Analysis of gravity-load-designed RC beam-column joints subjected to lateral loads

Lin, Xin

2007

Lin, X. (2007). Analysis of gravity-load-designed RC beam-column joints subjected to lateral loads. Doctoral thesis, Nanyang Technological University, Singapore.

https://hdl.handle.net/10356/12044

https://doi.org/10.32657/10356/12044

Analysis of Gravity-Load-Designed RC Beam-Column Joints Subjected to Lateral Loads

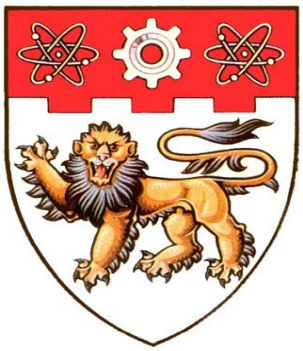

Lin Xin

School of Civil and Environmental Engineering

Nanyang Technological University

Singapore

Jun 2007

Analysis of Gravity-Load-Designed RC Beam-Column Joints Subjected to Lateral Loads

Lin Xin

A dissertation submitted to the Nanyang Technological University in fulfillment of the requirements for the degree of Doctor of Philosophy

School of Civil and Environmental Engineering

Nanyang Technological University

Singapore

Jun 2007

ABSTRACT

Gravity-load-designed structures widely exist in non-seismic zone, and some historical structures in seismic zone were designed based on gravity load long time ago. It is possible for gravity-load-designed structures to be subjected to lateral loads due to long-distance earthquake, explosion or strong wind. Then, the evaluation of the behaviour of gravity-load-designed structures under lateral load is necessary and important to ensure the safety of the occupants. In gravity-load-designed structures, seismic design principles are not satisfied. Because of this, beam-column joint may become the weakest component in the structures. Therefore, this study is conducted to model and investigate the behaviour of gravity-load-designed beam-column joints subjected to lateral loads.

To achieve different purposes, different models of gravity-load-designed beam-column joints were developed, such as the panel element for finite element analysis and joint element for frame analysis. Joint shear strength equation was also proposed to estimate the strength of gravity-load-designed beam-column joints.

To study the local behaviour of the beam-column joint subjected to lateral loads, especially the local strain distribution and local bond slip distribution in the joint, the finite element analysis should be carried out. In finite element analysis, a new double-panel element was developed to model both shear and bond behaviour, because these behaviour have been found to characterize the joint subjected to lateral loads. The shear behaviour in the double panel element was analysed with fixed-crack angle theory. Sophisticated material constitutive laws proposed by other researchers were utilised in the double panel element. The bond behaviour in the double panel element was analysed based on the displacement difference of concrete and reinforcement. In the new element, double nodes are used to represent concrete and reinforcement, and bond slip and stress are described in between concrete and reinforcement panels. Eligehausen et al' model was utilised to model the monotonic and cyclic local bond law. The element was implemented into finite element program, and was corroborated with typical bond experiments such as pull out, axial tension and push-pull tests.

Before using the double panel element to analyse beam-column joint subjected to

lateral loads, constitutive models such as concrete compression model and bond model were modified according to the characteristic of the joint. Then, 14 specimens failed in shear or bond were collected, and the analytical load-deflection curves from the double panel element with modified constitutive law were compared with experimental data to show the efficiency and accuracy of double-panel element. Besides load-deflection curves, contribution of the beam and column flexure, joint shear deformation and bond slip to the total story drift was analysed and compared with experimental results to show the significant contribution of joint shear deformation and fixed-end-rotation deformations to the total story drift. Another observed fact in the experiment, the initial tension of tensile beam reinforcement turns into compression due to bond-slip in the joint, can also be simulated in the analysis.

To study the global overall behaviour of the GLD structures subjected to lateral loads, the frame analysis is usually carried out. In frame analysis, a model of 12-dof joint element was developed to take into account the softening of the beam-column joint under lateral loads. A model with a combination of spring elements was developed to take into account the fixed-end-rotation at interface between the joint and adjacent members. The 12-dof joint element was degenerated from 8-node quadrilateral panel element. It has 9 Gauss points to describe non-constant strain field in the joint. The combination of spring elements considers both rotational and translational bond slip effect at beam end interface. In gravity-load-designed structures, beams are usually asymmetrical doubly reinforced. In this case, the bond slips at top and bottom reinforcement are not identical, and then translational displacement occurs together with rotational displacement at the interface. Constitutive models of the 12-dof joint element and spring elements were established considering the characteristics of the joints. Parameters in the models are verified through experimental results. The models of two elements were implemented into frame analysis program. Analytical results with the two elements were compared with experimental results to show the efficiency and accuracy of newly developed elements.

Before the retrofitting and strengthening process, the designer needs to know the strength of the existing members or structures. One of the most difficult to predict is

the shear strength of the gravity-load-designed beam-column joints. To estimate the shear capacity of beam-column joints, a simple equation is required. In the design equation, the joint shear strength estimation is based on the combination of arch and truss mechanisms. For joint strength based on truss mechanism, the joint core was simplified into a panel, and plasticity theory is applied to analyse the strength. For joint strength based on strut mechanism, resistance is provided by diagonal strut. Parameters such as column axial load, concrete cylinder strength, shear transverse reinforcement ratio, reinforcement detailing, which influence the joint shear strength, is included in the joint strength estimation equation. Parameters in the constitutive laws are verified through experimental data. Finally, the accuracy of the formula was studied through the comparison with the experimental results.

ACKNOWLEDGMENT

I would like to express my sincere appreciation and profound gratitude to Dr. Paulus Irawan for his valuable guidance and persistence supervision in every stage of this study.

Special appreciation is extended to School of Civil & Environmental Engineering, Nanyang Technological University (NTU) who has generously provided my scholarship.

I would also wish to thank Nguyen Xuan Hoang and many friends for their help and friendship.

No word is sufficient to express gratitude to my beloved family members for their constant sacrifices and concerns. This work is dedicated to them in recognition of their endless love.

TABLE OF CONTENTS

LIST OF TABLES

LIST OF FIGURES

NOTATIONS

English letters

A_c = area of concrete, mm^2

A_s = area of reinforcing steel bar, mm^2

b_b = width of beams, mm

b_c = width of columns, mm

c = cover of beam, mm

d_b = diameter of reinforcing bar, mm

d_{bx} = diameter of reinforcing bar in x-direction, mm

d_{by} = diameter of reinforcing bar in y-direction, mm

d_x = displacement at column ends, mm

d_y = displacement at beam ends, mm

E_b = modules of bond, MPa

E_{bx} = modules of bond in x-direction, MPa

E_{by} = modules of bond in y-direction, MPa

E_c = modules of elasticity of concrete, MPa

E_s = modules of elasticity of steel, MPa

f_c' = concrete compressive strength, MPa

f_y = yield stress of reinforcing bar, MPa

h_b = depth of beams, mm

h_c = depth of columns, mm

L = embedded length, mm

L_b = clear length of beams, mm

L_c = clear length of columns, mm

P_b = shear force on the beam, N

P_c = shear force on the column, N

s = local bond slip, mm

s_{max} = historical maximum bond slip, mm

s_{min} = historical minimum bond slip, mm

s_x = local bond slip in x-direction, mm

s_y = local bond slip in y-direction, mm

u_c = displacement of concrete, mm

u_{cx} = displacement of concrete in x-direction, mm

u_{cy} = displacement of concrete in y-direction, mm

u_s = displacement of reinforcing bar, mm

u_{sx} = displacement of reinforcing bar in x-direction, mm

u_{sy} = displacement of reinforcing bar in y-direction, mm

V_b = shear force on the beam, N

V_c = shear force on the column, N

Greek letters

α = Rotational angle; angle between the principle compressive stress of concrete (d-axis) and the longitudinal steel bars (l-axis)

α_2 = Fixed angle; angle between the applied principle compressive stress (2-axis) and the longitudinal steel bars (l-axis)

ε_0 = concrete compressive strain at peak stress, mm/mm

τ_x = local bond stress in x-direction, MPa

τ_y = local bond stress in y-direction, MPa

τ = local bond stress, MPa

ε_{cx} = normal strain in concrete in x-direction, mm/mm

ε_{cy} = normal strain in concrete in y-direction, mm/mm

σ_{cx} = normal stress in concrete in x-direction, MPa

σ_{cy} = normal stress in concrete in y-direction, MPa

ρ = reinforcing bar ratio

ρ_x = reinforcing bar ratio in x-direction

ρ_y = reinforcing bar ratio in y-direction

γ_{cxy} = shear strain in concrete in global coordinates, mm/mm

τ_{cxy} = shear stress in concrete in global coordinates, MPa

ε_c = strain in concrete, mm/mm

ε_{sx} = strain in reinforcing bar in x-direction, mm/mm

ε_{sy} = strain in reinforcing bar in y-direction, mm/mm

ε_s = strain in reinforcing bar, mm/mm

σ_c = stress in concrete, MPa

σ_{sx} = stress in reinforcing bar in x-direction, MPa

σ_{sy} = stress in reinforcing bar in y-direction, MPa

σ_s = stress in reinforcing bar, MPa

Abbreviation

ACI	American Concrete Constitute
AIJ	Architectural institute of Japan
CEB	Comité Européen du Béton (European Committee for Concrete)
EC	Euro Code
FE	Finite Element
fib	fédération internationale du béton (International Federation for Structural Concrete)
FIP	Fédération Internationale de la Précontrainte (International Federation for Prestressing)
GLD	Gravity Load Design
RC	Reinforced Concrete

CHAPTER 1 INTRODUCTION

1.1 Background

It is known that not all structures were designed to resist significant lateral loads. Many old buildings, especially historical structures, were built based on gravity loads only. In non-seismic zone, structures were usually designed based on gravity loads and notional horizontal load. But it is possible for these structures to be subjected to relatively larger lateral loads due to long-distance earthquake, ground shock due to explosion or strong wind. Then, the evaluation of the behaviour of gravity-load-designed (GLD) structures under lateral load is necessary and important to ensure the safety of the occupants.

The gravity-load-designed structures generally possess reinforcement details that conform to the code of non-seismic design. The following detailing may result: 1) little or no transverse shear reinforcement in beam-column joints; 2) discontinuous positive (bottom) beam flexural reinforcement in the beam-column joints and 3) insufficient anchorage length for the longitudinal bars in the beam-column joints. In

Beam-column joint shear failure

Beam-column joint shear failure

Figure 1-1 Beam-column joint failure at Kocaeli (Turkey) earthquake

the modern seismic design code, the beam-column joint is usually designed so rigid and strong that the strength of joint under lateral load is satisfied and the deformation of joint under lateral load can be neglected. On the contrary, beam-column joint may be the weakest component in the gravity-load-designed structures. As a result, joint failure may occur (Figure 1-1).

In earthquake-load-designed reinforced concrete structures, beam-column joints are designed stronger than the adjacent beams and columns. But when reinforced concrete frames designed for gravity loads are subjected to lateral loads, the shear force in the joint is much larger compared with shear force in the adjacent members and bond deterioration is prone to occur in the joint. The most vulnerable part of the RC frames is the joint. Therefore, it is important to investigate the strength of gravity-load-designed beam-column joint subjected to lateral load.

Beam-column joints are usually designed to be rigid in earthquake-load-designed reinforced concrete structures. Hence, the shear deformation of joint contributes little to the total story drift of the frame compared to the contribution from other deformation, such as deformation of the beams and the columns. In GLD structures, the contribution of fixed-end rotation due to slip in the joint and shear deformation of joint could be large to the total story drift. Noguchi and Naganuma (1984) found that in some cases the contribution of slip and joint distortion can be as high as 30% to the total story drift. Therefore, it is important to investigate the deformation of gravity-load-designed beam-column joint subjected to lateral load.

Based on the researches conducted in the past, two mechanisms were found to dominate in the joint shear transfer. One is the diagonal concrete arch mechanism. In this mechanism shear force is transferred directly from one corner to another corner through diagonal concrete strut. The other is truss mechanism. In truss mechanism, reinforcement act as tension member, and concrete acts as compression strut. These two components form truss mechanism to resist joint shear force.

The bond demand in the beam-column joints under lateral loads was found larger

than that under gravity loads. To transfer the force from reinforcing bars to concrete, higher bond stress in the joint occurs. If the anchorage is not sufficient, the pull-out of beam longitudinal bars at the beam-joint interface will occur and it will be the main cause of beam fixed-end rotation that can contribute significantly to the overall beam deflection.

1.2 Problem statement

The importance of the beam-column joint in GLD structures subjected to lateral loads to the total behaviour of the structures has been realised by researchers, and some experimental studies (Bracci et al, 1992, Aycardi et al, 1992) have been conducted on the shear performance and poor bond condition of these beam-column joints. Analytical study based on these softened joints is very few due to the complexity of the problem.

To study the global and local behaviour of the beam-column joint subjected to lateral loads, especially the local strain distribution and local bond slip distribution in the joint, the finite element analysis should be carried out.

Since shear and bond performances are two main characteristics of the GLD beam-column joints subjected to lateral loads, emphasis is put on the models to describe the shear and bond behaviour.

So far, the performance of the panel under shear or other complex in-plane loads has been studied quite extensively by researchers, such as Vecchio and Collins (1986), Okamura and Maekawa (1991) and Hsu et al (Pang and Hsu, 1996; Belarbi and Hsu, 1994 and Belarbi and Hsu, 1995). Sophisticated material constitutive models have been developed through experiments. Nonlinear finite element analysis programs have been developed based on these models.

Under lateral loads, more force should be transferred from reinforcement to concrete in the joint because forces on the reinforcement at the two opposite sides of the joint are in the same direction, while under gravity loads, these forces are in an opposite direction. Thus, bond stress in the joint subjected to lateral loads is

much larger than bond stress in the joint subjected to gravity loads. Slip at the interface of reinforcing bars and concrete may be significant.

To incorporate the bond slip, bond-link element and bond-zone element were applied in two-dimensional problems by Ngo and Scordelis (1967) and Keuser and Mehlhorn (1987). Because the advantage of bond zone element is in its ability to describe nonlinear slip effect, some researchers developed different types of bond zone elements for the analysis of trusses and frames with bond slip. As beam-column joints are modelled as two-dimensional elements, concrete and reinforcement are modelled by panel elements. In this case, bond zone element to describe bond effect between the two panels is required, and needs to be developed.

To study the global overall behaviour of the GLD structures subjected to lateral loads, the frame analysis is usually carried out. For GLD structures, the frame analysis programs can not assume the joint to be rigid. It should model the softening of the joint and also the possibility of the bond slip inside the joint. As the softening of joint and the bond slip will affect the overall behaviour of GLD structures significantly, special joint element has to be developed for this purpose.

Some researchers (D'Ambrisi and Filippou, 1999, Ghobarah and Biddah, 1999, Biddah and Ghobarah, 1999 and Youssef and Ghobarah, 2001) have included shear deformation to the additional rotation at the member ends. The simple rotation spring element was utilised to analyse the shear deformation of soft joint. Softened truss theory (Hsu, 1998) was utilised to calculate the shear stiffness by Biddah and Ghobarah (1999). However, the effect of varying axial loading can not be included in the rotational spring element. Another drawback of the rotational spring element is that it can only analyse constant strain field, while strain in the joint is obviously non-uniform.

Other researchers (Ghobarah and Biddah, 1999 and Youssef and Ghobarah, 2001) have also modelled the fix-end rotation at the interface of beam and joint due to bond deterioration. The simple rotational spring element was utilised to analyse the

slip effect. This simulation is based on symmetric arrangement of reinforcement in the beam. In the case of gravity-load-designed structures, reinforcement is usually arranged asymmetrically in beams. In this condition, slip effect at interface includes not only rotation, but also translation, which can not be described by the rotational spring element. Therefore, an element to include bond slip effect of both rotation and translation needs to be developed.

There is sometimes a need to retrofit or strengthening the old structures, especially the historical buildings, so that it can withstand larger lateral loads due to the ground shocks. Before the retrofitting and strengthening process, the designer needs to know the strength of the existing members or structures. One of the most difficult to predict is the shear strength of the beam-column joints. In this case, a simple equation to estimate the shear capacity of beam-column joints in gravity-load-designed structures is required. Parameters such as column axial load, concrete cylinder strength, shear transverse reinforcement ratio, reinforcement detailing, which influence the joint shear strength, should be included in the joint strength estimation equation.

1.3 Objectives and scope of the study

The main objective of this study is to model and investigate the shear strength and deformation of gravity-load-designed beam-column joints subjected to lateral loads. To achieve different purposes, different models are developed, such as the panel element for finite element analysis and model of joint element for frame analysis. Equation is also proposed to estimate the joint strength.

For finite element analysis, a double-panel element is developed to model the beam-column joint with the bond slip of longitudinal bars. In the double-panel element, nonlinear behaviour of concrete and reinforcement panel is described in each panel, and nonlinear behaviour of bond is described between the two panels. Monotonic and cyclic constitutive laws of concrete, reinforcement and bond are utilised so that this element can be applied to analyse beam-column joint subjected

monotonic and cyclic lateral loads.

For frame analysis, a 12-dof joint element is developed to take into account the joint shear deformation. Combining this element with existing frame element program, it will be able to predict the global structural behaviour with relatively soft beam-column joints. The joint element has three degrees of freedom in each node and is used to connect four beam or column members. Nonlinear behaviour of concrete and reinforcement is described in the macro element. A model with a combination of spring elements is also developed to take into account the fixed-end rotation at interface between the joint and the beams. The combination of springs can include both rotational and translational displacement to model slip in asymmetrically doubly-reinforced beams. After that, the 12-dof joint element is conducted with spring elements to model the relatively soft joints with bond slip.

Finally, to estimate the joint strength, a simple equation is proposed based on the combination of arch and truss mechanisms.

The elements and equation are developed to analyse the behaviour of gravity-load-designed interior beam-column joints subjected to in-plane loads only. Bond model is based on pull-out failure, and no splitting bond failure is assumed. Moreover, the bond failure due to insufficient splicing length is not considered.

1.4 Report organization

This report presents research work on the analysis of gravity-load-designed beam-column joints subjected to lateral loads and consists of seven chapters.

Chapter one presents the background of the GLD beam-column joints subjected to lateral loads, and states the need to do the modelling of the joint for finite element analysis, for frame analysis and the need to estimate the shear strength of beam-column joints. After that, the objectives and scope are specified and organization is introduced. Chapter two reviews previous researches on the behaviour of reinforced concrete beam-column joints subjected to lateral loads and researches on the modelling of shear and bond-slip. Chapter three develops a new

double-panel element including bond-slip effect. The new element is implemented into finite element program WCOMD. Verification on typical bond-slip experiments such as pull out, axial tension and push-pull tests is carried out both on monotonic and cyclic loads. Chapter four utilises the newly developed double-panel element to analyse beam-column joints subjected to lateral loads. Some parameters in the constitutive laws are verified before they are applied in the beam-column joint analysis. Analytical results on several specimens are compared with experimental results to show the effectiveness and accuracy of the element. Chapter five describes the development of a 12-dof joint element to simulate relatively soft beam-column joints. A model with combination of spring elements is developed to consider the fixed-end rotation due to bond slip at the interface of the joint and beams. Verification is carried out for monotonic loads. Chapter six presents the development of a simple equation to estimate the shear strength of beam-column joints based on the combination of arch and truss mechanisms. Analytical predictions by the new equation are compared with several experiment results to show the accuracy of the equation. Conclusion and future work are presented in chapter seven.

CHAPTER 2 LITERATURE REVIEW

2.1 Behaviour of gravity-load-designed beam-column joint

Although gravity-load-designed (GLD) structures are designed without the consideration of lateral loads, such as structures in Singapore and other non-seismic regions, they may be subjected to lateral loads from long-distance earthquakes and ground shock due to explosion. The deficient detailing of GLD beam-column joints can lead to inferior structural performance when they are subjected to lateral loads. Therefore, some researchers (Yin, 2001, Kunnath et al, 1995, Pessiki et al, 1990, Bracci et al, 1992, Aycardi et al, 1992) have carried out experimental studies on the performance of these GLD beam-column joints subjected to lateral loads.

The global and local behaviour of the GLD beam-column joints in the experiment will be summarised.

2.1.1 Global experimental behaviour

1. Crack sequence and failure mode

Since the seismic provision is not satisfied in the GLD frames, the joint may become the weakest part of the structure when it is subjected to lateral loads. Severe damage may occur in the joint, and failure mode of the structure can be joint failure. A typical crack pattern from specimen tested by Yin (2001) is shown in Figure 2-1.

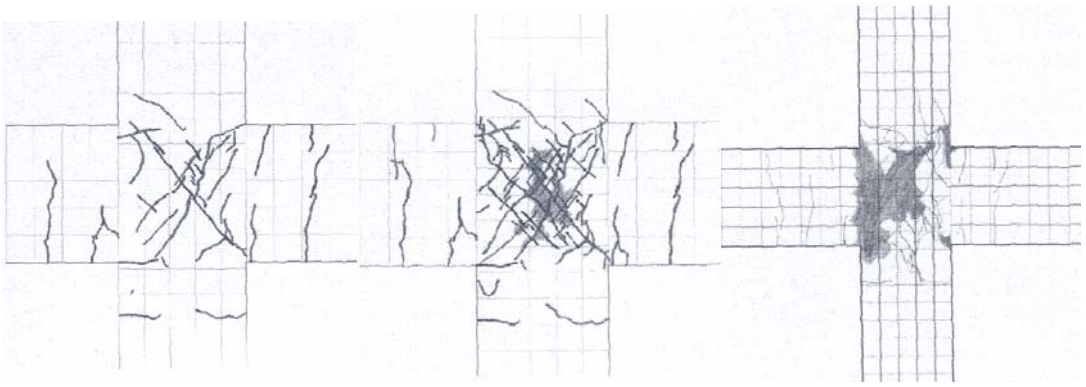

(1) 1% Story Drift (2) 2% Story Drift (3) 3% Story Drift

Figure 2-1 Crack pattern at different story drift (Yin, 2001)

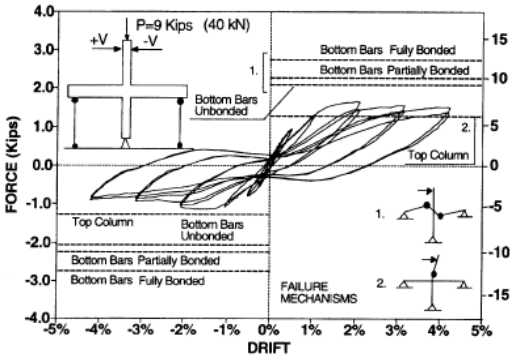

Figure 2-2 Force-Drift relation of shear failure joint (Aycardi et al, 1994)

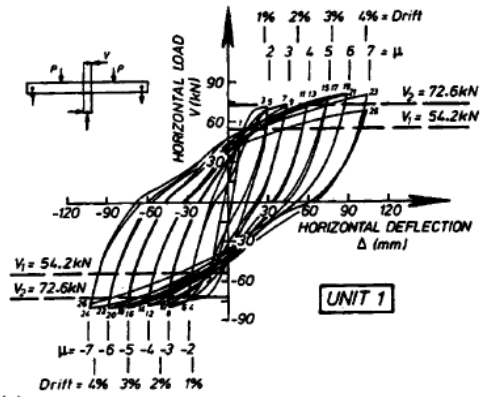

Figure 2-3 Force-Drift relation of beam failure joint (Park and Ruitong, 1988)

At 1% story drift ratio, minor cracks are found in the beams and joint, and the number of cracks in the joint is larger than that in the beams. At 2% story drift ratio, the crack width and crack number have increased much especially in the joint, and minor spalling is observed in the joint panel. At 4% story drift ratio, major spalling is found in the joint panel, and the joint can take no more loads.

2. Hysteresis response

In the gravity-load-designed frames, the joint deformed much before plastic hinge occurs at beam ends. Then, hysteresis curve can have severe pinching loops (Figure 2-2). This is in contrast with ductile beam-column joint, for which plastic hinge occurs at beam ends, and the hysteresis curve shows spindling loops (Figure 2-3). The pinching hysteresis loops of soft joint are caused by inelastic deformations due to shear and bond mechanisms after extensive diagonal cracking in the joint panel.

3. Element contribution to global displacement

The behaviour of soft joint can be identified from the large contribution of joint deformation to global drift angle compared to the rigid joint. In the ductile assemblage of beam-column joint, the contribution of joint deformation on the drift angle remains low compared to the contribution of beam flexure (Figure 2-4(a)). In a typical non-ductile assemblage of beam-column joint, the joint contributes a small portion to the drift angle at the beginning. With the increment of drift angle, damage

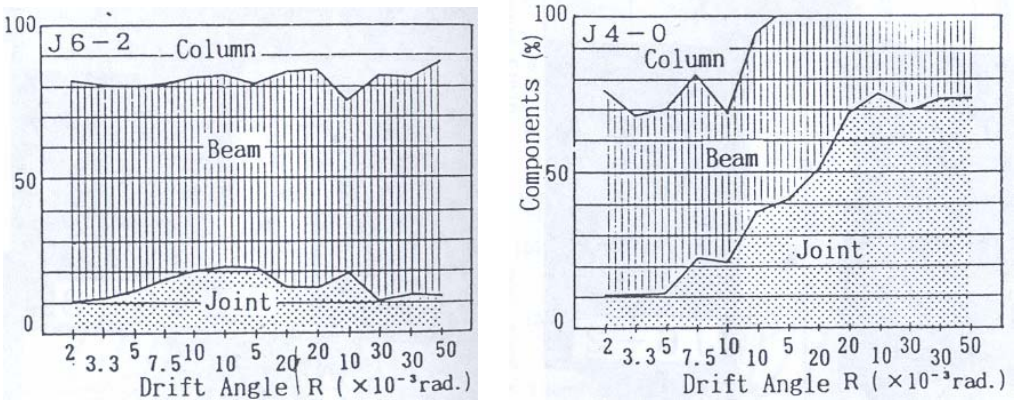

(a) Ductile assemblage of beam-column joint

(b) Non-ductile assemblage of beam-column joint

Figure 2-4 Drift angle component (Sugano et al, 1991)

in the joint becomes more severe, and the joint panel becomes softer. Then, the contribution of joint deformation increases substantially with drift angle. It exceeds 50% at the total drift angle of 2% as shown in Figure 2-4(b).

2.1.2 Local experimental behaviour

1. Strain distribution in the longitudinal reinforcement in the beam

A typical observed distribution of tensile stress along the longitudinal bar through joint core is plotted in Figure 2-5. As shown in Figure 2-5, when story drift is small, the stress of top reinforcement at left interface between the joint and the beam is compression because the section is subjected to negative moment. When the story drift increases, the stress of top reinforcement at left interface does not increase with

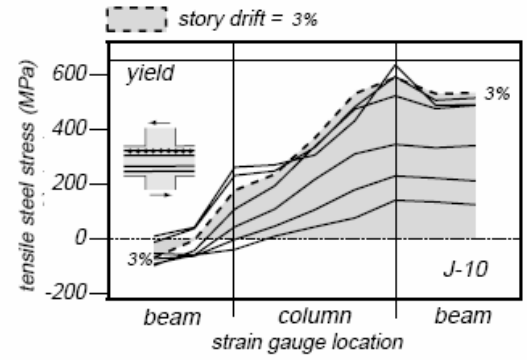

Figure 2-5 Observed stress in beam longitudinal reinforcement (Shiohara, 1998)

the increment of moment., but decreases and even changes into tension. It is due to bond deterioration.

2.2 Constitutive models for 2-D reinforced concrete

2.2.1 Constitutive models for 2-D concrete

2.2.1.1 Introduction

Concrete is a non-homogenous, anisotropic material whose response is nonlinear even under small stress levels. Furthermore, concrete exhibits a different behaviour under tension and compression stresses (Balan et al, 2001). In compression, the response hardens up to a peak stress value that depends on the level of lateral confinement. The post-peak behaviour depends in general on the level of lateral confinement. Under low confinement, the post-peak response is brittle softening. For increasing confinement stresses, the response of concrete changes to ductile hardening. Under tensile stresses, concrete cracks and eventually loses its strength entirely. The complex nonlinear behaviour of concrete makes it a difficult material to model. The main theories on different categories are reviewed below:

2.2.1.2 Linear elastic theory and nonlinear elastic theory

The simplest constitutive equation comes from linear elastic theory, which is

$$\sigma_{ij} = C_{ijkl}\varepsilon_{kl} \tag{2-1}$$

where C_{ijkl} is a constant tensor

However, the linear elastic theory was used only to establish the constitutive law of concrete under small stress levels. When the compressive stress under uniaxial compression is below $f_c'/3$, the stress-strain relation of concrete is linear, with f_c' being the uniaxial compressive cylinder strength (Chen, 1982). Otherwise, the behaviour of concrete is nonlinear, which cannot be characterized by the linear elastic theory.

In the nonlinear elastic theory, the material modulus is not a constant any more, but

also a function of stress state. There are two formulations for nonlinear elastic theory, the total stress-strain model and incremental formulation of non-linear elasticity.

a. Total stress-strain model of nonlinear elasticity

One version is hyperelasticity and it is based on the total stress-strain model. In this formulation, the current state of stresses in the material is dependent upon the current state of strains only, thereby, total stress-strain model represents a path-independent response. This behaviour is expressed by

$$\{\sigma\} = [D_s(\sigma)]\{\varepsilon\} \tag{2-2}$$

where D_s is the matrix of secant modulus

However, concrete is a path-dependent material. Its behaviour depends not only on current stress and strain, but also on their history. So the applicability of path-independent formulations is limited to describing concrete under proportionally increasing mechanical loads. According to the hyperelastic formulation, the strains are covered completely upon unloading, which is not generally encountered in concrete.

b. Incremental formulation of non-linear elasticity

This approach is based on an incremental formulation of the constitutive laws of concrete, which is known as the hypoelastic formulation. This model takes the following form:

$$\{d\sigma\} = [D_t(\sigma)]\{d\varepsilon\} \tag{2-3}$$

where D_t is the matrix of tangent modulus

With this formulation, it is possible to represent the path-dependent characteristics of concrete in which the state of stresses in the material is dependent not only on the current state of strains but also on their history. However, this approach has also reversible characteristic although this deficiency appears only in the incremental sense. The applicability of this formulation is still limited to monotonic loading conditions, but the loading is not necessarily proportional. These limitations can be

overcome by introducing loading and unloading criteria (Chen and Saleeb, 1982) to reflect the irreversibility of concrete deformations. This approach is known as a "variable modulus" model.

2.2.1.3 Plasticity theory

Plasticity theory consists of three basic components: yield surface, flow rule and hardening law. The relation between strain and stress increments in the theory of plasticity can be described by the following equations.

The yield condition limits the elastic domain. It depends on the stress state σ_{ij} and a hardening function q. It has the form

$$f\left(\sigma_{ij}, q\right) \leq 0 \tag{2-4}$$

where q is a function of the hardening parameter κ, expressed as

$$q = h\left(\kappa\right) \tag{2-5}$$

The hardening parameter is generally given in the form of a rate equation as

$$\dot{\kappa} = \dot{\lambda} \cdot k\left(\sigma_{ij}, \varepsilon_{kl}^{p}\right) \tag{2-6}$$

If the yield condition is equal to zero, plastic flow occurs. The flow rule prescribes in which way the plastic flow develops. The direction of the flow vector is determined by the gradient of the plastic potential function g. The amount of the plastic flow is determined by the plastic multiplier $\dot{\lambda}$:

$$\dot{\varepsilon}_{ij}^{p} = \dot{\lambda} \cdot \frac{\partial g}{\partial \sigma_{ij}} = \dot{\lambda} \cdot \left(g_{\sigma}\right)_{ij} \tag{2-7}$$

As mentioned, plastic flow can only occur if the state is plastic ($f = 0$). This can be expressed by

$$\dot{\lambda} \cdot f\left(\sigma_{ij}, q\right) = 0 \tag{2-8}$$

Furthermore, the plastic multiplier $\dot{\lambda}$ cannot be negative:

$$\dot{\lambda} \geq 0 \tag{2-9}$$

During plastic flow the yield condition must remain equal to zero, which can be expressed by

$$\dot{f} = \left(f_\sigma\right)_{ij} \cdot \dot{\sigma}_{ij} + f_q \cdot \dot{q} = 0 \tag{2-10}$$

The capabilities of the various plasticity models for plain concrete depend heavily on the form of the components, i.e. the yield condition, flow rule and hardening law.

a. Yield conditions

The yield condition at failure describes the strength surface of plain concrete. There are many formulations of yield conditions which fulfil these aspects by means of different mathematical formulations. Among these, there are formulations proposed by Willam and Warnke (1974), Ottosen (1977), Menétrey and Willam (1995). In commercial finite element codes it is still often common to use a Mohr-Coulomb or a Drucker-Prager yield surface. These formulations differ mainly in the number and kind of material parameters required for the calibration.

b. Flow rule

The flow rule prescribes the evolution and the amount of the plastic strain, and the ratio of axial and lateral inelastic deformations. The evolution itself is determined by the gradient of the plastic potential; if the plastic potential has the same form as the yield surface, the flow rule is called associated. For concrete, an associated flow rule overestimates the volumetric expansion reported in experiments.

c. Hardening law

The subsequent yield surfaces, which characterize the progressive yielding of material, can be obtained by applying appropriate hardening plasticity laws. There are three types of hardening law, which are isotropic hardening law, kinematic hardening law and mixed hardening law. Among them, the mixed hardening law is a combination of the two preceding cases, which leads to a more general mixed-hardening (Hodge, 1957).

The plasticity theory is also applied together with elastic theory to characterize

elastic and plastic states of concrete.

2.2.1.4 Fracture theory

Fracture theory focuses on developing numerical models to simulate the fracture behaviour of quasi-brittle materials, such as mortar, concrete, rock or bricks, used in civil engineering structures. Even in two dimensions, the modelling of the fracture behaviour of these materials is a complex problem. Traditionally, the numerical methods based on the FEM are classified in two groups: 'smeared crack approach' and 'discrete crack approach'.

In discrete crack model, cracks occur between finite elements, and gaps between elements represent crack width. The spring between nodes can be used to represent tension stiffening, which takes into account the remaining tensile strength in the reinforced concrete after cracks occur.

Since spring elements are used to simulate the crack opening, the location of crack should be known from the beginning. Another limitation of this model is the mesh of structure depends on the location of cracks and remeshing may be necessary.

Another method is smeared crack model. In smeared crack model, width of crack is modelled through the elongation of element between two cracks. Today, the smeared crack approach is mostly used by researchers in nonlinear analysis of reinforced concrete structures to model the cracking behaviour of concrete, since its implementation in a finite element analysis is simpler than that of discrete crack model.

In the smeared crack approach the fracture is represented in a smeared manner; an infinite number of parallel cracks of infinitely small opening are (theoretically) distributed (smeared) over the finite element (Bažant and Planas, 1997). The cracks are usually modelled on a fixed finite element mesh. Their propagation is simulated by the reduction of the stiffness and the strength of the material. The constitutive laws, defined by stress-strain relations, are non-linear and show a strain softening. This approach was pioneered with fixed-crack orthotropic secant models (Rashid,

1968; Cervenka, 1970; Suidan and Schnobrich, 1973) and rotating crack models (Cope et al., 1980; Gupta and Akbar, 1984; Willam et al., 1987).

The fracture theory is also applied together with plasticity theory to characterize the total constitutive model of concrete. It is difficult for the traditional plasticity constitutive models for concrete to represent the stress-strain relation of descending part in stress-strain space, because plastic slip does not lead to strain softening, i.e., the stress decreases at increasing strain. It is also difficult for these stress-based models to determine the descending part, or unloading part, of the stress-strain curve, because the stress increments are both negative during descending part and softening part. The plastic fracture model is strain-based model that can solve this problem.

2.2.2 Constitutive models for reinforcement in concrete

There are two typical elements to model reinforcement. They are discrete element and distributed element. In the discrete element, reinforcement is modelled as one dimensional bar. Nodes of the reinforcement element and concrete element coincide and related to represent bond behaviour. Obvious limitation of this model is that the mesh of structures will depend on the location of reinforcement. The second model smeared the reinforcement into the whole plane, so it has the same shape with concrete panel.

The smeared reinforcement model is relatively easier to be implemented into finite element program especially in the case of perfect bond.

2.3 Constitutive equations for 2D reinforced concrete

According to experimental data, the behaviour of concrete at relatively high stress level, and particularly near failure, exhibits stress (or strain)-induced anisotropy. Orthotropic models are formulated and used to describe the nonlinear behaviour of concrete under biaxial compressive states of stress. A typical representative model of orthotropic model was reviewed by Chen and Saleeb (1982). This hypoelastic

model is mostly for concrete under biaxial compression. For cracked reinforced concrete, it shows quite different properties along and perpendicular to crack. So, in the model, orthotropic constitutive equations should be presented first at crack coordinates, and transformed into x-y coordinates. Based on different assumptions of rotating or fixed crack, rotating or fixed crack models were proposed by researchers (Vecchio and Collins, 1986; Okamura and Maekawa, 1991; Pang and Hsu, 1996; Belarbi and Hsu, 1994 and Belarbi and Hsu, 1995). The focus of this dissertation is on shear dominated behaviour of cracked reinforced concrete. Therefore, the constitutive models of reinforced concrete in this dissertation are based on fixed crack approach (Okamura and Maekawa, 1991).

2.3.1 Incremental biaxial orthotropic model

In the case of plane stress conditions, the incremental orthotropic stress-strain relation referred to the principle axes is expressed in

$$\begin{Bmatrix} d\sigma_{11} \\ d\sigma_{22} \\ d\tau_{12} \end{Bmatrix} = \frac{1}{1-\nu_1\nu_2} \begin{bmatrix} E_1 & \nu_2 E_1 & 0 \\ \nu_1 E_2 & E_2 & 0 \\ 0 & 0 & (1-\nu_1\nu_2)G \end{bmatrix} \begin{Bmatrix} d\varepsilon_{11} \\ d\varepsilon_{22} \\ d\gamma_{12} \end{Bmatrix} \tag{2-11}$$

where

E_1, ν_1 and E_2, ν_2 are tangent elastic modulus along the principle axes of orthotropic axes 1 and 2, respectively.

G is the tangent shear modulus associated with axes of axes 1 and 2.

The tangent modulus E_1 and E_2 in the principle direction of orthotropic axes are obtained from the corresponding stress-strain relations of Eq. (2-12)

$$\sigma = \frac{E_0 \varepsilon}{(1-\nu\alpha)\left[1+\left(\frac{1}{1-\nu\alpha}\frac{E_0}{E_s}-2\right)\left(\frac{\varepsilon}{\varepsilon_p}\right)+\left(\frac{\varepsilon}{\varepsilon_p}\right)^2\right]} \tag{2-12}$$

where

E_0 is the initial tangent modulus of elasticity in uniaxial loading

$E_s = \sigma_p / \varepsilon_p$ = secant modulus of elasticity at the peak.

v is Poisson's effect in uniaxial loading

α = ratio of the principle stress in the orthogonal direction to the principle stress in the direction considered

σ_p ε_p are peak stress and strain

The strength parameters, σ_p , in major and minor directions can be determined from a biaxial strength envelope such as that shown in Figure 2-6 or from its analytical formula in Eq. (2-13)

Tension-tension region: $\sigma_1 = f_t^{'} \geq \sigma_2$

Tension-compression region: $\sigma_1 = \left(1 + 0.8\frac{\sigma_2}{f_c^{'}}\right) f_c^{'}$ (2-13)

Compression-compression region: $\left(\frac{\sigma_1}{f_c^{'}} + \frac{\sigma_2}{f_c^{'}}\right)^2 + \frac{\sigma_2}{f_c^{'}} + 3.65\frac{\sigma_1}{f_c^{'}} = 0$

The ductility parameters, ε_p , corresponding to σ_p in the two principle directions can be determined from the test results for different values of the stress ratio, α.

The hypoelastic formulation described above, Eq. (2-11), is mostly used for concrete under biaxial compression.

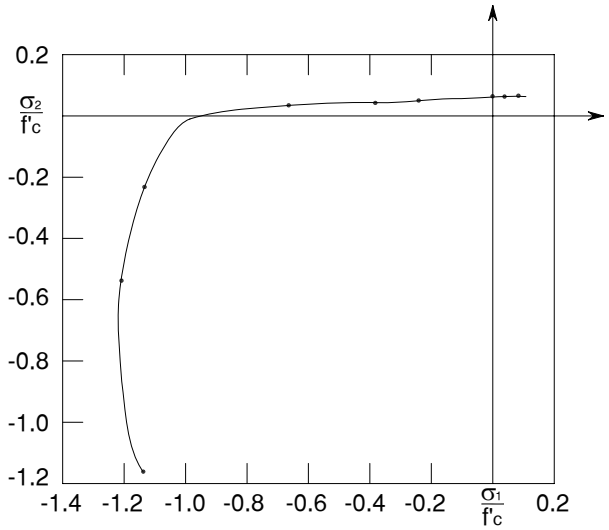

Figure 2-6 Biaxial strength envelope of concrete

(Kupfer et al, 1969)

2.3.2 Rotating- and fixed- crack approaches

For cracked reinforced concrete, behaviours on parallel crack direction and orthogonal crack direction show great difference. So, post-crack reinforced concrete can be modelled as orthotropic material referring to crack coordinates. Based on that, Vecchio and Collins proposed modified compression-field model (1986). In their analysis, they applied rotating-crack angle approach, while Okamura and Maekawa used fixed crack approach (1991). Hsu and his co-workers developed rotating-crack angle and fixed-crack angle softened-truss models (Pang and Hsu, 1996; Belarbi and Hsu, 1994 and Belarbi and Hsu, 1995).

Generally, in these models, stresses and strains can be considered in terms of average values when the areas are large enough to include several cracks and the longitudinal and transverse reinforcement is uniformly distributed over the element. Consequently, all these models are based on smeared crack and smeared reinforcement.

Total stress carried by reinforced concrete is the sum of averaged stresses of cracked concrete and reinforcement at equilibrium, as shown in Figure 2-7(a) to Figure 2-7(c). For the cracked concrete, the concrete stress comprises the average stresses parallel and normal to crack, and average shear stress transfers along cracks.

The smeared crack approach may be classified into the smeared fixed-crack angle approach and smeared rotating-crack angle approach. The fixed-crack angle approach treats a crack as being geometrically fixed once generated (Figure 2-7(f)), and anisotropy is inherently taken into account since the normal and shear transfers are independently modelled.

The smeared rotating-crack angle approach assumes that the crack direction always coincides with the principal direction of average strain. Accordingly, the crack direction will be changed or rotated depending on the stress condition (Figure 2-7(g)). Since basically there is no shear stress in the principal planes, no shear transfer model is needed. Only normal stress-strain relations in the direction normal

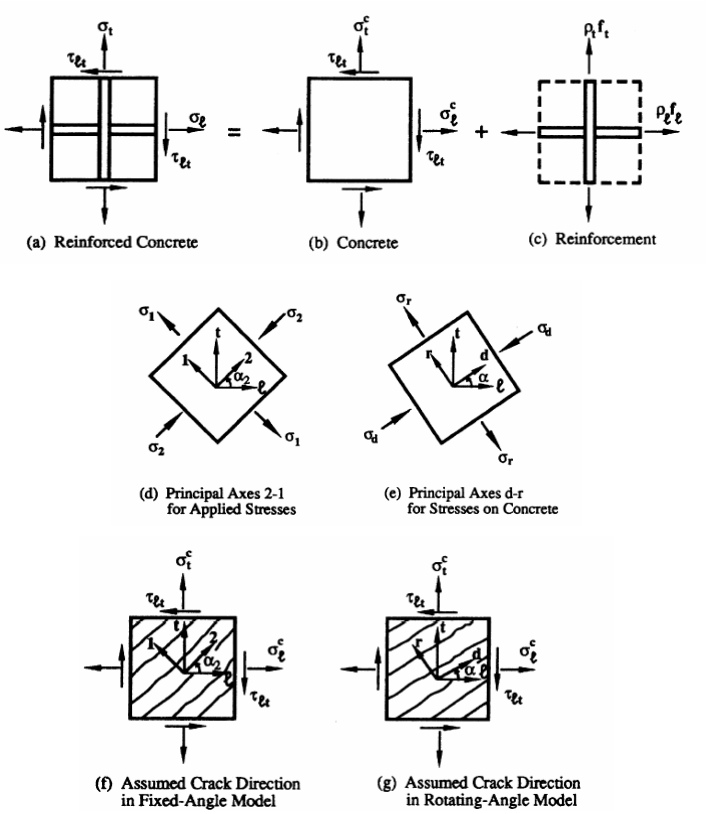

Figure 2-7 Reinforced concrete membrane elements subjected to in-plane stresses (Hsu, 1998)

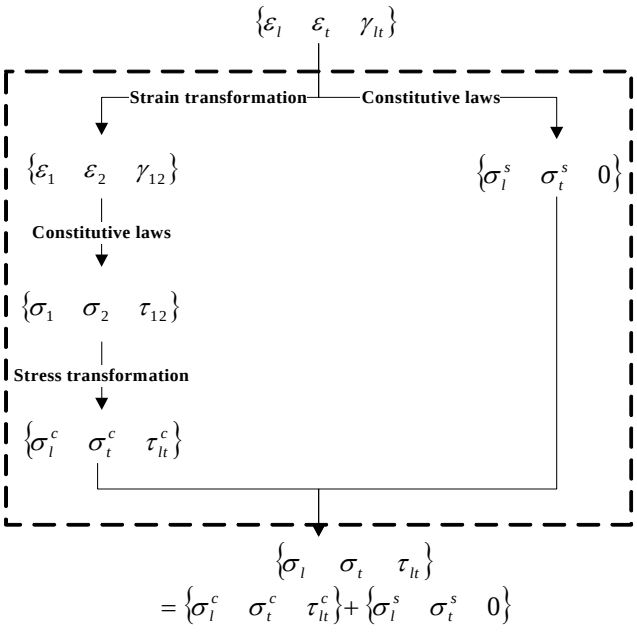

Figure 2-8 Flow chart of solution procedure for fixed-crack theory

and parallel to crack are needed.

Fixed-crack approach is taken as an example to illustrate the solution procedure. To calculate concrete stress on global coordinate l-t, firstly, concrete strain in global coordinate is transformed into concrete strain in crack coordinate 1-2. With the known stress-strain relation of concrete in crack coordinate 1-2, concrete stress in crack coordinate 1-2 can be calculated. Then, the calculated concrete stress in crack coordinate 1-2 will be transformed into concrete stress in global coordinate. For reinforcement stress in global coordinate l-t, it can be calculated through the stress-strain relation of reinforcement if the layout coincides with global coordinate. Finally, the stress of reinforced concrete in global coordinate can be calculated as the sum of stress of concrete and reinforcement in global coordinate. The whole process is illustrated in Figure 2-8.

2.4 Uniaxial constitutive models for concrete and reinforcement in 2D reinforced concrete model

2.4.1 Uniaxial concrete compression model in 2D reinforced concrete

Researchers (Vecchio and Collins, 1986 and Belarbi and Hsu, 1995) found the principle compression stress σ_2 was not only a function of the principle strain ε_2, but also a function of the co-existing principle tensile strain ε_1. Formulas of uniaxial concrete compression model including soften stress coefficient were proposed based on that. Furthermore, formulas to consider soften stress coefficient in high strength concrete (Vecchio et al., 1994 and Zhang and Hsu, 1998) were proposed. Among these, Maekawa and Okamura's model (1983) is a fixed crack approach model with an elasto-plastic and fracturing constitutive law included. Since this model can be used in general cases, it is adopted in this dissertation.

The model idealizes the concrete as the combination of continuum fracture and plasticity, which represents loss of elastic strain energy absorption capacity and the permanent deformation, respectively. The compressive stress is expressed in terms

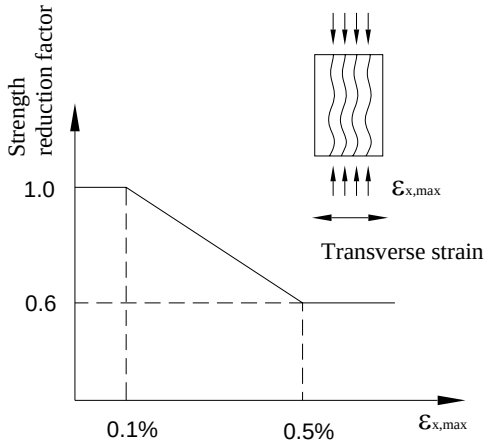

Figure 2-9 Strength reduction factor proposed by Okamura and Maekawa (1991)

of total strain, plastic strain and fracture parameter. When crack occurs in concrete, effective concrete strength will be reduced by a factor as a function of tensile strain in the orthogonal direction. The compressive concrete model is expressed as

$$\sigma_{cc} = \omega \cdot K_0 \cdot E_{c0} \cdot \left(\varepsilon - \varepsilon_p\right) \tag{2-14}$$

where

ω is strength reduction factor due to crack, as a function orthogonal tensile strain, shown in Figure 2-9.

ε_p is the plastic strain, $\varepsilon_p = \beta\left(\frac{\varepsilon}{\varepsilon_c} - \frac{20}{7}\left(1 - \exp\left(-0.35\frac{\varepsilon}{\varepsilon_c}\right)\right)\right)\varepsilon_c$

β is strain-rate factor, $\beta = 1$ for dynamic load

and $\beta = 1.5 - 2$ for static load

K_0 is the fracture parameter,

$$K_0 = \exp\left(-0.73 \cdot \frac{\varepsilon}{\varepsilon_c} \cdot \left(1 - \exp\left(-1.25 \cdot \frac{\varepsilon}{\varepsilon_c}\right)\right)\right) \cdot \left(1 + 0.227 \cdot \frac{\varepsilon}{\varepsilon_c}\right)$$

$E_{c0} = 2$

ε_c is the strain at peak stress

2.4.2 Uniaxial concrete tension model in 2D reinforced concrete model

The property of tensile has close relation with crack, so the criteria of crack and tension stiffening are two important aspects of uniaxial concrete tension model.

Some researchers (Collins et al., 1996 and Belarbi and Hsu 1994) considered concrete tensile strength is a function of compressive strength only. Okamura and Maekawa (1991) included the effect of biaxial stress conditions to determine crack strength.

$$\begin{aligned} &\left(\sigma_1 / f_t\right)^3 + \left(\sigma_2 / f_c\right) = 1 \qquad && \sigma_2 < 0 \\ &\left(\sigma_1 / f_t\right) + 0.3\left(\sigma_2 / \sigma_1\right)^2 = 1 \qquad && \sigma_2 \geq 0 \end{aligned} \tag{2-15}$$

where

f_t is uniaxial crack strength $f_t = 0.20 f_c^{'2/3}$

Concrete between the cracks in RC members can resist portion of the applied tension force even after cracking, which is known as tension stiffening effect. Due to bond transfer at the interface of concrete and reinforcement, concrete between the cracks can develop local tensile stresses even after cracks occur. Different formulas (Vecchio and Collins, 1986; Belarbi and Hsu, 1994; Collins et al., 1996; Stevens et al., 1991) were proposed to take into account the tension stiffening effect. In this dissertation, the formula proposed by Okamura and Maekawa (1991) were adopted.

The relation between average stress and average strain after cracking proposed by Okamura and Maekawa (1991) is expressed as,

$$\sigma = f_t\left(\varepsilon_{tu} / \varepsilon\right)^c \tag{2-16}$$

where

ε_{tu} is the cracking strain

f_t is uniaxial tensile strength

c is the stiffening parameter (0.4 for deformed bar, 0.2 for welded wire meshes)

2.4.3 Concrete shear model

The shear modular for uncracked plain concrete material is well known. Liu, Nilson, and Slate (1972) theoretically derived the equation for uncracked concrete to take concrete as an uncracked orthogonal material. Based on that, Vecchio (1989) proposed a modified orthogonal shear modular. Pang and Hsu (1996) derived an empirical formula from experimental data. Pang and Hsu's formula agrees well with experimental data, but it is quite complex. So, Zhu, Hsu, and Lee (2001) derived a simple formula based an assumption that the principle stress angle equals to the principle strain angle. Okamura and Maekawa (1991) used normalized shear strain to take into account of effect of tensile strain based on the contact density theory. Accuracy comparison between Zhu, Hsu and Lee's model and Okamura and Maekawa's model has been conducted with experimental data of normal strength concrete specimens subjected to shear dominated loads (Collins et al. 1985) and high strength concrete specimens subjected to shear dominated loads (Vecchio et al. 1994). The comparison showed Okamura and Maekawa's model is more accurate in predicting shear strain-stress curves. In this dissertation, the formula proposed by Okamura and Maekawa (1991) were adopted.

The shear transfer model of cracked concrete proposed by Okamura and Maekawa (1991) is based on the contact density theory. In this model, the rough crack surface is idealized as a set of numerous infinitesimal contact units having various inclinations. The simplified shear transfer model can be expressed as,

$$\tau_{st} = f_{st}\frac{\beta^2}{\beta^2+1} \tag{2-17}$$

where

f_{st} is the shear transfer strength, $f_{st} = 3.8 f_c^{'1/3}$ ($f_c^{'}: MPa$)

β is normalized shear strain, $\beta = \gamma_{cr}/\varepsilon_t$

γ_{cr} is shear strain due to crack

ε_t is tensile strain normal to crack

2.4.4 Embedded reinforcement model

In smeared crack model, the constitutive law of embedded bars is different from the constitutive law of bare bars. In crack concrete element, the stress of bars is not distributed uniformly along the element. The stress of bars in crack is obviously larger than that between cracks, so average stress of embedded bars will be different from average stress of bare bars. Some embedded reinforcement model (Belarbi and Hsu, 1994; Stevens et al., 1991) included the effect of reinforcement ratio and tensile strength of concrete into consideration. In this dissertation, the formulas proposed by Salem (Salem and Maekawa, 1999) and Shima and Okamura (Shima et al, 1987) were adopted.

In the formula proposed by Salem (Salem and Maekawa, 1999), the average yield stress can be expressed as,

$$f_{y0} = f_y - \frac{f_t}{2\rho} \tag{2-18}$$

where

f_y is the bare bar yield stress

f_{y0} is the average yield stress of bar embedded in concrete

f_t is uniaxial tensile strength

ρ is the reinforcement ratio

The post-yield stiffness, proposed by Shima and Okamura (Shima et al, 1987), is expressed in terms of yield stress of plain bar, average yield stress, bond properties of the bar, the strength of concrete, difference in steel ratio between two directions and the angle between the crack and bar axis.

$$E_{sh} = 100\left(f_y - f_{y0}\right)\cdot K_p K_y K_h K_a K_c K_k \tag{2-19}$$

Where

$$K_p = \rho_x^{0.5\rho_x}$$

$$K_h = \left(\rho_y / \rho_x\right)^{0.067}$$

$$K_y = \left(400/ f_y\right)^{0.1\left(\rho_y/\rho_x\right)\csc\theta}$$

$$K_a = \left(\csc\theta\right)^{0.2}$$

$$K_c = \left(30/ f_c^{'}\right)^{0.25}$$

$K_k = 1$ for deformed bar and $K_k = 0.72$ for welded wire meshes

ρ_x, ρ_y are reinforcement ratio in each direction $\rho_x \geq \rho_y$

2.5 Modelling of bond in the panel element

Two typical different elements have been proposed to include the bond-slip effect in the finite element analysis of RC structures. One is bond link element; the other is bond zone element (contact element). Bond-link element consists of two orthogonal springs which connect and transfer shear and normal forces between a reinforcement node and an adjacent concrete node (Figure 2-10). Since the link has no physical dimensions, the two connected nodes are in the same location in the finite element of undeformed structure.

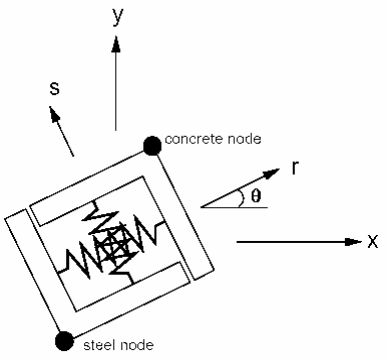

Figure 2-10 Bond link element
(Kwak and Filippou, 1990)

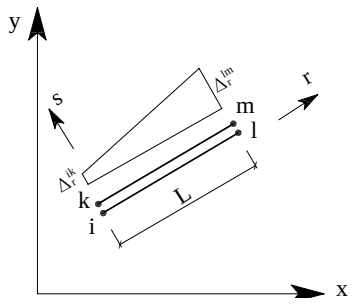

Figure 2-11 Bond zone element
(Keuser and Mehlhorn, 1987)

In the bond zone element (contact element), the contact surface between reinforcing bars are modelled by a material model, which represents the special properties of the bond zone (Figure 2-11).

Stiffness matrix of bond link element can be expressed as

$$\begin{Bmatrix} R_r^{ik} \\ R_t^{ik} \end{Bmatrix} = \pi \cdot d_s \cdot L \begin{bmatrix} G_r & 0 \\ 0 & G_t \end{bmatrix} \begin{Bmatrix} \Delta_r^{ik} \\ \Delta_t^{ik} \end{Bmatrix} \tag{2-20}$$

while, stiffness matrix of bond zone element can be expressed as

$$\begin{Bmatrix} R_r^{ik} \\ R_r^{lm} \\ R_t^{ik} \\ R_t^{lm} \end{Bmatrix} = \frac{\pi}{6} \cdot d_s \cdot L \begin{bmatrix} 2G_r & G_r & 0 & 0 \\ G_r & 2G_r & 0 & 0 \\ 0 & 0 & 2G_t & G_t \\ 0 & 0 & G_t & 2G_t \end{bmatrix} \begin{Bmatrix} \Delta_r^{ik} \\ \Delta_r^{lm} \\ \Delta_t^{ik} \\ \Delta_t^{lm} \end{Bmatrix} \tag{2-21}$$

where d_s = diameter of reinforcement

L = length of element

G_r, G_t = bond slip modular in r and t direction

In 1987, Keuser and Mehlhorn compared dissipated energy for bond-link element and bond-zone element with theoretical analysis, and concluded that the bond-link element was not well suited to model non-constant slip curves and bond-zone element could give better approximations of nonlinear slip curves with few elements.

With the development of experimental method, accurate local bond slip models were proposed for both monotonic and cyclic behaviours. Many researchers included the nonlinear behaviour into bond zone element. Some researchers (Ayoub and Filippou, 1999, Monti et al, 1997a and Monti, et al, 1997b) developed truss element with bond slip, and other researchers (Spacone and Limkatanyu, 2000, Limkatanyu and Spacone, 2002 and Monti and Spacone, 2000) developed beam element with bond slip.

The problem solved by Ayoub and Filippou (1999) is taken an example to illustrate the method in developing the element with bond slip. The developed truss element

with slip is to analyse bond behaviour of an anchored reinforcing bar as shown in Figure 2-12.

Governing equations include equilibrium equations, compatibility equations and constitutive laws. In this case, deformation of concrete is so small that it was neglected in the model.

Equilibrium: $\sigma_{,x} = \frac{4}{d_b} q$ (2-22)

Compatibility: $u_{,x} = \varepsilon$ (2-23)

Stress-strain relationship: $\sigma = \sigma(\varepsilon)$ (2-24)

Bond stress-slip relationship: $q = q(u)$ (2-25)

Displacement field $u(x) = a(x)u$ (2-26)

where $a(x)$ = displacement interpolation functions

The equilibrium equation is written in weighted integral form by invoking the principle of virtual displacements:

$$\int_0^L \delta u^T(x)[\sigma_{,x}^i(x) - \frac{4}{d_b} q^i(x)]dx = 0 \quad (2\text{-}27)$$

where δu = the virtual displacements in the role of a weight function.

Through integration, Eq. (2-27) can be simplified,

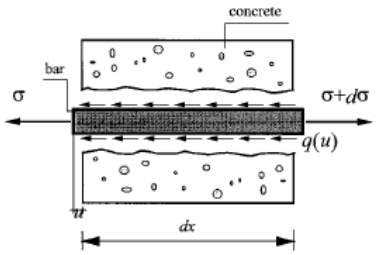

Figure 2-12 Anchored reinforcing bar problems in seismic analysis: Boundary conditions and infinitesimal segment of anchored reinforcing bar (Ayoub and Filippou, 1999)

$$(K_s^{i-1} + K_b^{i-1})\Delta u^i = P - Q_s^{i-1} - Q_b^{i-1} \tag{2-28}$$

where

$$K_s^{i-1} = \int_0^L a_{,x}^T(x) k_s^{i-1}(x) a_{,x}(x) dx$$

$$K_b^{i-1} = \int_0^L a^T(x) \frac{4}{d_b} k_b^{i-1}(x) a(x) dx$$

$$Q_s^{i-1} = \int_0^L a_{,x}^T(x) \sigma^{i-1}(x) dx$$

$$Q_b^{i-1} = \int_0^L a^T(x) \frac{4}{d_b} q_b^{i-1}(x) dx$$

$$k_s^{i-1} = \frac{\sigma^i(x) - \sigma^{i-1}(x)}{\Delta\varepsilon^i}$$

$$k_b^{i-1} = \frac{q^i(x) - q^{i-1}(x)}{\Delta u^i}$$

However, in the analysis of beam-column joint subjected to lateral loads, a panel element with bond slip is required and needs to be developed. Moreover, the deformation of concrete in the beam-column joints can not be neglected.

2.6 Constitutive model of bond

2.6.1 Mechanism of bond

Bond between concrete and reinforcement is a complex phenomenon which allows longitudinal forces to be transferred from the reinforcement to the surrounding concrete in reinforced concrete structures. Due to force transfer, the shear stress in reinforcing bars changes along their length, as does the stress in the concrete. Wherever steel strains differ from concrete strains, a relative displacement between the steel and the concrete i.e. slip does occur, but this lack of compliance is also the effect of the highly-localized strains in the concrete layer closest to the reinforcement (interface).

To understand this phenomenon, the mechanism of microstructure in interface is

investigated.

The force transfer is a combination of resistance due to adhesion (V_a), mechanics anchorage due to bearing of the lugs (V_b), and frictional resistance (V_f) shown in Figure 2-13. Adhesion is related to the shear strength of the steel-concrete interface, and is a result primarily of chemical bonding. Bearing forces perpendicular to the lug face arise as the bar is loaded and tries to slide. These bearing forces, in turn, give rise to frictional forces along the bar-concrete interface. The latter forces are

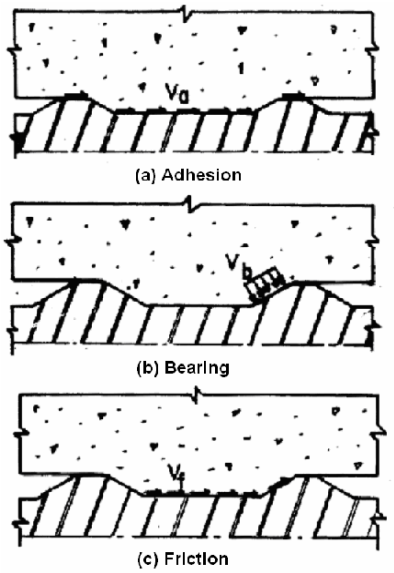

Figure 2-13 Three components of bond resistance

(ACI 408.2R-92, 1992)

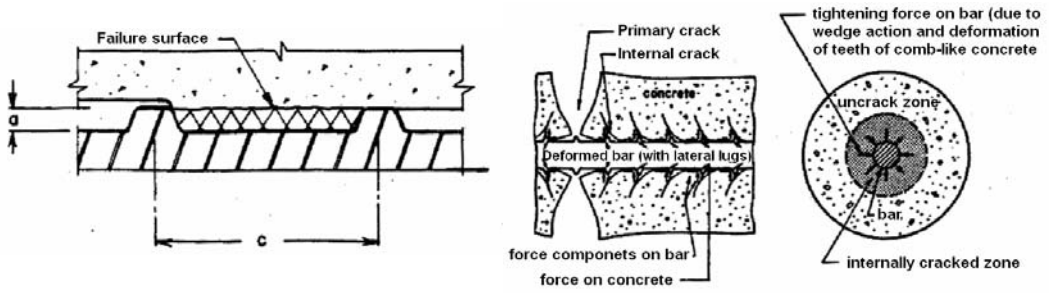

(a) Pull-out failure (b) Splitting failure

Figure 2-14 Two failure modes

(ACI 408.2R-92, 1992)

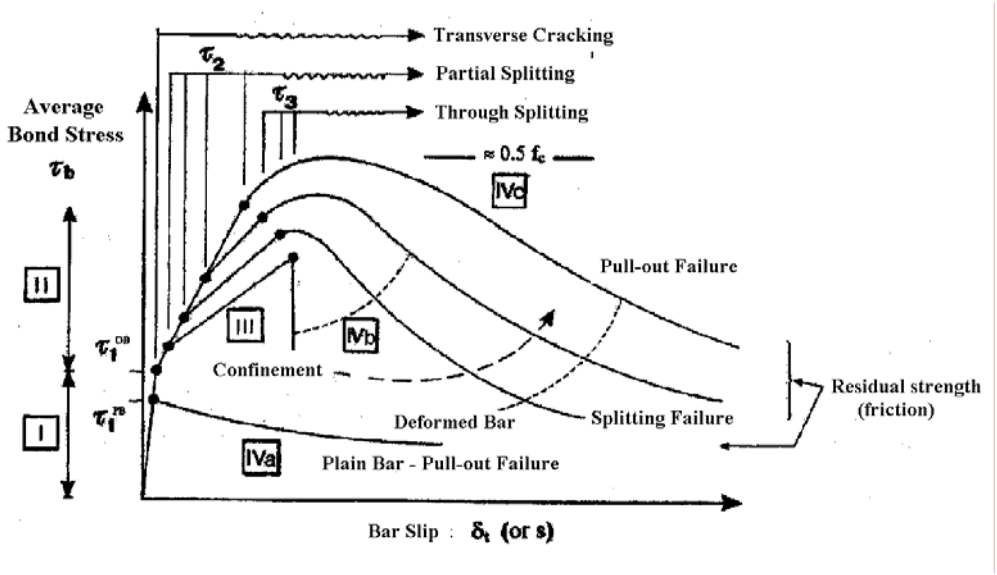

Figure 2-15 Local bond stress-slip model

(Comite euro-international du beton, 1996)

important component when failure is governed by splitting.

The first type of failure mode (Figure 2-14(a)) is a direct pullout of the bar, which occurs when sufficient confinement is provided to the bar. The concrete surrounding the bar immediately fails due to the shearing of the concrete between the lugs. The second type of failure mode (Figure 2-14(b)) is a splitting of the concrete cover when the cover or confinement is insufficient.

The resistant mechanisms upon which the steel-to-concrete bond is based are already well-known, the interaction between the concrete and a bar subjected to a pull-out force is characterized by four different stages by CEB (1996) as shown in Figure 2-15.

Stage Ⅰ (uncracked concrete): for low bond-stress values, $\tau \le \tau_1 = (0.2 - 0.8) f_{ct}$, bond efficiency is assured mostly by chemical adhesion, and no bar slip occurs, but highly localized stresses arise close to lug tips. Chemical adhesion is also accompanied by the micromechanical interaction associated with microscopically rough steel surface, but on the whole chemical and physical adhesion plays a minor role, as confirmed by the low bond performances of plain bars, where chemical

adhesion and microinterlocking are soon followed by the sliding of the bars.

Stage Ⅱ (first cracking): for high bond stress values ($\tau > \tau_1$), the chemical adhesion breaks down; in deformed bars the lugs induce large stresses in the concrete and transverse microcracks originated at the tips of the lug allowing the bar to slip, but the wedging action of the lugs remains limited and there is no concrete splitting

StageⅢ: for still higher bond stress value $\tau > (1-3) f_{ct}$, the longitudinal cracks (splitting crack) spread radically, owing to the wedging action which is enhanced by the crushed concrete stuck to the front of the lugs. The outward component of the pressure is resisted by the hoop stresses in the surrounding concrete; as a consequence, the surrounding concrete exerts confinement action on the bar, and bond strength and stiffness are assured mostly by the interlocking among the reinforcement, the concrete struts radiating from the bar and the splitting reaches the outer surface of the concrete member. Afterwards, a more or less sudden failure occurs depending on the transverse confinement. However, in relatively long anchorage with moderate confinement, a pullout failure usually occurs even after partial splitting, owing to the simultaneous presence of different stages along the bonded length. Hence, bond failure may be defined as a “splitting-induced pull-out failure”. In the case of heavy transverse reinforcement or large concrete cover partial splitting is prevented by their confining action and concrete splitting remains limited to a cracked core around the bar

StageⅣa: in plain concrete bars this stage immediately follows the breakage of adhesion bond; force transfer is provided by friction and strongly affected by the transverse pressure; concrete shrinkage and bar roughness favour friction, while interface wear long the sliding plane reduces the radial compressive stresses, and in the end the bond stress is also reduced.

StageⅣb: in the case of deformed bars confined by light-to-medium transverse reinforcement, the longitudinal cracks (splitting cracks) break out through the whole cover and bar spacing, and the bond tends to fail abruptly. On the other hand, a

sufficient amount of transverse reinforcement can assure bond efficiency in spite of concrete splitting, because of the confinement action developed by the reinforcement.

StageⅣc: in the case of deformed bars confined by heavy transverse reinforcement, partial splitting does not occur and bond failure is caused by bar pull-out. The force transfer mechanism changes from rib bearing to friction, and shear resistance of the keys can be considered as a criterion for this transition.

ACI 408 committee (1992) listed 12 mains factors affecting the bond performance. They are: concrete compression strength, cover, bar size, anchorage length, rib geometry, steel yield strength, amount and distribution of transverse steel, casting position, vibration and revibration, strain (or stress) range, type and rate of loading, temperature and surface condition.

Comite euro-international du beton (1996) classified them into four types: geometry and stress level of the reinforcing unit, concrete quality and state of stress, technological aspects and environmental effects and load-time history.

2.6.2 Terminology of local bond model

According to ACI committee 408 (1992), “bond stress” refers to the stresses along the bar-concrete interface which modify the stresses along the length of the bar by transferring load between bar and surrounding concrete. The difference in tensile force between two sections along a member ΔF is given by Eq. (2-29), as indicated in Figure 2-16

$$\Delta F = T_1 - T_2 \tag{2-29}$$

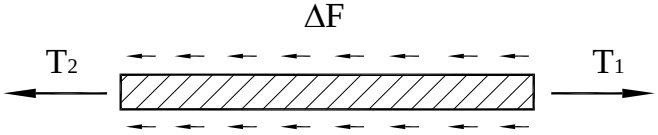

Figure 2-16 Equilibrium forces on free body of reinforcement

Bond stress is defined as a shear force per unit area of bar between two sections along the bar. It is given by:

$$\tau_b = \frac{q}{\sum o} = \frac{\Delta F}{\Delta L \sum o} = \frac{\Delta f_s (\pi d_d^2 / 4)}{\Delta L (\pi d_b)} = \frac{d_b \Delta f_s}{4 \Delta L} \tag{2-30}$$

where $q =$ change of bar force per unit length of bar

$\sum o =$ nominal perimeter of the bar

$d_b =$ nominal diameter of the bar

$\Delta f =$ change of steel over length ΔL

$A_s =$ area of bar

$\Delta L =$ length of bar over which bond stress is computed

The definition of local slip is originally given as the relative displacement between the bar and the surrounding concrete. The displacement of surrounding concrete is difficult to attain in experiments. Tassios and Yannopoulos (1981) specified the displacement of concrete as mean displacement at the cross section. Okamura and Maekawa (1991) defined the slip as relative displacement from a fixed point in concrete. In pull-out test, the local slip is obtained by taking the summation of the integration of strains from the free-end. In axial tension tests, the local slip is obtained by investigating the strains from the zero-slip point to the point concerned.

2.6.3 Monotonic local bond model

The monotonic local model is based on the assumption that the relationship between local bond stress and local slip is uniquely given for any loading and for any position along the reinforcing bars. Some researchers (Tassios and Yannopoulos, 1981 and Jiang et al, 1984) doubted if there exists such a unique curve. Jiang, et al (1984) investigated into three types of specimens and drew a conclusion that the relationship between the bond stress and slip at the steel-concrete interface is not

unique but varied from location to location. Their conclusion should be investigated more due to two reasons. First their experimental data are too focused on local strain, which is much affected by micro-cracks. Many models described here is bar-scale model, not rib-scale model. Second, the bond stress is not only a function of bond slip, but also a function of bar stress state. The factor of reinforcement strain reviewed by ACI 408 committee (1992) was included in the model of Okamura and Maekawa (1991).

Nowadays, it is generally accepted by most researchers that there exists such a unique curve of bond stress and bond slip. Several models of relationship of bond stress and bond slip (Noguchi and Naganuma 1984, Ueda et al, 1986, Eligehausen et al, 1983) have been proposed. Most of the proposed models can describe the trends: bond stress increases with increment of slip initially and after a certain value, bond stress would drop due to loss of bearing resistance and the initial stiffness of

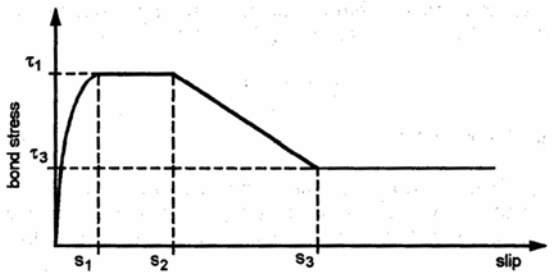

Figure 2-17 Analytical model for local bond stress-slip relationship (Eligehausen et al, 1983)

Table 2-1 Characteristic values of Eligehausen's model

	s_1	s_2	s_3	τ_1	τ_3	α
	[mm]	[mm]	[mm]	[MPa]	[MPa]	
Tension	1.00	3.00	10.50	13.50	5.00	0.4
Compression	1.00	3.00	10.50	13.50	5.00	0.4

Table 2-2 Characteristic values of CEB-FIP Model Code

	s_1 [mm]	s_2 [mm]	s_3 [mm]	τ_1 [MPa]	τ_3 [MPa]	α
Confined concrete	1.00	3.00	Clear rib spacing	$2.5\sqrt{f_{ck}}$	$\sqrt{f_{ck}}$	0.4
Unconfined concrete	0.60	0.60	10	$2.0\sqrt{f_{ck}}$	$0.3\sqrt{f_{ck}}$	0.4

bond stress-slip curve was quite large and gradually would drop due to loss of chemical adhesion. These trends agree well with mechanism of bond (Figure 2-15).

One of the widely accepted local bond stress-slip model was proposed by Eligehausen et al (1983) as shown in Figure 2-17.

Ascending part can be expressed as in Eq. (2-18). Characteristic values of monotonic envelope of the model are described in Table 2-1.

$$\tau = \tau_1 \left(\frac{s}{s_1} \right)^{\alpha} \qquad 0 \le s \le s_1 \tag{2-31}$$

Considering the influencing factors of concrete strength and diameter of reinforcement, Soroushian et al (1988 and 1991) modified peak value of Eligehausen's model.

$$\tau_1 = (20 - d_b / 4)\sqrt{f_c^{'} / 30} \tag{2-32}$$

CEB-FIP Model Code (1993) developed two bond stress-slip curves for different confinement. The model still takes the form of Eligehausen's model and accepted characteristic values are given in Table 2-2.

Okamura and Maekawa (1991) developed a steel strain dependent bond model by considering the influencing factors of steel strain and it is expressed as

$$\tau = f_c \frac{0.73\left[\ln\left(1 + 5000 s / d_b\right)\right]^3}{1 + \varepsilon_s 10^5} \tag{2-33}$$

2.6.4 Cyclic local bond model

Eligehausen's cyclic model (1983) is introduced here. In Figure 2-18, typical branch is described.

Branches a and b describe the positive and negative monotonic envelope. The same bond stress-slip relation is assumed regardless of whether bar is pulled or pushed. Branch c describes the unloading branch. When the load is reversed at some slip value, unloading takes place along a steep straight line until friction bond resistance is reached. The slope of unloading branch is taken as $K = 180N/mm^3$. Branch d describes the reloading branch. The reloading curve is described by a fourth degree polynomial starting from the frictional bond resistance value and leading to the intersection between the reduced envelope and previous unloading curve. For simplicity, the reloading curve is taken as a steep line after friction part before it reaches the envelope curve. The slope of reloading steep line is taken the same as reloading stiffness, that is $K = 180N/mm^3$. Branch e describes the reduced bond stress-slip envelope. Reduced envelopes are obtained from monotonic envelopes by

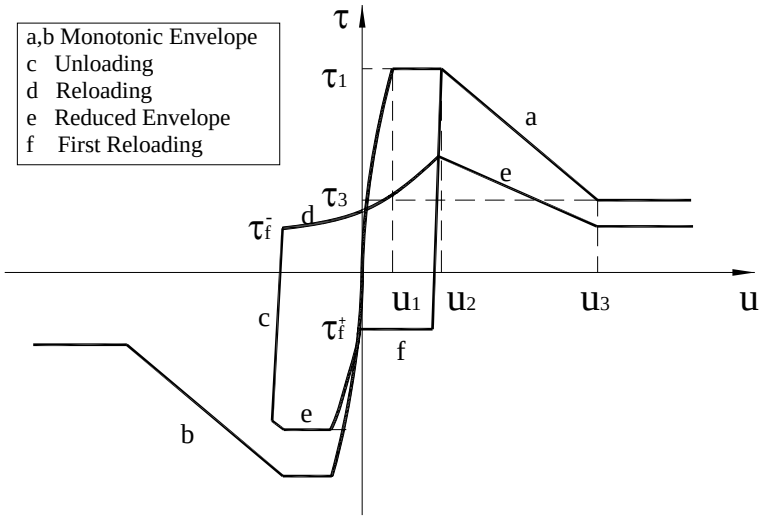

Figure 2-18 Cyclic rules for bond stress-bond slip

(Eligehausen et al, 1983)

reducing characteristic bond stress τ_1 and τ_3 through reduction factors, which are formulated as a function of one parameter called the "damage factor", d. For the case of no damage, d is taken as 0, and the reloading branch reaches the monotonic envelope. For the case of full damage, d is taken as 1, and bond is completely destroyed. The characteristic of monotonic envelope seems to depend on the damage experience by concrete, particularly, the length of concrete key between the lugs of bar that has been sheared off. Thus, the damage factor is expressed in terms of dimensionless dissipated energy factor E / E_0.

The reduced characteristic bond $\tau_1(N)$ can be expressed as,

$$\tau_1(N) = \tau_1 \cdot (1-d) \tag{2-34}$$

$$d = 1 - e^{-1.2(E/E_0)^{1.1}} \tag{2-35}$$

where

E is the total dissipated energy,

E_0 is the energy absorbed under monotonically increasing slip up to the value u_3 and is used as a normalization parameter.

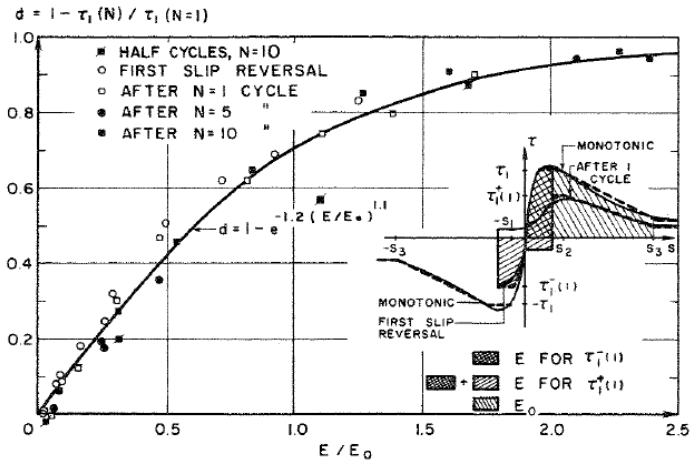

Figure 2-19 Sketch to calculate absorbed energy

(Eligehausen et al, 1983)

The reduced characteristic bond $\tau_3(N)$ can be expressed as

$$\tau_3(N) = \gamma \cdot \tau_3(N=1) \tag{2-36}$$

$$\gamma = 1 - \frac{d}{2-d} \tag{2-37}$$

Branch f describes the friction branch. When the load is reversed for the first time, monotonic loading curve goes directly after unloading curve.

The friction value is determined by historical maximum bond slip. It can be calculated through Eq. (2-38) and (2-39)

$$\frac{\tau_f^-}{\tau_3} = \begin{cases} \frac{0.9}{0.5} \cdot \frac{Slip_{Max}^+}{u_3} + 0.1 & Slip_{Max}^+ \le 0.5u_3 \\ 1 & Slip_{Max}^+ > 0.5u_3 \end{cases} \tag{2-38}$$

$$\frac{\tau_f^+}{\tau_3} = \begin{cases} \frac{0.9}{0.5} \cdot \frac{Slip_{Max}^-}{u_3} + 0.1 & Slip_{Max}^- \le 0.5u_3 \\ 1 & Slip_{Max}^- > 0.5u_3 \end{cases} \tag{2-39}$$

2.7 Modelling of beam-column joints in simple behaviour model

To predict the strength and deformation of joints, previous researchers used the flow of force based on experimental observation or equilibrium equations of joints, and developed behaviour models. Two popular behaviour models are strut-and-tie model and two-dimensional panel model.

1. Strut-and-tie model

Through experimental observation, after cracks occur, concrete between parallel cracks functions as the strut to carry compression force, and reinforcement functions as the tie to carry tension force. This leads to strut-and-tie model.

Lay-out of concrete struts depends on location and angle of cracks, which are unknown at the beginning. Therefore lay-out of concrete strut depends mostly on the intuitions and judgments of designers.

Hwang and Lee (1999 and 2000) combined three types of strut lay-out together and proposed a new strut-and-tie model for predicting shear strength. The analytical

model bears the load through three mechanisms as shown in Figure 2-20. Diagonal mechanism only considers the concrete contribution, while horizontal and vertical mechanisms consider the contribution of both concrete and reinforcement. When simplifications (Zhang and Jirsa, 1982) are introduced, the dimension of strut and tie can be determined. When the proportion of the three mechanisms (Schafer, 1996) is known, the force on concrete and reinforcement can be calculated.

$$D = \frac{-1}{\cos\theta} \cdot \frac{R_d}{(R_d + R_h + R_v)} \cdot V_{jh} \tag{2-40}$$

$$F_h = \frac{R_h}{(R_d + R_h + R_v)} \cdot V_{jh} \tag{2-41}$$

$$F_v = \frac{1}{\cos\theta} \cdot \frac{R_v}{(R_d + R_h + R_v)} \cdot V_{jh} \tag{2-42}$$

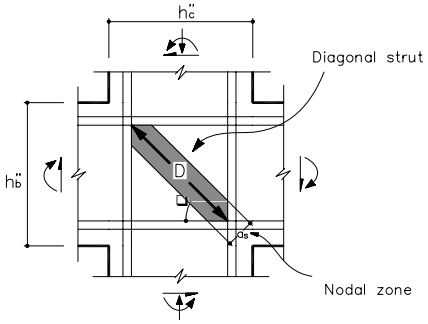

(a) Diagonal mechanism

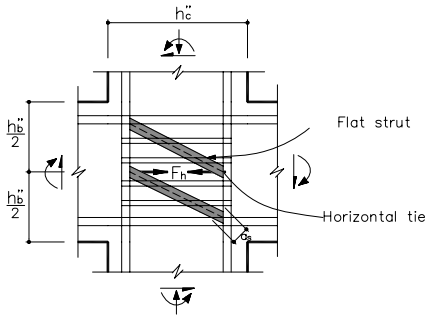

(b) Horizontal mechanism

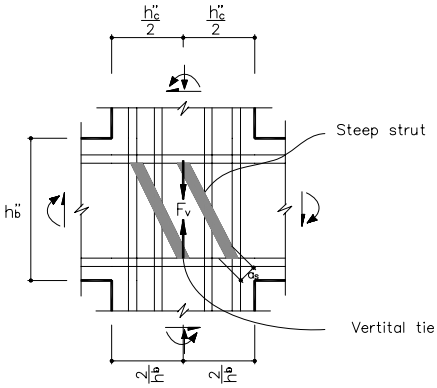

(c) Vertical mechanism

Figure 2-20 Joint-resisting mechanisms

(Hwang and Lee, 2000)

$$\sigma_{d,\max} = \frac{1}{A_{str}}\left[D - \frac{\cos(\theta - \tan^{-1}(\frac{h_b^{"}}{2h_c^{"}}))}{\cos(\tan^{-1}(\frac{h_b^{"}}{2h_c^{"}})} F_h - \frac{\cos(\tan^{-1}(\frac{2h_b^{"}}{h_c^{"}}) - \theta)}{\sin(\tan^{-1}(\frac{2h_b^{"}}{h_c^{"}})} F_v \right] \tag{2-43}$$

where D is the compressive force in the diagonal strut

F_h is the tension force in the horizontal tie

F_v is the tension force in the vertical tie

$\sigma_{d,\max}$ is the maximum compressive stress

R_d, R_h, R_v is the ratio of the joint shear resisted by the diagonal, horizontal and vertical mechanism

A_{str} is the effective area of diagonal strut

Through Eqs. (2-40) to (2-43), the stress in the reinforcement and concrete can be calculated, thus failure mode (concrete spalling or steel yielding) can be judged and shear strength can be determined.

According to bi-axial constitutive laws proposed by Zhang and Hsu (1998), compressive strength will drop due to crack strain in the other direction. Therefore, compatibility equation Eq. (2-44) is needed to determine crack strain, and further decide the reduced compressive strength.

$$\varepsilon_r + \varepsilon_d = \varepsilon_h + \varepsilon_v \tag{2-44}$$

where

ε_r is the crack strain to be calculated

ε_d is the diagonal compressive strain, depending on compressive stress

ε_h is the horizontal strain, depending on tensile stress of horizontal tie

ε_h is the vertical strain, depending on tensile stress of vertical tie

2. Two-dimensional panel model

Compared with strut-and-tie model, the direction of principal strain in

two-dimensional panel model is not assumed at the beginning, but to be obtained in the calculation. This method will avoid ambiguous lay-out of strut. To solve the problem, compatibility equations need to be added to the equations.

In 1992, Pantazopoulou and Bonacci developed a two-dimensional panel model. In this model, the joint is assumed as uniformly distributed compression field panel. In each section, normal and shear forces are both distributed uniformly as shown in Figure 2-21.

The failure of joint can either be the yielding of reinforcement in two directions or yielding in one direction with crushing in concrete.

For the first case, the strength of joint can be expressed as

$$v_n = \sqrt{\left\{\rho_t f_y + \frac{N_h}{bh}\right\}\left\{\rho_l f_y + \frac{N_v}{bd_w}\right\}} \tag{2-45}$$

where

ρ_t, ρ_l is the vertical and horizontal reinforcement ratio

N_h, N_v is the horizontal and vertical axial force

d_w is the depth of the column

h is the depth of the beam

For the second case, the strength of joint can be expressed as

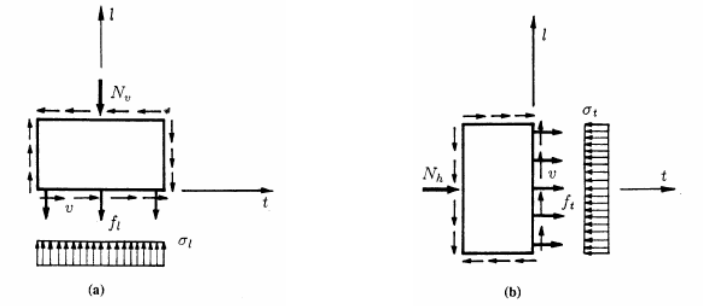

(a) Equilibrium of vertical forces (b) Equilibrium of horizontal forces

Figure 2-21 Equilibrium of forces in isolated bodies

(Pantazopoulou and Bonacci, 1992)

$$v_n = \sqrt{\left\{\left|f_c^{\max}\right| - \rho_t f_y - \frac{N_h}{bh}\right\}\left\{\rho_t f_y + \frac{N_h}{bh}\right\}} \tag{2-46}$$

where $f_c^{\max} = \lambda f_c^{'}$

$$\lambda = \frac{K}{0.8 - 0.34\varepsilon_1 / \varepsilon_0}$$

$$K = 1 + \rho_s \left| f_y / f_c^{'} \right|$$

ε_1 is the tensile strain

The deformation before the yielding of reinforcement is

$$\gamma = \frac{2}{E_s(1-\tan^2\theta)}\left[\frac{\tau}{\rho_l \rho_t}\left(\rho_l \tan^2\theta - \rho_t\right) + \left(\frac{N_v}{bd_w\rho_l} - \frac{N_h}{bh\rho_t}\right)\tan\theta\right] \tag{2-47}$$

All the behaviour models are based on equilibrium equations. These models can reflect the influence of main parameters such as strength of concrete and reinforcement, dimension of joint and ratio of reinforcement. However, due to their assumptions, behaviour model can only describe joints behaviour at certain stage only such as limit state. In addition, these models can not describe joint behaviour when the bond deteriorates.

2.8 Macro models of beam-column joints in frame analysis

Currently, there are some methods to deal with soft joint with bond slip. Ghobarah and Biddah (1999) used two rotational springs between beam and column nodes to represent the joint behaviour. D'Ambrisi and Filippou (1999) included joint behaviour in frame member element. Lowes, Mitra and Altoontash (2004) proposed a two-dimensional idealization of an interior beam-column building joint. The model includes eight bar-slip components that are intended to simulate bond slip at frame ends, one shear panel component that is intended to simulate shear behaviour of the joint core, and four interface-shear components that are intended to simulate loss of shear-transfer capacity at the joint-beam and joint-column perimeter under severe loading of the joint. Limkatanyu and Spacone (2003) proposed a joint model

comprising a beam-panel with bond interface, a column-panel with bond interface and a rigid-link member. These two panels are assumed to be independent of one another and are connected together through a rigid-link member to prevent spurious rigid body modes.

2.8.1 Macro model by Ghobarah and Biddah

In the model proposed by Ghobarah and Biddah (1999), the joint is represented by two types of rotational springs in series, one representing the joint shear deformation and the other representing the reinforcement bar bond slip. The locations of two types of springs are shown Figure 2-22 and Figure 2-23.

In the rigid joint, the joint is represented by one point, and has 3 degree-of-freedom (dof): horizontal dof, vertical dof, and beam and column ends share one rotation dof. In the soft joint, joint shear deformation can not be neglected. Therefore, the joint will have 4 degree-of-freedom with the additional one to represent joint deformation. The dof of beam and column ends are separated and related by a rotational spring as shown in Figure 2-22.

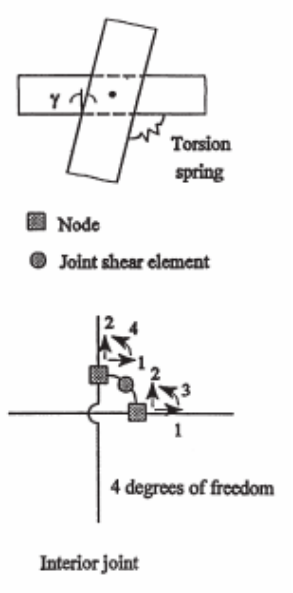

Figure 2-22 Idealization of the joint shear elements in frame analysis (Ghobarah and Biddah, 1999)

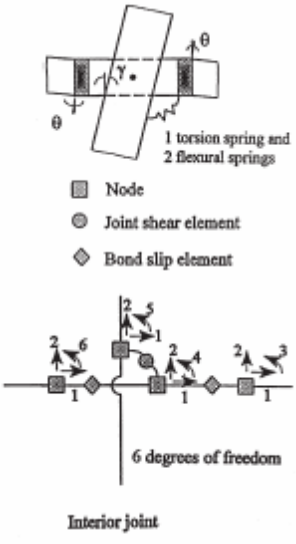

Figure 2-23 Idealization of joint shear and bond slip elements in frame analysis (Ghobarah and Biddah, 1999)

Bond slip effect causes beam fixed-end rotation, so bond slip element is represented by a torsional spring between beam and joint. Under reverse load, beam fixed-end rotation can occur in either side of the beams or columns, so three springs are needed in interior joint to represent the relative fixed end rotation, as indicated in Figure 2-23. When the effects of joint shear behaviour and bond slip are both included, joint element will have 6 dof for interior joint.

In the model proposed by Ghobarah and Biddah (1999), the hysteresis model for moment-rotation relationship of the joint is proposed based on the softened-truss model (Hsu, 1998). The joint is simplified into a panel subjected to shear force V_{jh} and axial force P_c (Figure 2-24). From softened-truss model, shear stress-shear strain relationship is obtained. From the Figure 2-24, the relationship between shear force and transferred moment can be established.

$$\sum M_b = 2M_b = \frac{V_{jh}}{\frac{1}{jd} - \frac{1}{L_c(1-\frac{h_c}{L_d})}} \tag{2-48}$$

where $\sum M_b$ = total beam moment to be transferred to the column by joint shear

jd = the moment arm of the beam

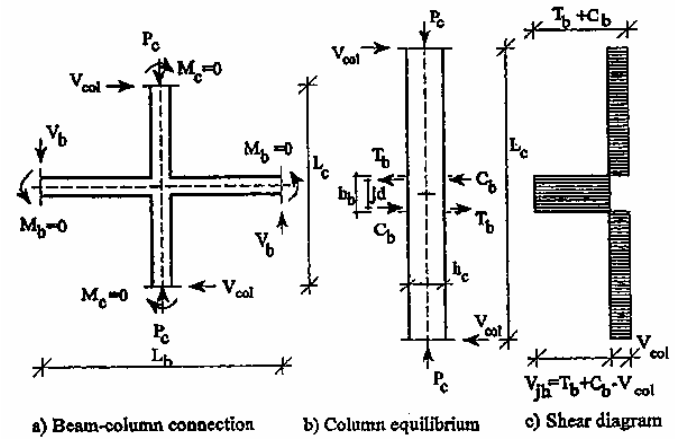

Figure 2-24 Equilibrium of interior beam-column joint

(Biddah and Ghobarah, 1999)

L_c = the length along the column between contra flexure point

L_b = the length along the beam between contra flexure point

h_c = the height of the column

At last, the model for moment-rotation relationship is established.

In the model proposed by Ghobarah and Biddah (1999), bond slip effect is present through one rotational spring. The rotation caused by bond slip can be expressed as

$$\theta = \frac{2\Delta_s}{d - d'} \tag{2-49}$$

where

Δ_s = bond slip at beam-joint interface

$d - d'$ = effective depth of the beam

Neglecting the concrete strain along the bar in the joint, the slippage Δ_s at the beam-column interface is given by the integration of the steel strain distribution over a length L_s, where L_s represents the distance from the beam-column interface to the point at which the bar begins to slip (Figure 2-25). Distribution of reinforcement stress is assumed to be linear in elastic phase, and bilinear in post-yield phase.

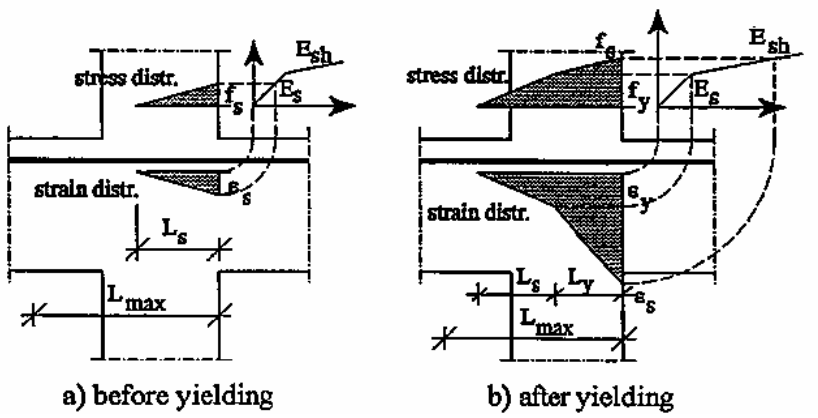

Figure 2-25 Stress and strain distribution assumption in the joint

(Biddah and Ghobarah, 1999)

2.8.2 Macro model by D'Ambrisi and Filippou

In the model proposed by D'Ambrisi and Filippou (1999), joint behaviour is included in frame member element. A reinforced concrete member is decomposed into sub-elements as shown in Figure 2-26(a). Each sub-element describes a different deformation mechanism that affects the hysteresis behaviour of critical region in RC elements.

The sub-elements used in this study as shown in Figure 2-26(a) are: (1) an elastic sub-element; (2) a spread plastic sub-element; (3) an interface bond-slip sub-element; and (4) a shear sub-element.

Bond slip effect is included through two rotational springs in bond-slip sub-element (Figure 2-26(b)), while joint shear behaviour is neglected in their model. In the model proposed by Ambrisi and Filippou (1999), bond slip model proposed by Filippou, Popov and Bertero (1983) was used.

Fixed-end rotations were computed from the pull-out of reinforcing bars using

$$\theta = \frac{u^l - u^u}{d} \tag{2-50}$$

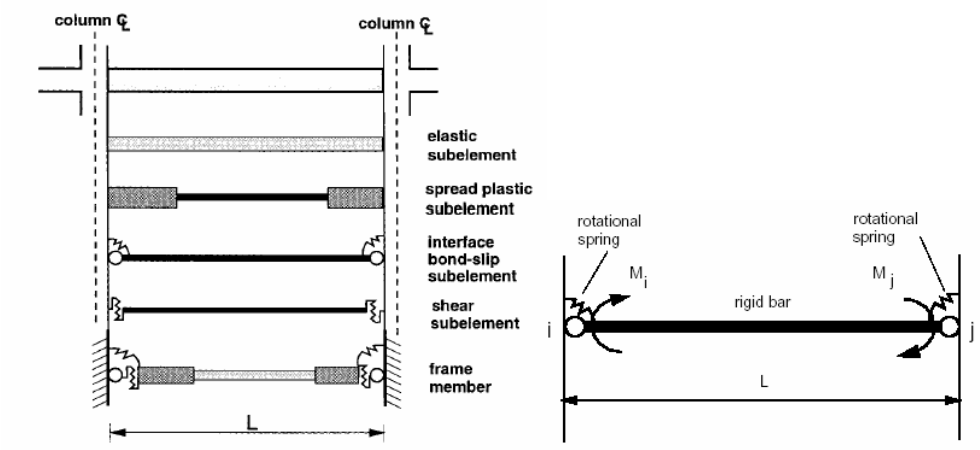

(a) Composition of superelement (b) Bond-slip subelement

Figure 2-26 Decomposition of RC frame member into different sub-elements (D'Ambrisi and Filippou, 1999)

where u^l = displacement of reinforcement at the lower layer

u^u = displacement of reinforcement at the upper layer

d= displacement between reinforcing layers

Displacement of reinforcement at the lower layer or upper layer can be calculated through equilibrium equations, compatibility equation and constitutive law.

$$A\frac{d\sigma_s}{dx} = q(u)\sum_0 \tag{2-51}$$

$$\varepsilon_s - \varepsilon_c = \frac{du}{dx} \tag{2-52}$$

$$\varepsilon_s = f(\sigma_s) \tag{2-53}$$

where A = reinforcing bar area

u = relative slip of steel versus surrounding concrete

q = bond stress

$\sum_0$ = reinforcing bar circumstance

2.8.3 Macro model by Lowes, Mitra and Altoontash

Lowes, Mitra and Altoontash (2004) proposed a two-dimensional idealization of an interior beam-column joint. The model includes eight bar-slip components that are intended to simulate stiffness and strength loss associated with bond-strength deterioration for beam and column longitudinal reinforcement embedded in the joint core, one shear panel component that is intended to simulate strength and stiffness loss associated with shear failure of the joint core, and four interface-shear components that are intended to simulate loss of shear-transfer capacity at the joint-beam and joint-column perimeter under severe loading of the joint. The joint model is depicted in Figure 2-27.

Unlike the typical displacement-based element formulation in which the displacement of the external nodes defines uniquely the element deformation state, the deformation state of the beam-column joint element is defined by the

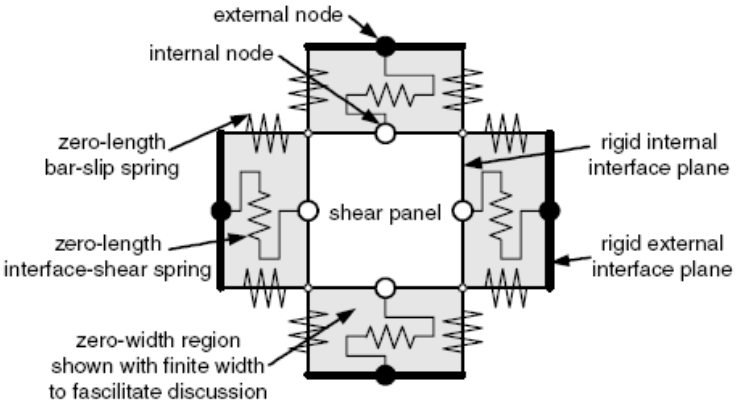

Figure 2-27 Component of the beam-column joint model

(Lowes, Mitra and Altoontash, 2004)

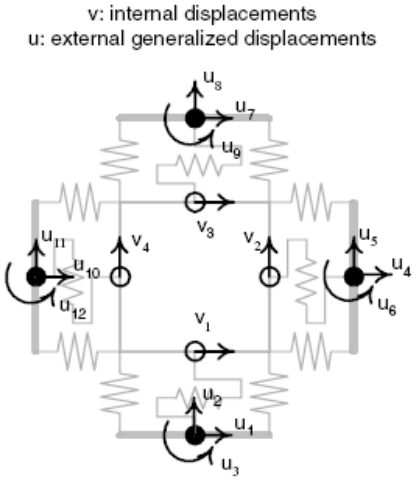

Figure 2-28 Internal and external displacement and rotations

(Lowes, Mitra and Altoontash, 2004)

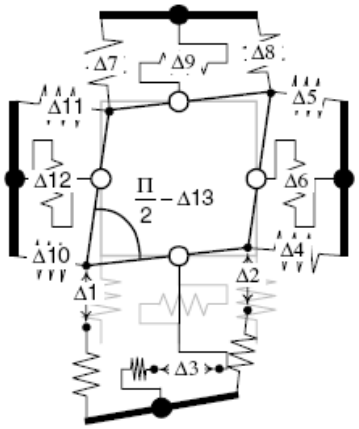

Figure 2-29 Component deformations of joint element

(Lowes, Mitra and Altoontash, 2004)

displacement of the external nodes and the four internal nodes (Figure 2-28). These displacement defines the deformation of the 12 uniaxial spring components and the single two-dimensional shear-panel component that compose the beam-column joint model. The shear-panel component is assumed to deform only in shear and thus to have a one-dimensional load-deformation response. Figure 2-29 shows the component deformations.

The deformation components of the joint element are defined as a function of the external and internal nodal displacements in (2-54):

$$\begin{Bmatrix} \Delta_1 \\ \Delta_2 \\ \Delta_3 \\ \Delta_4 \\ \Delta_5 \\ \Delta_6 \\ \Delta_7 \\ \Delta_8 \\ \Delta_9 \\ \Delta_{10} \\ \Delta_{11} \\ \Delta_{12} \\ \Delta_{13} \end{Bmatrix} = \begin{bmatrix} 0 & -1 & \frac{w}{2} & 0 & 0 & 0 & 0 & 0 & 0 & 0 & 0 & 0 & 0 & 0 & 0 & 1 \\ 0 & -1 & -\frac{w}{2} & 0 & 0 & 0 & 0 & 0 & 0 & 0 & 0 & 0 & 0 & 1 & 0 & 0 \\ 1 & 0 & 0 & 0 & 0 & 0 & 0 & 0 & 0 & 0 & 0 & 0 & -1 & 0 & 0 & 0 \\ 0 & 0 & 0 & 1 & 0 & \frac{h}{2} & 0 & 0 & 0 & 0 & 0 & 0 & -1 & 0 & 0 & 0 \\ 0 & 0 & 0 & 1 & 0 & -\frac{h}{2} & 0 & 0 & 0 & 0 & 0 & 0 & 0 & 0 & -1 & 0 \\ 0 & 0 & 0 & 0 & 1 & 0 & 0 & 0 & 0 & 0 & 0 & 0 & 0 & -1 & 0 & 0 \\ 0 & 0 & 0 & 0 & 0 & 0 & 0 & 1 & -\frac{w}{2} & 0 & 0 & 0 & 0 & 0 & 0 & -1 \\ 0 & 0 & 0 & 0 & 0 & 0 & 0 & 1 & \frac{w}{2} & 0 & 0 & 0 & 0 & -1 & 0 & 0 \\ 0 & 0 & 0 & 0 & 0 & 0 & 0 & 0 & 0 & 0 & 0 & 0 & 0 & 0 & -1 & 0 \\ 0 & 0 & 0 & 0 & 0 & 0 & 0 & 0 & 0 & -1 & 0 & -\frac{h}{2} & 1 & 0 & 0 & 0 \\ 0 & 0 & 0 & 0 & 0 & 0 & 0 & 0 & 0 & -1 & 0 & \frac{h}{2} & 0 & 0 & 1 & 0 \\ 0 & 0 & 0 & 0 & 0 & 0 & 0 & 0 & 0 & 0 & 1 & 0 & 0 & 0 & 0 & -1 \\ 0 & 0 & 0 & 0 & 0 & 0 & 0 & 0 & 0 & 0 & 0 & 0 & -\frac{1}{h} & \frac{1}{w} & \frac{1}{h} & -\frac{1}{w} \end{bmatrix} \begin{Bmatrix} u_1 \\ u_2 \\ u_3 \\ u_4 \\ u_5 \\ u_6 \\ u_7 \\ u_8 \\ u_9 \\ u_{10} \\ u_{11} \\ u_{12} \\ v_1 \\ v_2 \\ v_3 \\ v_4 \end{Bmatrix} \tag{2-54}$$

Furthermore, Eq. (2-54) can written as

$$\Delta = A \cdot \begin{Bmatrix} u \\ v \end{Bmatrix} \tag{2-55}$$

The element tangent matrix is defined as

$$K \cdot \partial U = K \cdot \begin{Bmatrix} \partial u \\ \partial v \end{Bmatrix} = \begin{bmatrix} K_{ee} & K_{ei} \\ K_{ie} & K_{ii} \end{bmatrix} \cdot \begin{Bmatrix} \partial u \\ \partial v \end{Bmatrix} = \begin{Bmatrix} \partial F \\ \partial \Phi \end{Bmatrix} = \begin{Bmatrix} \partial R \\ 0 \end{Bmatrix} \tag{2-56}$$

where

$$K = A^T \cdot k \cdot A$$

k is the matrix of component tangents

K_{ii} is the stiffness matrix of internal nodes

K_{ee} is the stiffness matrix of external nodes

K_{ie} is the stiffness matrix between internal nodes and external nodes

through static condensation of the global element tangent matrix, the element tangent is written as

$$\frac{\partial R}{\partial u} = K_{ee} - K_{ei} \cdot \left[K_{ii}\right]^{-1} \cdot K_{ie} \tag{2-57}$$

Though the model by Lowes, Mitra and Altoontash (2004) can include both bond slip and shear behaviour into analysis, this model is weak in analyzing shear behaviour subjected to combination of shear and normal forces because shear stress is affected by shear strain only in their model. So, the effect of axial force on strength and deformation behaviour of beam-column joint can not be studied with this model.

2.8.4 Macro model by Limkatanyu and Spacone

Limkatanyu and Spacone (2003) proposed a joint model based on two-node displacement-based RC frame model with bond-interfaces proposed by themselves (Limkatanyu and Spacone, 2002). The frame model with bond-interfaces will be reviewed before introduction on their joint element. Force components and their relation can be seen in Figure 2-30.

Equilibrium equation can be written as

$$\partial_B^T D_B(x) - \partial_b^T D_b(x) - p(x) = 0 \tag{2-58}$$

where

$D_B(x) = \left\{\overline{D}(x) : \overline{\overline{D}}(x)\right\}^T$ = the element section forces,

$\overline{D}(x) = \left\{N_B(x)\, M_B(x)\right\}^T$ = the beam section forces

$\overline{\overline{D}}(x) = \left\{N_1(x) \ldots N_n(x)\right\}^T$ = the bar forces

$D_b(x) = \{D_{b1}(x) \ldots D_{bn}(x)\}^T$ = the bond section forces

∂_B and ∂_b are differential operators

Compatibility equation describes the relationship between section deformation (including beam section deformation $\varepsilon_B(x)$ $\kappa_B(x)$ and steel axial deformation $\varepsilon_1(x) \ldots \varepsilon_n(x)$) and section displacement (including beam section displacement $u_B(x)$ $v_B(x)$ and $u_1(x) \ldots u_n(x)$). It can be written as

$$\varepsilon_B(x) = du_B(x)/dx \tag{2-59}$$

$$\kappa_B(x) = d^2 v_B(x)/dx^2 \tag{2-60}$$

$$\varepsilon_i(x) = du_i(x)/dx \tag{2-61}$$

$$u_{bi}(x) = u_i(x) - u_B(x) + y_i \frac{dv_B(x)}{dx} \tag{2-62}$$

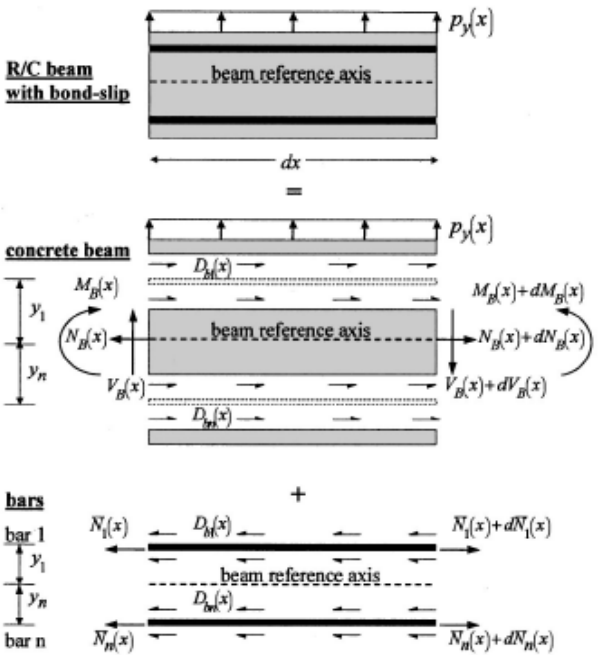

Figure 2-30 Reinforced concrete beam element with bond slip:

beam and bar components

(Limkatanyu and Spacone 2003)

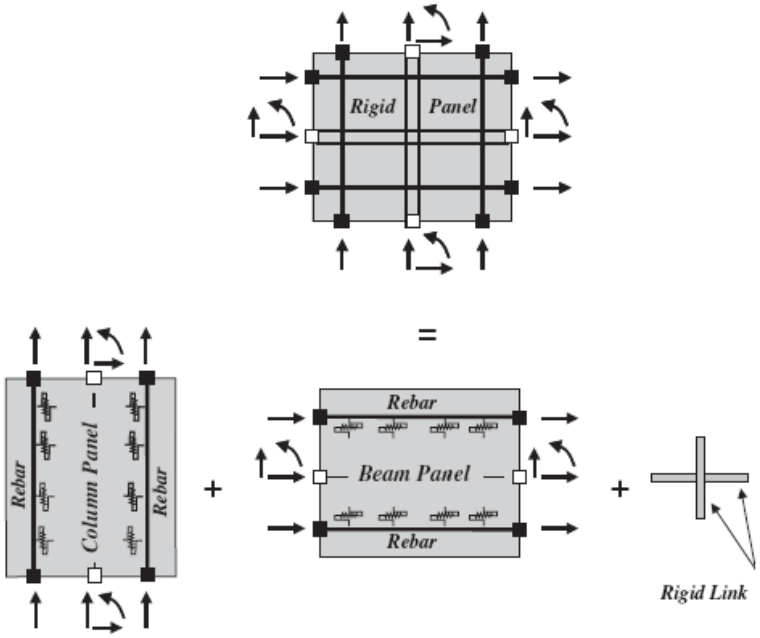

Figure 2-31 Rigid-panel joint element with bond-slip

(Limkatanyu and Spacone 2003)

With these equilibrium equations, compatibility equations and proper select constitutive laws, two-node displacement-based RC frame model with bond-interfaces can be developed.

The four-faced plane joint element with bond-slip is shown in Figure 2-31. The joint element comprises a beam-panel, a column-panel and a rigid-link member. These two panels are assumed to be independent of one another and are connected together through a rigid-link member to prevent spurious rigid body modes.

As mentioned by the authors, the proposed joint element is intended to account mostly for bond-slip effects, while softening of shear panel are not the concern in their study. This assumption makes the application of the joint element unable to be used for gravity-load-designed beam column joint.

2.9 Development of shear design equation for beam members

The method in development of shear design equation for beam members can be used in developing shear strength estimation in the joint. Ichinose (1992) illustrated

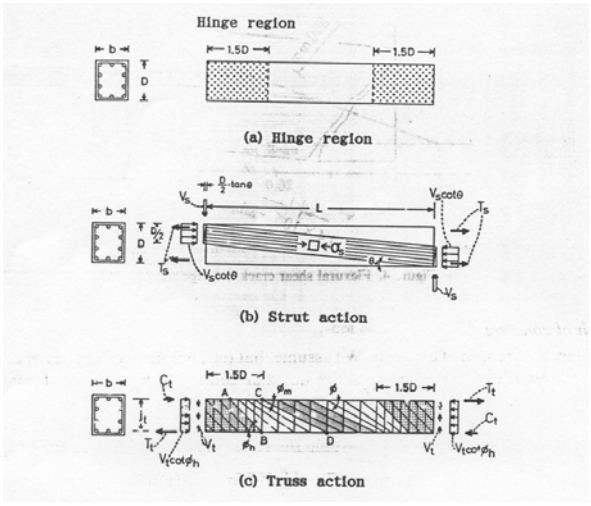

Figure 2-32 Shear resisting actions of a member with hinges at both ends (Ichinose, 1992)

the development of shear design equations for ductile beam members. In the design equations, both strut and truss action work together to take the load, and the distribution ratio between these two actions is explicitly expressed.

The member is divided into two parts, hinge region and unyielding region, as seen in Figure 2-32(a). In the two regions, the truss angle and the effective strength of concrete are different due to crack damage. Strut and truss actions in the member are illustrated in Figure 2-32 (b) and (c). Strut angle and truss angle are expressed as θ and ϕ.

Before the development of the equations, three assumptions are introduced.

Firstly, truss angle ϕ is limited at certain range to limit shear crack width (Thurlimann, 1979), and expressed as

$1 \le \cot\phi_m \le 2$ Out of hinge region

$1 \le \cot\phi_m \le \lambda \quad \lambda = \lambda(R_p)$ In hinge region (2-63)

where R_p is the hinge rotation (rad)

Secondly, effective strength of concrete is applied instead of original compressive concrete strength because of crack in orthogonal direction. Reduction factor ν is expressed in Eq. (2-64)

$$v = v_0 = 0.7 - \sigma_B / 200 \qquad \text{Out of hinge region}$$

$$\frac{v}{v_0} = \frac{v}{v_0}\left(R_p\right) \qquad \text{In hinge region} \qquad (2\text{-}64)$$

where R_p is the hinge rotation (rad)

Thirdly, the truss action always fails owing to the compressive crushing of the web concrete and/or the yielding of the web reinforcement

Finally, sum of concrete stress in truss action and strut action is limited by compressive concrete strength considering reduction due to cracks

In Figure 2-32(c) and Figure 2-33(a), the shear resisting strength in truss action can be obtained from a free body analysis in hinge region and out of hinge region separately as,

$$V_t = bj_t \rho_{wm} \sigma_{wy} \cot \phi_m \qquad (2\text{-}65)$$

$$V_t = bj_t \rho_{wh} \sigma_{wh} \cot \phi_h \qquad (2\text{-}66)$$

where

ϕ_m truss angle out of hinge region

ϕ_h truss angle in hinge region

ρ_{wm} reinforcement ration out of hinge region

ρ_{wh} reinforcement ration in hinge region

σ_{wy} steel stress out of hinge region

σ_{wh} steel stress out of hinge region

According to assumption, the truss action always fails owing to the compressive crushing of the web concrete and/or the yielding of the web reinforcement. Resisting shear strength of truss action can be calculated from Eq. (2-65).

In Figure 2-33(b), the maximum concrete stress can be obtained from a free body analysis in point C, and it is expressed in terms of stress of reinforcement in the

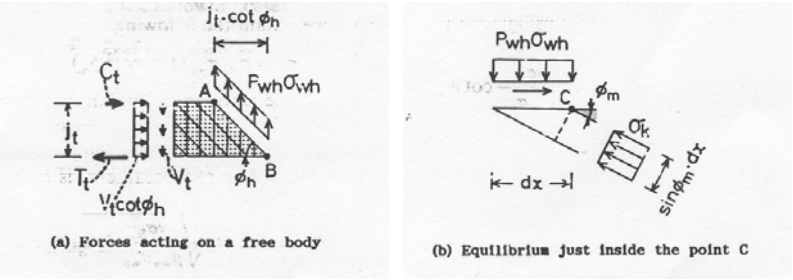

Figure 2-33 Detail of truss action

(Ichinose, 1992)

hinge region. Reinforcement in the hinge region may not yield, but the stress of reinforcement in the hinge region can be calculated from Eq. (2-65) to (2-66). Then, concrete stress σ_k can be expressed by steel stress out of hinge region.

$$\sigma_k = \frac{\rho_{wm}\sigma_{wy}\cot\phi_m\left(1+\cot^2\phi_m\right)}{\cot\phi_h} \tag{2-67}$$

The remaining of compressive concrete stress from the truss action works is strut action to resist shear loads, and it is expressed as,

$$\sigma_s = \nu\sigma_B - \sigma_k = (1-\beta)\nu\sigma_B \tag{2-68}$$

where

$$\beta = \frac{\sigma_k}{\nu\sigma_B} = \frac{\rho_{wm}\sigma_{wy}\cot\phi_m\left(1+\cot^2\phi_m\right)}{\nu\sigma_B\cot\phi_h}$$

Therefore shear resisting strength of strut action can be expressed as,

$$V_s = b(D/2)\sigma_s\tan\theta = b(D/2)(1-\beta)\nu\sigma_B\tan\theta \tag{2-69}$$

Finally, shear resisting strength is the superposition of truss and strut actions

$$V_u = V_t + V_s = bj_t\rho_{wm}\sigma_{wy}\cot\phi_m + b(D/2)(1-\beta)\nu\sigma_B\tan\theta \tag{2-70}$$

CHAPTER 3 REINFORCED CONCRETE ELEMENT WITH BOND-SLIP EFFECT

3.1 Introduction

The strength of reinforced concrete member depends on the compatibility condition of concrete and reinforcing bar to act together in resisting the external loads. The amount of force that the interface of concrete and reinforcement can transfer will affect the ultimate strength of reinforced concrete members. In cracked concrete, the residual tensile strength of concrete depends on concrete strength developed between cracks, which is related to the capacity of the interface of concrete and reinforcement to transfer the force. Several phenomena such as tension stiffening are related to bond behaviour between concrete and reinforcement. Hence, a clear understanding of bond behaviour is necessary to be able to simulate the behaviour of reinforced concrete members accurately. The bond mechanism and affecting factors have been reviewed by ACI 408.2R-92 (1992) and fib (2000), and several local bond stress-slip laws (Eligehausen et al, 1983 and Okamura and Maekawa, 1991) have been proposed.

Two different elements which include the bond-slip effect in the finite element analysis of RC structures have been reviewed in chapter 2. They are bond link element and bond zone element (contact element). Compared with bond link element, bond zone element can obtain higher accuracy with fewer elements (Keuser and Mehlhorn, 1987). Therefore, the bond zone element to describe the bond behaviour between concrete and reinforcement panels will be developed in this chapter.

Since bond zone elements connect concrete and reinforcement elements, bond zone element will have different types depending on the type of concrete and reinforcement elements. Whether concrete and reinforcement are modelled in truss elements or whether concrete and reinforcement are modelled in panel and truss

elements, different types of bond zone element should be developed to describe bond behaviour between concrete and reinforcement. Some researchers (Ayoub and Filippou, 1999, Monti et al, 1997a and Monti et al, 1997b) applied the element in the analysis of truss with bond slip. Other researchers (Spacone and Limkatanyu, 2000, Limkatanyu and Spacone, 2002 and Monti and Spacone, 2000) applied the element in the frame element with slip. However, in the analysis of beam-column joint subjected to lateral loads, a panel element with bond slip is required. So, in this chapter, a double-panel element will be developed to describe the behaviour of concrete panel, reinforcement panel and the bond-slip behaviour between the panels.

The double-panel element has 8 nodes representing concrete panel and 8 nodes representing reinforcement panel, and these 16 nodes are also used to represent the bond effect between concrete and reinforcement panels, as indicated in Figure 3-1. Crack is smeared into the concrete panel, while discrete reinforcement is smeared into reinforcement panel. Bond force around the discrete reinforcement is also smeared between concrete and reinforcement panels. Before the development of double-panel element, a simplified one dimensional double truss element will be developed first. The double truss element has 4 nodes, with 2 nodes to represent steel truss and 2 nodes to represent concrete truss and these 4 nodes are also used to

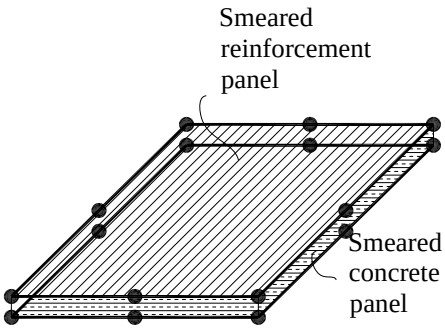

Figure 3-1 The RC panel element with bond slip

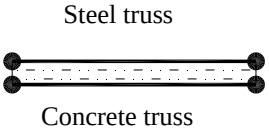

Figure 3-2 The RC truss element with bond slip

represent the bond between them, as indicated in Figure 3-2.

Suitable monotonic and cyclic local bond laws will be selected and some modifications will be carried out based on experimental data. Then, the double panel element is implemented into finite element program WCOMD. Comparison with pull-out, axial tension and push-pull tests will be carried out to show the efficiency and accuracy of the newly developed element.

3.2 Theory of 1-D bond slip element

3.2.1 Strong form

Reinforcement and concrete are analyzed separately. Equilibrium of forces in reinforcement and concrete is shown in Figure 3-3. In the free body of reinforcement, forces at the two ends of reinforcement are in equilibrium with bond force along length dx, which is equilibrated by the forces at two ends of concrete as shown in the free body of concrete. The equilibrium equations are expressed in Eqs. (3-1) and (3-2),

$$\frac{d\sigma_s(x)}{dx} - \frac{4}{d_b}\tau(x) = 0 \tag{3-1}$$

$$\frac{d\sigma_c(x)}{dx} + \frac{4\rho}{d_b}\tau(x) = 0 \tag{3-2}$$

Equation (3-1) and (3-2) can be expressed in matrix form as

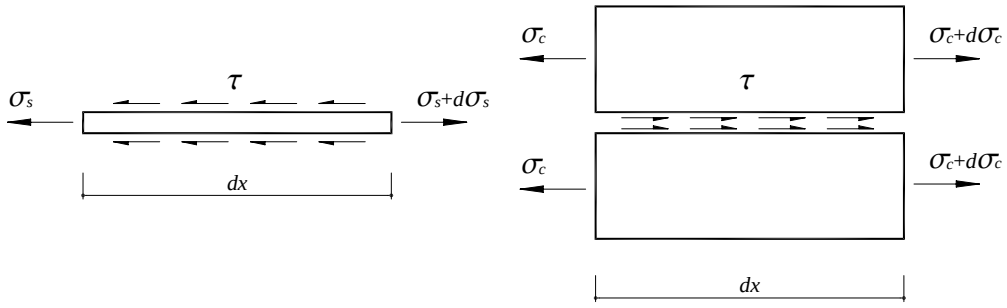

(a) Free body of reinforcement (b) Free body of concrete

Figure 3-3 Equilibrium forces in reinforcement and concrete

$$\frac{d\sigma(x)}{dx} + Q_e \cdot \tau(x) = 0 \tag{3-3}$$

where $\sigma = \begin{Bmatrix} \rho\sigma_s \\ \sigma_c \end{Bmatrix}$

$\tau = \begin{Bmatrix} \tau_b \\ \tau_b \end{Bmatrix}$

$Q_e = \begin{bmatrix} -\frac{4\rho}{d_b} & 0 \\ 0 & \frac{4\rho}{d_b} \end{bmatrix}$

3.2.2 Weak form

If displacement field of concrete and reinforcement is assumed as

$$u(x) = N(x)u \tag{3-4}$$

where $N(x)$ = shape functions

$u(x) = \begin{Bmatrix} u_s(x) \\ u_c(x) \end{Bmatrix}$

the slip in the element can be expressed by the displacement at the element nodes as

$$s = \begin{Bmatrix} s \\ s \end{Bmatrix} = \begin{Bmatrix} u_s - u_c \\ u_s - u_c \end{Bmatrix} = \begin{bmatrix} 1 & -1 \\ 1 & -1 \end{bmatrix} \begin{Bmatrix} u_s \\ u_c \end{Bmatrix} = T \cdot u(x) = T \cdot N \cdot u \tag{3-5}$$

where $T = \begin{bmatrix} 1 & -1 \\ 1 & -1 \end{bmatrix}$

The constitutive laws are expressed in matrix form in Eqs. (3-6) and (3-7).

$$\sigma = \begin{Bmatrix} \sigma_s \\ \sigma_c \end{Bmatrix} = \begin{bmatrix} \rho E_s & 0 \\ 0 & E_c \end{bmatrix} \begin{Bmatrix} \varepsilon_s \\ \varepsilon_c \end{Bmatrix} = D_{sc} \cdot N_{,x} \cdot u \tag{3-6}$$

$$\tau = \begin{Bmatrix} \tau_b \\ \tau_b \end{Bmatrix} = \begin{bmatrix} E_b & 0 \\ 0 & E_b \end{bmatrix} \begin{Bmatrix} s \\ s \end{Bmatrix} = D_b \cdot T \cdot N \cdot u \tag{3-7}$$

where, $D_{sc} = \begin{bmatrix} \rho E_s & 0 \\ 0 & E_c \end{bmatrix}$

$$D_b = \begin{bmatrix} E_b & 0 \\ 0 & E_b \end{bmatrix}$$

$$N_{,x} = \frac{\partial N}{\partial x}$$

Weighted residual method is introduced, and Eq. (3-3) is expressed in weighted integrated form as

$$\int_{-L/2}^{L/2} \delta u^T \left\{ \frac{d\sigma(x)}{dx} + Q_e \cdot \tau(x) \right\} = 0 \tag{3-8}$$

Equation (3-8) is multiplied by area of concrete, A_c, and integrated by parts,

$$A_c \left\{ \delta u^T \sigma \Big|_{-L/2}^{L/2} - \int_{-L/2}^{L/2} \delta \frac{du^T}{dx} \sigma dx + \int_{-L/2}^{L/2} \delta u^T Q_e \cdot \tau(x) dx \right\} = 0 \tag{3-9}$$

When Eqs. (3-4) and (3-5) are substituted into Eq. (3-9), Eq. (3-9) can be expressed as

$$\left\{ A_c \int_{-L/2}^{L/2} N_{,x}^T(x) D_{sc} N_{,x}(x) dx \right\} u - \left\{ A_c \int_{-L/2}^{L/2} N^T(x) \cdot Q_e \cdot D_b \cdot T \cdot N(x) dx \right\} u = P \tag{3-10}$$

Simplified form of Eq. (3-10) is

$$(K_{sc} - K_b) u = P \tag{3-11}$$

where

$K_{sc} = A_c \int_{-L/2}^{L/2} N_{,x}^T(x) \cdot D_{sc} \cdot N_{,x}(x) dx$, is the stiffness of concrete and reinforcement panels

$K_b = A_c \int_{-L/2}^{L/2} N^T(x) \cdot Q_e \cdot D_b \cdot T \cdot N(x) dx$, is the stiffness of bond to represent the interaction between concrete and reinforcement

$$Q_e = \begin{bmatrix} \frac{4\rho}{d_b} & 0 \\ 0 & -\frac{4\rho}{d_b} \end{bmatrix}$$

$$N_{,x} = \frac{\partial N}{\partial x}$$

$$T = \begin{bmatrix} 1 & -1 \\ 1 & -1 \end{bmatrix}$$

$$D_{sc} = \begin{bmatrix} \rho E_s & 0 \\ 0 & E_c \end{bmatrix}$$

$$D_b = \begin{bmatrix} E_b & 0 \\ 0 & E_b \end{bmatrix}$$

3.3 Theory of 2-D bond slip element

The method used in 1-D element is extended to 2-D element. In 2-D element, bond stress around the reinforcement will be described in two directions, so all equilibrium equations should be expressed in two directions.

3.3.1 Strong form

Reinforcement still behaves one dimensionally in the direction of the axes of the bars. The equilibrium of forces in the reinforcement is shown in Figure 3-4. Equations can be written as

$$\frac{d\sigma_{sx}}{dx} - \frac{4}{d_{bx}}\tau_x = 0 \tag{3-12}$$

$$\frac{d\sigma_{sy}}{dx} - \frac{4}{d_{by}}\tau_y = 0 \tag{3-13}$$

Two-dimensional equilibrium forces in the concrete is shown in Figure 3-5 and the equilibrium equations can be expressed as

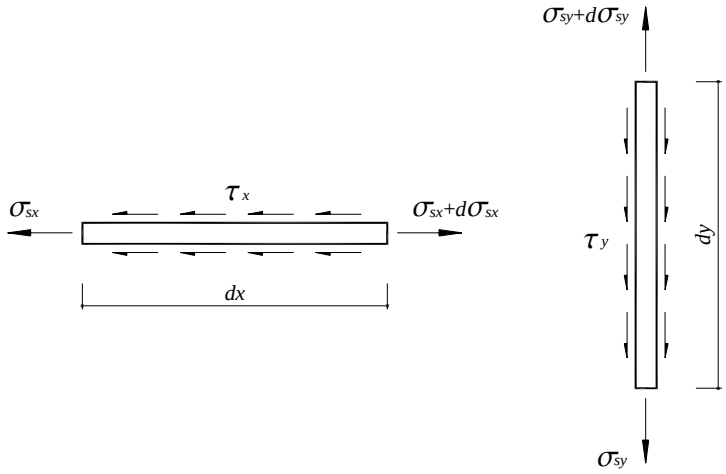

(a) Free body of reinforcement in x-direction

(b) Free body of reinforcement in y-direction

Figure 3-4 Two-dimensional equilibrium of forces in the reinforcement

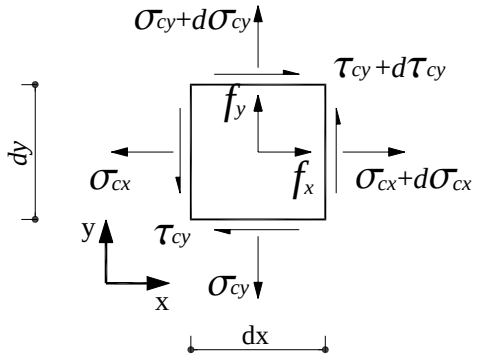

Figure 3-5 Two-dimensional equilibrium of forces in the concrete

$$\frac{d\sigma_{cx}}{dx}+\frac{d\tau_{cxy}}{dy}+f_x=0 \tag{3-14}$$

$$\frac{d\sigma_{cy}}{dy}+\frac{d\tau_{cxy}}{dx}+f_y=0 \tag{3-15}$$

f_x and f_y are bond stress functions as a body force of concrete.

Body force in x-direction due to bond stress is

$$f_x=\frac{n_x\,\pi\,d_{bx}\,\tau_x\,dx}{dx\,dy} \tag{3-16}$$

where, $n_x = \dfrac{\rho_x \, dy}{\pi \dfrac{d_{bx}^2}{4}}$ is number of reinforcement bars parallel to x-direction

When n_x is substituted into Eq. (3-16), body force in x-direction due to bond stress can be simplified as

$$f_x = \frac{4\rho_x}{d_{bx}} \tau_x \tag{3-17}$$

Similarly, for body force in y-direction due to bond stress, f_y, can be written as,

$$f_y = \frac{4\rho_y}{d_{by}} \tau_y \tag{3-18}$$

So, the equilibrium equations in concrete panel can be written as

$$\frac{d\sigma_{cx}}{dx} + \frac{d\tau_{cxy}}{dy} + \frac{4\rho_x}{d_{bx}} \tau_x = 0 \tag{3-19}$$

$$\frac{d\sigma_{cy}}{dy} + \frac{d\tau_{cxy}}{dx} + \frac{4\rho_y}{d_{by}} \tau_y = 0 \tag{3-20}$$

Bond slip in x- and y-directions are defined as

$$s_x = u_{sx} - u_{cx} \tag{3-21}$$

$$s_y = u_{sy} - u_{cy} \tag{3-22}$$

Strain of the reinforcement can be calculated from the difference of reinforcement displacement, and expressed as

$$\varepsilon_{sx} = \frac{\partial u_{sx}}{\partial x} \tag{3-23}$$

$$\varepsilon_{sy} = \frac{\partial u_{sy}}{\partial y} \tag{3-24}$$

Strain of the concrete can calculated from the difference of concrete displacement, and expressed as

$$\varepsilon_{cx} = \frac{\partial u_{cx}}{\partial x} \tag{3-25}$$

$$\varepsilon_{cy} = \frac{\partial u_{cy}}{\partial y} \tag{3-26}$$

$$\gamma_{cxy} = \frac{\partial u_{cy}}{\partial x} + \frac{\partial u_{cx}}{\partial y} \tag{3-27}$$

If bond stress can be expressed by bond slip, and concrete and reinforcement stresses can be expressed by concrete and reinforcement strain as shown in Eqs. (3-28) to (3-34)

$$\tau_x = \tau_x(s_x) \tag{3-28}$$

$$\tau_y = \tau_y(s_y) \tag{3-29}$$

$$\sigma_{sx} = \sigma_{sx}(\varepsilon_{sx}) \tag{3-30}$$

$$\sigma_{sy} = \sigma_{sy}(\varepsilon_{sy}) \tag{3-31}$$

$$\sigma_{cx} = \sigma_{cx}(\varepsilon_{cx}) \tag{3-32}$$

$$\sigma_{cy} = \sigma_{cy}(\varepsilon_{cy}) \tag{3-33}$$

$$\tau_{cxy} = \tau_{cxy}(\gamma_{cxy}) \tag{3-34}$$

the problem involving 18 unknowns (u_{cx}, u_{cy}, u_{sx}, u_{sy}, ε_{cx}, ε_{cy}, γ_{xy}, ε_{sx}, ε_{sy}, s_x, s_y, σ_{cx}, σ_{cy}, τ_{cxy}, σ_{sx}, σ_{sy}, τ_x and τ_y) can be solved through 18 independent equations (Eq. (3-12), Eq. (3-13) and Eqs. (3-19) to (3-34)).

3.3.2 Weak form

Firstly, Eqs. (3-12) to (3-15) are expressed in matrix form as

$$\begin{bmatrix} \frac{1}{\partial x} & 0 & \frac{1}{\partial y} & 0 & 0 \\ 0 & \frac{1}{\partial y} & \frac{1}{\partial x} & 0 & 0 \\ 0 & 0 & 0 & \frac{1}{\partial x} & 0 \\ 0 & 0 & 0 & 0 & \frac{1}{\partial y} \end{bmatrix} \begin{Bmatrix} \sigma_{cx} \\ \sigma_{cy} \\ \tau_{cxy} \\ \sigma_{sx} \\ \sigma_{sy} \end{Bmatrix} + \begin{bmatrix} \frac{4\rho_x}{d_{bx}} & 0 \\ 0 & \frac{4\rho_y}{d_{by}} \\ -\frac{4}{d_{bx}} & 0 \\ 0 & -\frac{4}{d_{by}} \end{bmatrix} \begin{Bmatrix} \tau_x \\ \tau_y \end{Bmatrix} = 0 \tag{3-35}$$

Equation (3-35) can be simplified as

$$\partial_{tt}\sigma + Q_e \cdot \tau = 0 \tag{3-36}$$

where $\sigma = \{\sigma_{cx} \quad \sigma_{cy} \quad \tau_{cxy} \quad \rho_x\sigma_{sx} \quad \rho_y\sigma_{sy}\}^T$

$$\tau = \{\tau_x \quad \tau_y\}^T$$

$$\partial_{tt} = \begin{bmatrix} \frac{1}{\partial x} & 0 & \frac{1}{\partial y} & 0 & 0 \\ 0 & \frac{1}{\partial y} & \frac{1}{\partial x} & 0 & 0 \\ 0 & 0 & 0 & \frac{1}{\partial x} & 0 \\ 0 & 0 & 0 & 0 & \frac{1}{\partial y} \end{bmatrix}$$

$$Q_e = \begin{bmatrix} \frac{4\rho_x}{d_{bx}} & 0 \\ 0 & \frac{4\rho_y}{d_{by}} \\ -\frac{4\rho_x}{d_{bx}} & 0 \\ 0 & -\frac{4\rho_y}{d_{by}} \end{bmatrix}$$

Weighted integration form of Eq. (3-36) can be expressed as

$$\int_\Omega \delta u^T(x,y) \cdot (\partial_{tt}\sigma + Q_e \cdot \tau) d\Omega = 0 \tag{3-37}$$

Eq. (3-37) is multiplied by t, and integrated by parts,

$$t\left\{\delta u^T(x,y)\sigma\Big|_\Gamma - \int_\Omega (\partial_{tt}\delta u^T(x,y))\sigma d\Omega + \int_\Omega \delta u^T(x,y) \cdot Q_e \cdot \tau \cdot d\Omega\right\} = 0 \tag{3-38}$$

where t is thickness of the panel

When shape function *N(x,y)* is assumed,

$$u(x,y) = \begin{Bmatrix} u_{cx}(x,y) \\ u_{cy}(x,y) \\ u_{sx}(x,y) \\ u_{sy}(x,y) \end{Bmatrix} = N(x,y)_{4\times 16} \begin{Bmatrix} u_{1x} \\ u_{1y} \\ \dots \\ u_{8x} \\ u_{8y} \end{Bmatrix} = N(x,y) \cdot u \tag{3-39}$$

Strain and stress of element can be expressed as

$$\begin{Bmatrix} \varepsilon_{cx} \\ \varepsilon_{cy} \\ \gamma_{cxy} \\ \varepsilon_{sx} \\ \varepsilon_{sy} \end{Bmatrix} = \begin{bmatrix} \frac{1}{\partial x} & 0 & 0 & 0 \\ 0 & \frac{1}{\partial y} & 0 & 0 \\ \frac{1}{\partial y} & \frac{1}{\partial x} & 0 & 0 \\ 0 & 0 & \frac{1}{\partial x} & 0 \\ 0 & 0 & 0 & \frac{1}{\partial y} \end{bmatrix} \begin{Bmatrix} u_{cx}(x,y) \\ u_{cy}(x,y) \\ u_{sx}(x,y) \\ u_{sy}(x,y) \end{Bmatrix} = \partial_{tt}^{T} u(x,y) = \partial_{tt}^{T} N(x,y) \cdot u \tag{3-40}$$

$$\begin{Bmatrix} \sigma_{cx} \\ \sigma_{cy} \\ \tau_{cxy} \\ \sigma_{sx} \\ \sigma_{sy} \end{Bmatrix} = \begin{bmatrix} E_{cx} & 0 & 0 & 0 & 0 \\ 0 & E_{cy} & 0 & 0 & 0 \\ 0 & 0 & G_c & 0 & 0 \\ 0 & 0 & 0 & \rho_x E_{sx} & 0 \\ 0 & 0 & 0 & 0 & \rho_y E_{sy} \end{bmatrix} \begin{Bmatrix} \varepsilon_{cx} \\ \varepsilon_{cy} \\ \gamma_{cxy} \\ \varepsilon_{sx} \\ \varepsilon_{sy} \end{Bmatrix} = D_{cs} \cdot \varepsilon = D_{cs} \cdot \partial_{tt}^{T} N \cdot u \tag{3-41}$$

Slip and bond stress of element can be expressed as

$$s = \begin{Bmatrix} s_x \\ s_y \end{Bmatrix} = \begin{bmatrix} -1 & 0 & 1 & 0 \\ 0 & -1 & 0 & 1 \end{bmatrix} \begin{Bmatrix} u_{cx}(x,y) \\ u_{cy}(x,y) \\ u_{sx}(x,y) \\ u_{sy}(x,y) \end{Bmatrix} = T_s \cdot N \cdot u \tag{3-42}$$

$$\tau = \begin{Bmatrix} \tau_x \\ \tau_y \end{Bmatrix} = \begin{bmatrix} E_{bx} & 0 \\ 0 & E_{by} \end{bmatrix} \begin{Bmatrix} s_x \\ s_y \end{Bmatrix} = D_b \cdot s = D_b \cdot T_s \cdot N \cdot u \tag{3-43}$$

When Eqs. (3-40) to (3-43) are substituted into Eq. (3-38), Eq. (3-38) can be rewritten as

$$t \cdot (\int_{\Omega} (\partial_{tt}^{T} N)^{T} \cdot D_{cs} \cdot \partial_{tt}^{T} N \cdot d\Omega - \int_{\Omega} N^{T} \cdot Q_e \cdot D_b \cdot T_s \cdot N \cdot d\Omega) \cdot u = P \tag{3-44}$$

If $\partial_{tt}^{T} N$ is defined as B, then Eq. (3-44) can be simplified as

$$K\,u = P \tag{3-45}$$

where $K = K_{sc} - K_b$

$K_{sc} = t \cdot \int_{\Omega} B^{T} \cdot D_{cs} \cdot B \cdot d\Omega$, is the stiffness of concrete and reinforcement panels

$K_b = t \cdot \int_\Omega N^T \cdot Q_e \cdot D_b \cdot T_s \cdot N \cdot d\Omega$, is the stiffness of bond to describe the interaction between concrete and reinforcement

$$B = \partial_{tt}^T N$$

$$\partial_{tt} = \begin{bmatrix} \frac{1}{\partial x} & 0 & \frac{1}{\partial y} & 0 & 0 \\ 0 & \frac{1}{\partial y} & \frac{1}{\partial x} & 0 & 0 \\ 0 & 0 & 0 & \frac{1}{\partial x} & 0 \\ 0 & 0 & 0 & 0 & \frac{1}{\partial y} \end{bmatrix}$$

$$D_{cs} = \begin{bmatrix} E_{cx} & 0 & 0 & 0 & 0 \\ 0 & E_{cy} & 0 & 0 & 0 \\ 0 & 0 & G_c & 0 & 0 \\ 0 & 0 & 0 & \rho_x E_{sx} & 0 \\ 0 & 0 & 0 & 0 & \rho_y E_{sy} \end{bmatrix}$$

$$Q_e = \begin{bmatrix} \frac{4\rho_x}{d_{bx}} & 0 \\ 0 & \frac{4\rho_y}{d_{by}} \\ -\frac{4\rho_x}{d_{bx}} & 0 \\ 0 & -\frac{4\rho_y}{d_{by}} \end{bmatrix}$$

$$T_s = \begin{bmatrix} -1 & 0 & 1 & 0 \\ 0 & -1 & 0 & 1 \end{bmatrix}$$

$$D_b = \begin{bmatrix} E_{bx} & 0 \\ 0 & E_{by} \end{bmatrix}$$

3.4 Transitional element

In normal RC element without the effect of bond slip, concrete and reinforcement share the same node. But in RC element considering the effect of bond slip (bond zone element), double nodes at the same point should be used to represent concrete and reinforcement, respectively. When the two elements are used in one model, the transitional element is needed to connect these two elements.

In Figure 3-6, Element Ⅱ is a transitional element to connect the normal R.C. element and bond zone element.

The transitional element *ikl* is degenerated from bond zone element *ijkl* on the condition that $u_i = u_j$ as shown in Figure 3-6.

The equation of the original element *ijkl* can be expressed as Eq. (3-46).

$$\begin{bmatrix} k_{ii} & k_{ij} & k_{ik} & k_{il} \\ k_{ji} & k_{jj} & k_{jk} & k_{jl} \\ k_{ki} & k_{kj} & k_{kk} & k_{kl} \\ k_{li} & k_{lj} & k_{lk} & k_{ll} \end{bmatrix} \begin{Bmatrix} u_i \\ u_j \\ u_k \\ u_l \end{Bmatrix} = \begin{Bmatrix} P_i \\ P_j \\ P_k \\ P_l \end{Bmatrix} \tag{3-46}$$

with the condition $\hat{u}_i = u_i = u_j$ and $\hat{P}_i = P_i + P_j$,

where $\hat{u}_i$ is the displacement of node i in the transitional element *ilk*

$\hat{P}_i$ is the force of node i in the transitional element *ilk*

The stiffness matrix of transitional element can be degenerated from Eq. (3-46).

$$K = \begin{bmatrix} k_{ii} + k_{ij} + k_{ji} + k_{jj} & k_{ik} + k_{jk} & k_{il} + k_{jl} \\ k_{ki} + k_{kj} & k_{kk} & k_{kl} \\ k_{li} + k_{lj} & k_{lk} & k_{ll} \end{bmatrix} \tag{3-47}$$

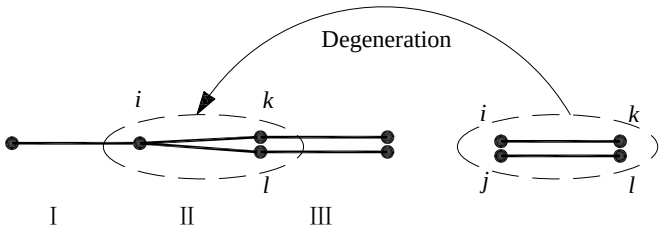

Figure 3-6 One-dimensional transitional element

Inside the program, the transitional element is considered a special double-panel element. The node, which is shared by concrete and reinforcement, is used twice to represent concrete and reinforcement nodes in double-panel element. In the process of assembling, stiffness condensation is automatically done.

3.5 Monotonic bond model used in the double-panel element

The widely used monotonic local bond stress-slip model proposed by Eligehausen et al (1983) is used as the local bond slip model of the double-panel element. The bond stress-slip curve is shown in Figure 2-17. Characteristic values of monotonic envelope of the model are described in Table 2-1. To take account of the effect of concrete strength f_c and diameter of reinforcement d_b, characteristic bond stress τ_1 is modified according to research of Soroushian et al (1988 and 1991), and expressed in Eq. (2-32).

3.6 Cyclic bond model used in the double-panel element

3.6.1 Original Eligehausen et al's (1983) model

The cyclic bond model proposed by Eligehausen et al (1983) is used in the double-panel element.

The stress path from positive to negative monotonic envelope can be divided into three branches as: unloading, negative friction and reloading paths, as shown in Figure 3-7(a), while the stress paths from negative monotonic to positive monotonic envelope can be divided into unloading, positive friction and reloading paths, as seen in Figure 3-7(b).

Unloading and reloading paths are stiff lines, and the slope of unloading and reloading paths is taken as $K = 180 N/mm^3$. Friction path is a flat line. The friction value varies with the maximum bond slip, and is expressed as in Eqs. (2-24) and (2-25).

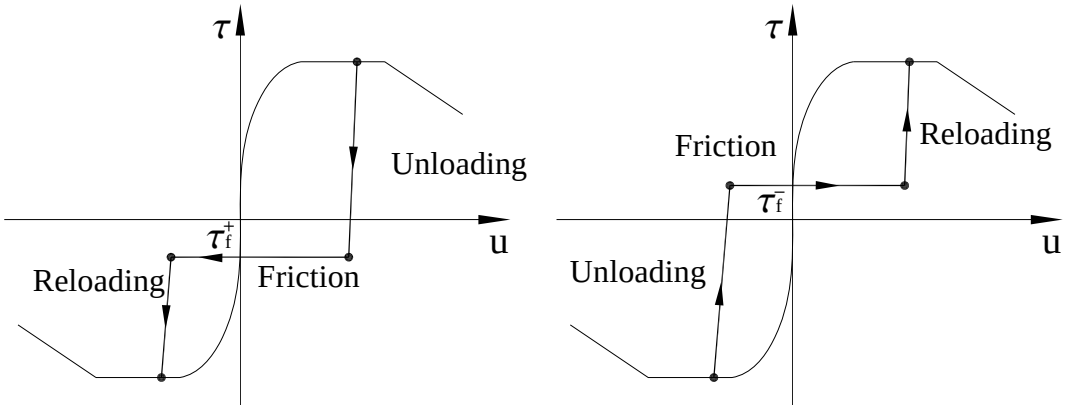

(a) Unloading from positive envelope (b) Unloading from negative envelope

Figure 3-7 Branches of cyclic curves in mathematical

Characteristic bond stress in the envelope can be reduced due to cyclic loads. Characteristic bond stress τ_1 and τ_3 can be formulated in terms of dimensionless dissipated energy. The formulas are written in Eqs. (2-34), (2-35), (2-36) and (2-37).

3.6.2 Modification of Eligehausen et al's (1983) cyclic model

In Eligehausen et al's (1983) cyclic law, the reloading path is simplified into a steep line followed by friction flat line, as illustrated by the lines in Figure 3-7. According to the recommendation of Balazs (1991), during the first loading, the bond stress-slip curves are concave in both directions. In all subsequent load phase, the curves were convex at first, and then became concave beyond a point of inflection close to the previous maximum slip. This characteristic of reloading curve can be seen from experimental bond stress-slip curve, shown in Figure 3-8.

However, the reloading path of the load-slip curve through analysis based on Eligehausen et al's (1983) model can not reflect the experimental behaviour accurately. The comparison between prediction with Eligehausen et al's (1983) model and experimental data are based on based on specimen tested by Balazs (1991). A reinforcing bar embedded in confined concrete is subjected to cyclic loads. Diameter of reinforcement is 8 mm, and the embedded length is 6 times of diameter. Concrete strength is 25 MPa, and the reinforcement yield stress is 414 MPa. In

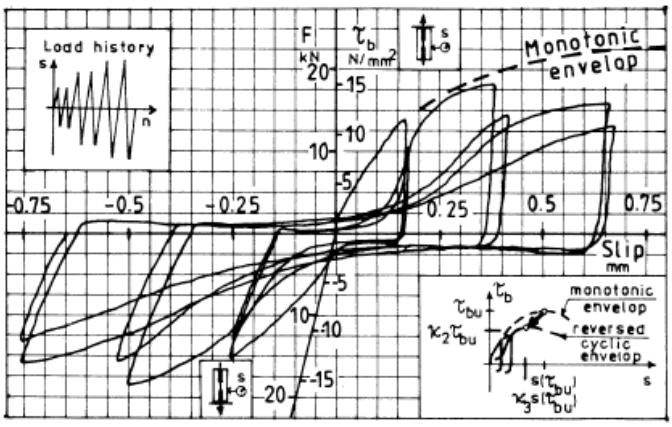

Figure 3-8 Experimental bond stress v.s slip

(Balazs, 1991)

positive cycle

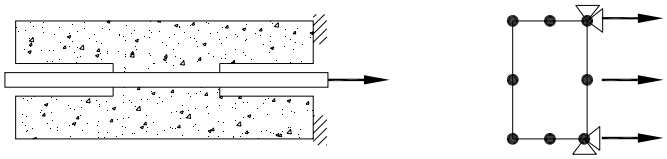

negtive cycle

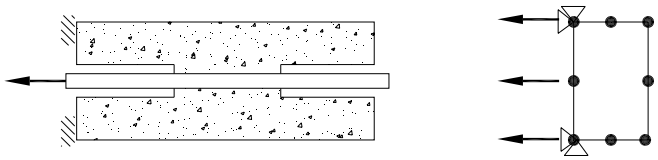

Figure 3-9 Modelling of cyclic pull-out test

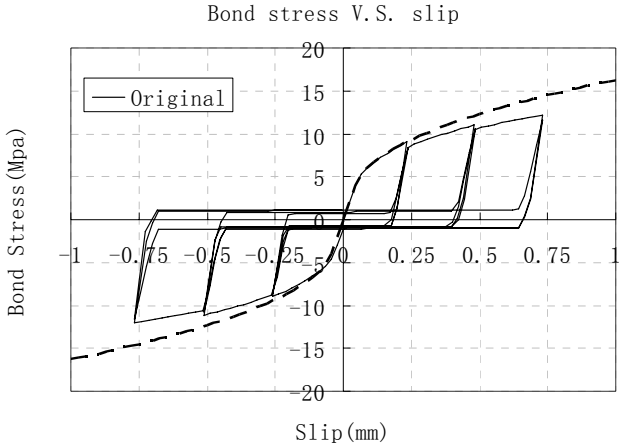

Figure 3-10 Bond stress v.s slip with original cyclic law

positive loading cycles, pull force is on the right end of the reinforcement, and the right end of concrete is fixed. While in negative loading cycles, pull is on the left end of the reinforcement, and the left end of concrete is fixed. Modelling of pull-out test is also shown in Figure 3-9. The results of experimental data and prediction with Eligehausen et al's (1983) model are shown in Figure 3-8 and Figure 3-10, respectively.

Through further investigation, it is found that the experimental behaviour of being convex first and concave later can be described by the curve of function $y = \arctan(x)$, where x is between ω_1 and 1. A function $y = \arctan(x)$, where x is between ω_1 and 1, can be used to do the mapping of reloading curve (shown in Figure 3-11).

Then, the reloading curve is written as

$$\frac{\tau - y_0}{s_{cy}} = \text{atan}\left(\frac{s - x_0}{s_{cx}}\right) \tag{3-48}$$

where

x_0 is the translation distance, $x_0 = s_{\max}\dfrac{-\omega_1}{1-\omega_1}$

y_0 is the translation distance, $y_0 = \bar{\tau_f} + (\tau_{\max} - \bar{\tau_f})\dfrac{-\text{atan}(\omega_1)}{\text{atan}(1.0) - \text{atan}(\omega_1)}$

s_{cy} is the scaling factor in y-direction, $s_{cy} = \dfrac{\tau_{\max} - \bar{\tau_f}}{\text{atan}(1.0) - \text{atan}(\omega_1)}$

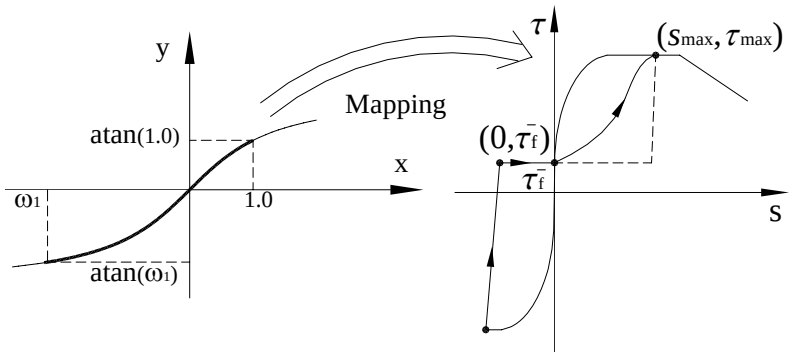

Figure 3-11 Modified reloading curve from scaling and mapping of atan(x)

s_{cx} is the scaling factor in x-direction, $s_{cx} = \dfrac{s_{\max}}{1-\omega_1}$

ω_1 is the parameter to determine the shape of reloading curve

Similarly, reloading to negative envelope can be derived based on scaling and mapping of the curve of a function $y = \arctan(x)$, where x is between -1 and ω_2

Then, the reloading curve can be expressed as

$$\frac{\tau - y_0}{s_{cy}} = \text{atan}\left(\frac{s - x_0}{s_{cx}}\right) \tag{3-49}$$

where

x_0 is the translation distance, $x_0 = s_{\min}\dfrac{\omega_2}{\omega_2 + 1}$

y_0 is the translation distance, $y_0 = \tau_f^+ - \left(\tau_f^+ - \tau_{\min}\right)\dfrac{\text{atan}(\omega_2)}{\text{atan}(\omega_2) - \text{atan}(-1.0)}$

s_{cy} is the scaling factor in y-direction, $s_{cy} = \dfrac{\tau_f^+ - \tau_{\min}}{\text{atan}(\omega_2) - \text{atan}(-1.0)}$

s_{cx} is the scaling factor in x-direction, $s_{cx} = \dfrac{s_{\min}}{\omega_2 + 1}$

ω_2 is the parameter to determine the shape of reloading curve

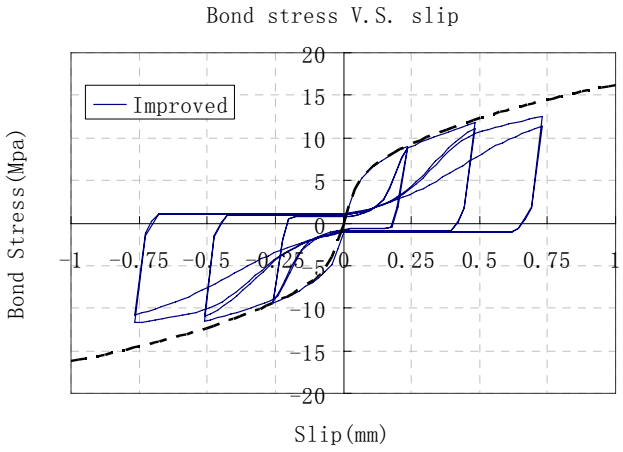

Figure 3-12 Bond stress v.s slip with improved cyclic law

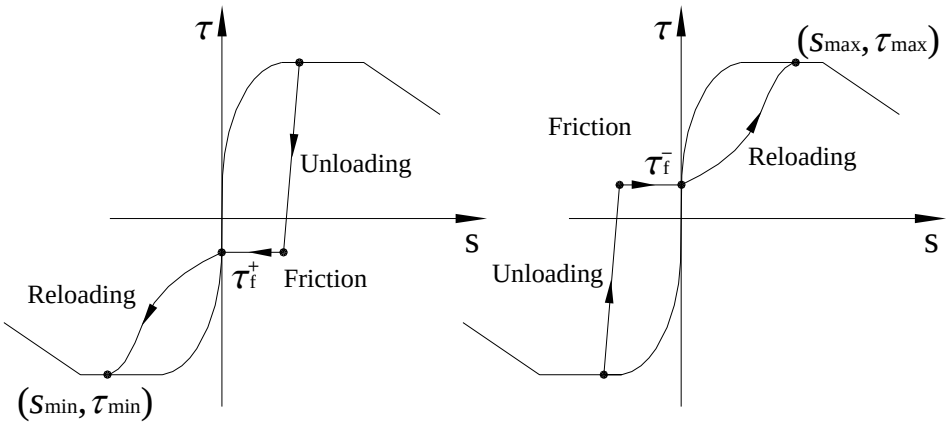

(a) Unloading from positive envelope (b) Unloading from negative envelope

Figure 3-13 Branches of cyclic curves in modified cyclic law

The parameter ω_1 or ω_2 determines the curvature of convex curve. If ω_1 or ω_2 approaches negative infinity, the curvature of reloading curve is big. The curve is similar to reloading curve of Eligehausen et al's (1983) model. If ω_1 or ω_2 approaches zero, the slope of reloading curve is relatively gentle. Through several trial, ω_1 and ω_2 are expressed as in Eq. (3-50)

$$\omega_2 = -\omega_1 = \frac{10}{s_{max}^2} \tag{3-50}$$

The modified cyclic model is shown in Figure 3-13. With it, the bond stress-slip curve is shown in Figure 3-12. Compared with the analysis with original model, the analysis with modified model can represent the behaviour shown in experiment better.

3.7 Verification with experimental data and analysis of local behaviour

The newly developed double-panel element is corroborated by the experimental results of pull-out, axial tension and push-pull tests. Besides the comparisons of the experiment with monotonic loading, the comparison is also conduct for experiment with cyclic push-pull test. Finally, the analysis of pull-out test is used as an example to study the effect of element numbers on the accuracy of the results.

After the verification with experimental data in term of load-displacement relationship, local behaviour such as steel and bond stress distributions are analyzed. Steel and bond distributions are obtained through strain and stress components on Gauss Points of the element. Nine Gauss points are used in the double panel elements. In each Gauss point, the element strain includes three main components: concrete strain (concrete normal strains in two directions and shear strain), reinforcement strain (reinforcement strains in two directions) and bond slip (bond slips in two directions). Similarly, in each Gauss point, the element stress includes three main components: concrete stress (concrete normal stresses in two directions and shear strain), reinforcement stress (reinforcement stresses in two directions) and bond stress (bond stresses in two directions). The observation and analysis of local behaviour are based on strains and stresses on the Gauss Points in the elements. Concrete strain and stress of the element can be obtained from concrete strain and stress at the Gauss Points. Since the reinforcement is distributed into the whole panel element, strain and stress of the reinforcement have to be calculated through the average of strain and stress at three Gauss Points perpendicular to strain or stress direction. Bond slip and stress along the reinforcement can be determined through similar ways.

3.7.1 Pull-out test

Four specimens of the pull-out tests were tested by Ueda et al (1986). Geometric and material properties are listed in Table 3-1. Pull force is applied on the right end of the reinforcement and concrete is fixed at the right end. On the other side, reinforcement and concrete are both free. Slip of the reinforcement is measured at the loading end. The reinforced concrete specimens are modelled by 4 double-panel elements. Loading and modelling of pull-out test is shown in Figure 3-14. The comparison of load-slip curve between analytical results and experimental data is shown in Figure 3-15.

The shape of the load-slip diagrams predicted by the analytical simulation generally

compares well with the experimental results for the four specimens,

Local behaviour of pull-out test is illustrated through the example of specimen S101, and shown in Figure 3-16 to Figure 3-18. To show local behaviour of pull-out test in the case of unyielding and yielding of the reinforcement, distributions of steel and bond are presented at three loading states: $P=20\%F_y$, $P=70\%F_y$ and $P=110\%F_y$, where P is the pull force at the end of reinforcement, F_y is the yielding strength of reinforcement.

It is observed in Figure 3-16 and Figure 3-17 that the maximum steel stress and bond slip both occur at the end near pulling force. As the bond transfers force to concrete, steel stress decreases along the specimen. In the mean time, bond slip and bond stress decrease along the specimen. When the pull force is small, bond from only part of the reinforcement is enough to transfer the pull force to concrete. So, steel and bond stresses decrease to zero around the middle of the specimen, as it is observed in the case of $P=20\%F_y$. When the pull

Table 3-1 Test program by Ueda et al (1986)

	Embedded length (mm)	Concrete strength (MPa)	Bar size (mm)	Reinforcement yield stress (MPa)
S101	610	19.9	32	414
S107	610	18.2	32	331
S61	406	23.8	19	469
S64	610	28.7	19	438

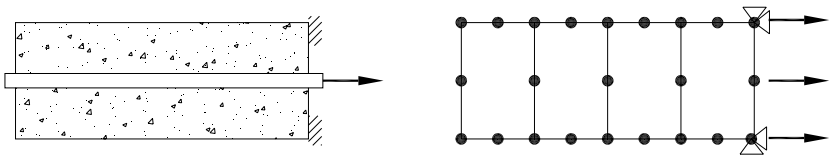

Figure 3-14 Loading and modelling of pull-out test

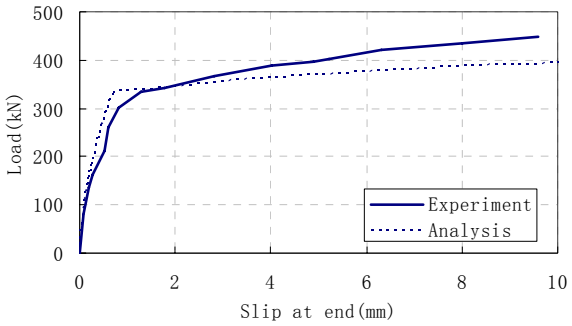

(a) Specimen S101

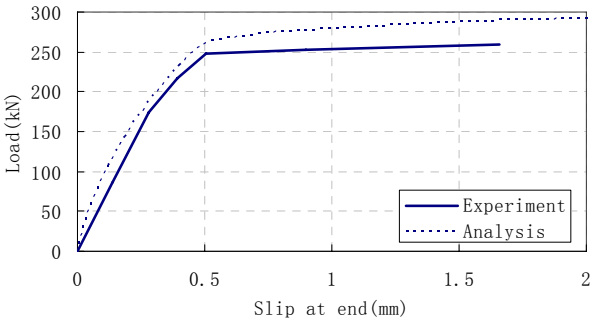

(b) Specimen S107

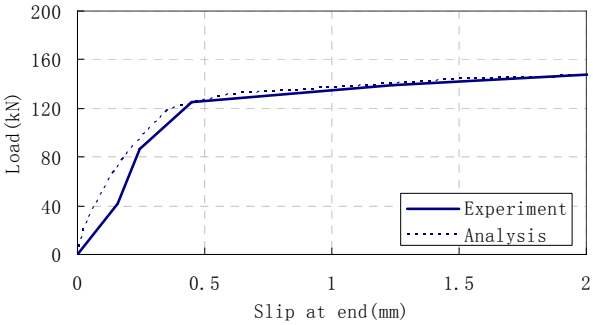

(c) Specimen S61

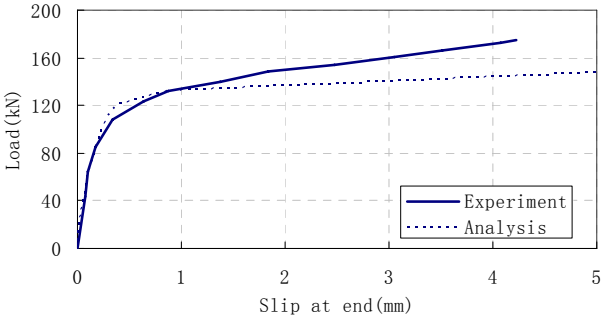

(d) Specimen S64

Figure 3-15 Comparison of analytical and experimental results for specimen S101, S107, S61 and S64

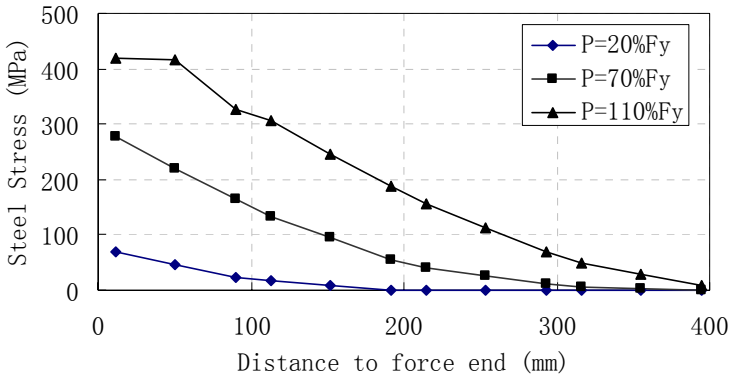

Figure 3-16 Distribution of steel stress along the specimen

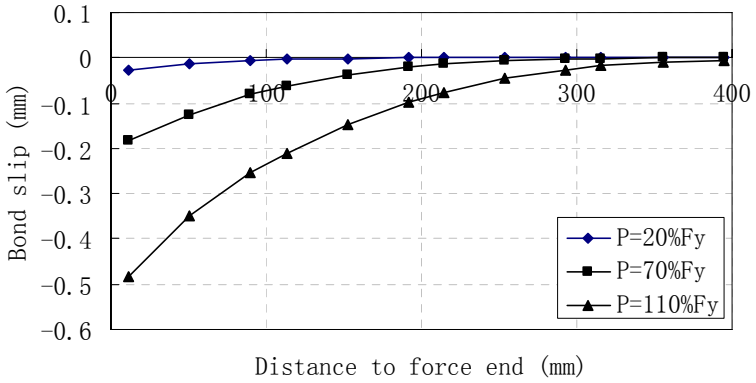

Figure 3-17 Distribution of bond slip along the specimen

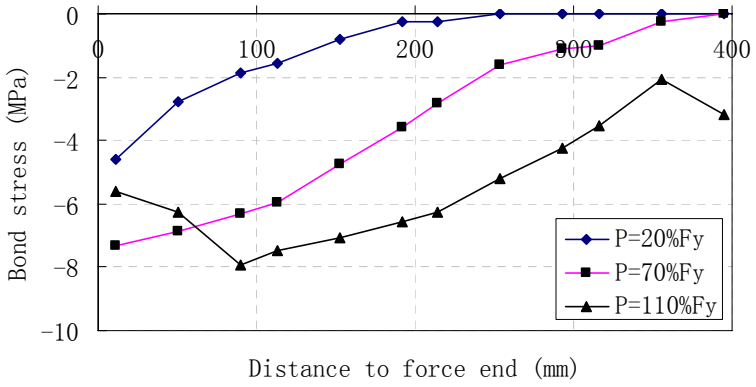

Figure 3-18 Distribution of bond stress along the specimen

force increases, bond from the whole reinforcement needs to work together to transfer the pull force to concrete. So, zero point of steel and bond stress move to

the free end, as it is observed in the case of P=70%F_y. When the pull force exceeds the yielding strength of the reinforcement, part of the reinforcement near the pull force yields. Bond constitutive law used in this dissertation takes into account of the effect of steel strain. When the reinforcement yields, steel strain increases a lot, and bond stress can decrease even though bond slip increases. It is simulated by the model and shown in Figure 3-18.

3.7.2 Axial tension test

The axial tension test was carried out by Doerr (Keuser and Mehlhorn, 1987). Diameter of reinforcement is 16 mm, and the embedded length is 508 mm. Concrete strength is 37.2 MPa, and the reinforcement yield stress is 420 MPa. Forces are applied at two ends of the reinforcement and concrete is fixed at two ends. The middle of specimen is weakened by a notch to obtain the first crack in the middle. The axial loaded specimen is modelled by 13 double-panel elements. The weakened middle part is simulated by lowering cracking strength in middle element. The detailing and modelling of axial tension test is shown in Figure 3-19.

The bar force distribution along the embedded length from the analysis is compared with experimental data as shown in Figure 3-20. The comparison between analytical

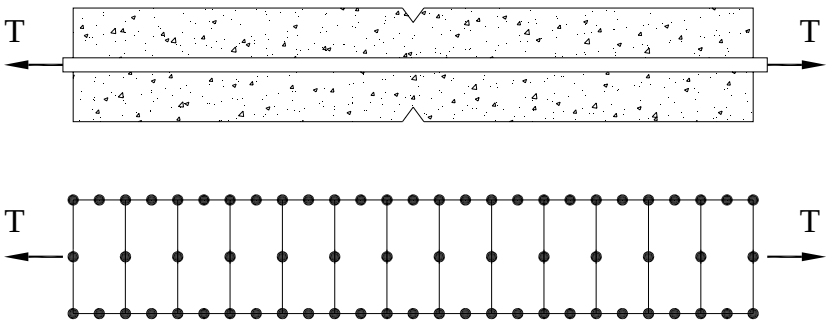

Figure 3-19 Detailing and modelling of axial tension test

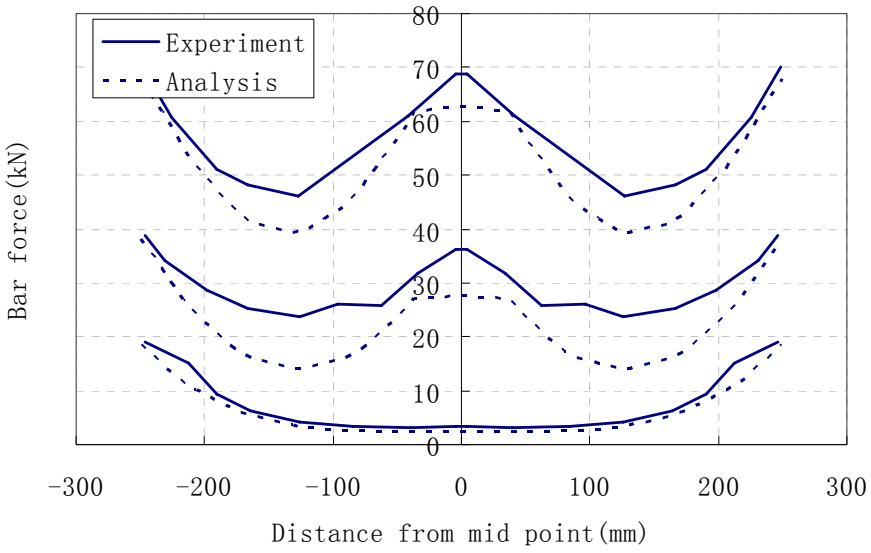

Figure 3-20 Comparison of bar force between experiment and analysis

and experimental results is done on three load levels: T=20kN, T=40kN and T=70kN.

The shape of the bar force distribution predicted by the analytical simulation generally compares well with the experimental results before crack occurs, when the crack occurs, the deviation between analytical and experimental results becomes larger. The analytical bar forces except at the two ends are smaller than the experimental results. From the equilibrium equation of reinforcement, the difference of force equals to the sum of bond force. Hence, in this case the bond stress in the analytical simulation is overestimated. One of the reasons can be that the bond stress-slip law used in analysis does not include the effect of crack in concrete, which can deteriorate the bond strength. The modification of bond-slip model to include this effect will be proposed in chapter 4. The improvement can be seen based on the modified bond slip curve.

The distributions of bond and concrete stresses are shown in Figure 3-21 to Figure 3-22.

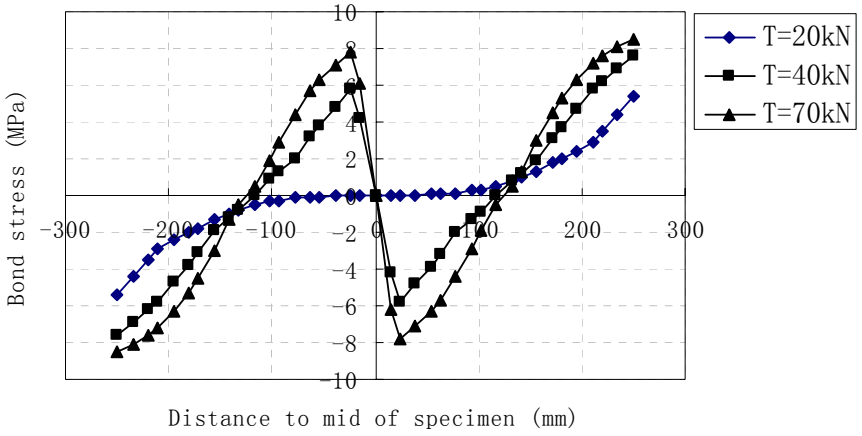

Figure 3-21 Distribution of bond stress along the specimen

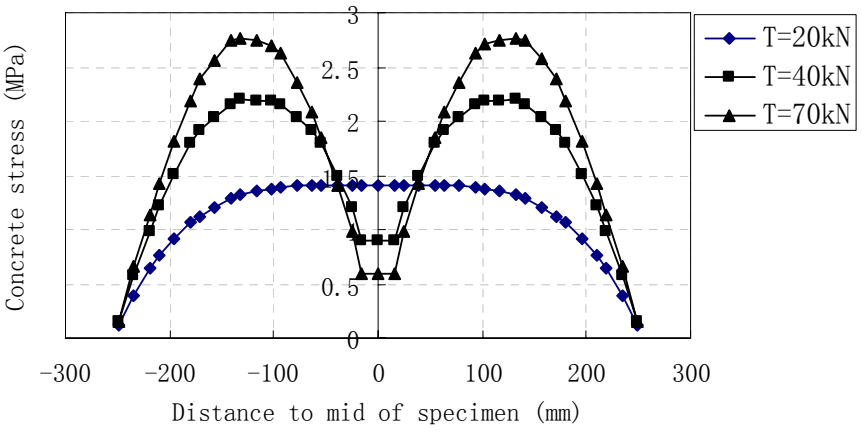

Figure 3-22 Distribution of concrete stress along the specimen

Before cracking, stress in the reinforcement reaches maximum at two ends of the specimen. As the bond transfers force to concrete, concrete stress reaches its peak in the middle of the specimen, as seen in the case of T=20kN. With the increment of axial force at two ends, concrete stress in the middle of the specimen will reach its tensile strength, and suddenly drop after that. To get the equilibrium in the middle of the specimen, steel stress increases sharply. And bond stress around the middle of the specimen increases sharply because of the change in steel stress, as seen in the case of T=40kN and T=70kN.

3.7.3 Monotonic push-pull test

In joints subjected to lateral loads, main bar in the joint is usually subjected to push force at one end and pull force at the other end. In this case, the bond condition is different from pull-out test or axial force tension. It is usually called push-pull test. Viwathanatepa et al (1979) tested several anchored reinforcing bars subjected to monotonic push-pull test. The specimen is an anchored #8 bar in a well confined block of 25 in width, which corresponds to an anchorage length of 25 times bar diameters. Concrete compression strength is 30 MPa, and the reinforcement yielding stress is 400 MPa. Two identical forces are applied at two ends of the reinforcement. And concrete is fixed at two ends. Modelling of push-pull test is shown in Figure 3-23. The comparison between analytical results and experimental data is shown in Figure 3-24. The comparison is done on the relationship between steel stress and displacement at the end. The steel stress–displacement diagrams

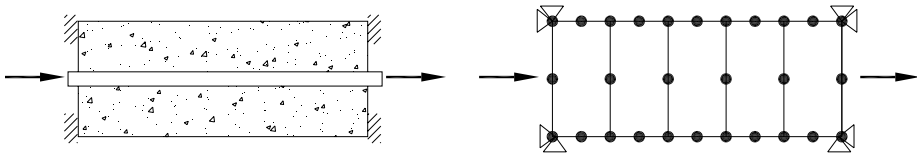

Figure 3-23 Detailing and modelling of monotonic push-pull test

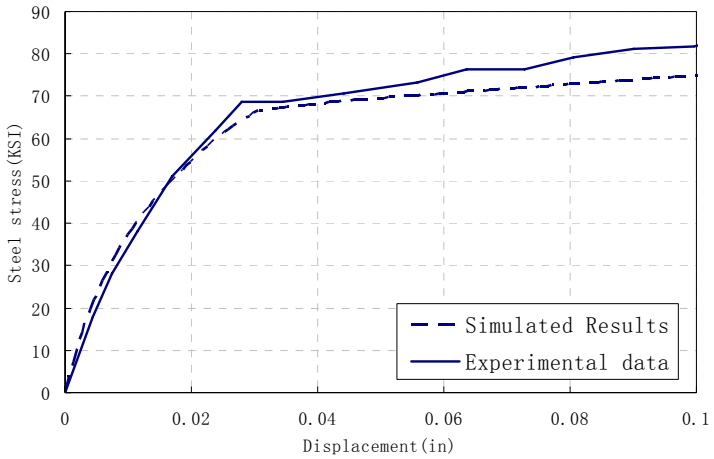

Figure 3-24 Steel stress v.s displacement comparison between experiment and analysis

predicted by the analytical simulation generally compares well with the experimental results.

To study the behaviour of push-pull test, strain and stress distributions of steel and bond are presented at three loading states: P=20%F_y, P=70%F_y and P=110%F_y, where P is the pull force at two ends of the specimen and F_y is the yielding strength of reinforcement.

Comparing the left half of specimen in push-pull test, as shown in Figure 3-25 and Figure 3-26, with the specimen in pull-out test, as shown in Figure 3-16 and Figure 3-18, it is found the distribution of steel stress is similar. Both reach maximum at the end near the pull force and zero at the other end. While bond stress distribution differs greatly, bond stress in push-pull test remains high in the whole specimen even where steel stress is zero, as shown in Figure 3-26.

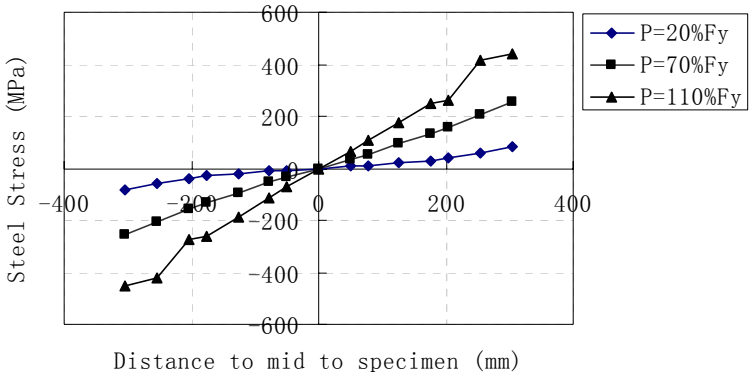

Figure 3-25 Distribution of steel stress along the specimen

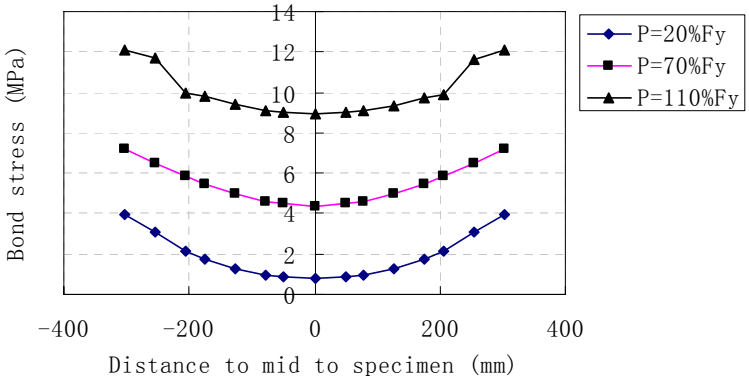

Figure 3-26 Distribution of bond stress along the specimen

3.7.4 Cyclic push-pull test

Viwathanatepa et al (1979) also tested several anchored reinforcing bars subjected to cyclic push-pull test. Detail of the specimen is similar to the one used in monotonic push-pull test. Detailing and modelling of push-pull test is shown in Figure 3-27. Steel stress-slip curve before the yielding of reinforcement in the analysis and experiment are shown respectively in Figure 3-28 and Figure 3-29. Steel stress-slip curve after the yielding of reinforcement in the analysis and experiment are shown respectively in Figure 3-30 and Figure 3-31, respectively.

From the comparison, it is found that the analytical simulation can model the pinching shape of cyclic curve before severe bond deterioration occurs, and it can also model the part that friction dominates after severe bond deterioration occurs.

The decreased envelope due to undergoing several cyclic loads can also be modelled by the analytical simulation. The reduction of peak stress is not obvious before yielding, while after yielding, the reduction is quite obvious, which are both reflected by experiment and analytical simulation.

Five loading states are used to show the distributions of steel stress and bond stress at different loading states. These five loading states are shown in Figure 3-32. State 1 represents the state of current maximum loading displacement, state 2 for the state of half current maximum loading displacement, state 3 for zero displacement state, state 4 for the state of half current minimum loading displacement and state 5 for the state of current minimum loading displacement.

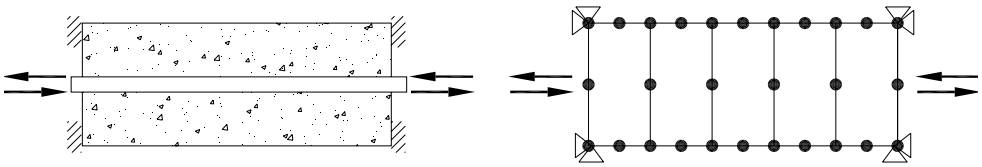

Figure 3-27 Detailing and modelling of cyclic push-pull test

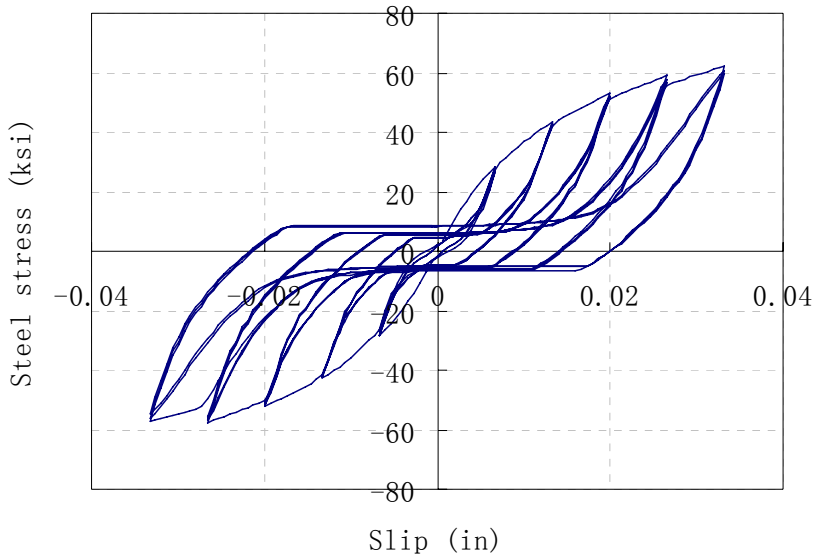

Figure 3-28 Analytical results of stress-slip response of anchored reinforcement under cyclic push-pull test before yielding of reinforcement.

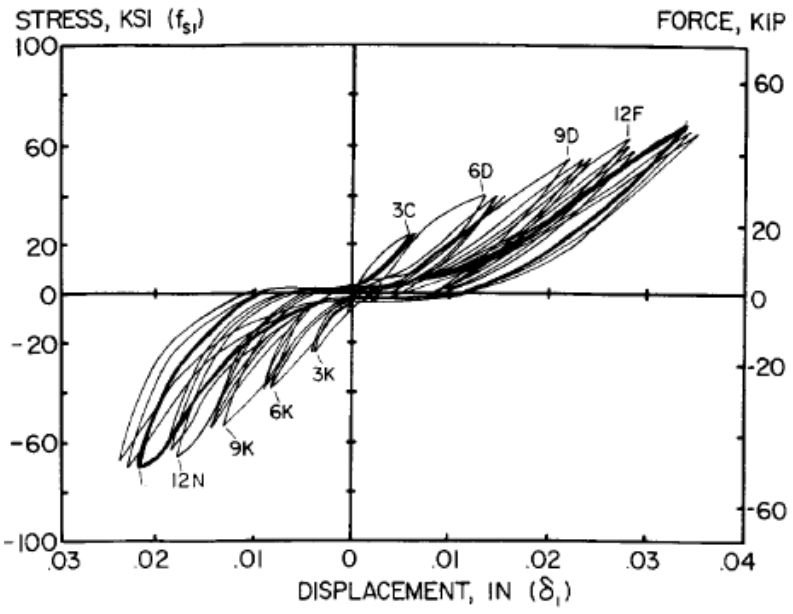

Figure 3-29 Experimental results of stress-slip response of anchored reinforcement under cyclic push-pull test before yielding of reinforcement.

(Viwathanatepa et al, 1979)

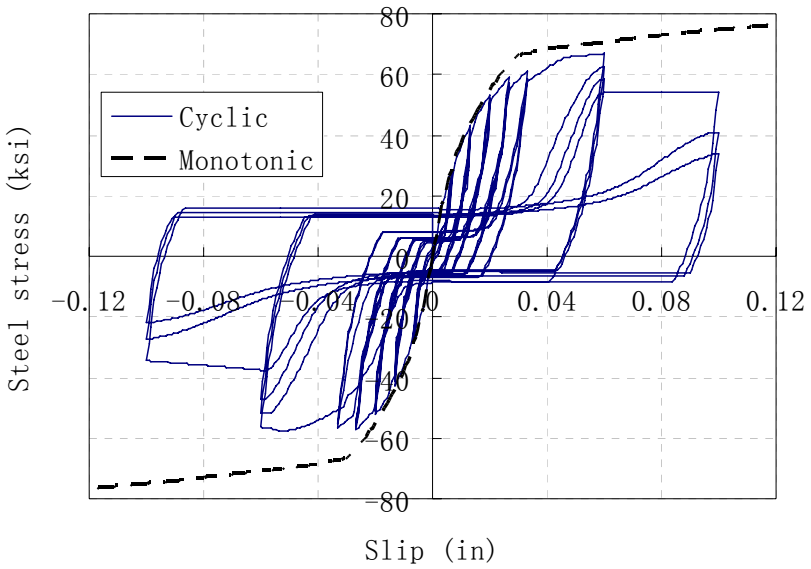

Figure 3-30 Analytical results of stress-slip response of anchored reinforcing bar under cyclic push-pull test after yielding of reinforcement

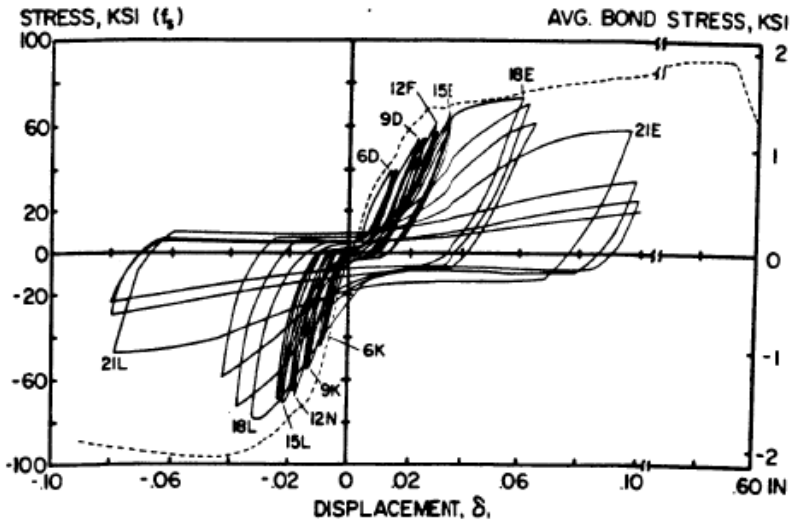

Figure 3-31 Experimental results of stress-slip response of anchored reinforcement under cyclic push-pull test after yielding of reinforcement (Viwathanatepa et al, 1979)

These five states are shown in the relationship between steel stress and slip at the end, as seen in Figure 3-33. Strain and stress distributions of steel and bond on these five states are shown in Figure 3-34 to Figure 3-37.

From Figure 3-33, it is observed that steel stress at the end reaches current maximum and current minimum in state 1 and state 5 respectively, while in state 2, 3 and 4, steel stress at the end of specimen stays low. The steel stress in the middle of the specimen at any loading state remains zero because of the symmetry of steel

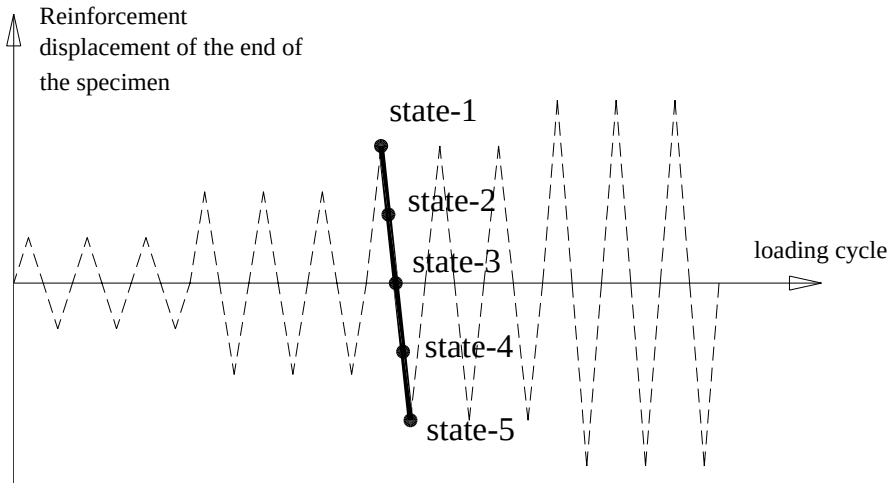

Figure 3-32 Five states from loading to unloading and reloading states

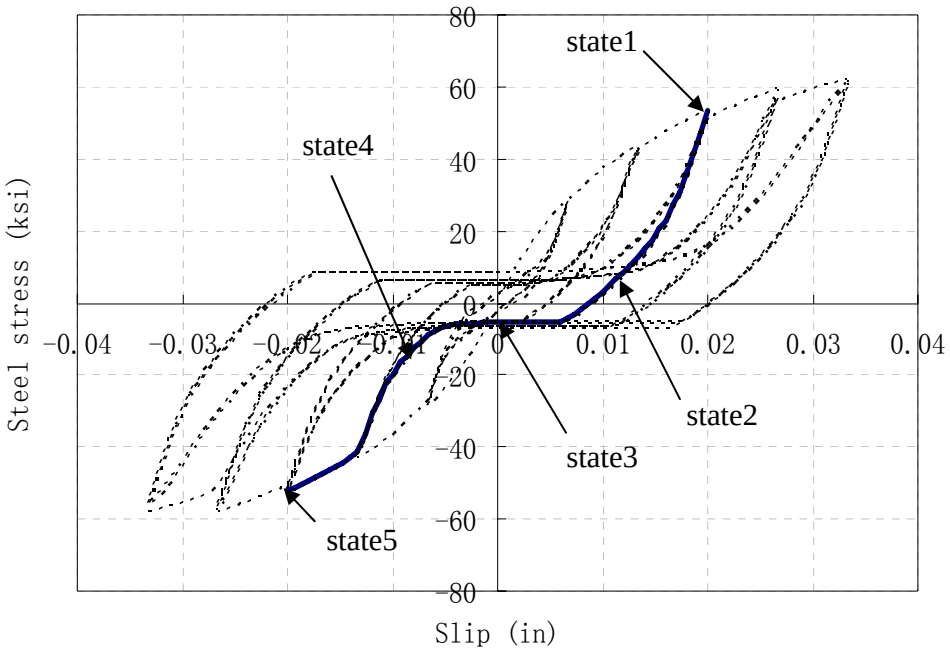

Figure 3-33 Five states from current maximum to current minimum in steel stress-slip relationship

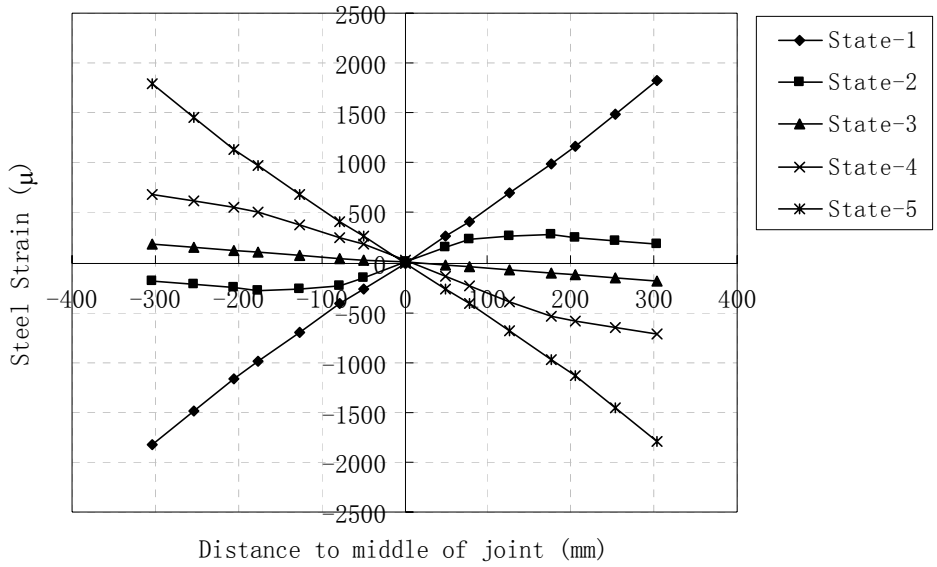

Figure 3-34 Distribution of steel strain along the specimen

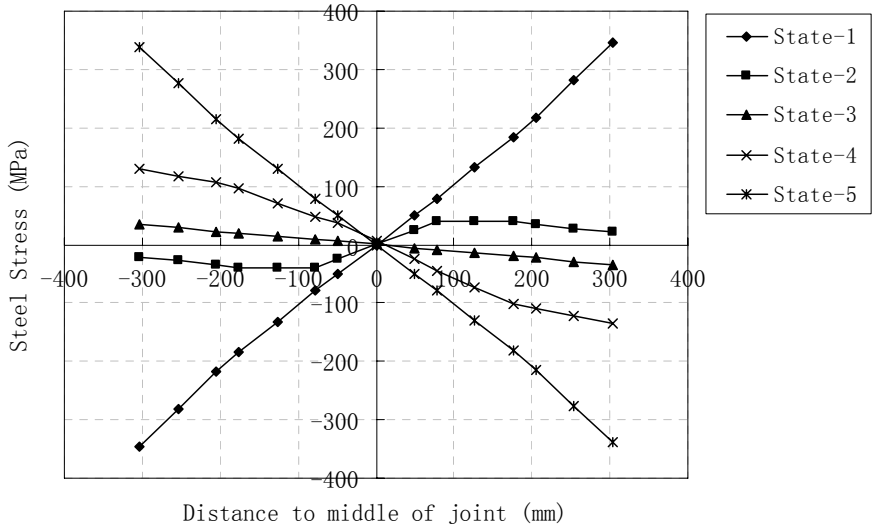

Figure 3-35 Distribution of steel stress along the specimen

stress in the specimen. These characteristics of steel stain and stress at two ends and the middle of the specimen can also be found in Figure 3-34 to Figure 3-35.

From Figure 3-33, it is observed that bond slip at the end reaches current maximum and current minimum in state 1 and state 5 respectively, while in state 2 and 4, bond slip at the end stays at half of current maximum and current minimum. From cyclic

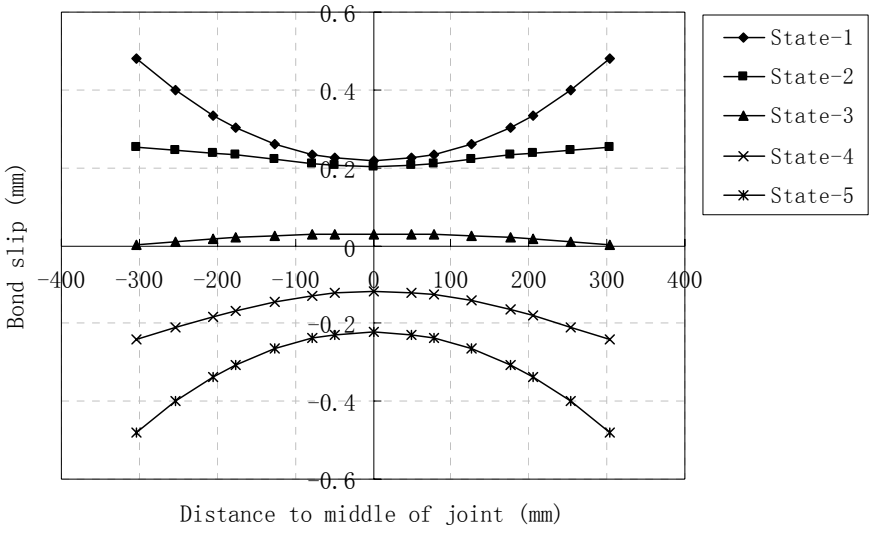

Figure 3-36 Distribution of bond slip along the specimen

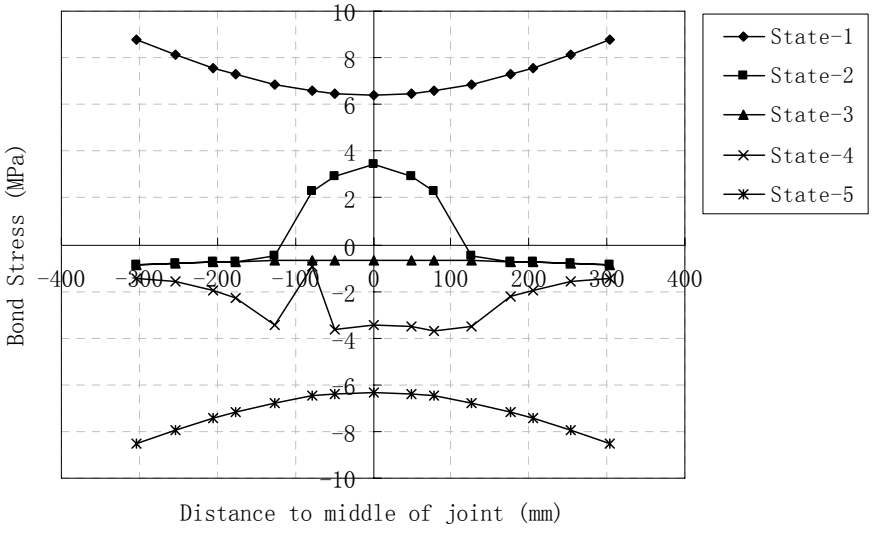

Figure 3-37 Distribution of bond stress along the specimen

rules for bond stress-bond slip relationship, as seen in Figure 2-18, when bond slip unloads to half maximum slip or reloads to half minimum slip (state 2 or state 4), bond stress at state 2 or state4 is in the friction branch, where bond stress is relatively low. These characteristics of bond slip and stress at two ends of the specimens can be found from Figure 3-36 and Figure 3-37. As for bond stress in the

middle of specimen in state 2 or state 4, because bond slip remains high compared with its peak, bond stress is still in the steep unloading branch, where bond stress is relatively high compared with bond stress at the end. This causes bond stress in the middle part drop only a little compared with sudden drop of bond stress at the end parts in state 2 or state 4. These characteristics of bond slip and stress in the middle of the specimens can be found from Figure 3-36 and Figure 3-37.

3.7.5 Effect of the number of element

The specimen S61 in pull-out test by Ueda et al (1986) is taken to study the efficiency of double-panel element. Detail of the specimen S61 can be referred to Table 3-1. Two different meshes are used in the modelling of pull-out test as shown in Figure 3-38. The specimen is modelled by 4 elements and 9 elements separately to see the effect of element number.

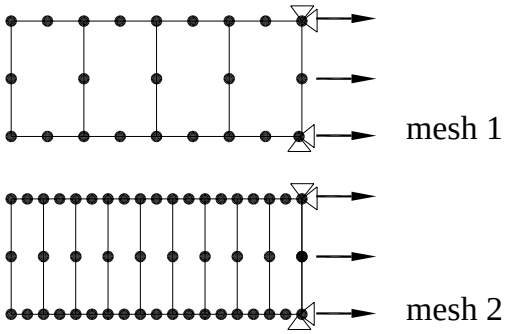

Figure 3-38 Two different meshes for pull-out test

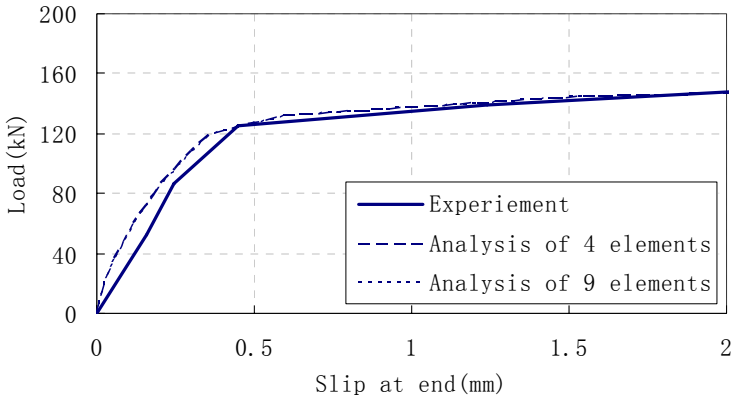

Figure 3-39 Comparison of analysis from two different meshes

The load-slip curve from two meshes is compared and shown in Figure 3-39. From the results, it is found that 4 elements are enough to simulate the case.

3.8 Conclusion

To describe bond-slip behaviour in a panel element, a new double-panel element combining concrete panel, reinforcement panel and bond interface is introduced. The double-panel element has 16 nodes with 8 nodes representing concrete panel and another 8 nodes representing steel panel. Bond effect is incorporated between concrete and reinforcement panels.

The stiffness matrix of the new double-panel element is developed in this chapter based on equilibrium forces in reinforcement and concrete, respectively. The analysis of concrete and reinforcement panels is based on fixed-cracked angle theory, and the local monotonic and cyclic bond slip behaviour is based on Eligehausen et al's (1983) model, except the reloading part is modified to better reflect the experimental results. The model is implemented in finite element program WCOMD, and verifications are done on monotonic pull-out test, axial tension test, push-pull test and cyclic push-pull test. From the comparisons, it is shown that the newly developed double-panel element can generally simulate the bond-slip behaviour well. The efficiency of double-panel element shows that a few elements are enough to simulate the pull-out test.

CHAPTER 4 MODELLING AND INVESTIGATION OF BEAM-COLUMN JOINTS SUBJECTED TO LATERAL LOADS

4.1 Introduction

As reviewed in chapter 2, there are two important behaviour in gravity-load-designed (GLD) beam-column joints subjected to lateral loads; they are shear and bond behaviour. So, it is very important to be able to accurately model these two behaviour in the analysis of GLD beam-column joints subjected to lateral loads.

Currently several finite element programs can describe 2D shear behaviour in cracked reinforced concrete accurately. WCOMD is one of them that can accurately predict the nonlinear behaviour of reinforced concrete. It was developed by the Concrete Laboratory at the University of Tokyo for 2D non-linear static and dynamic analysis of reinforced concrete structures. Fixed-crack angle theory is implemented in the program. WCOMD uses constitutive models based on the results achieved through numerous experiments and theoretical verifications.

The good match between WCOMD analytical results and experimental data in several shear panels subjected to cyclic shear loading has been shown (Maekawa et al, 2003), however, bond-slip behaviour between concrete and reinforcement was not modelled in WCOMD. A newly developed double-panel element will be applied to simulate the bond-slip behaviour in the analysis of beam-column joints. The accuracy and efficiency of the new element have been shown in chapter 3 through the analytical simulation on pull-out, axial tension and push-pull tests under both monotonic and cyclic loading. Combining the capability of modelling the shear and bond behaviour, the new double-panel element will be able to model beam-column joints better.

In this study, the newly developed double-panel element is implemented in WCOMD as one of its elements. It uses the same subroutines of input, nonlinear solver and output in WCOMD to read data files, solve nonlinear equations and write output files. Geometric modelling, model discretization and visualization of results

are done by a universal, adaptive and graphic user interface software GID.

Concrete and reinforcement constitutive models of the double-panel element are based on the constitutive models in WCOMD. Bond constitutive models of the double-panel element are based on Eligehausen's model. Some constitutive models are modified in order to include the special characteristics of the GLD beam-column joint subjected to lateral loads. After that, the effect of mesh size and the number of double-panel element are studied to get good results with less computer time. Loading and boundary conditions are modelled as close as the reality. Finally, several experimental data are collected and analysed using the newly developed double-panel elements.

4.2 Constitutive models

General description of the newly developed double-panel element is presented in chapter 3. And governing equations are expressed in Eq. (3-45). Constitutive models used in the double-panel element such as uniaxial concrete tension and compression model, shear concrete model, reinforcement model and bond model have been reviewed in chapter 2, and in this chapter, some of the constitutive models need to be modified due to special characteristic behaviour of the GLD beam-column joints subjected to lateral loads.

4.2.1 Concrete compression model

The pre-peak curve of stress-strain relationships is based on elasto-plastic and fracture model. When crack occurs in concrete, effective concrete strength will be reduced to consider the effect of crack in the orthogonal direction. In this model, compressive stress in cracked concrete is expressed in terms of total strain, plastic strain, fracture parameter and strength reduction factor. The compressive concrete model before peak stress is expressed in Eq. (2-14).

The post-peak curve of stress-strain relationships can be quite different depending on the type of concrete, amount of confinement and the applied load. Confinement will influence the slope of descending part as shown in Figure 4-1. It was observed by Hsu (Wang and Hsu, 2001) that there is a long plateau after peak point in the strain-control tests of panels using servo-control system. To describe this

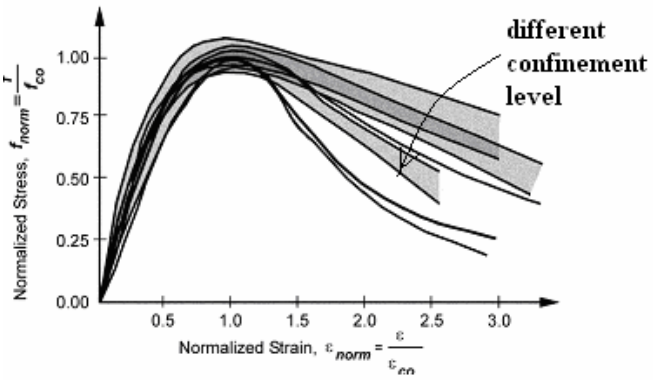

Figure 4-1 Normalized stress-strain relationship on different confinement (Lowes, 1999)

phenomenon, they replace a constant parameter 2 in the denominator of Eq. (4-1) by a constant parameter 4.

$$\sigma_2 = \zeta f_c^{'}\left[1-\left(\frac{\varepsilon_2/\zeta\varepsilon_0 - 1}{2/\zeta - 1}\right)^2\right] \quad \text{for} \quad \varepsilon_2/\zeta\varepsilon_0 > 1 \tag{4-1}$$

where

ζ is softening coefficient

ε_0 is concrete strain at maximum compressive stress

Considering possible factors to make the descending part of concrete compression stress-strain relationship gentler, the post-peak concrete compression model can be written in Eq. (4-2). Because no reduction on strain at peak stress in Okamura and Maekawa's model (1991), $\varepsilon_2/\varepsilon_0$ is used instead of $\varepsilon_2/\zeta\varepsilon_0$, and *k* is used instead $2/\zeta$ in the double-panel element for continuity of pre-peak and post-peak concrete compression curve.

The residual strength is assumed as 20% of peak stress in the post-peak concrete compression model, and can be written as in Eq. (4-3).

$$\sigma_2 = \zeta f_c^{'}\left[1-\left(\frac{\varepsilon_2/\varepsilon_0 - 1}{k-1}\right)^2\right] \quad \text{for} \quad 1 < \varepsilon_2/\varepsilon_0 \le 1+\sqrt{0.8}(k-1) \tag{4-2}$$

$$\sigma_2 = 0.2\zeta f_c^{'} \quad \text{for} \quad \varepsilon_2/\varepsilon_0 > 1+\sqrt{0.8}(k-1) \tag{4-3}$$

where *k* to be verified by experimental data

4.2.2 Concrete tension model

The relationship between average concrete stress and average concrete strain after cracking is expressed in Eq. (2-16).

4.2.3 Concrete shear model

The shear transfer model of cracked concrete is based on the contact density theory (Maekawa et al, 2003). In this model, the rough crack surface is idealized as a set of numerous infinitesimal contact units having various inclinations. The simplified shear transfer model is given in Eq. (2-17).

Nguyen (2005) found that, the shear transfer strength f_{st} in Okamura and Maekawa's model (1991) does not include the effect of reinforcement ratio and the yield strength of reinforcement. When reinforcement ratio is low, the shear transfer strength f_{st} in Okamura and Maekawa's model (1991) will be overestimated. He proposed an empirical formula, which gave more accurate prediction in shear panel problems.

$$f_{st} = c_1 \cdot \left(\rho \cdot f_y\right)^{c_2} \tag{4-4}$$

where

$$c_1 = 0.822 \cdot f_c^{\,0.406}$$

$$c_2 = 0.159 \cdot f_c^{\,0.303}$$

In beam-column joints, especially in gravity-load-designed beam-column joints, there is no shear reinforcement or the amount of shear reinforcement is nominal in the joint core. When the load increases or reverses, the principal plane does not always coincide with the cracks coordinate. In this case, shear transfer model plays an important role in simulating the GLD joints subjected to lateral loads, especially under reversed cyclic loads. The accuracy of the joint simulation will be affected by the accuracy of shear transfer model, especially when there is no reinforcement or when reinforcement ratio is low. In this case, the original shear transfer strength was modified according to Nguyen's proposed formula. The shear transfer model is expressed as

$$\tau_{st} = f_{st} \frac{\beta^2}{\beta^2 + 1} \tag{4-5}$$

where

f_{st} is the shear transfer strength proposed by Nguyen (2005)

β is normalized shear strain, $\beta = \gamma_{cr} / \varepsilon_t$

γ_{cr} is shear strain due to crack

ε_t is tensile strain normal to crack

4.2.4 Reinforcement model

The modelling of the reinforcing bar in concrete is based on the properties of the bar and the effect of bonding between bar and concrete. The average yield stress proposed by Salem (Salem and Maekawa, 1999) can be written as in Eq. (2-18).

The post-yield stiffness, proposed by Shima and Okamura (Shima et al, 1987), is expressed in terms of yield stress of plain bar, average yield stress, bond properties of the bar, the strength of concrete, difference in steel ratio in two directions and the angle between the crack and bar axis. The post-yield stiffness is expressed in Eq. (2-19).

4.2.5 Bond model

As reviewed in chapter 2, Eligehausen et al's bond model (Eligehausen et al, 1983) is one of the most widely used bond models (Figure 2-17). Ascending part can be expressed as in Eq. (2-31). Characteristic values of monotonic envelope of the model are described in Table 2-1. In this model, initially the bond stress increases with the increment of slip and after it reaches the peak, bond stress will drop due to loss of bearing resistance. Initial stiffness of bond stress-slip curve was quite large and gradually will drop due to the loss of chemical adhesion. These characteristics agree well with the mechanism of bond. Bond stress is also affected by the following factors and modification should be done to take into account their effects.

1. Effect of concrete strength and diameter of reinforcement

   Considering the influencing factors of concrete strength and diameter of reinforcement, Soroushian et al (1988 and 1991) modified peak value of Eligehausen's model as shown in Eq. (2-32).

2. Effect of steel strain

   Okamura and Maekawa (1991) observed from the experiments that the

bond-slip relationship in the pull-out test with long embedded length is different from that in the extremely short embedded length and bond stress deteriorates much when reinforcement yields. Through this observation, they included the effect of steel strain into bond-slip relationship.

$$\tau(\varepsilon, s) = \tau_0(s) g(\varepsilon) \tag{4-6}$$

where

$\tau_0(s)$ is bond stress when strain is zero

$g(\varepsilon)$ is a function of steel strain, $g(\varepsilon) = \dfrac{1}{1+10^5 \varepsilon}$

ε is strain of a bar

3. Effect of bond deterioration due to crack

Ueda and Sato (2002) found that the deterioration of bond near the section where crack occurs affected the tension stiffness of concrete and needed to be considered in predicting the tension stiffness of concrete. Their study on bond behaviour in cracked concrete was based on a discrete model. When an unbonded zone of 2.5D (D: bar diameter) was considered at both sides of the cracked section in their analysis, good match with experimental data can be obtained.

In the smeared crack model, local crack is not considered explicitly. The effect of crack has to be expressed as function of tensile strain. For simplicity, a function as written in Eq. (4-7) is taken to consider the effect of bond deterioration due to crack.

$$h(\varepsilon_c) = \frac{1}{1+m\varepsilon_c} \tag{4-7}$$

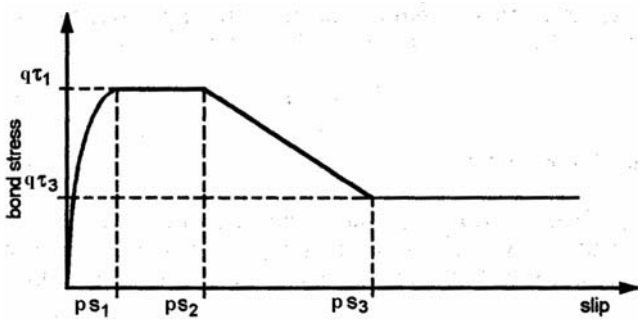

Figure 4-2 Analytical model for local bond stress-slip relationship

where

m is determined through verifications on axial tension test

ε_c is the average concrete tensile strain due to cracks

As seen from Figure 2-15, when bond strength is reduced due to crack or unconfinement, initial stiffness will not change, but slip at the peak stress will be less. Therefore, the effect of bond deterioration due to crack is reflected not only on peak bond stress, but also on slip at the peak bond stress. In the bond model, it is assumed that the initial stiffness of bond stress-slip curve with reduced peak stress does not change.

The original Eligehausen et al's bond model (1983) was modified based on the factors mentioned. The modified relationship between bond stress and bond slip is shown in Figure 4-2. τ_1 and τ_3 are characteristic bond stress, and s_1, s_2 and s_3 are original characteristic bond slip. p is the reduction factor for characteristic slip due to reduction in bond slip. Reduction factor p can be calculated from Eq. (4-8).

$$p = \exp\left(\log\left(\frac{1}{1+m\varepsilon_c} \right) \Big/ 0.4 \right) \tag{4-8}$$

where

m is determined through verifications on axial tension test

ε_c is the average concrete tensile strain due to cracks

q is the reduction factor for characteristic bond stress due to reduction in bond stress. Reduction factor q can be calculated from. (4-9).

$$q = g(\varepsilon_s)h(\varepsilon_c) \tag{4-9}$$

where

$g(\varepsilon_s)$ is a function of steel strain, $g(\varepsilon_s) = \dfrac{1}{1+10^5\varepsilon_s}$

$h(\varepsilon_c)$ is a function of tensile strain of concrete, $h(\varepsilon_c) = \dfrac{1}{1+m\varepsilon_c}$

4.2.6 Comparison on the analytical results by using different concrete compression models

Firstly, Okamura and Maekawa's model (1991) is selected as the concrete compressive model both before and after peak and is expressed in Eq. (2-1). The accuracy of the model is checked through comparison with experimental results of specimen C1B (Yin, 2001) as shown in Figure 4-3. Specimen C1B is a beam-column joint subjected to lateral loads. It is fixed at the column ends, and opposite vertical loads are applied at the two beam ends. Details of specimen C1B are given in Table 4-1.

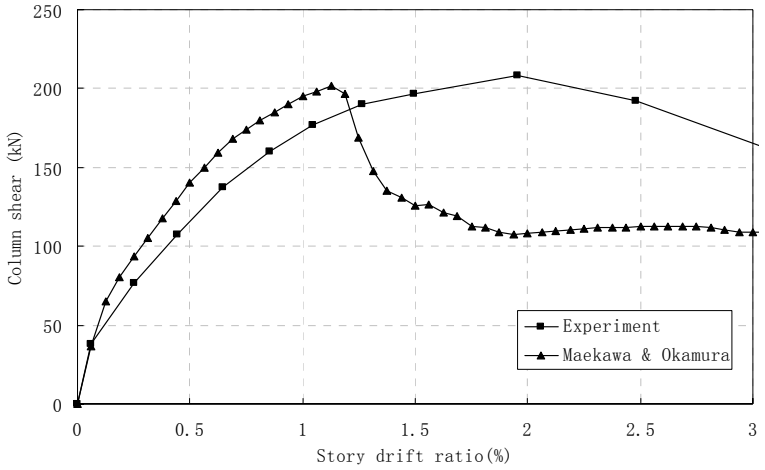

Figure 4-3 Story drift ratio v.s. column shear on specimen C1B with original Maekawa & Okamura's model

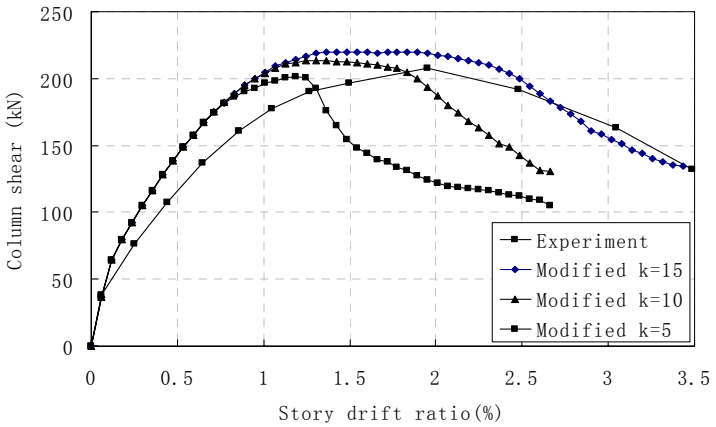

Figure 4-4 Story drift ratio v.s. column shear on specimen C1B with modified compressive models

From Figure 4-3, it is found that the Okamura and Maekawa's model (1991) gives a relatively good prediction on peak value of column shear, but after peak, the curve drops very significantly. When post-peak curve of compression concrete is made relatively flat, as what was proposed by Wang and Hsu (2001), the simulated relationship between column shear and story drift ratio is improved as shown in Figure 4-4.

Another possible reason to make post-peak curve relatively flat is the good confinement of joint core. For joints without transverse beams or horizontal shear reinforcement, confinement can be obtained from adjacent members. The compression force in the diagonal strut in the joint is from the compression forces in the adjacent members, which are in horizontal or vertical directions. These compression forces in the adjacent members can be decomposed into the forces along and orthogonal to diagonal direction. The forces orthogonal to the diagonal direction contribute to the effect of confinement on the diagonal strut.

Based on that, the modification of post-peak curve of concrete compression stress-strain relationship is necessary. The post-peak curve of stress-strain relationship will be modified according to Eq. (4-2).

Different value of k was tried, and the simulated results are compared with experimental results in Figure 4-4. With the increment of k, the relationship between column shear and story drift ratio around the peak tends to be flat. Among these three simulated curves, curve with $k=15$ matches best the experimental data. So, constant value of k is taken as 15 in Eq. (4-2).

4.2.7 Comparison on bond models

Crack has been found to affect bond behaviour and a factor has been introduced to take into account this effect as given in Eq. (4-7). Constant parameter m in Eqs. (4-8) and (4-9) is taken as 0, 500 and 1000, and simulated results based on that are compared with axial tension test data by Doerr (Keuser and Mehlhorn, 1987). Details of the specimen have been mentioned in chapter 3.

Modelling of the axial tension test is shown in Figure 3-19. Comparison between experimental and simulated results of bar force distribution in half of the specimen is shown in Figure 4-5. Because of symmetry, only half of the results are shown.

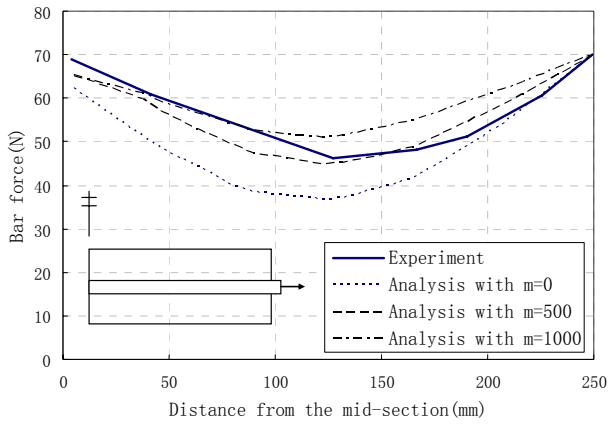

Figure 4-5 Comparison of bar force distribution between experiment and analysis

When constant parameter *m* is taken as 0, there is no reduction in the bond stress due to crack. Hence, bond stress is the largest. From the equilibrium equation of steel bar Eq. (3-1), the larger the bond stress $\tau(x)$, the larger steel stress difference is expected. Consequently, smaller bar force at quartered point will be obtained. Therefore, bar force distribution with *m* is equal to 0 is the lowest. Compared with experimental results, bar force distribution with *m* is equal to 500 is considered the best and will be used in the bond model.

4.3 Selection of mesh size and the extension of double-panel element used in the adjacent members

4.3.1 Selection of mesh size

From observations in the experiments, strain and stress varies in the joint area which is geometrically relatively smaller compared with its adjacent members such as beams and column. It is important to find out the number of elements which will be sufficient to simulate the complex behaviour of the GLD beam-column joint subjected to the lateral loads. Comparisons are done between two different meshes of specimen C1B. In the coarse mesh model, a joint is modelled by 4×4 elements for the analysis of beam-column joint, while 6×8 elements are used in the fine mesh model as shown in Figure 4-6.

From the comparison in Figure 4-7, it is found that mesh size does not affect the results very much. To save computer time, a relatively coarse mesh of joint with 4×4 elements is adopted for the analytical simulation.

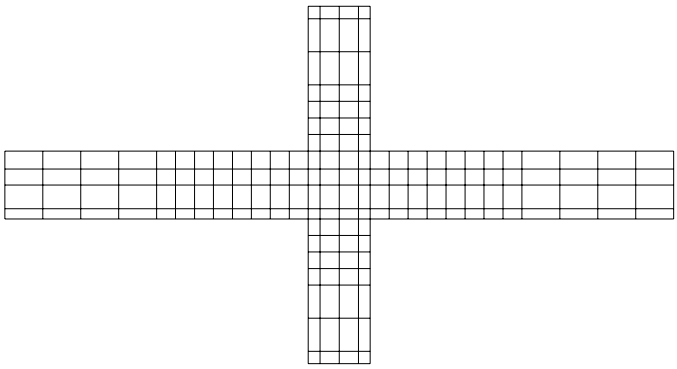

(a) Joint modelled by 4×4 elements (coarse mesh model)

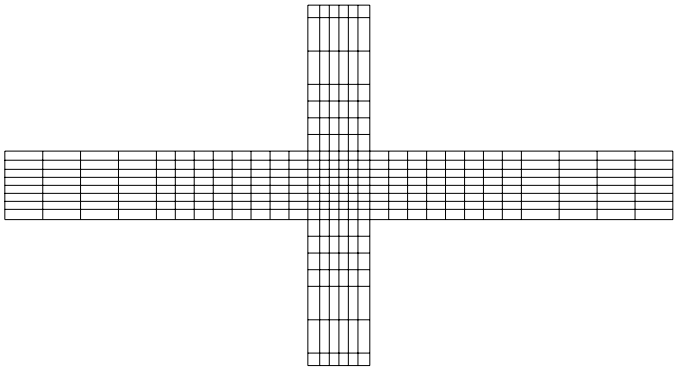

(b) Joint modelled by 6×8 elements (fine mesh model)

Figure 4-6 Mesh of specimen C1B

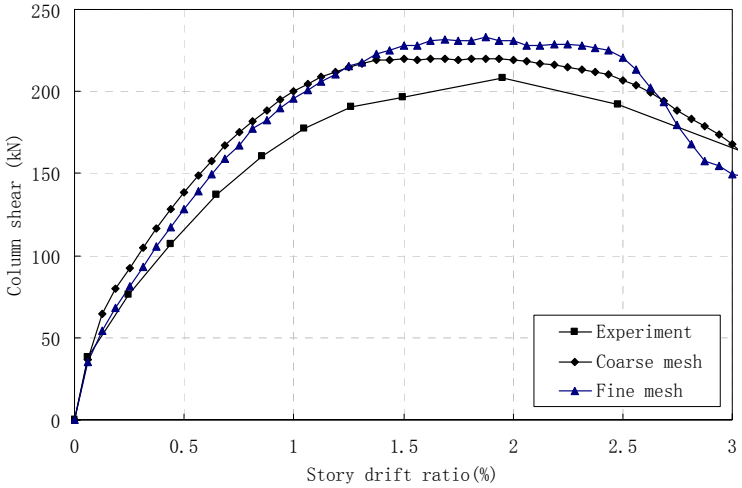

Figure 4-7 Comparison of analytical results with coarse and fine mesh models

4.3.2 Extension of double-panel elements used in adjacent members

The advantage of double-panel element compared with normal panel element is in its capacity to simulate the bond behaviour, while the disadvantage is more computer time needed for the analysis. In places where bond deterioration is severe, double-panel elements has to be used, while in other places where bond deterioration is negligible, normal panel elements should be used to save the computer time. In between these two, transition elements can be utilised.

To find out the extent of the application of double-panel elements in the joint and adjacent members to describe the behaviour of GLD beam-column joints subjected to lateral loads, comparison with different extension of double-panel elements used to model adjacent members is carried out. Joints with different extent of adjacent members are simulated with double-panel element. The adjacent members simulated with double-panel elements range from 0 to the full length of members as shown in Figure 4-8. In the finite element meshes, the dark areas represent double-panel elements and transition elements. Transition elements are located at the end of the dark areas of adjacent members. Comparison of analytical results with different extent of the application of double-panel element and perfect bond is shown in Figure 4-9.

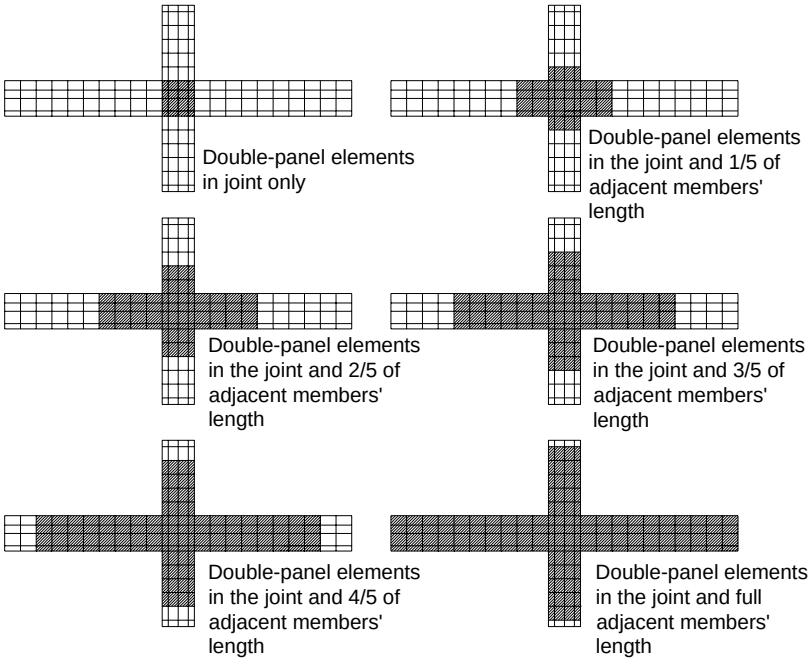

Figure 4-8 Different mesh method of specimen C1B

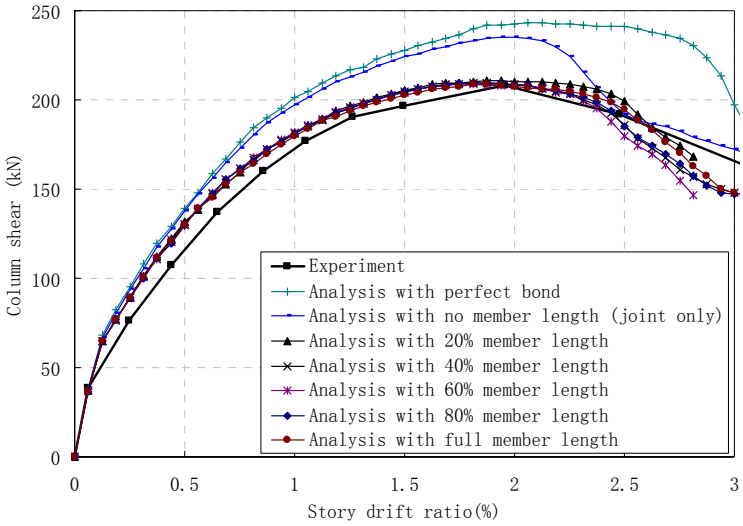

Figure 4-9 Results comparison on specimen C1B with different mesh method

When severe bond deterioration area was not modelled by double-panel elements, joint strength from analytical simulation will be larger than the experimental result, which is reflected by analysis with perfect bond and the analysis with no adjacent members were modelled with double-panel element in Figure 4-9. Other curves are all close to the experimental result. Therefore, only the joint and 20% length of the adjacent member length modelled with double-panel elements and transition elements will be used in the subsequent analysis.

4.4 Modelling of load and boundary conditions

There are two kinds of load applied to the GLD beam-column joint subjected to lateral loads. One is the opposite vertical loads at beam ends and the other is the axial load at the column end. To obtain the descending part of load-deflection curve, displacement control method should be used in the finite element method. However, if the axial load at the column end is simulated through fixed displacement at the column end, the axial force in the column will not remain constant with the increment of the loads at the beam ends. In specimen C1A by Yin (2001), the applied axial load is 600 kN, and the fluctuation of axial force is shown in Figure 4-10. Unless the axial force is accurately added and described, the effect of axial force on the strength of joint can not be accurately simulated. In the experiment, the

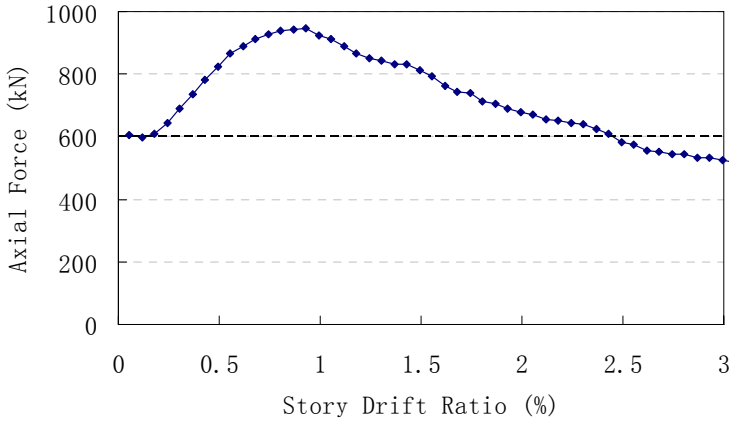

Figure 4-10 Axial force fluctuates with lateral loads

force applied at the column end is necessary to be adjusted to obtain a constant axial force.

In analytical simulation, axial load is applied through force control method, while the loads at the beam ends is applied through displacement control to simulate the post-peak behaviour of the GLD beam-column joints subjected to lateral loads.

4.5 Comparison of the analytical with experimental results

4.5.1 Details of specimen

Four groups of specimens are selected for the comparison purpose. These 14 specimens were set-up and tested by Yin (2001), Fujii (1991), Hegger (2004) and Teng (2003). All the specimens failed in shear or bond. In the set-up of these specimens, the application of lateral load is applied either at beam ends or at column end as shown in Figure 4-11. Details of the specimens are listed in Table 4-1, and general geometric properties of specimens are shown in Figure 4-12.

In the joint and adjacent members, bond deterioration can occur when the assemblage is subjected to lateral loads. Then, these areas are modelled with double-panel element. Other areas are modelled with normal panel elements. Between these two elements, transitional elements are used. The finite element meshes are shown in Figure 4-13. Axial force is applied at top column end, and vertical displacement is applied at beam ends.

4.5.2 Monotonic load-deflection curve

Comparison of the analytical results is conducted with the experimental results of four groups of specimens. The relationship between column shear force and story drift ratio is shown in Figure 4-14 to Figure 4-17. From the comparison, the analytical results with and without bond slip effect are both shown, and compared with experimental results.

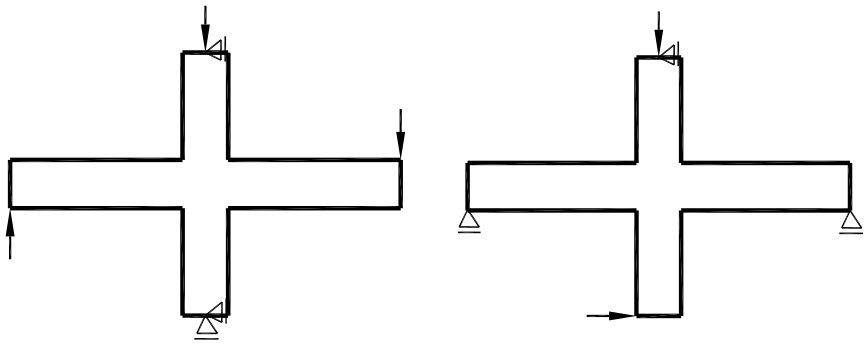

(1) Mode 1 (2) Mode 2

Figure 4-11 Loading modes of beam-column joints subjected to lateral loads

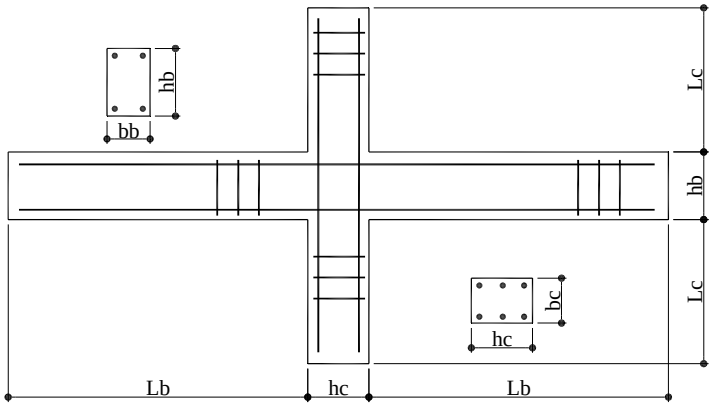

Figure 4-12 Geometric properties of specimens

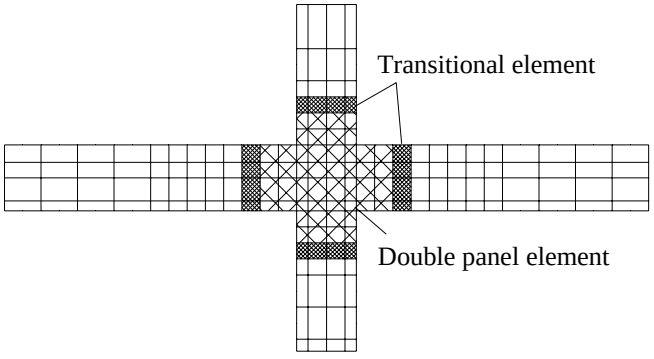

Figure 4-13 Finite element mesh of specimens

Table 4-1 Details of specimens

Specimens		Material property					Geometric property						
		Concrete strength	Beam main bar	Beam shear bar	Column main bar	Column shear bar	Length		Beam section		Column section		Axial load
		fc (MPa)	fyb (MPa)	fybs (MPa)	fyc (MPa)	fycs (MPa)	Lb (mm)	Lc (mm)	bb (mm)	hb (mm)	bc (mm)	hc (mm)	P (kN)
Yin (2001)	**C1B**	23.7	500	380	500	380	2450	1173	300	550	350	500	0
	C1A	23.7	500	380	500	380	2450	1173	300	550	350	500	650
	C4B	23.7	500	380	500	380	2500	1173	300	400	400	400	0
	C4A	23.7	500	380	500	380	2500	1173	300	400	400	400	600
Fujii (1991)	**A1**	41	1090	297	656	297	890	625	160	250	220	220	150
	A2	41	417	297	656	297	890	625	160	250	220	220	150
	A3	41	1090	297	656	297	890	625	160	250	220	220	450
	A4	41	1090	297	656	297	890	625	160	250	220	220	450
Hegger (2004)	**RA2**	66.1	555	555*	555	555*	850	680	150	300	150	240	458
	RA3	43.6	555	555*	555	555*	850	680	150	300	150	240	502
	RA4	66.1	555	555*	555	555*	850	680	150	300	150	240	336
	RA5	56.2	555	555*	555	555*	850	680	150	300	150	240	499
	RA7	79.7	555	555*	555	555*	850	680	150	300	150	240	457
Teng (2003)	**S1**	33	510	530	510	530	1850	1113	200	400	300	400	441

*The yield stress of shear reinforcement in beams and column is not given in the paper.

It is assumed in the analysis to guarantee no shear failure in the beams or columns.

Table 4-1 Details of specimens (continued)

Specimen		Reinforcement Arrangement							Loading Arrangement[1]
		Beam			Column			Joint Horizontal Shear bar	
		Top bar	Bot bar	Shear bar	Side bar	Mid bar	Shear bar		
Yin (2001)	**C1B**	5 ϕ 32	2 ϕ 32	2 ϕ 10@200	2 ϕ 25	2 ϕ 25	3 ϕ 10@150	0	1
	C1A	5 ϕ 32	2 ϕ 32	2 ϕ 10@200	2 ϕ 25	2 ϕ 25	3 ϕ 10@150	0	1
	C4B	6 ϕ 32	3 ϕ 32	2 ϕ 10@200	3 ϕ 25	2 ϕ 25	3 ϕ 10@150	0	1
	C4A	6 ϕ 32	3 ϕ 32	2 ϕ 10@200	3 ϕ 25	2 ϕ 25	3 ϕ 10@150	0	1
Fujii (1991)	**A1**	8 ϕ 10	8 ϕ 10	2 ϕ 10@200[#]	5 ϕ 13	6 ϕ 13	2 ϕ 10@200[#]	3-2 ϕ 6	1
	A2	8 ϕ 10	8 ϕ 10	2 ϕ 10@200[#]	5 ϕ 13	6 ϕ 13	2 ϕ 10@200[#]	3-2 ϕ 6	1
	A3	8 ϕ 10	8 ϕ 10	2 ϕ 10@200[#]	5 ϕ 13	6 ϕ 13	2 ϕ 10@200[#]	3-2 ϕ 6	1
	A4	8 ϕ 10	8 ϕ 10	2 ϕ 10@200[#]	5 ϕ 13	6 ϕ 13	2 ϕ 10@200[#]	4-4 ϕ 6	1
Hegger (2004)	**RA2**	4 ϕ 14	4 ϕ 14	2 ϕ 10@200[#]	4 ϕ 20	0	2 ϕ 10@200[#]	4-2 ϕ 6	1
	RA3	4 ϕ 14+1 ϕ 12	4 ϕ 14+1 ϕ 12	2 ϕ 10@200[#]	4 ϕ 20	0	2 ϕ 10@200[#]	5-2 ϕ 8	1
	RA4	2 ϕ 20+2 ϕ 16	2 ϕ 20+2 ϕ 16	2 ϕ 10@200[#]	2 ϕ 20+3 ϕ 16	0	2 ϕ 10@200[#]	5-2 ϕ 8	1
	RA5	4 ϕ 12+1 ϕ 12	4 ϕ 12+1 ϕ 12	2 ϕ 10@200[#]	4 ϕ 20	0	2 ϕ 10@200[#]	5-2 ϕ 6	1
	RA7	4 ϕ 16+1 ϕ 12	4 ϕ 16+1 ϕ 12	2 ϕ 10@200[#]	4 ϕ 20	0	2 ϕ 10@200[#]	5-2 ϕ 10	1
Teng (2003)	**S1**	5 ϕ 16	3 ϕ 16	2 ϕ 10@200[#]	5 ϕ 20	2 ϕ 20	2 ϕ 10@200[#]	4-3 ϕ 10	2

[1]Loading arrangement is illustrated in Figure 4-11

[#]The amount of shear reinforcement in beams and column is not given in the paper.

It is assumed in the analysis to guarantee no shear failure in the beams or columns.

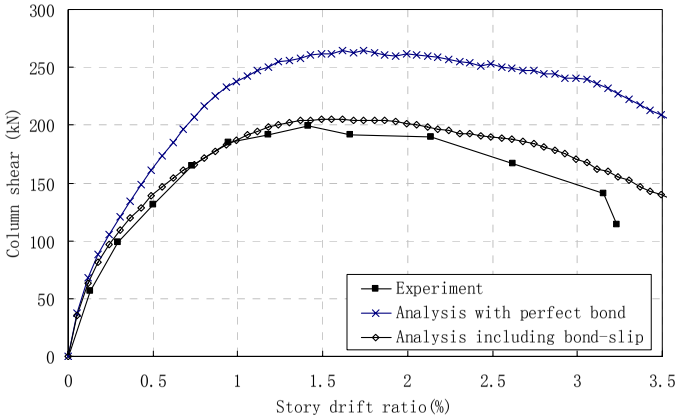

(a) Specimen C1A

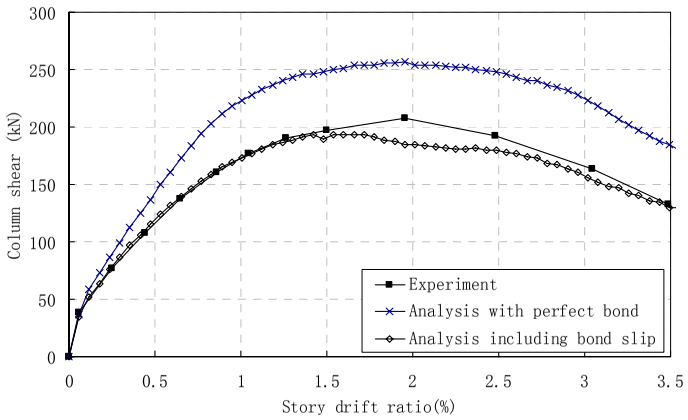

(b) Specimen C1B

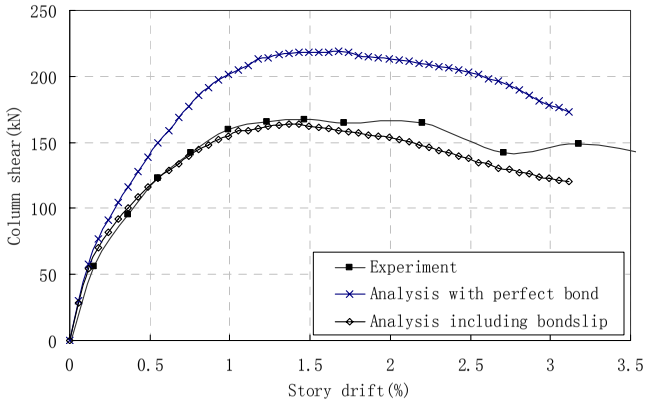

(c) Specimen C4A

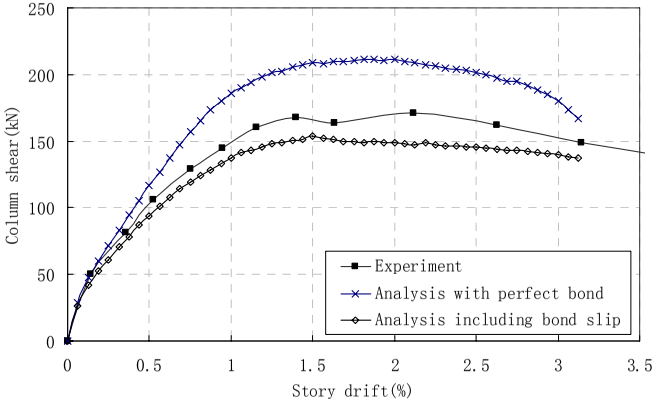

(d) Specimen C4B

Figure 4-14 Comparison of analytical results with Yin's (2001) experimental results

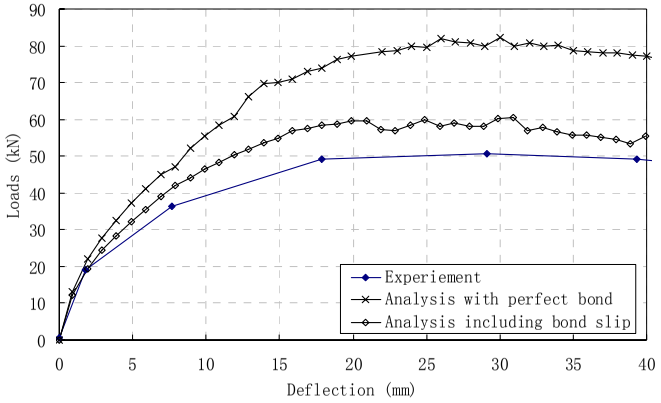

(a) Specimen A1

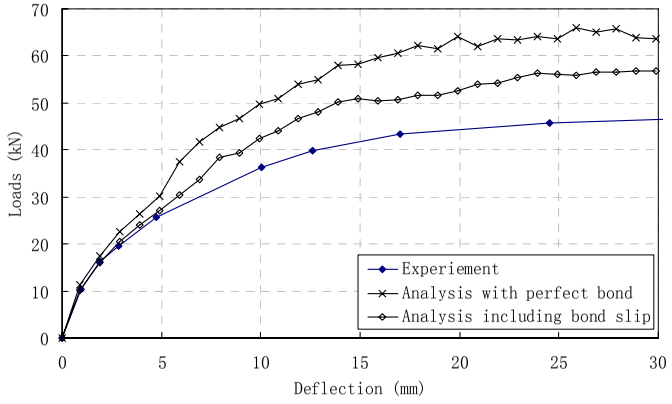

(b) Specimen A2

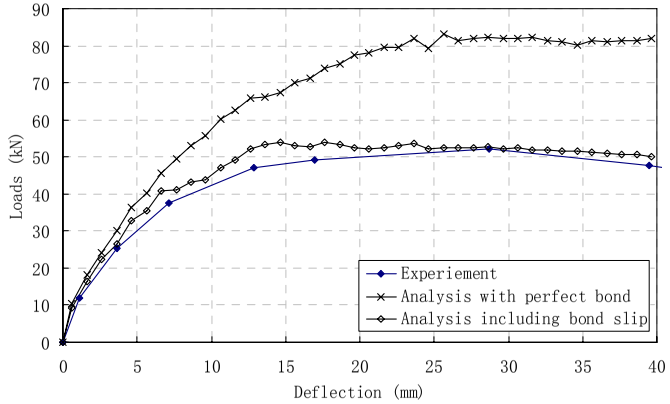

(c) Specimen A3

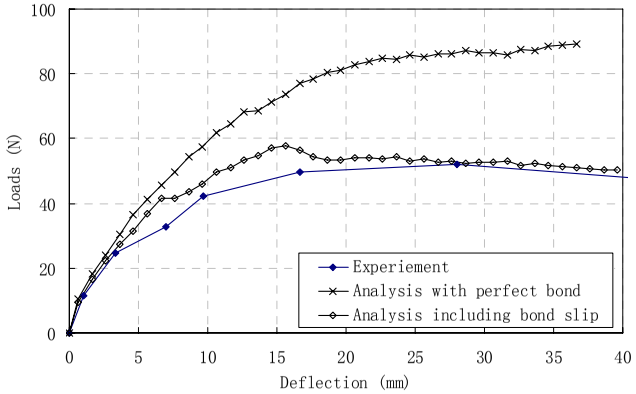

(d) Specimen A4

Figure 4-15 Comparison of analytical results with Fujii's (1991) experimental results

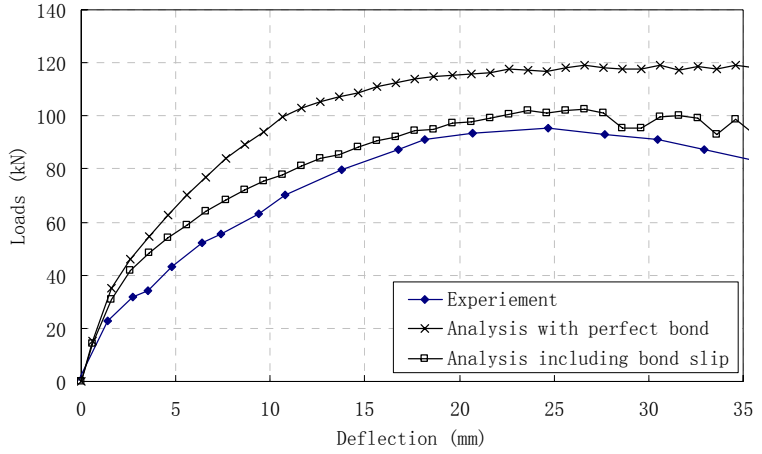

(a) Specimen R2

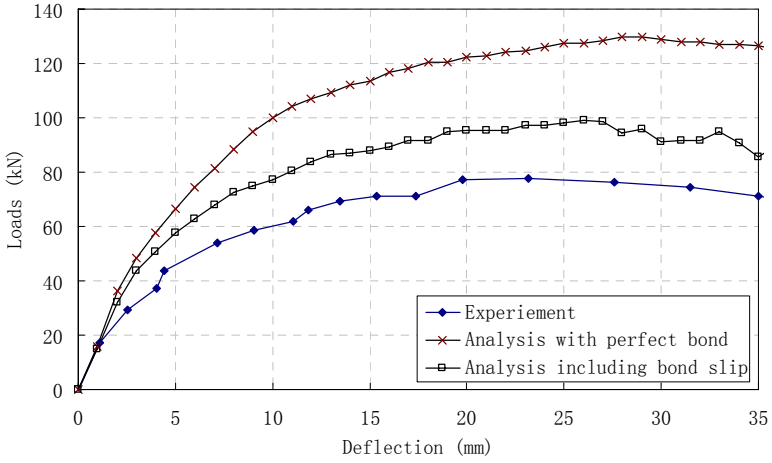

(b) Specimen R3

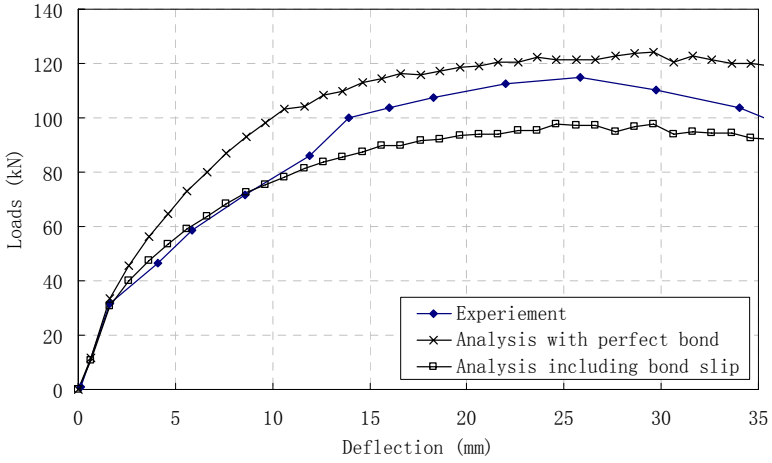

(c) Specimen R4

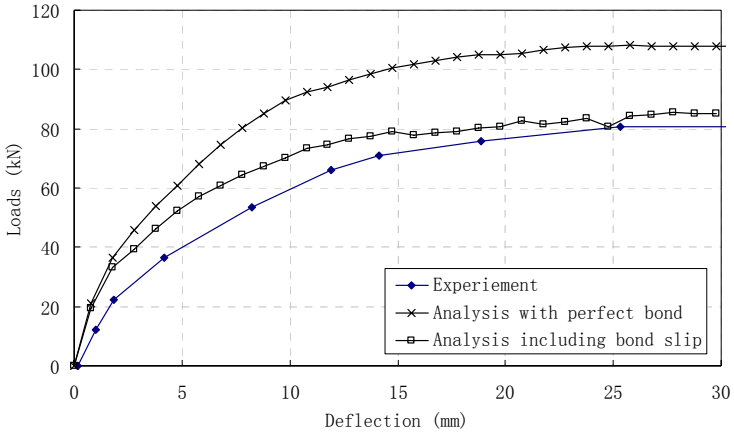

(d) Specimen R5

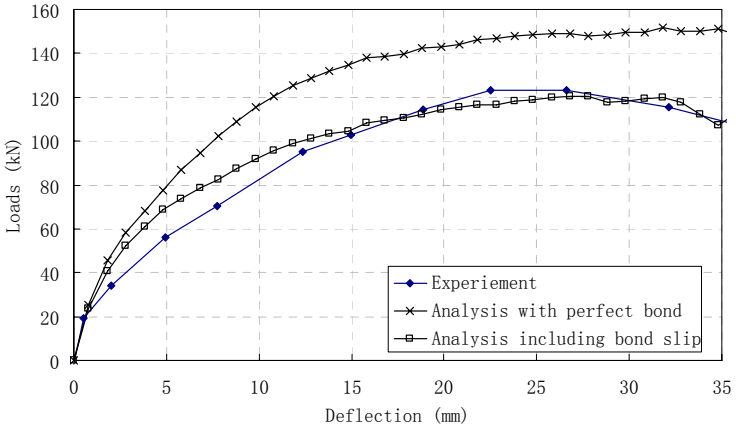

(e) Specimen R7

Figure 4-16 Comparison of analytical results with Hegger's (2004) experimental results

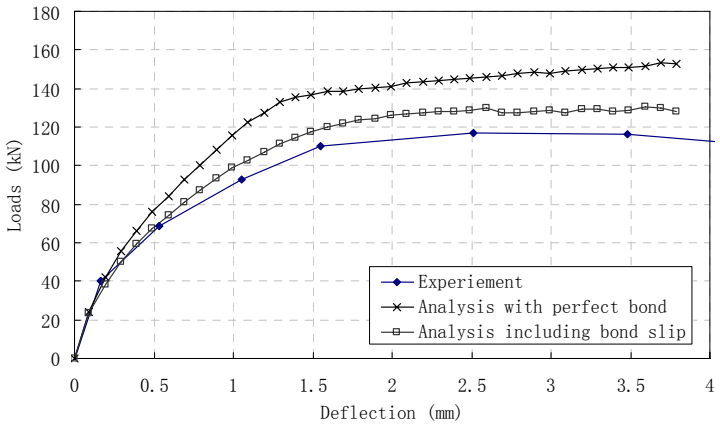

Figure 4-17 Comparison of analytical results with Teng's (2003) experimental results of specimen S1

It is found that the analytical results improve much when bond slip effect is considered, and in most cases, the analytical results with bond-slip modelling generally match the experimental results. It shows the importance of modelling the bond-slip behaviour in the beam-column joint to simulate the behaviour of GLD beam-column joint subjected to lateral loads accurately. The perfect bond analysis will overestimate the shear strength of the beam-column joint subjected to lateral loads.

4.5.3 Cyclic load-deflection curve

The effectiveness and accuracy of the beam-column joint modelling mentioned previously is also scrutinised under reversed cyclic loading. The comparison of analytical and experimental results is conducted by using four specimens of Yin (2001). Details of the specimens are listed in Table 4-1. The opposite vertical loading cycles at two beam ends are shown in Figure 4-18 to simulate the applied reversed cyclic load. The curves of column shear force-story drift ratio for the four specimens are depicted in Figure 4-19 to Figure 4-22.

From the figures, the analytical peak column shear forces are close to experimental results, but the post-peak envelope curves from the analysis descend faster than those from the experiment. Curves of shear load-story drift in experimental and analytical results both give pinching shapes due to shear and bond dominated behaviour. The pinching shape for the experimental results is more obvious.

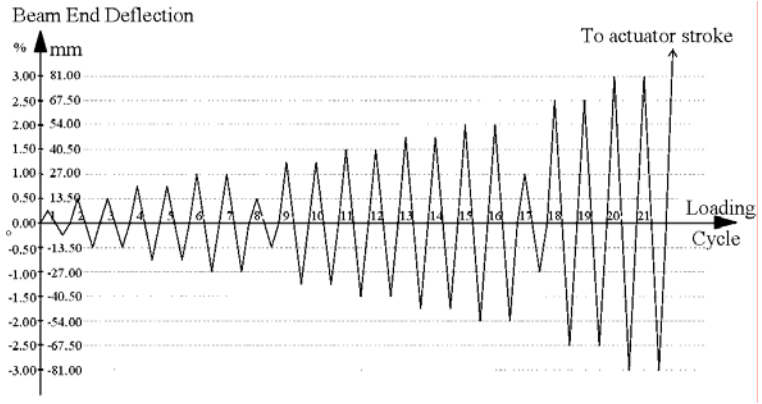

Figure 4-18 Loading history in experiment (Yin, 2001)

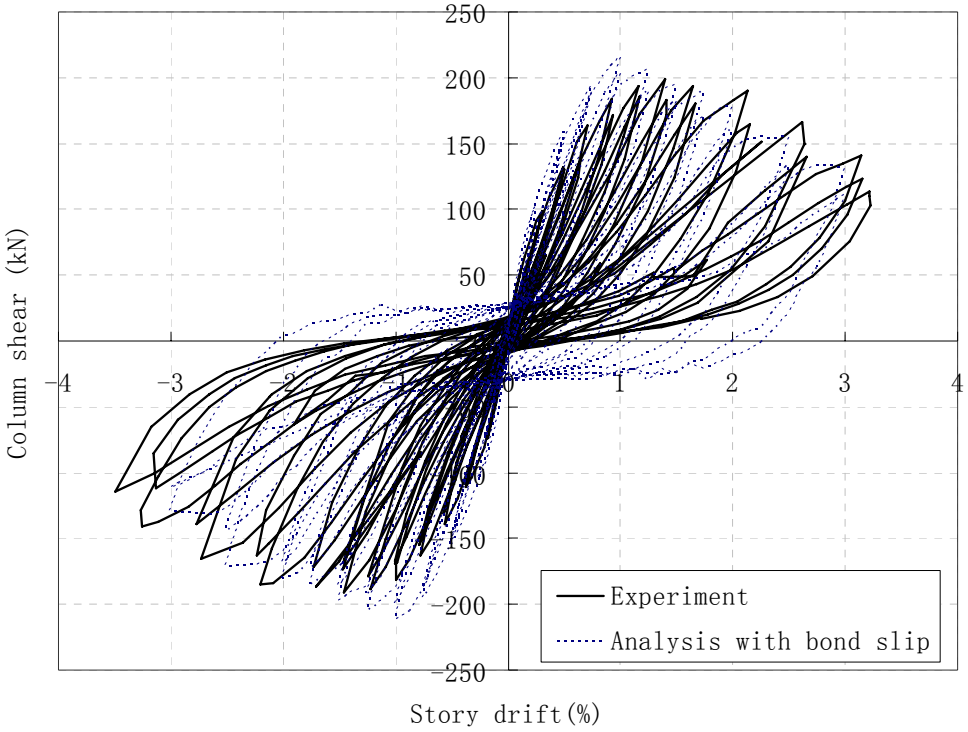

Figure 4-19 Comparison of analytical and experimental results of specimen C1A by Yin (2001)

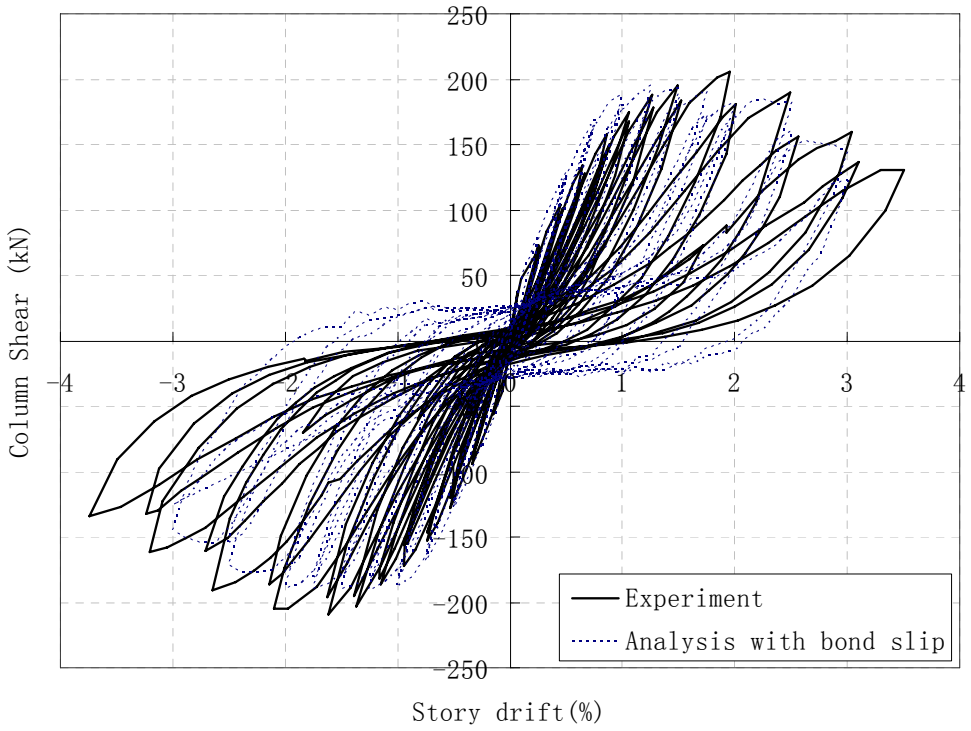

Figure 4-20 Comparison of analytical and experimental results of specimen C1B by Yin (2001)

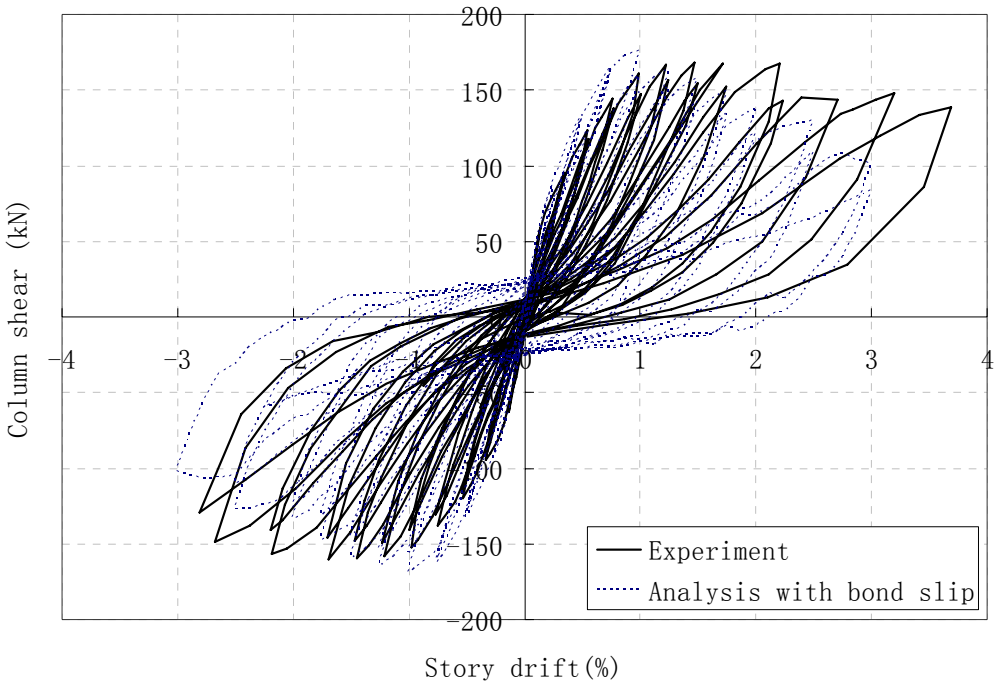

Figure 4-21 Comparison of analytical and experimental results of specimen C4A by Yin (2001)

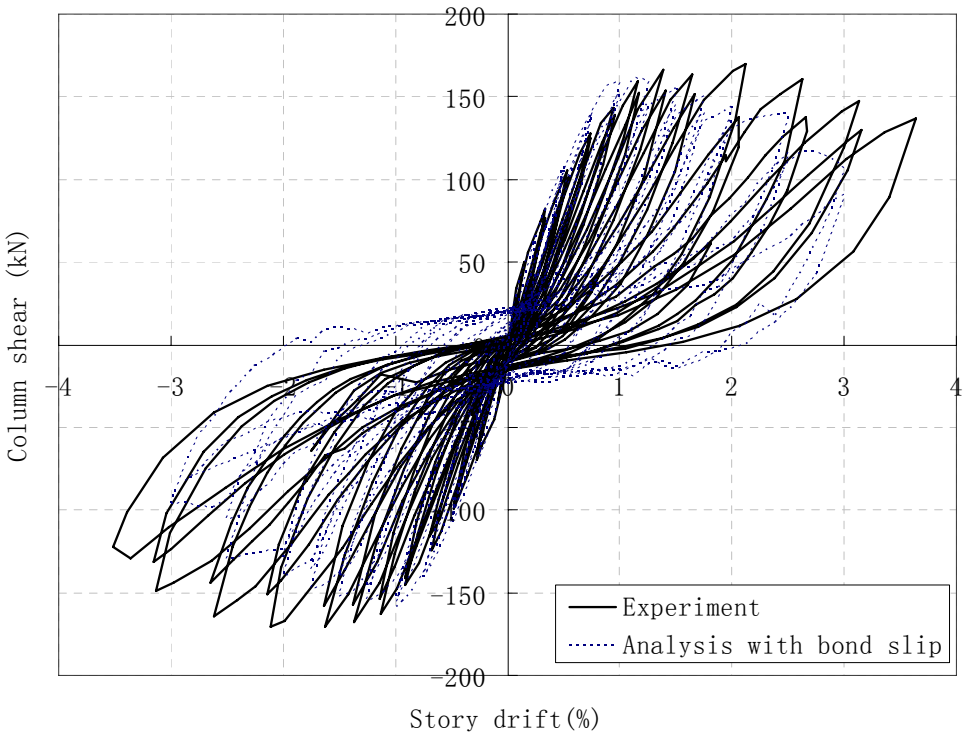

Figure 4-22 Comparison of analytical and experimental results of specimen C4B by Yin (2001)

4.6 Comparison of other behaviour of GLD beam-column joint subjected to lateral loads

Shear performance and bond deterioration behaviour, which are the two characteristics of GLD beam-column joint under lateral loads, can be observed from their contribution to the total story drift and strain distribution of beam reinforcement in the joint. In the following illustration, contribution of shear to total drift ratio in specimens C1A, C1B, C4A and C4B and beam main bar strain distribution in the joint on specimen C1A are shown.

4.6.1 Deflection contribution of joint

Generally, there are six components contributing to the total story drift. They are elastic beam and column deformation, plastic beam and column deformation, joint

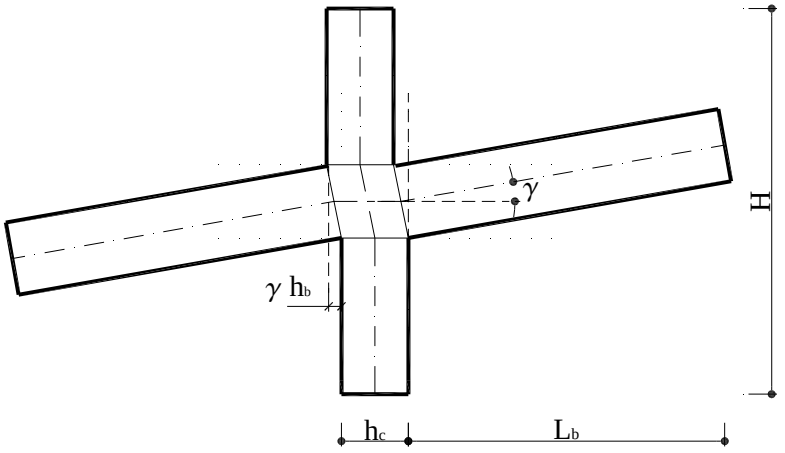

Figure 4-23 Joint shear deformation contribution

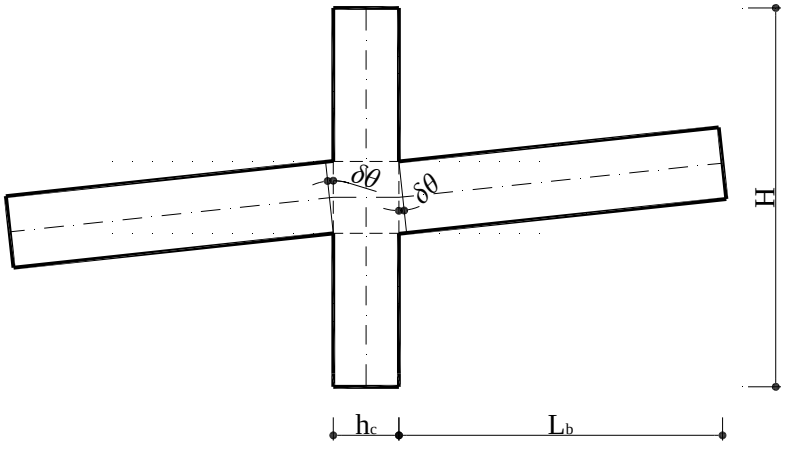

Figure 4-24 Fix-end-rotation deformation contribution

shear deformation and fixed-end-rotation deformation due to slip. In seismic design, beam-column joint is usually designed to be rigid and bond slip is prevented through the limitation of column depth-beam bar diameter ratio. In this case, the contribution of joint shear deformation and fixed-end-rotation deformation to total story drift ratio is negligible. In the gravity-load-designed frames, seismic design principles are not followed. In this case, joint shear deformation and fixed-end-rotation deformation may dominate the contribution to the total story drift ratio.

The joint shear deformation and fixed-end-rotation deformation contribution are shown in Figure 4-23 and Figure 4-24, respectively. These contributions are expressed in Eqs. (4-10) and (4-11),

$$\theta_{j,shear} = \gamma L_b / \left(L_b + h_c / 2\right) - \gamma h_b / H \tag{4-10}$$

$$\theta_{j,bond} = \delta\theta L_b / \left(L_b + h_c / 2\right) \tag{4-11}$$

In experiment, the joint shear deformation γ was acquired from the differential measurement through inclinometers. Fixed-end-rotation due to bond slip was included in joint shear deformation. Hence, the comparisons can only be based on the contribution of the sum of joint shear and fixed-end-rotation to total story drift.

The comparison between analytical results and experiment on shear deformation and fixed-end-rotation deformation is shown in Figure 4-25 to Figure 4-28. Both the analytical and experimental results show that shear deformation and fixed-end-rotation deformation contribute more than 50% of total story drift ratio when the total story drift is more than 1.5%. With the increase of story drift ratio, shear deformation and fixed-end-rotation deformation contribute more.

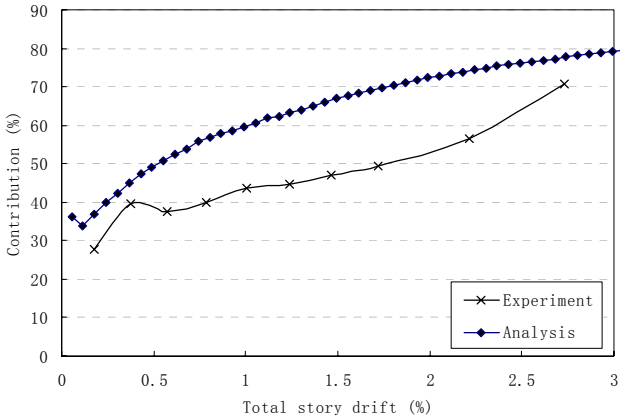

Figure 4-25 Comparison on joint shear deformation contribution - specimen C1A by Yin (2001)

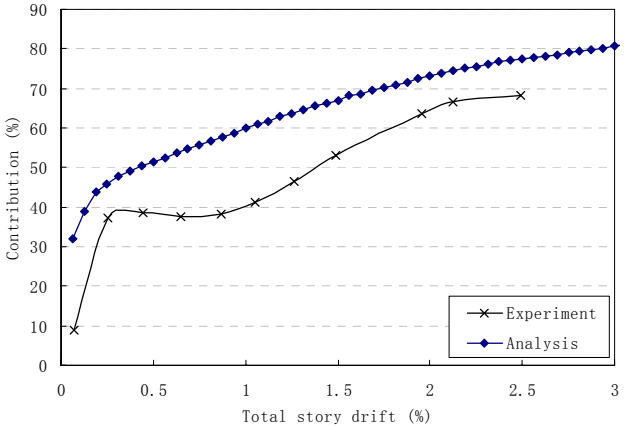

Figure 4-26 Comparison on joint shear deformation contribution - specimen C1B by Yin (2001)

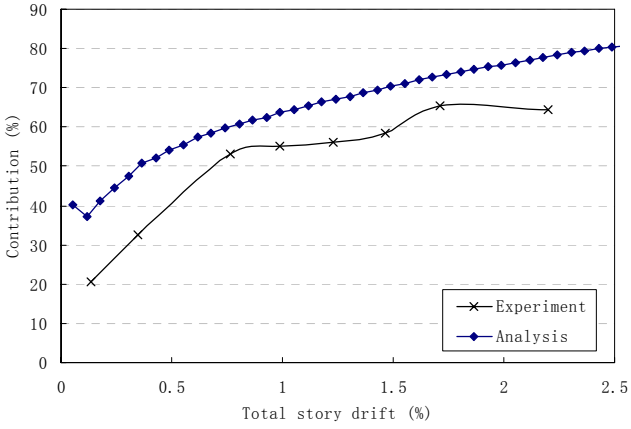

Figure 4-27 Comparison on joint shear deformation contribution - specimen C4A by Yin (2001)

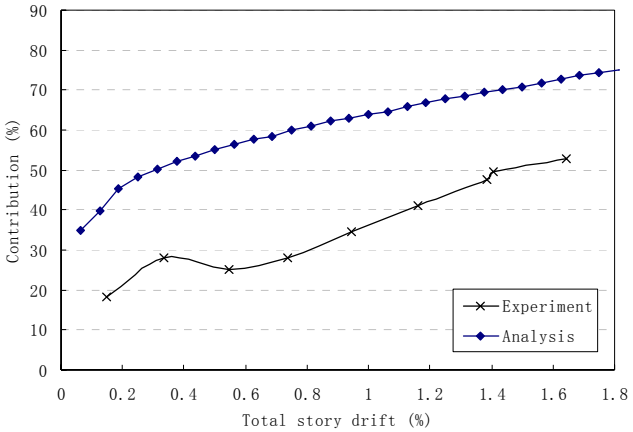

Figure 4-28 Comparison on joint shear deformation contribution - specimen C4B by Yin (2001)

To investigate the contribution of each component to total story drift, contributions of each component of the four specimens from the analysis are drawn in Figure 4-29 to Figure 4-32. In the figures, the components of total story drift ratio are classified into 5 categories: joint shear, fixed-end-rotation, beam and column plastic deformation, beam and column elastic deformation and others. The category of others comes from unaccounted shear deformation.

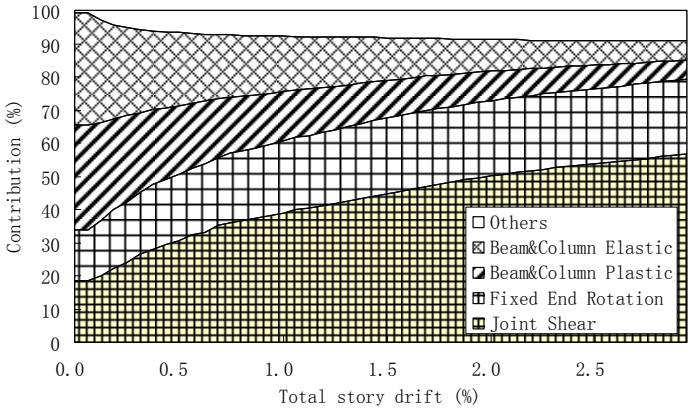

Figure 4-29 Contribution of each component to total displacement based on the analysis of specimen C1A by Yin (2001)

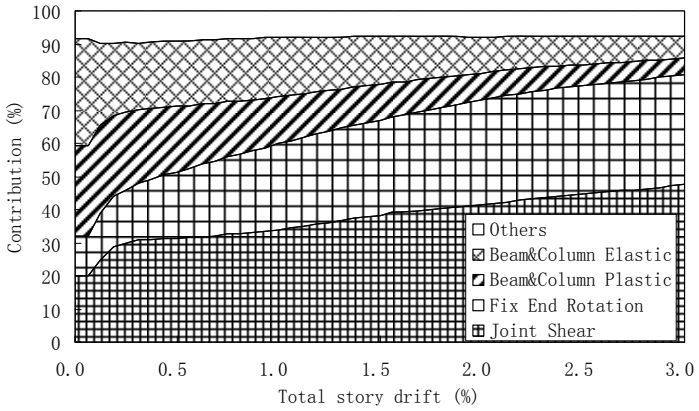

Figure 4-30 Contribution of each component to total displacement based on the analysis of specimen C1B by Yin (2001)

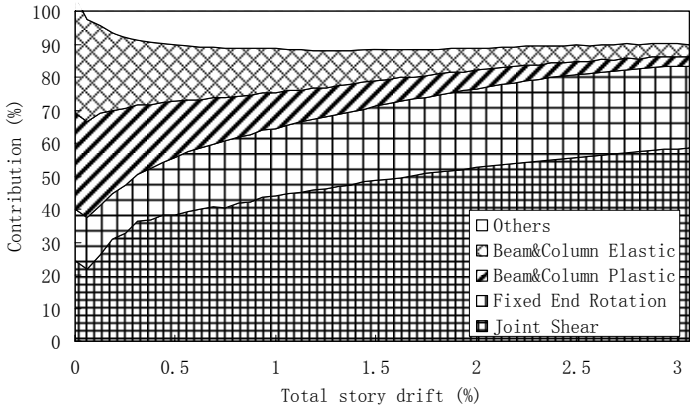

Figure 4-31 Contribution of each component to total displacement based on the analysis of specimen C4A by Yin (2001)

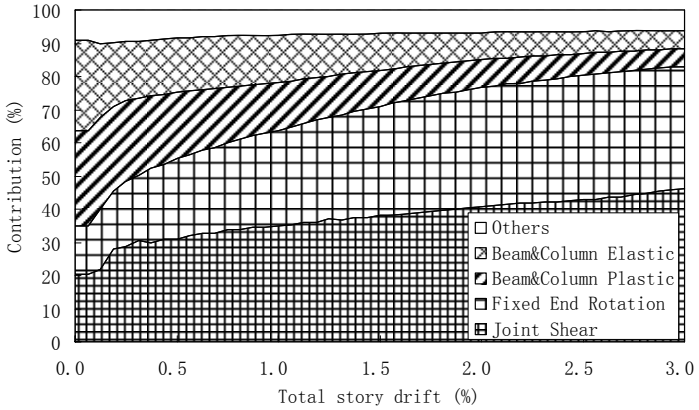

Figure 4-32 Contribution of each component to total displacement based on the analysis of specimen C4B by Yin (2001)

It is illustrated in the figures that fixed-end-rotation and joint shear deformations are the two main contributors to the total story drift ratio when the story drift ratio is more than 0.5%, while contribution of deformation of beams and columns are less. With the increase of story drift ratio, contribution of joint shear and fixed-end-rotation to the total story drift is higher.

4.6.2 Steel strain distribution in the joint

Top of the beam bar of specimen C1B of Yin (2001) is selected to see its stain distribution around the joint. The comparison is done at different story drift ratio between the analytical and experimental results as shown in Figure 4-33. Column depth is 500 mm and is shown between two dashed lines in the figures.

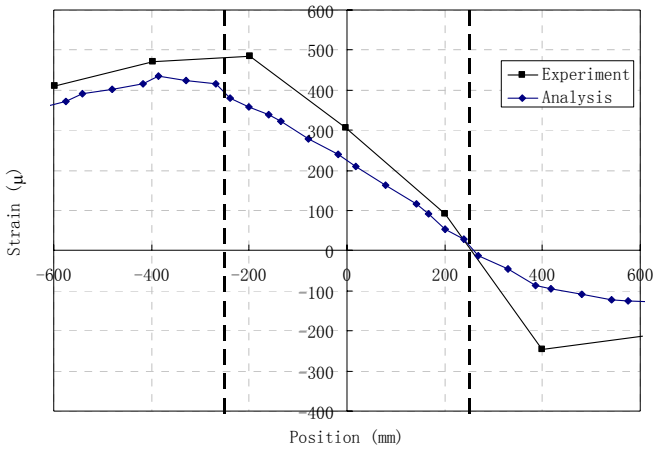

(a) Steel strain distribution (top bar) at story drift ratio of 0.3%

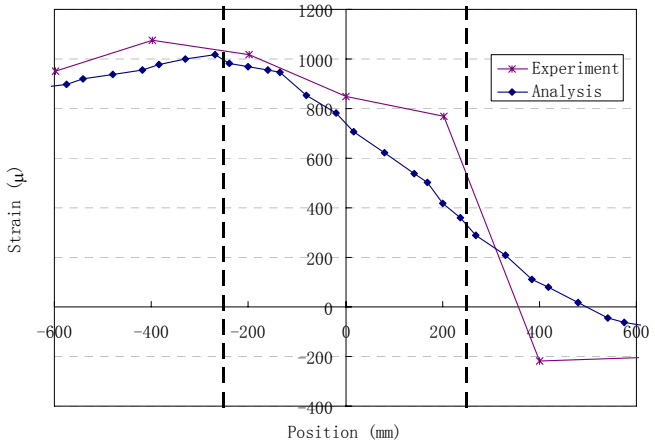

(b) Steel strain distribution (top bar) at story drift ratio of 0.93%

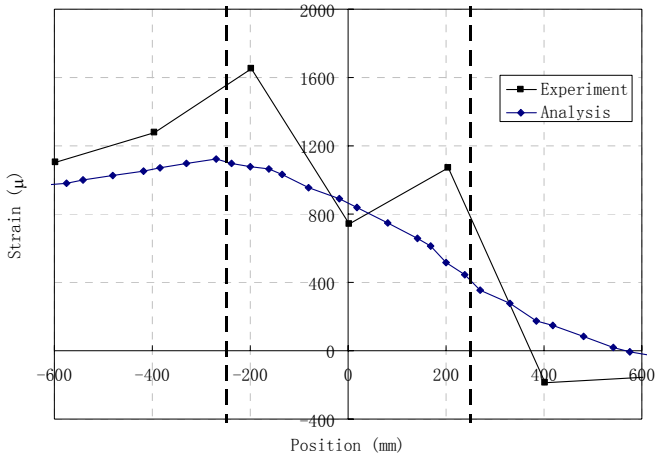

(c) Steel strain distribution (top bar) at story drift ratio of 1.40%

Figure 4-33 Comparison on steel strain distribution on top bar of specimen C1A by Yin (2001)

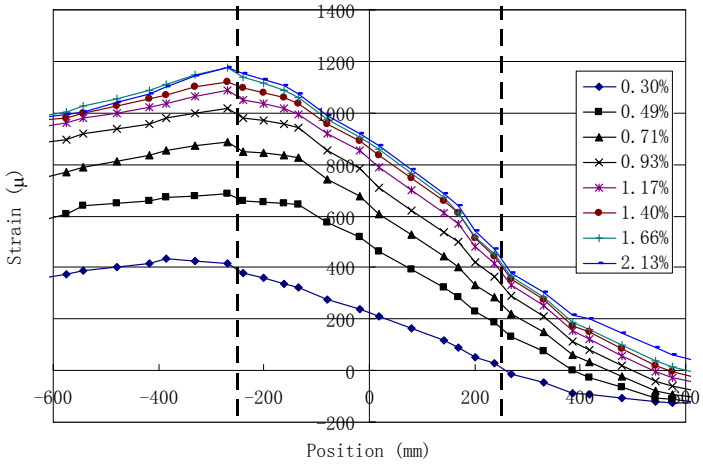

Figure 4-34 Simulated top beam bar strain distribution at different drift ratio of specimen C1A by Yin (2001)

In Figure 4-33(a), the analytical and experimental strain of top beam reinforcement at the interface between the joint and the right beam is in compression because of the positive moment at this section when bond deterioration in the joint is not severe. With the increase of story drift ratio, bond deterioration in the joint becomes severe. In this case, there is not enough development length for compression reinforcement, and then the compression strain of top beam reinforcement at the interface between the joint and the right beam decreases with the increase of story drift ratio, or even turns into tension, which is reflected by both analytical and experimental results

shown in Figure 4-33(b) and (c).

The complete response of beam bar strain distribution of the beam-column joint from the elastic stage to the collapse level is plotted in Figure 4-34. It is found that reinforcement strain does not increase much after story drift ratio reaches 1.4%, and there is no yielding of top beam reinforcement. Therefore, it is believed that the bond-slip instead of the yielding of reinforcement contributes for the ductility of beam-column joint subjected to lateral loads.

4.6.3 Bond slip and stress distribution in the joint

Top of the beam bar of specimen C1A of Yin (2001) is selected to see its bond slip and stress distributions in the joint. The simulated bond slip and stress at different story drift ratio are shown in Figure 4-35 and Figure 4-36. Column depth is 500 mm and is drawn as two vertical dashed lines in the figures to define the joint range.

It is observed in Figure 4-34 that when beam-column joint is subjected to lateral loads, top longitudinal beam bar embedded in the joint is subjected to tension at one side of the joint and compression at the opposite side of the joint. The situation is similar to the specimen in push-pull test where bond condition is severe in the whole area. So, in Figure 4-35, it is observed that bond slip remains high in the joint. While in Figure 4-36, it is observed, the maximum bond stress occurs at the

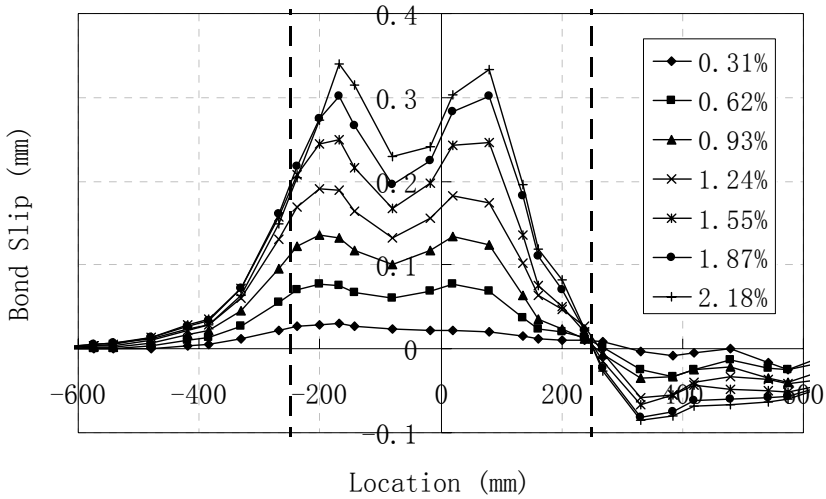

Figure 4-35 Bond slip distribution along top reinforcement in the beam

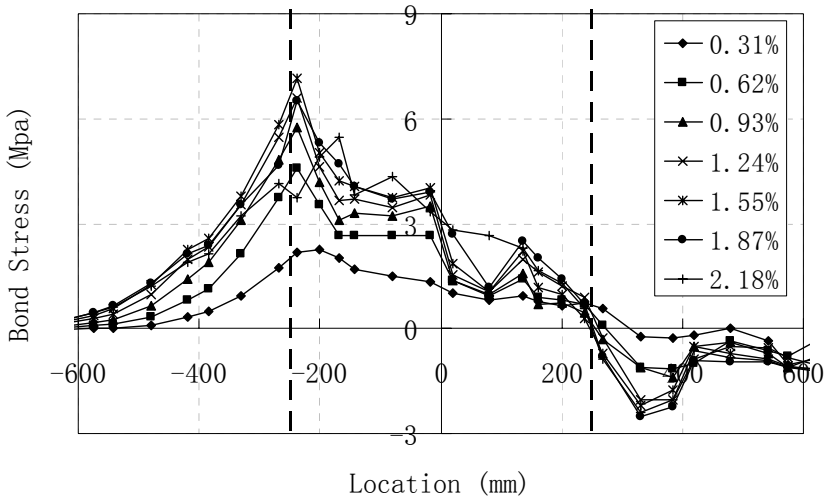

Figure 4-36 Bond stress distribution along top reinforcement in the beam

compression end. It is because at tension end or near tension end, concrete is damaged due to cracks. The constitutive law of bond slip-bond stress is not only a function of bond slip, but also a function of concrete tensile strain. When concrete is severely damaged, bond strength decreases. This makes maximum bond stress occurr only at compression end even though bond slip is high in the whole joint.

To study steel and bond behaviour from current maximum to current minimum displacement state, five loading states are selected.

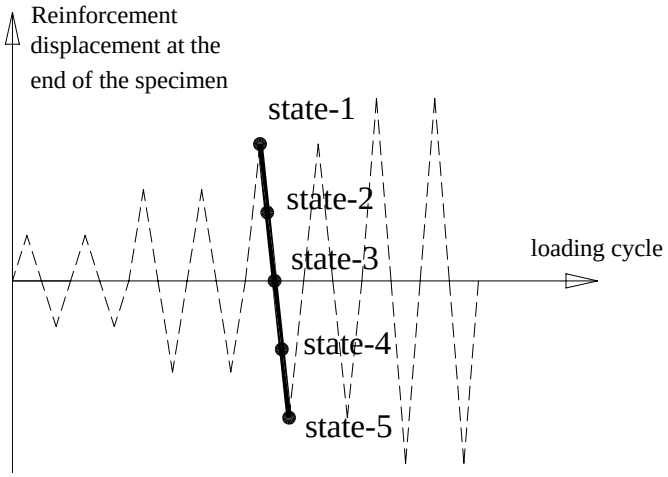

Figure 4-37 Five states from current maximum to current minimum displacement state

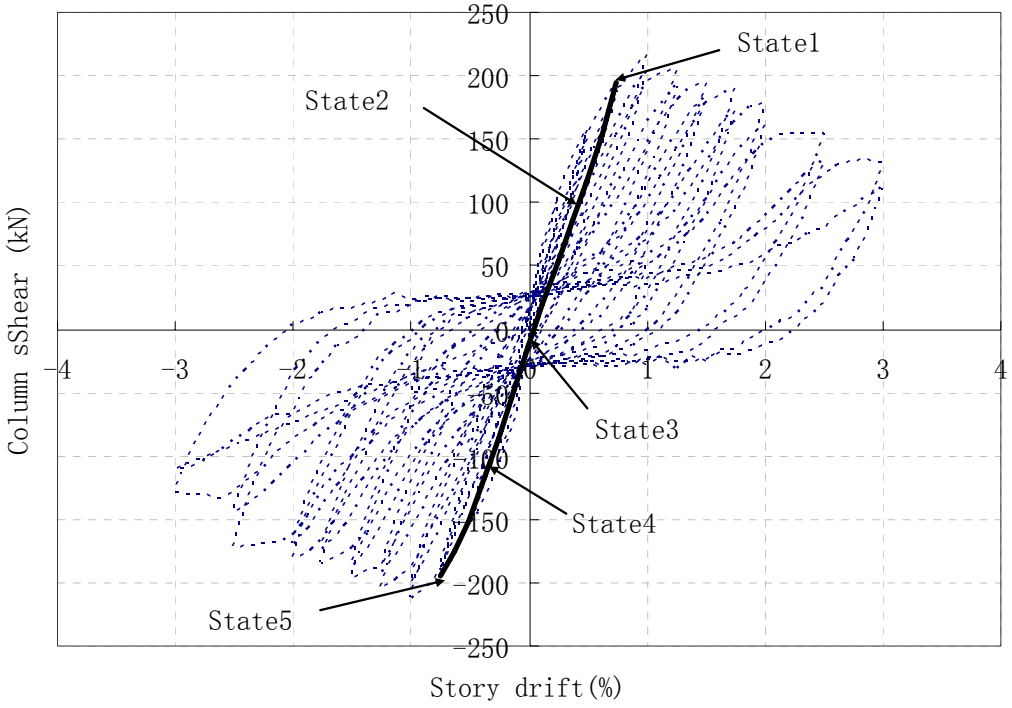

Figure 4-38 Five states from current maximum to current minimum displacement state in column shear-story drift relationship

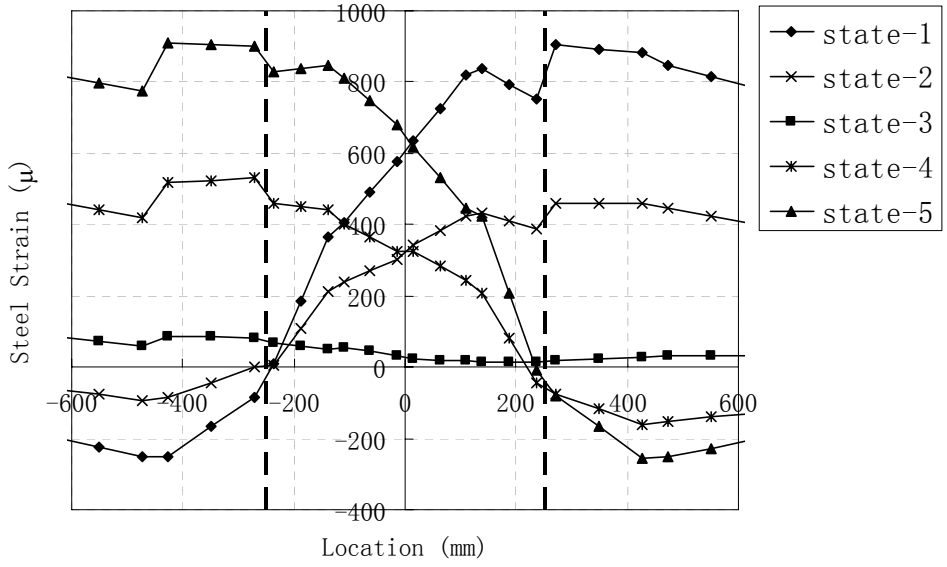

Figure 4-39 Distribution of steel strain along top longitudinal bar in the beam

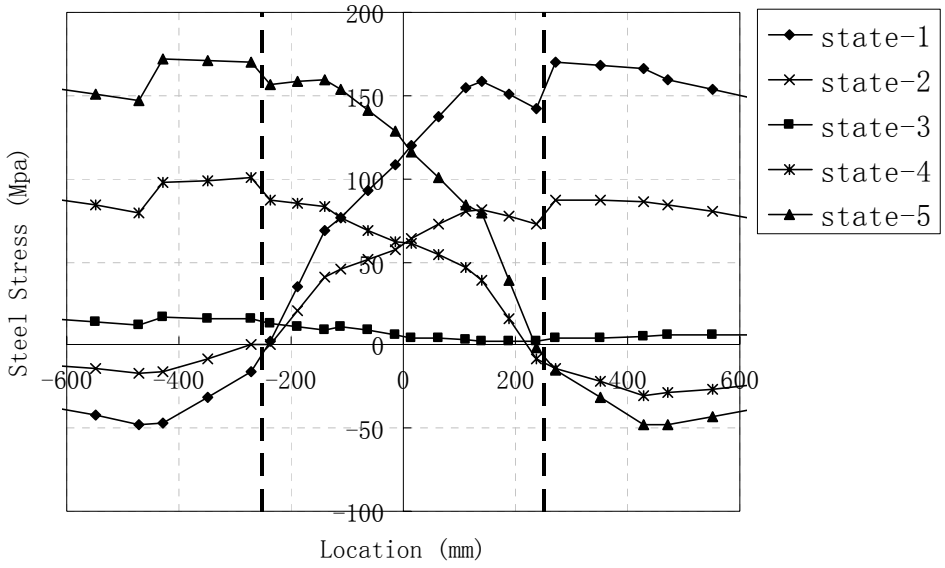

Figure 4-40 Distribution of steel stress along top longitudinal bar in the beam

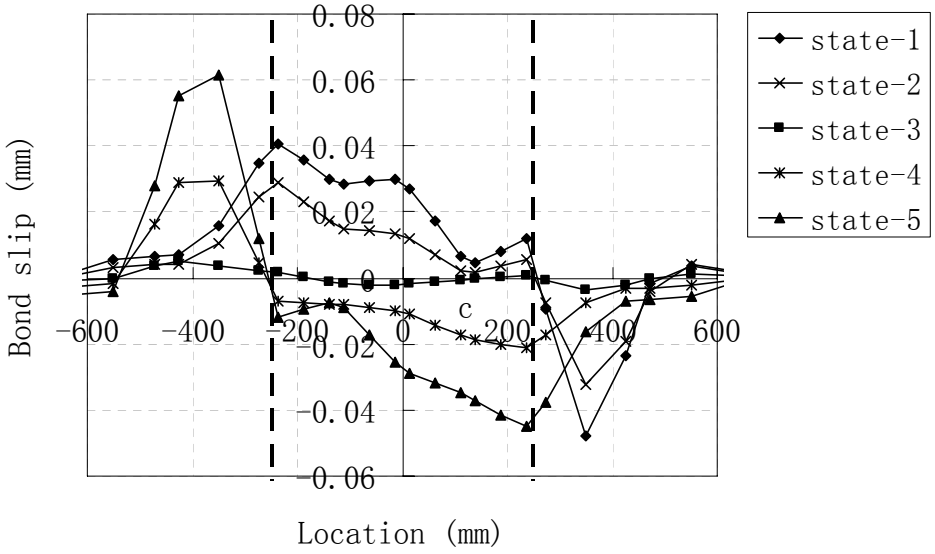

Figure 4-41 Distribution of bond slip along top longitudinal bar in the beam

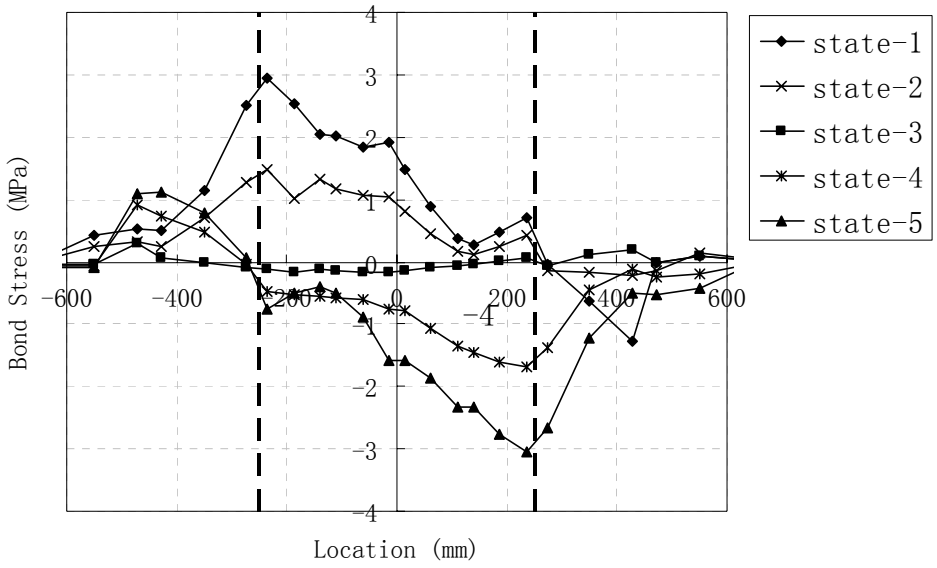

Figure 4-42 Distribution of bond stress along top longitudinal bar in the beam

Five loading states are shown in Figure 4-37. State 1 represents the state of current maximum loading displacement, state 2 for the state of half current maximum loading displacement, state 3 for zero displacement state, state 4 for the state of half current minimum loading displacement and state 5 for the state of current minimum loading displacement.

These five states are shown in relationship between column shear and story drift ratio as seen in Figure 4-38. Steel and bond distribution on these five states are shown in Figure 4-39 to Figure 4-42.

From Figure 4-39 and Figure 4-40, it is observed that in state 1 and state 5 steel strain and stress in tension end are higher than that in compression end. It is because the moment at the beam end is formed by a pair of forces, tension force from the tension reinforcement, compression forces from the compression reinforcement and concrete. These two forces are identical, so tension force from the tension reinforcement is higher than compression force from the compression reinforcement when subjected to the moment. It is also observed that in state 2 and state 4, steel strain and stress are approximately half of current maximum and current minimum at two ends. It is due to linear unloading and reloading curve of column shear, as shown in Figure 4-38.

These characteristics of bond slip and bond stress distributions can be found from

Figure 4-41 to Figure 4-42. It is observed that both bond slip and bond stress reach maximum or minimum at the ends where tension or compression reinforcement reaches its maximum.

4.7 Conclusion

To accurately simulate GLD beam-column joints subjected to lateral loads, the model is required to be able to simulate shear and bond-slip behaviour. The newly developed double-panel element combines the modelling of shear and bond-slip behaviour. Therefore, it is able to better simulate the behaviour of GLD beam-column joint subjected to lateral loads.

Constitutive models of concrete and reinforcement of WCOMD are used in the double-panel element. Eligehausen et al's (1983) model is used to model bond slip in the double-panel element. To utilise these element into the analysis of beam-column joints subjected to lateral loads, some parameters of the constitutive models are modified such as post-peak curve of compression concrete model, shear strength of shear transfer model and reduction of characteristic bond stress and slip due to reinforcement strain and concrete crack.

Finally, 14 specimens tested by four groups of researchers, which all fail in shear or bond, are selected. Monotonic load-deflection curves of analytical and experimental results are compared to show the effectiveness and accuracy of the modelling by using the newly developed double-panel element. Also, the comparison on reversed cyclic load-deflection between analytical and experiment results is done to show the ability of double-panel element to simulate the load-deflection curve. Pinching hysteresis loops of load-deflection curves due to shear and bond deterioration are obtained from the analytical simulation, which is in accordance to the experimental results.

Besides load-deflection curves, contribution of the beam and column flexure, joint shear deformation and bond slip to the total story drift is analysed and compared with experimental results to show the significant contribution of joint shear deformation and fixed-end-rotation deformations to the total story drift. Another observed fact in the experiment, the initial tension of tensile beam reinforcement turns into compression due to bond-slip in the joint, can also be simulated in the analysis.

CHAPTER 5 DEVELOPMENT OF REINFORCED CONCRETE BEAM-COLUMN JOINT ELEMENT FOR FRAME ANALYSIS

5.1 Introduction

Frame analysis is usually used to analyse the overall behaviour of frame structures subjected to different types of loading and it can model the structure with fewer degrees-of-freedom and less computer time. Compared to finite element analysis, the frame analysis is simpler, while it still gives relatively accurate results on global behaviour. Frame analysis is not suitable if local strain and stress distributions need to be investigated.

In seismic-load-designed structures, the joint is designed to be rigid by limiting the nominal shear stress, and significant bond slip at the interface is prevented by limiting the ratio of column depth to beam bar diameter. However, these requirements are usually not satisfied in gravity-load-designed structures.

The joint is usually modelled by one point, which has large stiffness and 3 degree-of-freedom as shown in Figure 5-1(a) in seismic-load-designed frames. In gravity-load-designed (GLD) frames, the joint must be modelled with more degree-of-freedom to simulate significant joint deformation.

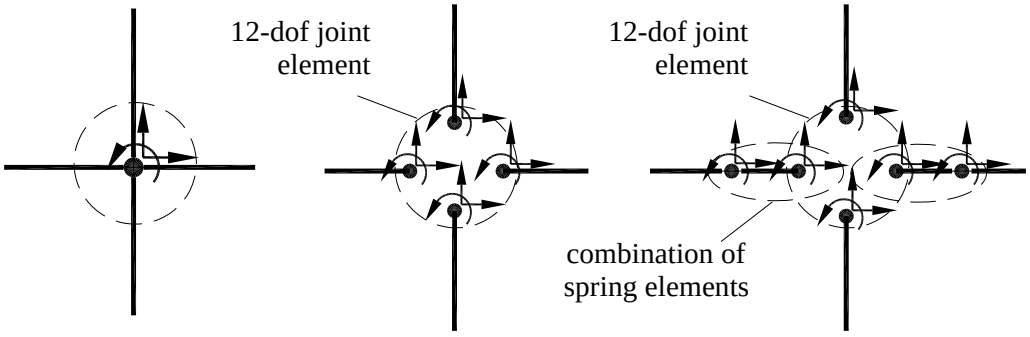

(a) Rigid joint (b) Soft joint (c) Soft joint with slip

Figure 5-1 Modelling of joint in frame analysis

As reviewed in chapter 2, some researchers (D'Ambrisi and Filippou, 1999; Ghobarah and Biddah, 1999; Youssef and Ghobarah, 2001) developed joint element to take into account the joint strength degradation and joint deformation for frame analysis. Shear deformation contributes additional rotation at the interface between the joint and its adjacent members, and they utilised a spring or a set of springs to simulate shear deformation of the joint. In their joint elements, the constant strain field of the joint is assumed. However, strains and stresses differ much from one location to another location in the GLD beam-column joint subjected to lateral loads. For this case, a 12 degree-of-freedom joint element with nine gauss points will be developed to represent the non-constant strain field in the joint. This element can be seen in Figure 5-1(b).

As reviewed in chapter 2, for the fixed-end rotation due to slip, the researchers (D'Ambrisi and Filippou, 1999, Ghobarah and Biddah, 1999, Youssef and Ghobarah, 2001) used a rotational spring at the interface between members and the joint to simulate the slip effect. Rotational spring simulating fixed-end rotation due to crack is applicable for symmetrical doubly-reinforced beam cases, but for asymmetrical doubly-reinforced beams, there is translational displacement besides rotational displacement at the interface between the joint and its adjacent members. Therefore, in this chapter, a combination of springs including rotational and translational springs is used instead of only a rotational spring to deal with a more general case as shown in Figure 5-1(c).

The 12-dof joint element and combination of rotational and translational spring element are applied into a newly developed Matlab nonlinear frame analysis program MBFEA. This program can analyse frames with soft joint and the slip at the interface between joints and adjacent members.

5.2 Development of 12 degree-of-freedom joint element

The 8-node quadrilateral element can simulate non-constant strain field, but it has 3 nodes at its edge and 2 degree-of-freedom for each node (Figure 5-2(a)). In this case,

it can not be directly connected to beam-column element with 3-dof node at its end. Therefore, the 8-node quadrilateral element has to be degenerated into 12-dof element as shown in Figure 5-2(b), so that it can be connected to the beam-column element.

The 12-dof joint element has 4 nodes with 3-dof at each node. Beams or columns can be connected to the joint through each of its node. The stiffness matrix of the 12-dof element can be degenerated from the 8-node quadrilateral element. The displacement relationship between the 8-node quadrilateral element, which has 16 degree-of-freedom, and 12-dof joint element can be expressed by considering the translational displacement of the node in 12-dof joint element as the translational displacement of the mid node of the 8-node quadrilateral element and the rotational displacement of the node in 12-dof joint element as the rotation of the corresponding edge in the 8-node quadrilateral element.

The translational displacement relationship can be written as

$$u_1 = \bar{u}_8 \tag{5-1}$$

$$v_1 = \bar{v}_8 \tag{5-2}$$

$$u_2 = \bar{u}_5 \tag{5-3}$$

$$v_2 = \bar{v}_5 \tag{5-4}$$

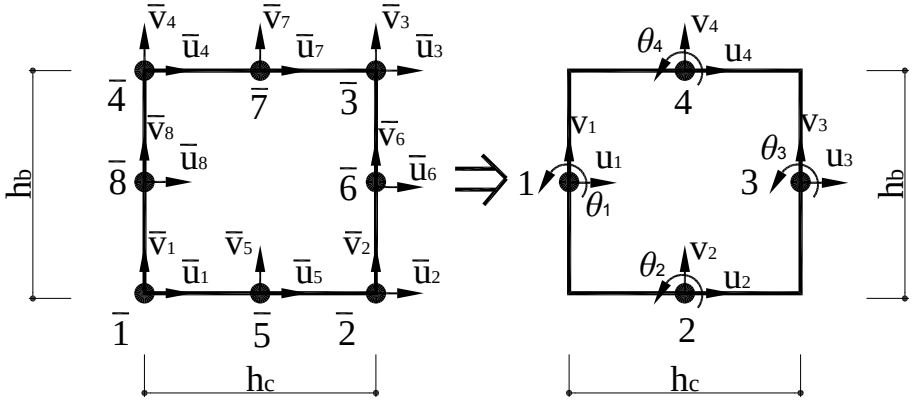

(a) Quadrilateral element (b) 12-dof joint element

Figure 5-2 A 12-dof joint element degenerated from 8-node quadrilateral panel

$$u_3 = \bar{u}_6 \tag{5-5}$$

$$v_3 = \bar{v}_6 \tag{5-6}$$

$$u_4 = \bar{u}_7 \tag{5-7}$$

$$v_4 = \bar{v}_7 \tag{5-8}$$

The edge of the 8-node quadrilateral element is assumed to remain plane after deformation, so the rotational displacement of the node in the 12-dof joint element can be defined as the rotation of the corresponding edgy in the 8-node quadrilateral element.

The rotational displacement relationship can be written as

$$\theta_1 = \frac{\bar{u}_8 - \bar{u}_4}{h_b/2} = \frac{\bar{u}_1 - \bar{u}_8}{h_b/2} \tag{5-9}$$

$$\theta_2 = \frac{\bar{v}_2 - \bar{v}_5}{h_c/2} = \frac{\bar{v}_5 - \bar{v}_1}{h_c/2} \tag{5-10}$$

$$\theta_3 = \frac{\bar{u}_2 - \bar{u}_6}{h_b/2} = \frac{\bar{u}_6 - \bar{u}_3}{h_b/2} \tag{5-11}$$

$$\theta_4 = \frac{\bar{v}_3 - \bar{v}_7}{h_c/2} = \frac{\bar{v}_7 - \bar{v}_4}{h_c/2} \tag{5-12}$$

where

u, v, θ are degrees of freedom of 12-dof element

$\bar{u}, \bar{v}$ are degrees of freedom of 8-node element

h_b, h_c are depth of beams and columns

From 8 translational displacement relationship equations in Eqs. (5-1) to (5-8) and 8 rotational displacement relationship equations in Eqs. (5-9) to (5-12), u, v, θ can be solved from

$$\bar{u}_1 = u_1 + \frac{h_b}{2} \cdot \theta_1 \tag{5-13}$$

$$\bar{v}_1 = v_2 - \frac{h_c}{2}\cdot\theta_2 \tag{5-14}$$

$$\bar{u}_2 = u_3 + \frac{h_b}{2}\cdot\theta_3 \tag{5-15}$$

$$\bar{v}_2 = v_2 + \frac{h_c}{2}\cdot\theta_2 \tag{5-16}$$

$$\bar{u}_3 = u_3 - \frac{h_b}{2}\cdot\theta_3 \tag{5-17}$$

$$\bar{v}_3 = v_4 + \frac{h_c}{2}\cdot\theta_4 \tag{5-18}$$

$$\bar{u}_4 = u_1 - \frac{h_b}{2}\cdot\theta_1 \tag{5-19}$$

$$\bar{v}_4 = v_4 - \frac{h_c}{2}\cdot\theta_4 \tag{5-20}$$

$$\bar{u}_5 = u_2 \tag{5-21}$$

$$\bar{v}_5 = v_2 \tag{5-22}$$

$$\bar{u}_6 = u_3 \tag{5-23}$$

$$\bar{v}_6 = v_3 \tag{5-24}$$

$$\bar{u}_7 = u_4 \tag{5-25}$$

$$\bar{v}_7 = v_4 \tag{5-26}$$

$$\bar{u}_8 = u_1 \tag{5-27}$$

$$\bar{v}_8 = v_1 \tag{5-28}$$

These 16 equations can be written into a matrix form as

$$\bar{u} = T_e \cdot u \tag{5-29}$$

where

$$\bar{u} = \{\bar{u}_1 \quad \bar{v}_1 \quad \bar{u}_2 \quad \bar{v}_2 \quad \bar{u}_3 \quad \bar{v}_3 \quad \bar{u}_4 \quad \bar{v}_4 \quad \bar{u}_5 \quad \bar{v}_5 \quad \bar{u}_6 \quad \bar{v}_6 \quad \bar{u}_7 \quad \bar{v}_7 \quad \bar{u}_8 \quad \bar{v}_8\}^T$$

$$u = \{u_1 \quad v_1 \quad \theta_1 \quad u_2 \quad v_2 \quad \theta_2 \quad u_3 \quad v_3 \quad \theta_3 \quad u_4 \quad v_4 \quad \theta_4\}^T$$

$$T_e = \begin{bmatrix}
1 & 0 & \frac{h_b}{2} & 0 & 0 & 0 & 0 & 0 & 0 & 0 & 0 & 0 \\
0 & 0 & 0 & 0 & 1 & -\frac{h_c}{2} & 0 & 0 & 0 & 0 & 0 & 0 \\
0 & 0 & 0 & 0 & 0 & 0 & 1 & 0 & \frac{h_b}{2} & 0 & 0 & 0 \\
0 & 0 & 0 & 0 & 1 & \frac{h_c}{2} & 0 & 0 & 0 & 0 & 0 & 0 \\
0 & 0 & 0 & 0 & 0 & 0 & 1 & 0 & -\frac{h_b}{2} & 0 & 0 & 0 \\
0 & 0 & 0 & 0 & 0 & 0 & 0 & 0 & 0 & 0 & 1 & \frac{h_c}{2} \\
1 & 0 & -\frac{h_b}{2} & 0 & 0 & 0 & 0 & 0 & 0 & 0 & 0 & 0 \\
0 & 0 & 0 & 0 & 0 & 0 & 0 & 0 & 0 & 0 & 1 & -\frac{h_c}{2} \\
0 & 0 & 0 & 1 & 0 & 0 & 0 & 0 & 0 & 0 & 0 & 0 \\
0 & 0 & 0 & 0 & 1 & 0 & 0 & 0 & 0 & 0 & 0 & 0 \\
0 & 0 & 0 & 0 & 0 & 0 & 1 & 0 & 0 & 0 & 0 & 0 \\
0 & 0 & 0 & 0 & 0 & 0 & 0 & 1 & 0 & 0 & 0 & 0 \\
0 & 0 & 0 & 0 & 0 & 0 & 0 & 0 & 0 & 1 & 0 & 0 \\
0 & 0 & 0 & 0 & 0 & 0 & 0 & 0 & 0 & 0 & 1 & 0 \\
1 & 0 & 0 & 0 & 0 & 0 & 0 & 0 & 0 & 0 & 0 & 0 \\
0 & 1 & 0 & 0 & 0 & 0 & 0 & 0 & 0 & 0 & 0 & 0
\end{bmatrix} \tag{5-30}$$

Then, the degenerated stiffness matrix of the 12-dof joint element can be expressed as,

$$[K]_{12-dof} = T_e^{\,T}[K]_{8-node}T_e \tag{5-31}$$

where

$[K]_{8-node}$ is the stiffness matrix of 8-node quadrilateral element

In deriving the stiffness of the 8-node quadrilateral element, elastic material model is utilsed to calculate the constitutive matrix D before concrete cracking, while fixed-angle softened-truss model is utilised to calculate the nonlinear constitutive matrix D after concrete cracking. Flowchart to construct the stiffness matrix of the 12-dof joint element is given in Figure 5-3.

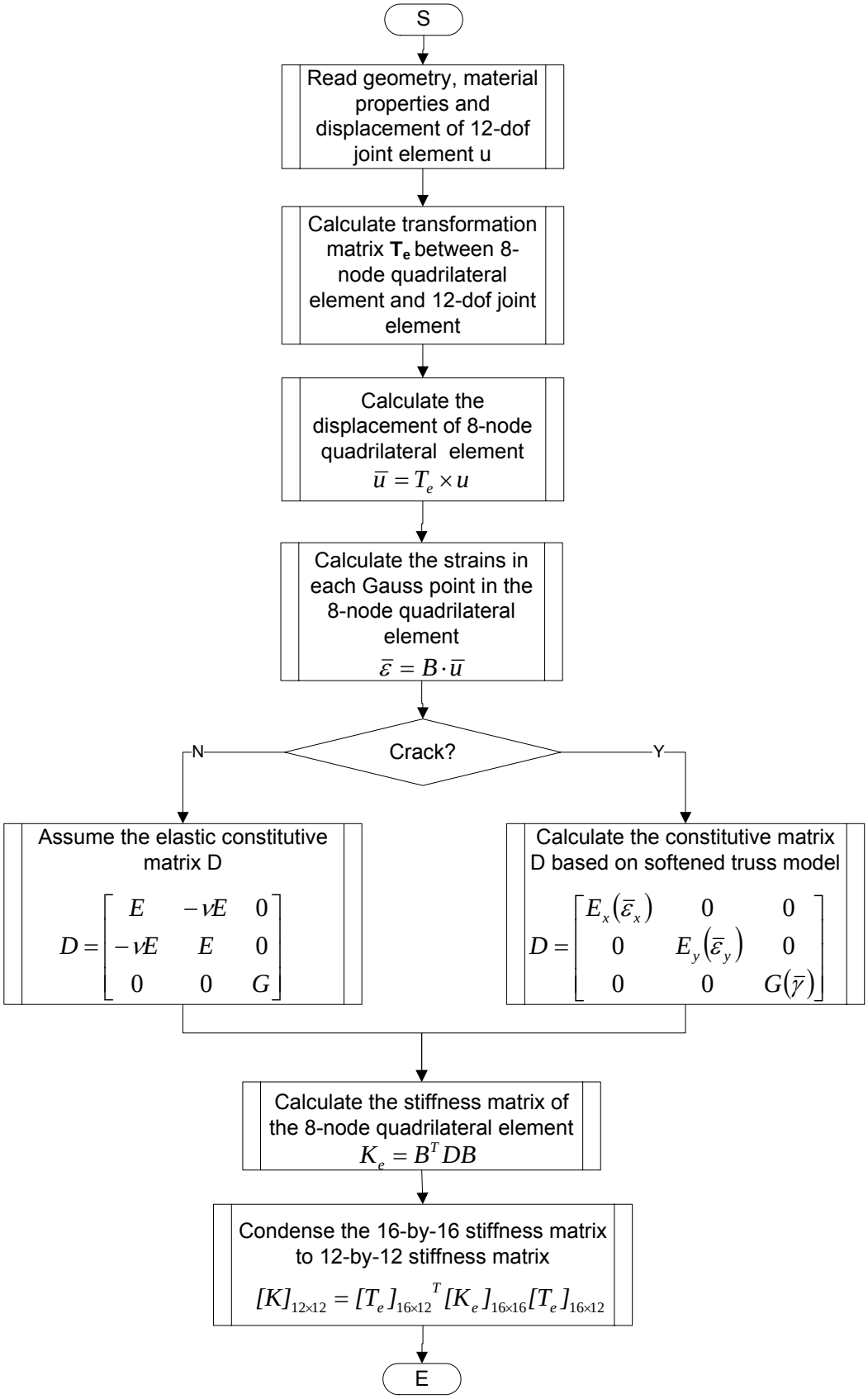

Figure 5-3 Flowchart to construct stiffness matrix of 12-dof joint element

5.3 Development of the spring elements to consider bond slip

5.3.1 Bond slip consideration in symmetrical doubly-reinforced beams

In the symmetrical doubly-reinforced beam subjected to lateral loads, forces in the main longitudinal bar can be compression at one end, and tension at another end. Hence, bond stress is relatively high between concrete and longitudinal bars in the joint, and bond slip may be significant. At interface section between joint and beam, when top reinforcement is slipped to the right, and bottom reinforcement is slipped to the left, additional rotation is introduced as shown in Figure 5-4. Thus, fixed-end rotation at the interface section is simulated with a rotational spring element. The soft joint with additional fixed-end rotation at the interface between the joint and beam due to the bond slip can be modelled by the 12-dof joint element with two rotational springs as shown in Figure 5-5.

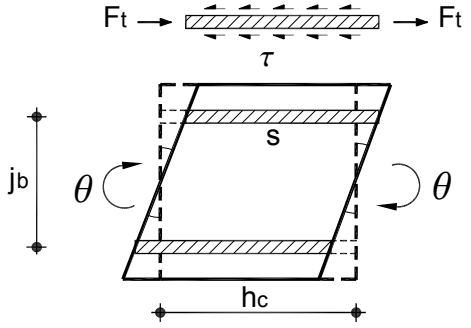

Figure 5-4 Additional rotation at beam ends due to slip

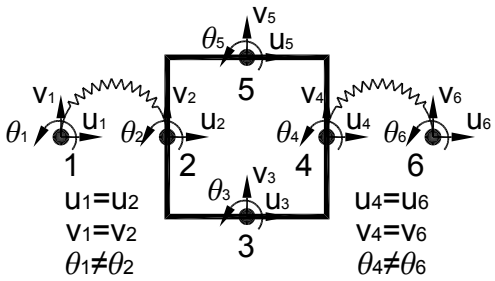

Figure 5-5 A 12-dof joint element with two rotational springs to consider bond slip

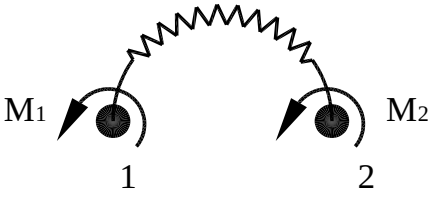

Figure 5-6 Forces on spring element

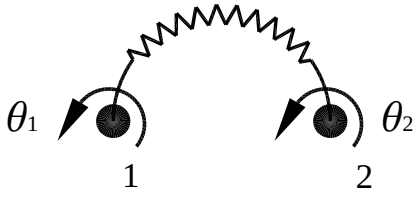

Figure 5-7 Deformation on spring element

The moments in the spring element (Figure 5-6) is a couple formed by the forces on the top and bottom main bars, which are shown in Figure 5-4. From the free-body analysis of top main bar (Figure 5-4), the force on the main bar can be expressed in terms of bond stress, perimeter of the main bar and embedded length as

$$F_t = \frac{E_b(s) \cdot s \cdot l_s \cdot h_c}{2} \tag{5-32}$$

Moment in the rotational spring can be expressed as

$$M_1 = F_t \cdot j_b = \frac{E_b(s) \cdot s \cdot l_s \cdot h_c}{2} \cdot j_b \tag{5-33}$$

where

F_t is the force on main bar

$E_b(s)$ is the bond stiffness

s is the slip at the interface

l_s is the sum of perimeter of main bars

h_c is the embedded length of main bar in the joint, which is identical to depth of column

j_b is the distance between top and bottom main bars

Deformation of the rotational spring can be expressed as

$$\theta_1 - \theta_2 = \frac{s}{j_b / 2} \tag{5-34}$$

where

θ_1, θ_2 are rotations of the spring elements (Figure 5-7)

And the stiffness of the rotational spring due to slip is calculated as

$$k_b = \frac{M_1}{\theta_1 - \theta_2} = E_b(s) \cdot \frac{j_b}{2} \cdot \frac{l_s}{2} \cdot h_c \cdot j_b \tag{5-35}$$

where $s = \frac{j_b}{2} \cdot (\theta_1 - \theta_2)$ (5-36)

Then, the stiffness equation of the rotational spring element can be written in a matrix form as

$$\begin{Bmatrix} M_1 \\ M_2 \end{Bmatrix} = \begin{bmatrix} k_b & -k_b \\ -k_b & k_b \end{bmatrix} \begin{Bmatrix} \theta_1 \\ \theta_2 \end{Bmatrix} \tag{5-37}$$

5.3.2 Bond slip consideration in asymmetrical doubly-reinforced beams

In the previous derivation, it was assumed that the amount of top longitudinal main bar is the same as the amount of bottom longitudinal main bar in the beam. While in gravity-load-designed beams, the amount of top and bottom main bar can be significantly different. In this case, bond slip at the interface between the joint and the beam can cause translation in addition to rotation. So, the effect of slip on the interface has to be described by a combination of springs as shown in Figure 5-8. The combination of spring includes rotational and translational springs to take into account the rotational and translational deformation due to bond slip. The forces and deformations on the joint element with a combination of spring elements are shown in Figure 5-9 and Figure 5-10.

From Figure 5-11, slip at the top and the bottom bars can be calculated through relative displacement, and expressed as,

$$s_{top} = \Delta x + \frac{j_b}{2} \cdot \Delta\theta = u_2 - u_1 + \frac{j_b}{2} \cdot (\theta_1 - \theta_2) \tag{5-38}$$

$$s_{bot} = \Delta x - \frac{j_b}{2} \cdot \Delta\theta = u_2 - u_1 - \frac{j_b}{2} \cdot (\theta_1 - \theta_2) \tag{5-39}$$

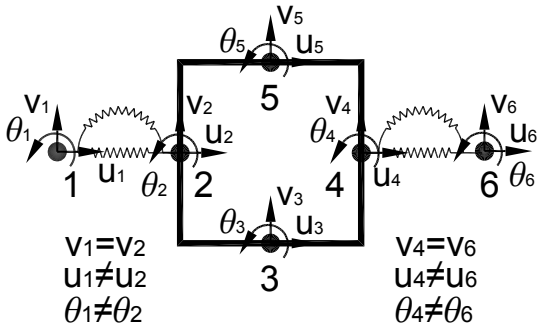

Figure 5-8 A 12-dof joint element with rotational and translational springs to consider bond slip

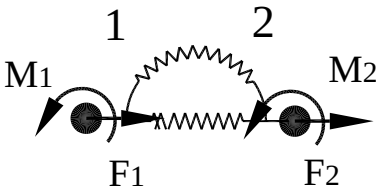

Figure 5-9 Forces on combination of spring elements

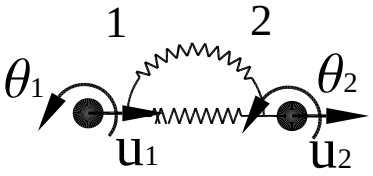

Figure 5-10 Deformation on combination of spring elements

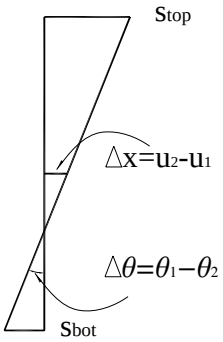

Figure 5-11 Relative displacement on interface section between node 1 and 2

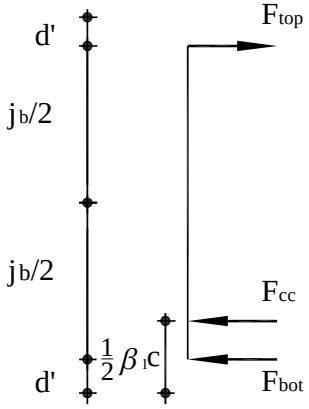

Figure 5-12 Forces on interface section between node 1 and 2

where

u_1, u_2 are translational displacement (see Figure 5-10)

θ_1, θ_2 are rotational displacement (see Figure 5-10)

Δx is relative translational displacement, $\Delta x = u_2 - u_1$ (see Figure 5-11)

$\Delta\theta$ is relative translational displacement, $\Delta\theta = \theta_1 - \theta_2$ (see Figure 5-11)

j_b is the distance between top and bottom main bars (see Figure 5-12)

d' is the clear cover of the beam (see Figure 5-12)

c is the depth of compression zone

β_1 is the stress block depth factor

The depth of compression zone c is assumed to be the same as that without bond slip. Then, the depth of compression zone c is still a function of moment M_1.

From Figure 5-12, force and moment in the combination of spring elements can be expressed as

$$M_2 = F_{bot}\frac{j_b}{2} + F_{cc}\left(\frac{j_b}{2} - \left(\frac{1}{2}\beta_1 c - d'\right)\right) - F_{top}\frac{j_b}{2} \tag{5-40}$$

$$F_2 = F_{bot} + F_{cc} + F_{top} \tag{5-41}$$

where

F_{bot} is the force in bottom longitudinal main bar

F_{top} is the force in top longitudinal main bar

F_{cc} is the compression force of concrete

F_{bot} and F_{top} can be calculated through the free-body analysis of bottom and top bars, and F_{cc} can be calculated through the analysis on the equivalent rectangular stress block of concrete under compression.

$$F_{bot} = \frac{1}{2}E_b(s_{bot})s_{bot}l_{s,bot}h_c \tag{5-42}$$

$$F_{top} = \frac{1}{2}E_b(s_{top})s_{top}l_{s,top}h_c \tag{5-43}$$

$$F_{cc} = -f_c b_b \beta_1 c \tag{5-44}$$

where

E_b is the bond stiffness

s_{bot} is the slip of bottom bar

s_{top} is the slip of top bar

$l_{s,bot}$ is the perimeter of bottom bars

$l_{s,top}$ is the perimeter of top bars

b_b is the width of beams

When Eqs. (5-38) to (5-39) are substituted into Eqs. (5-42) to (5-44), F_{bot} and

F_{top} can be rewritten as

$$F_{bot} = \frac{1}{2}E_b(s_{bot})\cdot l_{s,bot}\cdot h_c(u_2-u_1)+\frac{1}{2}E_b(s_{bot})\cdot l_{s,bot}\cdot h_c\cdot\frac{j_b}{2}(\theta_1-\theta_2) \tag{5-45}$$

$$F_{top} = \frac{1}{2}E_b(s_{top})\cdot l_{s,bot}\cdot h_c(u_2-u_1)-\frac{1}{2}E_b(s_{top})\cdot l_{s,bot}\cdot h_c\cdot\frac{j_b}{2}(\theta_1-\theta_2) \tag{5-46}$$

Then, by substituting Eqs. (5-45) to (5-46) into Eqs. (5-40) and (5-41), force and moment in the combination of spring elements can be expressed as

$$M_2 = \left(\frac{1}{2}\left(E_b(s_{bot})\cdot l_{s,bot}+E_b(s_{top})\cdot l_{s,top}\right)\cdot h_c\left(\frac{j_b}{2}\right)^2-\varpi_M\right)(\theta_2-\theta_1) + \frac{1}{2}\left(E_b(s_{bot})\cdot l_{s,bot}-E_b(s_{top})\cdot l_{s,top}\right)\cdot h_c\cdot\frac{j_b}{2}(u_2-u_1) \tag{5-47}$$

$$F_2 = \frac{1}{2}\left(E_b(s_{bot})\cdot l_{s,bot}-E_b(s_{top})\cdot l_{s,top}\right)\cdot h_c\cdot\frac{j_b}{2}\cdot(\theta_2-\theta_1) + \left(\frac{1}{2}\left(E_b(s_{bot})\cdot l_{s,bot}+E_b(s_{top})\cdot l_{s,top}\right)\cdot l_s\cdot h_c-\varpi_F\right)\cdot(u_2-u_1) \tag{5-48}$$

where

$$\varpi_M = \frac{f_c\cdot b_b\cdot\beta_1\cdot c\left(\frac{j_b}{2}-\left(\frac{1}{2}\beta_1 c-d'\right)\right)}{\theta_2-\theta_1}$$

$$\varpi_F = \frac{f_c\cdot b_b\cdot\beta_1\cdot c}{u_2-u_1}$$

So, the stiffness matrix of the spring elements can be written as

$$\begin{Bmatrix}F_1\\M_1\\F_2\\M_2\end{Bmatrix} = \begin{bmatrix}k_{uu} & k_{u\theta} & -k_{uu} & -k_{u\theta}\\ k_{u\theta} & k_{\theta\theta} & -k_{u\theta} & -k_{\theta\theta}\\ -k_{uu} & -k_{u\theta} & k_{uu} & k_{u\theta}\\ -k_{u\theta} & -k_{\theta\theta} & k_{u\theta} & k_{\theta\theta}\end{bmatrix}\begin{Bmatrix}u_1\\\theta_1\\u_2\\\theta_2\end{Bmatrix} \tag{5-49}$$

where

$$k_{uu} = \frac{1}{2}\left(E_b(s_{bot})\cdot l_{s,bot}+E_b(s_{top})\cdot l_{s,top}\right)\cdot l_s\cdot h_c-\varpi_F \tag{5-50}$$

$$k_{u\theta} = \frac{1}{2}\left(E_b(s_{bot})\cdot l_{s,bot}-E_b(s_{top})\cdot l_{s,top}\right)\cdot h_c\cdot\frac{j_b}{2} \tag{5-51}$$

$$k_{\theta\theta} = \frac{1}{2}\left(E_b(s_{bot})\cdot l_{s,bot}+E_b(s_{top})\cdot l_{s,top}\right)\cdot h_c\cdot\left(\frac{j_b}{2}\right)^2-\varpi_M \tag{5-52}$$

5.4 Constitutive model used in 12-dof joint element with spring elements

5.4.1 Concrete compression model

The concrete compression model in MBFEA follows the concrete compression model described in sub-chapter 4.2.1 except the compression model after peak. Before the peak, the concrete compression model is based on elasto-plastic fracture model, and expressed in Eq. (2-14). After the peak, the concrete compression model expressed in Eqs. (4-2) and (4-3) is simplified into a straight line, and expressed in Eq. (5-53). The residual strength is assumed as 20% of peak stress in the post-peak concrete compression model. The post-peak compression model can be written as

$$\sigma_2 = 1 - \frac{(k-1)\varepsilon_0}{\varepsilon - \varepsilon_0}\zeta f_c' \qquad \text{for} \quad 1 < \varepsilon_2/\varepsilon_0 \le 1 + 0.8(k-1) \tag{5-53}$$

$$\sigma_2 = 0.2\zeta f_c' \qquad \text{for} \quad \varepsilon_2/\varepsilon_0 > 1 + 0.8(k-1) \tag{5-54}$$

The parameter *k* in Eqs. (5-53) and (5-54) is taken as 15 according to verification in sub-chapter 4.2.6 if size effect is not considered. Because the joint is simulated by one element only, whose size is relative large, the size effect should be considered if more accurate results are required.

In recent years, researchers (Markeset and Hillerborg, 1995, Lertsrisakulrat et al, 2000 and Soltani et al, 2005) realised that the failure of concrete loaded in compression is localized to a fracture zone. Localization means that the descending branch of the compressive stress-strain curve becomes size dependent, and the stress-strain curve can therefore not be regarded as a pure material property. The compressive stress-strain curves varying with specimen size are shown in Figure 5-13.

Markeset and Hillerborg (1995) proposed the compressive damage zone (CDZ) model to calculate the compressive stress-strain curve considering the localization of compression failure. The model is assumed to consist of three curves (Figure 5-14). The first curve is the stress-strain curve for the material loaded up to the

compressive strength $f_c^{'}$ and then unloaded. The second curve shows the relationship between the stress and the average additional strain ε_d within the damage zone, related to the formation of longitudinal cracks and a corresponding additional lateral strain within this damage zone. The third curve is a stress-deformation curve, related to localized deformation. The complete compressive stress-strain curve contributes from these three curves is shown in Figure 5-15. For specimen length L is greater than damage zone L_d, the average strain becomes

$$\varepsilon_m = \varepsilon + \varepsilon_d \frac{L_d}{L} + \frac{w}{L} \tag{5-55}$$

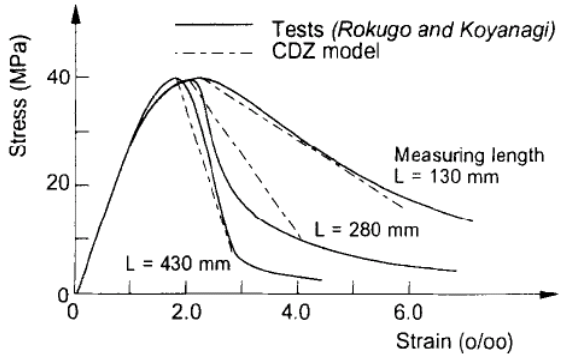

Figure 5-13 Influence of specimen length on the stress-strain curve (Markeset and Hillerborg, 1995)

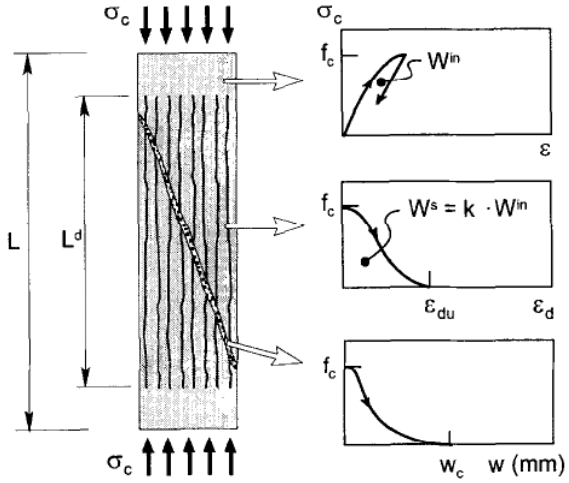

Figure 5-14 Illustration of the CDZ model on a specimen loaded in uniaxial compression (Markeset and Hillerborg, 1995)

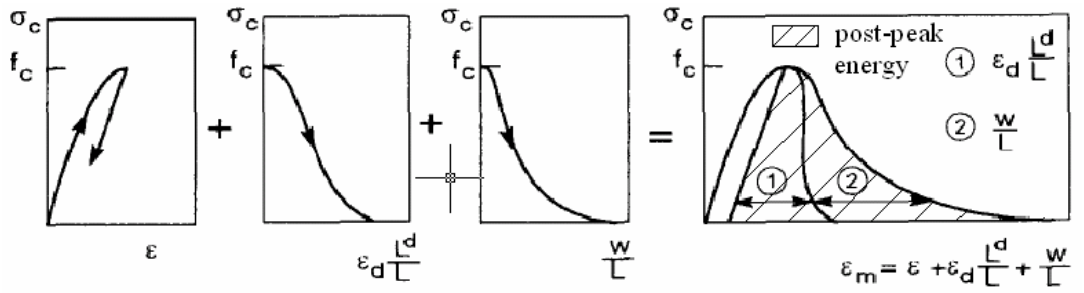

Figure 5-15 Composition of the complete stress-strain curve

(Markeset and Hillerborg, 1995)

where

ε_d is the additional strain within the damage zone

L_d is the length of the damage zone

L is the length of the specimen

w is the localized deformation (mm)

As indicated by Eq. (5-55), the post-peak energy G_{fc} (seen in Figure 5-15) is independent of the specimen length when specimen length L is greater than damage zone L_d. The post-peak energy G_{fc} differs in each research (Markeset and Hillerborg, 1995, Lertsrisakulrat et al, 2000 and Soltani et al, 2005). But they all agreed on constant post-peak energy when the element length is greater than the length of the damage zone.

As recommended by Soltani et al (2005), when element length is less than the length of the damage zone, size effect will not affect the compressive softening model of the finite element. And the length of the damage zone is recommended by Soltani et al (2005) to be 200mm.

Therefore, in the 12-dof joint element when the length of element is less than 200mm, the post-peak curve is expressed as Eqs. (5-53) and (5-54), and the parameter *k* in Eqs. (5-53) and (5-54) is taken as 15. When the length of element is greater than 200mm, the post-peak curve is expressed as Eqs. (5-53) and (5-54), and

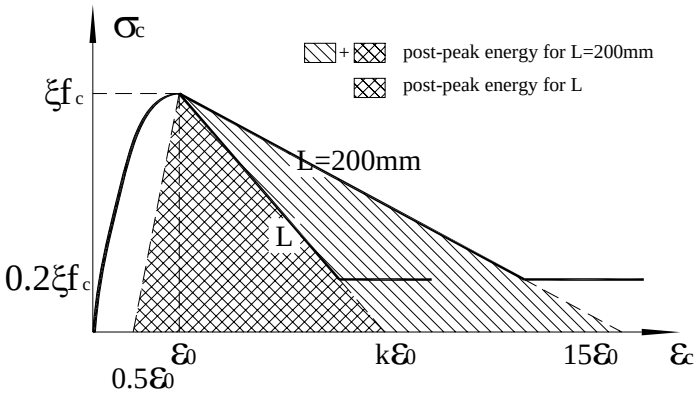

Figure 5-16 Post-peak curve on different element size

the parameter *k* in Eqs. (5-53) and (5-54) can be calculated based on constant post-peak energy G_{fc}, as shown in Figure 5-16. The equation of equivalent energy for element length 200mm and L indicated by Figure 5-16 is expressed as

$$\frac{1}{2}\xi f_c^{'}\cdot(15-0.5)\cdot 200=\frac{1}{2}\xi f_c^{'}\cdot(k-0.5)\cdot L \tag{5-56}$$

k can be solved from Eq. (5-56).

Considering the cases of element length in compression direction both greater and less than the length of damage zone, parameter *k* can be expressed as

$$\begin{aligned} k &= 15 && \text{for } L \le 200\text{mm} \\ k &= 14.5\frac{200}{L}+0.5 && \text{for } L > 200\text{mm} \end{aligned} \tag{5-57}$$

5.4.2 Concrete tension model

The concrete tension model in MBFEA follows the concrete tension model described in sub-chapter 4.2.2. The relation between average stress and average strain after cracking expressed in Eq. (2-16) is used.

5.4.3 Concrete shear model

The concrete shear transfer model in MBFEA follows the concrete shear model in sub-chapter 4.2.3. The shear transfer model expressed in Eq. (4-5) is used.

5.4.4 Reinforcement model

The reinforcement model in MBFEA follows the reinforcement model in sub-chapter 4.2.4. The modelling of the reinforcing bar in concrete must be based on the properties of the bar and the effect of bonding between bar and concrete. Yield stress of the reinforcement is expressed in Eq. (2-18), and post-yield modulus is expressed in Eq. (2-19).

5.4.5 Bond model

In the case of beam-column joints subjected to lateral loads, main bars running through joint are subjected to pull and push force at two ends. Actually the relationship between average bond stress and slip at the interface between the joint and adjacent members should be used in the spring elements to model the fixed-end-rotation at the interface between the joint and adjacent members. When the embedded length is relatively long, the average bond stress will differ much with the local bond stress. In this case, an average bond stress model needs to be developed instead of the local bond stress model.

At first, a bottom main bar in the joint in the case of specimen C1B (Yin, 2001) subjected to push and pull force at two ends is taken as an example to show the difference between average bond model and local bond model. It is a 32mm reinforcing bar embedded in 500mm concrete. Concrete compressive strength is 25MPa. Boundary condition and force are simplified as shown in Figure 5-17.

One dimensional truss element with slip can be simulated by the element in frame analysis program MBFEA. The derivation of 1D truss element with slip has been elaborated in chapter 3, and its stiffness equation is expressed in Eq. (3-11).

The specimen C1B is modelled with 8 elements. In each element, there are four nodes. Two nodes represent steel nodes, and two nodes represent concrete nodes. Concrete nodes are fixed at two ends and forces are on steel nodes at the two ends as shown in Figure 5-18. Young's modulus of concrete and reinforcement are assumed to be constant, and the local bond model proposed by Eligehausen et al

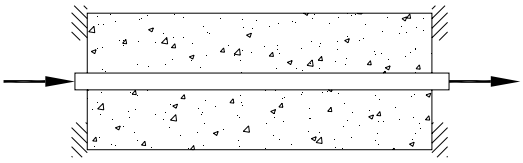

Figure 5-17 Simplification of bottom main bar in the joint

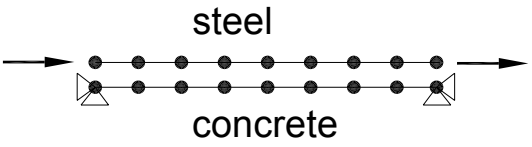

Figure 5-18 Mesh and boundary condition of 1D FEM

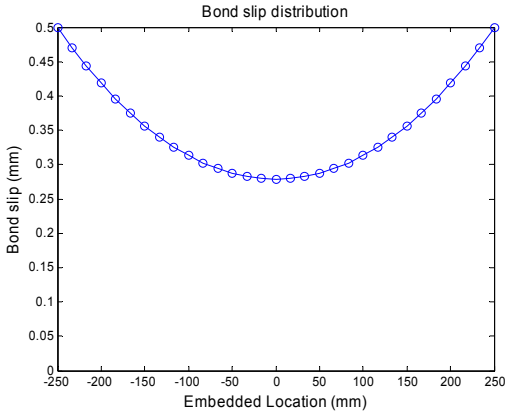

Figure 5-19 Bond slip distribution

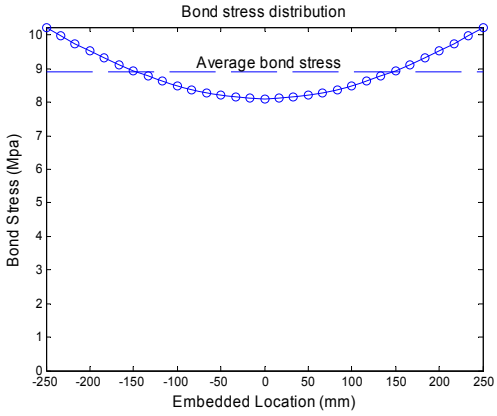

Figure 5-20 Bond stress distribution

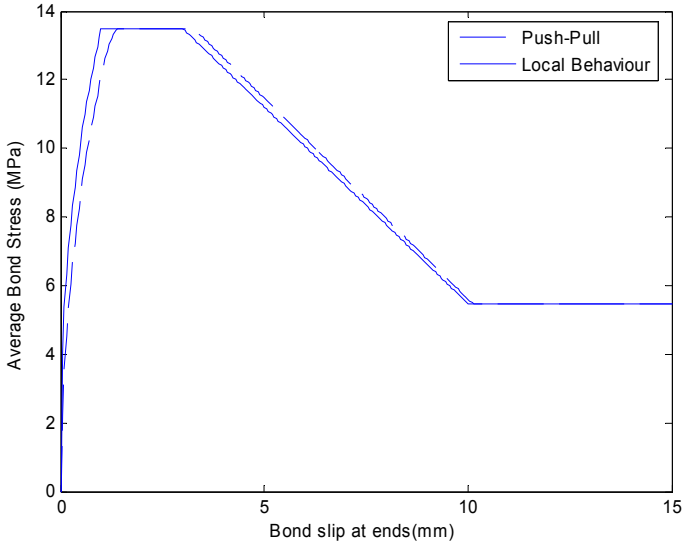

Figure 5-21 Average bond stress in push-pull test

(1983) is used. The formula has been reviewed in sub-chapter 2.6.3.

The bond-slip and bond stress distribution calculated by program MBFEA are shown in Figure 5-19 and Figure 5-20. The average bond stress in the push-pull experiment can be obtained from it. The bond stiffness used in 12-dof will be calculated from the relationship between average bond stress and end slip as

$$\bar{\tau} = \frac{F}{n \cdot l_s \cdot \frac{L}{2}} \tag{5-58}$$

where

F is the force at bar ends

n is the number of reinforcement

l_s is the perimeter of one bar

L is the embedded length

Comparing the calculated average bond stress-slip relationship with the local bond stress-bond slip relationship in Figure 5-21, it is found that the average bond stress-slip relationship only changes the characteristic slip s_1. Therefore, the average bond stress-slip relationship applied in the push-pull test can be proposed based on local bond stress-slip relationship with the modification on the characteristic slip s_1, and expressed as

$$\tau = \begin{cases} \tau_1 \left(\dfrac{s}{\beta \cdot s_1} \right)^{\alpha} & s \le \beta \cdot s_1 \\ \tau_1 & \beta \cdot s_1 < s \le s_2 \\ \tau_1 - \dfrac{s - s_2}{s_3 - s_2} \times (\tau_1 - \tau_3) & s_2 < s \le s_3 \\ \tau_3 & s > s_3 \end{cases} \tag{5-59}$$

Factor β is to take into account the modification on the characteristic slip s_1 and it is mostly affected by the ratio of embedded length to diameter of reinforcement L/d_b. When embedded length is small, the average bond behaviour is similar to local bond behaviour. When embedded length is long, the difference of bond behaviour and local bond behaviour becomes obvious. So, when the ratio of embedded length

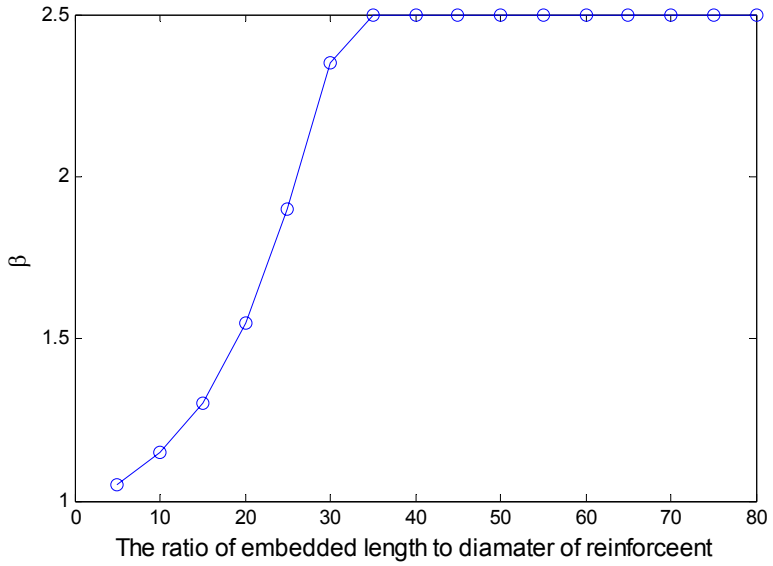

Figure 5-22 The relationship between β and the ratio of embedded length to diameter of reinforcement L/d_b

to diameter of reinforcement approaches 0, β approaches 1. With the increment of the ratio of embedded length to diameter of reinforcement, β increases.

Following the method mentioned above, different β can be calculated based on different embedded length L. Afterwards, the relationship between β and the ratio of embedded length to diameter of reinforcement L/d_b is plotted in Figure 5-22, and the curve can be approximated with a simple formula as

$$\beta = \begin{cases} 0.0018 \times \left(\frac{L}{d_b}\right)^2 - 0.012 \times \frac{L}{d_b} + 1.1 & \frac{L}{d_b} \le 35 \\ 2.5 & \frac{L}{d_b} > 35 \end{cases} \tag{5-60}$$

5.5 Effective reinforcement area in 12-dof joint element

In the joint, there are horizontal and vertical main bars and transverse shear reinforcements. In the 12-dof joint element, only one element is used to represent the whole joint. The reinforcement is assumed to be uniformly distributed in the whole element.

Based on the development of 12-dof joint element, there are some factors that will

increase the strength of the joint.

1. Assumption of plane boundary of the joint

   When the 12-dof joint element is degenerated from 8-node quadrilateral element, the boundary of the panel is assumed to remain plane after deformation. From the results of 2-D plane finite element analysis, it is found that the interface between joint and adjacent members is often curved because of non-uniformly shear stress along the interface (Figure 5-23). With the additional constraints, the joint element is expected to be stiffer and stronger.

2. Modelling of joint behaviour with different mesh

   With fewer elements, the joint has fewer degrees of freedom. Therefore, the joint element represented by one element is expected to be stiffer and stronger. This effect can be shown from the comparison of two cases with finite element program WCOMD.

   Case 1 is simulated with fine mesh as shown in Figure 5-24(a). Case 2 is simulated with coarse mesh, and joint is simulated with one element as shown

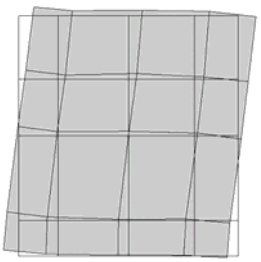

Figure 5-23 Typical deformed joint compared with original one

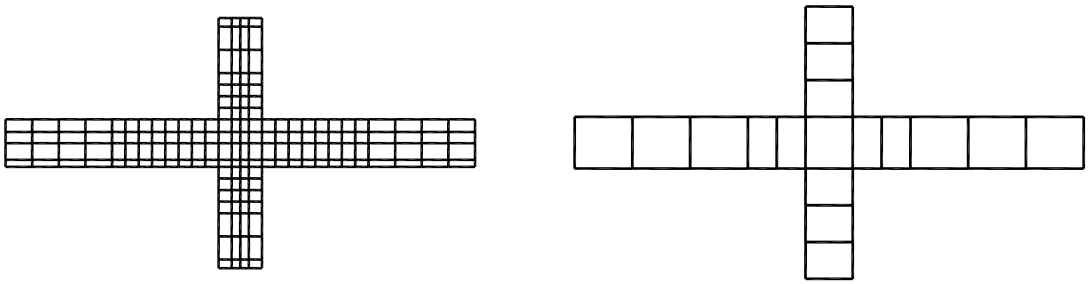

(a) Fine mesh (b) Coarse mesh

Figure 5-24 Mesh of specimen C1B by Yin (2001)

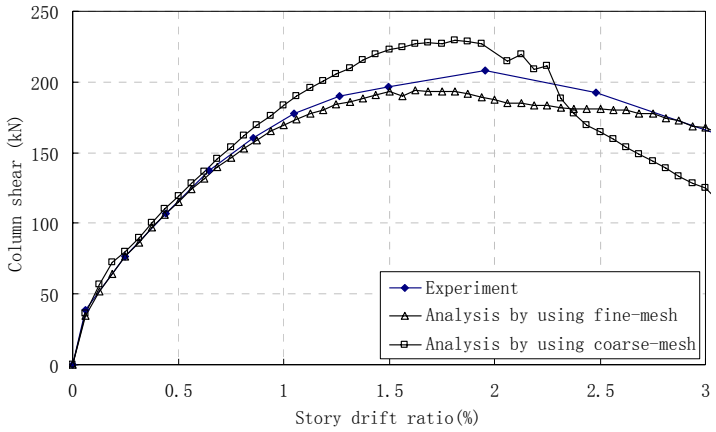

Figure 5-25 Results comparison between fine mesh and coarse mesh - specimen C1B by Yin (2001)

(a) Results with fine mesh (b) Results with coarse mesh

Figure 5-26 Crack pattern at story drift ratio of 1.5% - specimen C1B by Yin (2001)

in Figure 5-24(b). The comparison is done based on specimen C1B by Yin (2001). Details of specimen C1B can be found in Table 4-1. The comparison of results is shown in Figure 5-25. It is found that the analysis with coarse mesh gives higher strength of the joint.

Further observation on crack pattern on two cases, it is found that with more elements to represent the joint, crack occurs earlier, while with fewer elements, crack occurs much later in the joint as shown in Figure 5-26. As the cracks in the transverse direction affect the compressive concrete strength, it will also

affect the shear strength of joint.

Considering the factors mentioned above, the joint strength needs to be reduced in order to get more accurate results. For the modelling of the joint with one element, the high estimation of joint strength is because the lumped main reinforcement is smeared into the whole joint. In the joint, the main bars are usually concentrated near at the edge of the joint. When the dimensions of the joint are large, i.e. greater than 7.5 times of diameter of the reinforcement, simulating the joint with the smeared main reinforcement will overestimate the strength of the joint. In this case, effective main reinforcement should be used by reducing the amount of main bars to be smeared in the joint. The effective reinforcement amount in the joint can be expressed as

$$A_{s,eff} = A_{s,shear} + \lambda \cdot A_{s,main} \tag{5-61}$$

where

λ is the effectiveness factor for main reinforcement

$A_{s,shear}$ is the amount of transverse shear reinforcement

$A_{s,main}$ is the amount of main reinforcement

When more amount of main reinforcement is used, the effectiveness of the additional reinforcement is less, so reduction factor should be smaller. Therefore, the ratio of the amount of transverse shear reinforcement to the total amount of transverse shear and main reinforcement is used as the variable for the reduction factor λ.

By curve-fitting from experimental results, λ can be expressed as,

$$\lambda = 2.11 \times \mathrm{r} + 0.41 \le 1 \tag{5-62}$$

where $r = \dfrac{A_{sShear}}{A_{sShear} + A_{sMain}}$

5.6 Verification

5.6.1 Experimental data

The experimental results of four groups of specimens by Yin (2001), Fujii (1991), Hegger (2004) and Kitayama(1991) are selected The failure modes of all the specimens are either shear or bond failure. These specimens include cases with and without axial loading, with and without transverse reinforcement, high strength concrete up to 66 MPa and high strength reinforcement up to 1090 MPa. Details of the specimens can be found in Table 5-1. In the set-up of these specimens, the load is applied either at beam ends or at column end as shown in Figure 4-11.

5.6.2 Modelling for frame analysis

In frame analysis with rigid joint and no slip between main longitudinal bars and concrete, the sub-assemblage is modelled with four beam elements as shown in Figure 5-27. In this case, joint is not modelled separately. In frame analysis considering soft joint, the sub-assemblage is modelled with four beam elements and a 12-dof joint element as shown in Figure 5-28. In frame analysis considering soft joint and fixed-end rotation, the sub-assemblage is modelled with four beam elements, a 12-dof joint element and combination of spring elements at beam-column interface as shown in Figure 5-29.

5.6.3 Modelling of beam element

After crack occurs, beam elements will behave nonlinearly, and affect the lateral drift together with joint element. After the crack, the moment-curvature relationship of the beams is calculated based on the effective moment of inertia (ACI 318-05, 2005). After the yielding, moment capacity is assumed to remain constant.

Table 5-1 Details of specimens for frame analysis

Specimens		Material property			Beam				Column				
		Concrete strength	Beam reinforcement	Column reinforcement	Dimension		Reinforcement area		Dimension		Reinforcement area	Axial loading	Loading Mode[1]
		f_c (MPa)	f_{yb} (MPa)	f_{yc} (MPa)	b_b (mm)	h_b (mm)	Top bar (mm^2)	Bot bar (mm^2)	b_c (mm)	h_c (mm)	(mm^2)	(kN)	
Yin (2001)	C1B	23.7	500	500	300	550	4021	1609	350	500	982	0	1
	C1A	23.7	500	500	300	550	4021	1609	350	500	982	650	1
	C4B	23.7	500	500	300	400	4826	2413	400	400	982	0	1
	C4A	23.7	500	500	300	400	4826	2413	400	400	982	600	1
Fujii (1991)	A1	41	1090	656	160	250	628	628	220	220	664	150	1
	A3	41	1090	656	160	250	628	628	220	220	664	150	1
	A4	41	1090	656	160	250	628	628	220	220	664	450	1
Hegger (2004)	RA2	66.1	555	555	150	300	626	626	150	240	1257	45.8	1
	RA4	66.1	555	555	150	300	1030	1030	150	240	1030	33.6	1
	RA5	56.2	555	555	150	300	565	565	150	240	1257	49.9	1
Kitayama (1991)	J1	26.1	409	409	200	300	796	796	300	300	1061	180	2

[1]Loading mode is illustrated in Figure 4-11

Table 5-1 Details of specimens for frame analysis (continued)

Specimens		Joint							Slip			
		Yield stress in x-dir	Yield stress in y-dir	Thickness	Reinforcement area				Diameter of top bars	Number of top bars	Diameter of bot bars	Number of bot bars
					in x-direction		in y-direction					
		f_{xy} (MPa)	f_{yy} (MPa)	t (mm)	Main Bar (mm^2)	Shear Bar (mm^2)	Side Bar (mm^2)	Mid Bar (mm^2)	(mm)		(mm)	
Yin (2001)	C1B	500	500	500	5630	0	1964	1964	32	2	32	5
	C1A	500	500	500	5630	0	1964	1964	32	2	32	5
	C4B	500	500	400	7238	0	2945	1964	32	3	32	6
	C4A	500	500	400	7238	0	2945	1964	32	3	32	6
Fujii (1991)	A1	1090	656	220	1257	170	1327	796	10	8	10	8
	A3	1090	656	220	1257	170	1327	796	10	8	10	8
	A4	1090	656	220	1257	452	1327	796	10	8	10	8
Hegger (2004)	RA2	555	555	240	1232	226	2513	0	14	4	14	4
	RA4	555	555	240	2061	503	2463	0	18	4	18	4
	RA5	555	555	240	1131	283	2513	0	12	5	12	5
Kitayama (1991)	J1	409	409	300	1593	170	1328	796	13	6	13	6

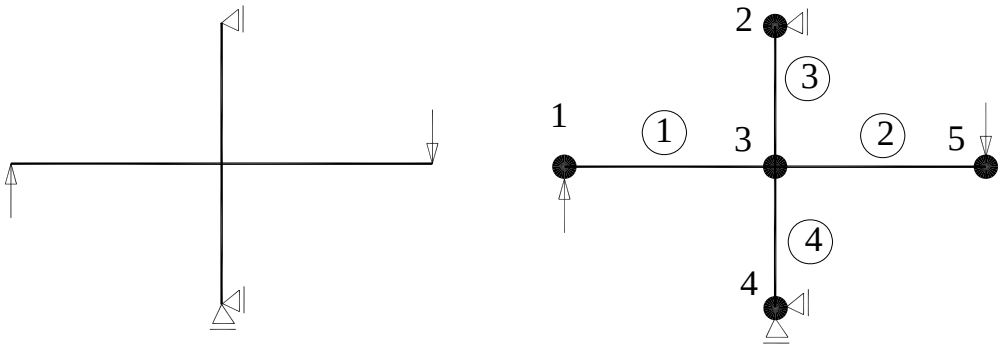

Figure 5-27 Modelling of frame analysis with rigid joint

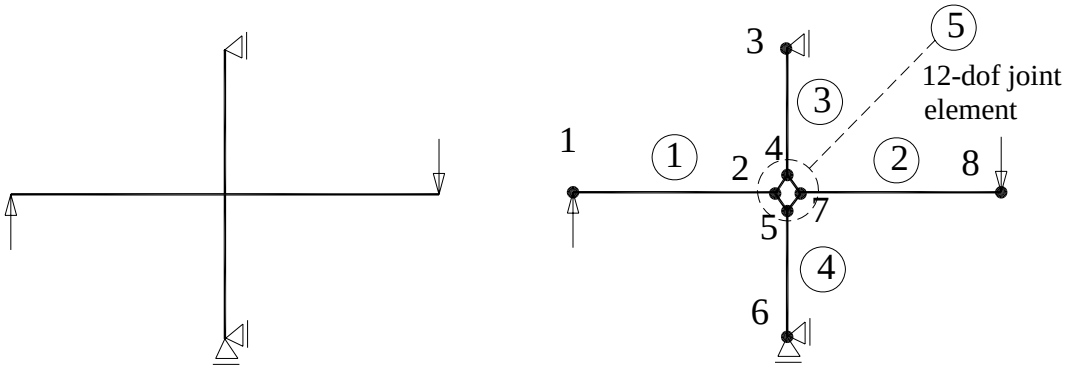

Figure 5-28 Modelling of frame analysis with 12-dof joint element

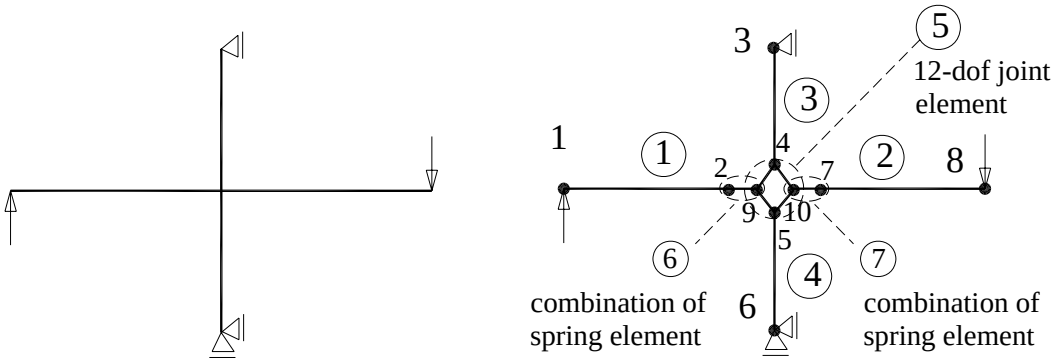

Figure 5-29 Modelling of frame analysis with 12-dof joint element and spring elements

5.6.4 Results and discussions

The analytical results from 12-dof joint element and spring elements are compared with the experimental results from four groups of specimens. Analytical results with and without the effect of slip are compared in the verification and shown in Figure 5-30 to Figure 5-33.

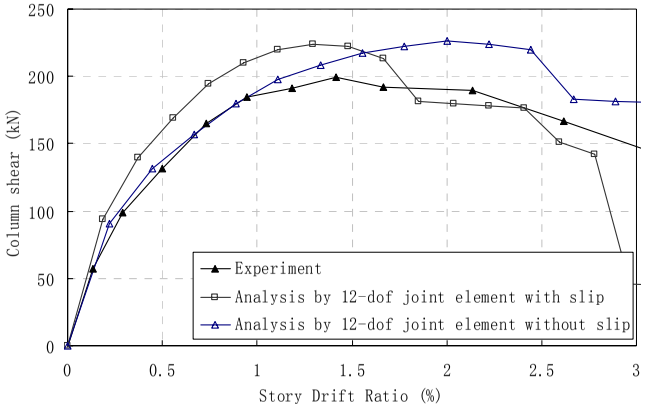

(a) Specimen C1A

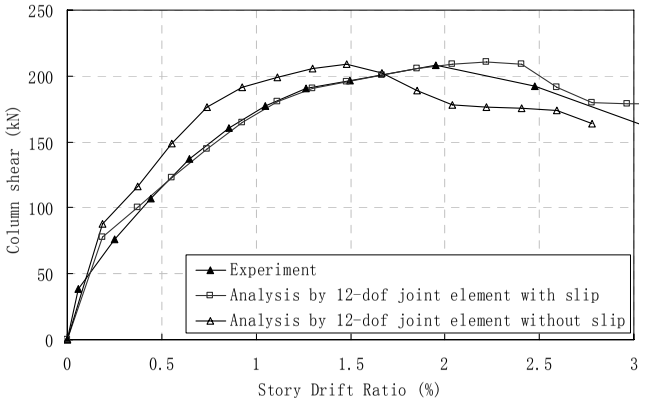

(b) Specimen C1B

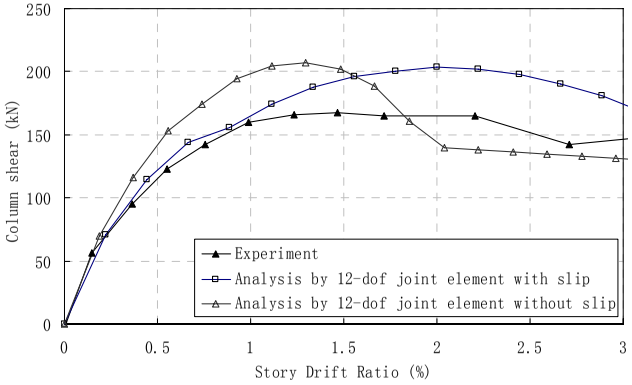

(c) Specimen C4A

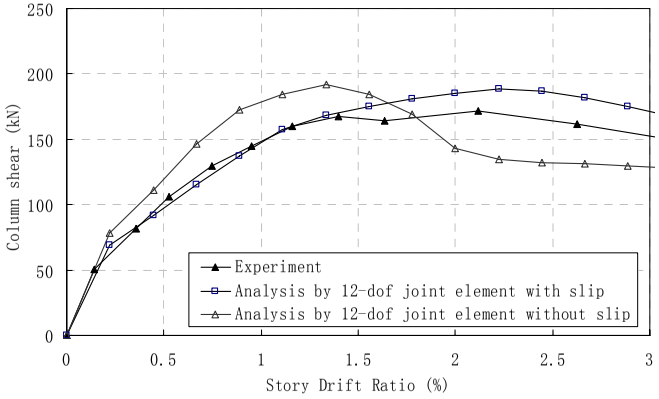

(d) Specimen C4B

Figure 5-30 Verification with Yin's (2001) experimental results

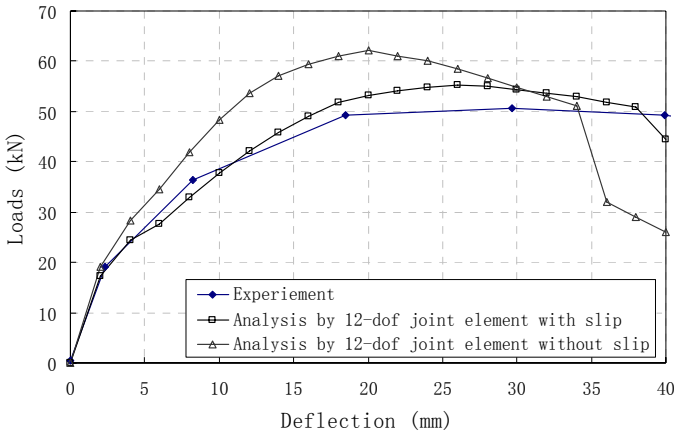

(a) Specimen A1

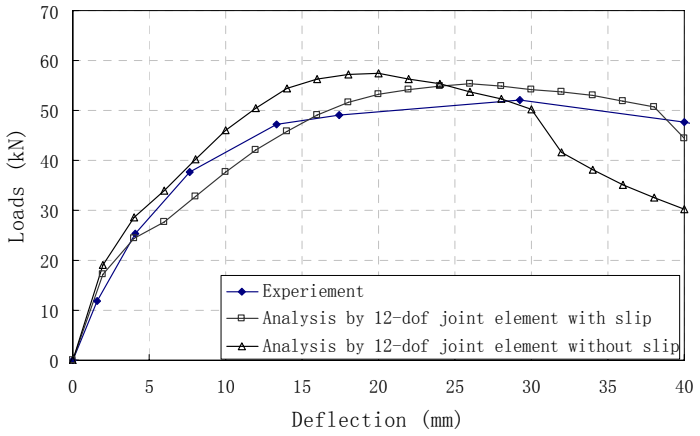

(b) Specimen A3

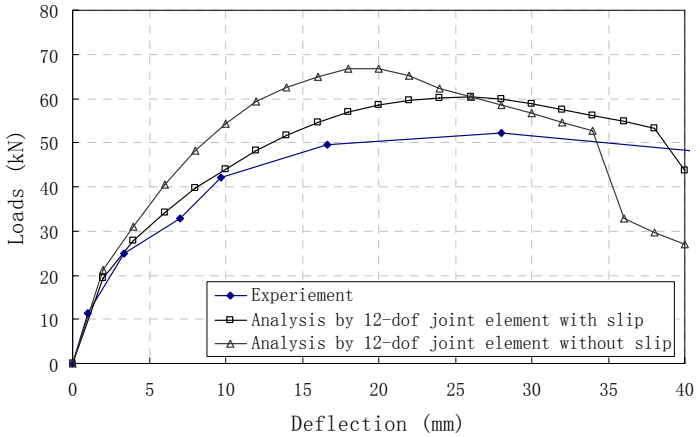

(c) Specimen A4

Figure 5-31 Verification with Fujii's (1991) experimental results

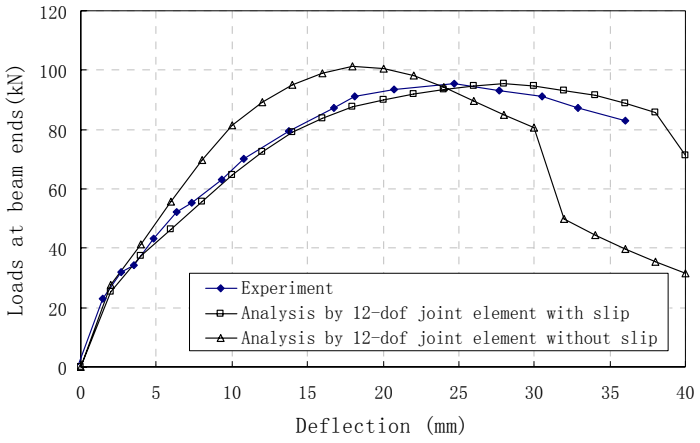

(a) Specimen RA2

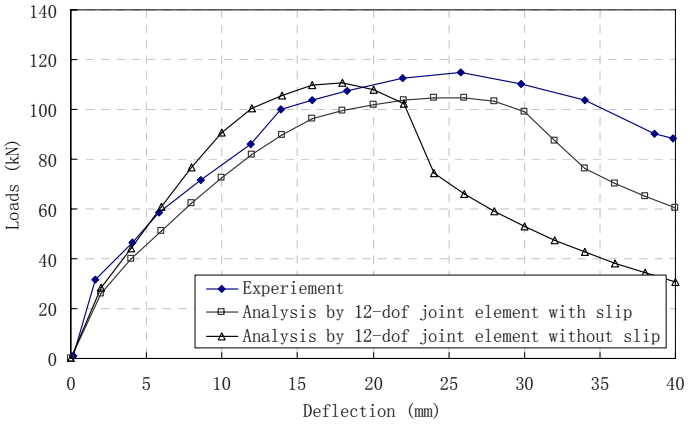

(c) Specimen RA4

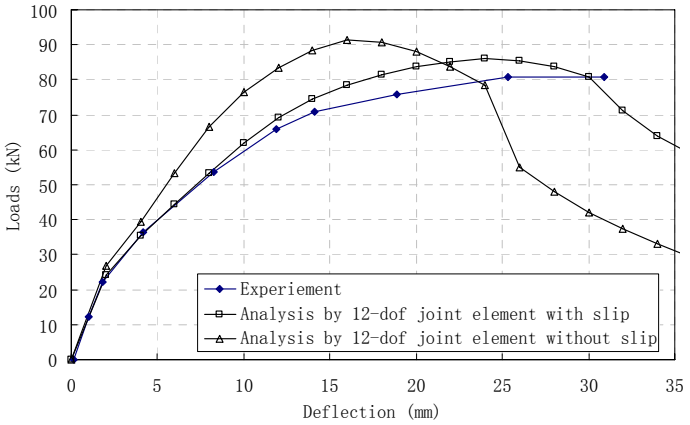

(d) Specimen RA5

Figure 5-32 Verification with Hegger's (2004) experimental results

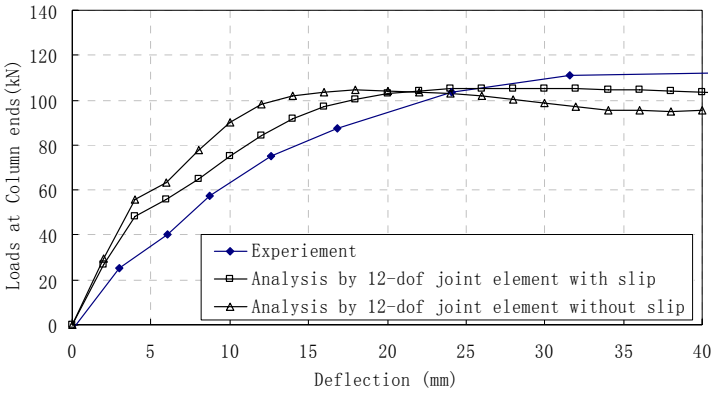

Specimen S1

Figure 5-33 Verification with Kitayama's (1991) experimental results

In the comparison of analytical results with experimental results shown from Figure 5-30 to Figure 5-33, the analyses by using 12-dof joint element with slip elements predict closer peak strength, better deflection at the peak strength and better descending curves compared to the analyses without slip elements. Compared to the analyses without slip elements, the analyses by using 12-dof joint element with slip elements improve the deflection at peak strength through the introduction the fixed-end-rotation due to effect of bond slip, which is important in modelling these specimens. Compared to the descending curve by the analyses without slip elements, the descending curves by the analyses with slip elements are all relatively more gentle, which represent the bond slip dominated phenomenon instead of compression dominated phenomenon. This phenomenon agrees with the experimental results. In summary, the analyses by using 12-dof joint element with slip elements can simulate shear and bond slip behaviours in structures with soft joint and bond slip at the interface between the joint and adjacent members.

5.7 Conclusion

A 12-dof joint element is developed and utilized in Matlab frame analysis program MBFEA. The 12-dof joint element is degenerated from of 8-node quadrilateral element. It has 9 gauss points to simulate the non-constant strain field of the joint. In each gauss point, shear modulus is calculated based on the fixed-angle soften truss model. With this element, the strength and deformation of frames with soft joints can be calculated by using frame analysis.

A model of spring elements is also developed to take into account the strength and stiffness reduction due to bond-slip. Considering asymmetrical reinforcement arrangement in gravity-load-designed structures, a combination of rational and translational spring element is used to consider of both fixed-end rotation and translation due to bond-slip.

To obtain more accurate results, constitute models in the 12-dof joint element and spring elements are established considering the characteristics of modelling of the joint with macro elements. Effective reinforcement area is used in modelling concentrated reinforced joint with smeared method. Parameters in the models are verified through experimental results.

Finally, four groups of specimens are selected, and comparison between experimental results and analytical results is done to show the effectiveness and accuracy of the element. Compared with the analysis without slip elements, the analysis with slip elements simulates the experimental results better. So, the 12-dof joint element with spring elements can be utilised in frame analysis to simulate soft joint with fixed-end-rotation.

CHAPTER 6 SHEAR STRENGTH ESTIMATION OF BEAM-COLUMN JOINTS

6.1 Introduction

The safety of reinforced concrete structures depends on the ability of structural designers to predict the structural response both globally and locally. It is still a challenge to precisely predict the shear strength of beam-column joint in the reinforced concrete frame structures. This requires understanding on the complex behaviour of beam-column joints. Substantial efforts have been spent to understand the behaviour through experiments (Agbabian et al, 1994, Attaalla, 1997 and Durrani and Wight, 1985). The findings from the experiments combined with engineering judgment have provided valuable and simple design guidelines. It is, therefore, understandable that shear strength estimation of beam-column joints in reinforced concrete structures are often or even entirely empirical. However, empirical formulas can pose the danger of false sense of security unless a designer possesses a good understanding of joint behaviour and of the reasons for possible unsatisfactory response when these formulas are applied to situations that may be outside the range simulated in the tests (Paulay, 1989).

Despite numerous studies conducted on the beam-column joints, existing shear strength estimation generally does not give accurate prediction. Currently, the concept of truss and arch mechanisms in the joint is widely accepted. In truss mechanism, horizontal reinforcement, vertical reinforcement and concrete form the truss to resist the shear force, while in arch mechanism, only concrete around the diagonal contributes to resist the shear forces. However, the complex interaction of these two mechanisms involved in the joint behaviour makes the shear strength estimation of the beam-column joint a challenging problem.

This chapter presents a simple equation to predict the shear strength of the beam-column joints based on the combination of truss and arch mechanisms. The equation can be used to estimate the shear strength of not only gravity-load-designed but also seismic-load-designed beam-column joints.

6.2 Basis for shear strength equation

In this model, joint core is simplified into plain stress panel subjected to shear force. Therefore, the model is applicable in cases of beam-column joint subjected to in-plane forces only.

Concrete contributes in both arch and truss mechanisms, and the total of concrete contribution is limited by the effective concrete compressive strength. In truss mechanism, concrete and reinforcement in x- and y- directions act together to resist the shear force, while in arch mechanism, only concrete sustains the shear force. Hence, concrete plays two important roles in two mechanisms.

The total shear strength of the beam-column joint contributed from truss and arch mechanisms can be expressed as

$$V_j = V_j^t\left(\sigma_c^t,...\right) + V_j^a\left(\sigma_c^a,...\right) \tag{6-1}$$

where

V_j^t is shear resistance from truss mechanism

V_j^a is shear resistance from arch mechanism

The sum of concrete compressive stress in truss and arch mechanisms is limited by the effective concrete compressive strength and can be expressed as

$$\sigma_c^t + \sigma_c^a = v \cdot f_c^{'} \tag{6-2}$$

where

σ_c^t is concrete compressive stress in truss mechanism

σ_c^a is concrete compressive stress in arch mechanism

v is the factor of effective concrete compressive strength

According to low-bound plasticity theory (Nielsen, 1998), the actual resistance is based on maximum plastic resistance of the structure. Concrete compression capacity will be utilised in the truss mechanism as much as possible until the yielding of reinforcement. After that, the remaining concrete compression capacity will be utilised in the arch mechanism.

In arch mechanism, shear force is approximately transferred in the diagonal direction of the joint. Then, arch angle θ can be expressed as,

$$\tan\theta = \frac{h_b}{h_c} \tag{6-3}$$

According to research by Thurlimann (Thurlimann, 1979), shear crack width should be limited by applying limit on truss angle. Ichinose (1992) applied the limit on $\cot\phi_m$ for shear formula in the beam. The $\cot\phi_m$ must be less than 2. Beam-column joint may be subjected to shear force in two opposite directions. To limit the width of shear cracks in two opposite directions, truss angle is taken as

$$1/2 \le \cot\phi_m \le 2 \tag{6-4}$$

There are four kinds of possible failure modes in the derivation of shear strength of beam-column joints. They are:

(1) Reinforcement yielding in x- and y- directions and concrete crushing.

(2) Reinforcement yielding in x- direction and concrete crushing.

(3) Reinforcement yielding in y- direction and concrete crushing.

(4) Concrete crushing without steel yielding.

Theoretically, joint core will deform arbitrary when reinforcement in both directions yields. In reality, it is surrounded by adjacent members that the compatibility of deformation of joint and adjacent members has to be satisfied. So when reinforcement yields in both directions, the joint will not suddenly lose its strength until the crushing of concrete.

Since the derivation is based on plasticity theory, only the equilibrium equations are needed.

In the truss mechanism, equilibrium equations are

$$\sigma_c^t \cos^2\phi_m + \rho_{wx}\sigma_{wx} = 0 \tag{6-5}$$

$$\sigma_c^t \sin^2\phi_m + \rho_{wy}\sigma_{wy} = -\sigma_y \tag{6-6}$$

$$\tau_t = -\sigma_c^t \sin\phi_m \cos\phi_m \tag{6-7}$$

where ρ_{wx} and ρ_{wy} are reinforcement ratios in x- and y- directions

σ_{wx} is steel stress in x-direction, and $\sigma_{wx} \le f_{wx}$

σ_{wy} is steel stress in y-direction, and $\sigma_{wy} \le f_{wy}$

σ_y is normal stress in y-direction due to column axial load, $\sigma_y = \dfrac{N}{h_c \cdot b_c}$

σ_c^t is the concrete stress in truss mechanism

τ_t is the shear stress in truss mechanism

In the truss mechanism, vertical shear resistance can be expressed as

$$V_{jv}^t = t \cdot j_{bt} \cdot \tau_t \tag{6-8}$$

while in the arch mechanism, vertical shear resistance can be expressed as

$$V_{jv}^a = t \cdot c \cdot \sigma_c^a \cdot \sin\theta = t \cdot c \cdot \left(\nu \cdot f_c^{'} - \sigma_c^t\right) \cdot \sin\theta \tag{6-9}$$

Then, the total vertical shear resistance in the joint is

$$V_{jv} = V_{jv}^t + V_{jv}^a = t \cdot j_{bt} \cdot \tau_t + t \cdot c \cdot \left(\nu \cdot f_c^{'} - \sigma_c^t\right) \cdot \sin\theta \tag{6-10}$$

where

t is thickness of the joint

τ_t is nominal shear stress of truss mechanism

c is width of the diagonal strut

j_{ct} is the arm lever of columns

σ_c^a is the concrete stress in arch mechanism

σ_c^t is the concrete stress in truss mechanism

v is the factor of effective concrete compressive strength

6.3 Shear strength equation

Shear stress and concrete stress in truss mechanism can be calculated from Eqs. (6-5) to (6-7) and be written as

$$\tau_t = \left(\rho_{wy}\sigma_{wy} + \sigma_y\right) \cdot \cot\phi \tag{6-11}$$

where

$$\cot\phi = \sqrt{\frac{\rho_{wx}\sigma_{wx}}{\rho_{wy}\sigma_{wy} + \sigma_y}}$$

$$\sigma_c^t = -\left(\rho_{wx}\sigma_{wx} + \rho_{wy}\sigma_{wy} + \sigma_y\right) \tag{6-12}$$

When Eqs. (6-11) and (6-12) are substituted into Eqs. (6-8) and (6-9), vertical shear resistance in joint core V_{jv} can be calculated as

$$V_{jv} = V_{jv}^{t} + V_{jv}^{a} = t \cdot j_{bt} \cdot \left(\rho_{wy}\sigma_{wy} + \sigma_{y}\right)\cot\phi + t \cdot c \cdot \left(1-\beta\right) \cdot \nu f_{c}^{'} \cdot \sin\theta \tag{6-13}$$

And the horizontal shear resistance can be calculated as

$$V_{jh} = V_{jh}^{t} + V_{jh}^{a} = t \cdot j_{ct} \cdot \left(\rho_{wy}\sigma_{wy} + \sigma_{y}\right)\cot\phi + t \cdot c \cdot \left(1-\beta\right) \cdot \nu f_{c}^{'} \cdot \cos\theta \tag{6-14}$$

where

$$\cot\phi = \sqrt{\frac{\rho_{wx}\sigma_{wx}}{\rho_{wy}\sigma_{wy} + \sigma_{y}}}$$

$$\beta = \frac{\rho_{wx}\sigma_{wx} + \rho_{wy}\sigma_{wy} + \sigma_{y}}{\nu\sigma_{B}}$$

σ_{y} is normal stress in y-direction due to axial column load, $\sigma_{y} = \dfrac{N}{h_{c} \cdot b_{c}}$

$$\theta = \arctan\left(\frac{h_{b}}{h_{c}}\right)$$

t is thickness of the joint

c is width of the diagonal strut

j_{bt} is the arm lever of beams

j_{ct} is the arm lever of columns

$\nu f_{c}^{'}$ is the effective compressive concrete strength

The vertical shear resistance in joint core V_{jv} can be determined if the reinforcement stresses in x- and y-directions, σ_{wx} and σ_{wy}, are determined. According to different failure modes, the reinforcement stresses in x- and y-directions, σ_{wx} and σ_{wy}, can be different. There are four failure modes in truss mechanism. In the failure modes governed by crushing of concrete, the derivation of the reinforcement stresses can be different based on two cases: the concrete crushing due to truss and arch mechanisms and the concrete crushing due to truss mechanism only.

In any case, the following inequalities should be satisfied

$$\rho_{wx}\sigma_{wx} + \rho_{wy}\sigma_{wy} + \sigma_{y} = \left(-\sigma_{c}^{t}\right) \le \nu f_{c}^{'} \tag{6-15}$$

$$\sigma_{wx} \le f_{wx} \tag{6-16}$$

$$\sigma_{wy} \le f_{wy} \tag{6-17}$$

Failure mode 1: Steel yielding in both directions

In this mode, steel yields in x- and y-directions. Hence,

$$\sigma_{wx} = f_{wx} \tag{6-18}$$

$$\sigma_{wy} = f_{wy} \tag{6-19}$$

The derivation of this failure mode is based on the following inequalities

$\rho_{wx}\sigma_{wx} + \rho_{wy}\sigma_{wy} + \sigma_y = \left(-\sigma_c^t\right) \le \nu f_c^{'}$ and $1/2 \le \cot\phi_m \le 2$.

If $x = \dfrac{\rho_{wx} f_{wx}}{\nu f_c^{'}}$, $y = \dfrac{\rho_{wy} f_{wy}}{\nu f_c^{'}}$ and $r = \dfrac{\sigma_y}{\nu f_c^{'}}$, these inequalities can be simplified as

$x + y + r \le 1$ and $\dfrac{1}{4} \le \dfrac{x}{y+r} \le 4$

Failure mode 2: Steel yielding in x-direction and concrete crushing

Case 1: Concrete crushing due to truss and arch mechanisms

In this case, only reinforcement in x-direction yields, while the full capacity of reinforcement in y-direction can not be mobilized because of the limit on the truss angle, $\cot\phi_m = 1/2$. Hence,

$$\sigma_{wx} = f_{wx} \tag{6-20}$$

σ_{wy} can be solved by using Eq. (6-5), Eq. (6-6) and $\cot\phi_m = 1/2$, and it can be written as

$$\sigma_{wy} = \frac{4\rho_{wx} f_{wx} - \sigma_y}{\rho_{wy}} \tag{6-21}$$

The derivation of this mode is based on the following inequalities

$\rho_{wx}\sigma_{wx} + \rho_{wy}\sigma_{wy} + \sigma_y = \left(-\sigma_c^t\right) \le \nu f_c^{'}$ and $\sigma_{wy} \le f_{wy}$.

If $x = \dfrac{\rho_{wx} f_{wx}}{\nu f_c^{'}}$, $y = \dfrac{\rho_{wy} f_{wy}}{\nu f_c^{'}}$ and $r = \dfrac{\sigma_y}{\nu f_c^{'}}$, these inequalities can be simplified as

$0 \le x \le 0.2$ and $\dfrac{x}{y+r} \le \dfrac{1}{4}$

Case 2: Concrete crushing due to truss mechanism only

In this case, reinforcement in x direction yields, and concrete strength is fully utilised in truss mechanism. Hence,

$$\sigma_{wx} = f_{wx} \tag{6-22}$$

σ_{wy} can be solved by using Eq. (6-5) and Eq. (6-6) , and it can be expressed as

$$\sigma_{wy} = \frac{\nu f_c^{'} - \rho_{wx} f_{wx} - \sigma_y}{\rho_{wy}} \tag{6-23}$$

The derivation of this mode is based on the following inequalities

$\sigma_{wy} \le f_{wy}$, $1/2 \le \cot\phi_m \le 2$ and $\rho_{wx}\sigma_{wx} \le \rho_{wy}\sigma_{wy} + \sigma_y$

If $x = \frac{\rho_{wx} f_{wx}}{\nu f_c^{'}}$, $y = \frac{\rho_{wy} f_{wy}}{\nu f_c^{'}}$ and $r = \frac{\sigma_y}{\nu f_c^{'}}$, these inequalities can be simplified as

$x + y + r > 1$ and $0.2 \le x \le 0.5$

Failure mode 3: Steel yielding in y-direction and concrete crushing

Case 1: Concrete crushing due to truss and arch mechanisms

In this case, only reinforcement in y-direction yields, while the full capacity of reinforcement in x-direction can not be mobilized because of the limit on the truss angle, $\cot\phi_m = 2$. Hence,

$$\sigma_{wy} = f_{wy} \tag{6-24}$$

σ_{wx} can be solved by using Eq. (6-5), Eq. (6-6) and $\cot\phi_m = 2$, and it can be expressed as

$$\sigma_{wx} = 4\frac{\rho_{wy} f_{wy} + \sigma_y}{\rho_{wx}} \tag{6-25}$$

The derivation of this mode is based on the following inequalities

$\rho_{wx}\sigma_{wx} + \rho_{wy}\sigma_{wy} + \sigma_y = \left(-\sigma_c^t\right) \le \nu f_c^{'}$ and $\sigma_{wx} \le f_{wx}$.

If $x = \frac{\rho_{wx} f_{wx}}{\nu f_c^{'}}$, $y = \frac{\rho_{wy} f_{wy}}{\nu f_c^{'}}$ and $r = \frac{\sigma_y}{\nu f_c^{'}}$, these inequalities can be simplified as

$0 \le y + r \le 0.2$ and $\frac{x}{y + r} \ge 4$

Case 2: Crushing due to truss mechanism only

In this case, reinforcement in y-direction yields, and concrete strength is fully utilised in truss mechanism. Hence,

$$\sigma_{wy} = f_{wy} \tag{6-26}$$

σ_{wx} can be solved by using Eq. (6-5) and Eq. (6-6) , and it can be expressed as

$$\sigma_{wx} = \frac{\nu f_c^{'} - \rho_{wy} f_{wy} - \sigma_y}{\rho_{wy}} \tag{6-27}$$

The derivation of this mode is based on the following inequalities

$\sigma_{wx} \le f_{wx}$, $1/2 \le \cot\phi_m \le 2$ and $\rho_{wx}\sigma_{wx} \ge \rho_{wy}\sigma_{wy} + \sigma_y$.

If $x = \frac{\rho_{wx} f_{wx}}{\nu f_c^{'}}$, $y = \frac{\rho_{wy} f_{wy}}{\nu f_c^{'}}$ and $r = \frac{\sigma_y}{\nu f_c^{'}}$, these inequalities can be simplified as

$x + y + r > 1$ and $0.2 \le y + r < 0.5$

Failure mode 4: Concrete crushing only

In this case, there is no reinforcement yielding in the both directions. So, σ_{wx} and σ_{wy} are unknown. Together with ϕ and τ, there are four unknowns in three equations (Eqs. (6-5) to (6-7)). According to low-bound plasticity theory (Nielson, 1998), the actual resistance is based on the maximum plastic resistance of the structure. To make τ maximum, $\sin\phi_m = \frac{1}{\sqrt{2}}$ and $\cos\phi_m = \frac{1}{\sqrt{2}}$ should be satisfied. So, σ_{wx} and σ_{wy} can be solved by using Eq. (6-5) and Eq. (6-6), and they can be expressed as

$$\sigma_{wx} = \frac{1/2\,\nu f_c^{'}}{\rho_{wx}} \tag{6-28}$$

$$\sigma_{wy} = \frac{1/2\,\nu f_c^{'} - \sigma_y}{\rho_{wy}} \tag{6-29}$$

The derivation of this mode is based on the following inequalities

$\sigma_{wx} \le f_{wx}$ and $\sigma_{wy} \le f_{wy}$

If $x = \frac{\rho_{wx} f_{wx}}{v f_c^{'}}$, $y = \frac{\rho_{wy} f_{wy}}{v f_c^{'}}$ and $r = \frac{\sigma_y}{v f_c^{'}}$, these inequalities can be simplified as

$x > 0.5$ and $y + r > 0.5$

Altogether there are six cases in the above derivation. Steel stress in x- and y-direction and conditions of each case can be summarized as

Case 1:

$\sigma_{wx} = f_{wx}$ for $(x + y + r \le 1)$ and $(1/4\, x \le y + r \le 4x)$

$\sigma_{wy} = f_{wy}$

Case 2:

$\sigma_{wx} = f_{wx}$ for $(0 \le x \le 0.2)$ and $(y + r \ge 4x)$

$\sigma_{wy} = \frac{4\rho_{wx} f_{wx} - \sigma_y}{\rho_{wy}}$

Case 3:

$\sigma_{wx} = f_{wx}$ for $(x + y + r \ge 1)$ and $(0.2 \le x \le 0.5)$

$\sigma_{wy} = \frac{v f_c^{'} - \rho_{wx} f_{wx} - \sigma_y}{\rho_{wy}}$

Case 4:

$\sigma_{wx} = 4\frac{\rho_{wy} f_{wy} + \sigma_y}{\rho_{wx}}$ for $(0 \le y + r \le 0.2)$ and $(y + r \le 1/4\, x)$

$\sigma_{wy} = f_{wy}$

Case 5:

$\sigma_{wx} = \frac{v f_c^{'} - \rho_{wy} f_{wy} - \sigma_y}{\rho_{wy}}$ for $(x + y + r \ge 1)$ and $(0.2 \le y + r \le 0.5)$

$\sigma_{wy} = f_{wy}$

Case 6:

$\sigma_{wx} = \frac{1/2 \cdot v f_c^{'}}{\rho_{wx}}$ for $(x \ge 0.5)$ and $(y + r \ge 0.5)$

$\sigma_{wy} = \frac{1/2 \cdot v f_c^{'} - \sigma_y}{\rho_{wy}}$

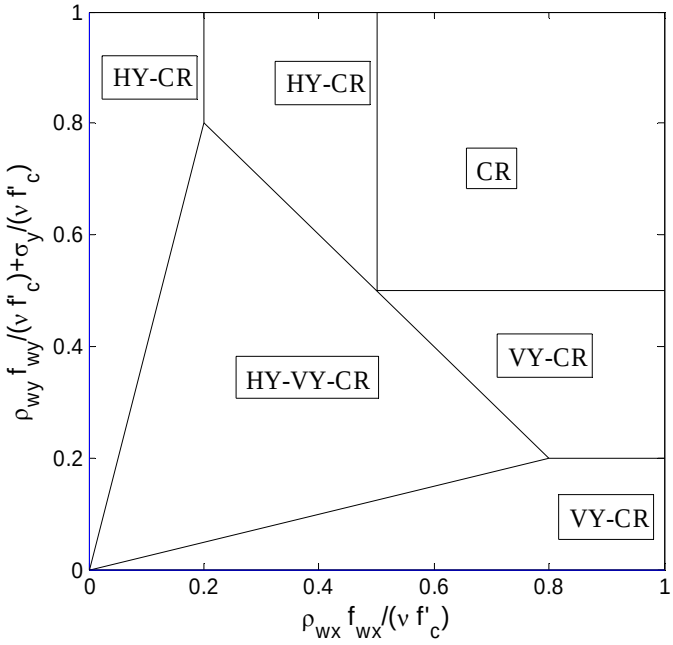

Failure modes:

HY-VY-CR: horizontal and vertical reinforcement yielding with concrete crushing

HY-CR: horizontal reinforcement yielding and concrete crushing

VY-CR: vertical reinforcement yielding and concrete crushing

CR: concrete crushing

Figure 6-1 Failure modes of shear strength

6.4 Discussion on equation

6.4.1 Failure mode of the joint

Altogether there are four failure modes: horizontal and vertical reinforcement yielding with concrete crushing, horizontal reinforcement yielding and concrete crushing, vertical reinforcement yielding and concrete crushing and concrete crushing. The failure mode varies according to different combination of reinforcement ratio, yield stress of reinforcement, the effective compressive strength of concrete and axial stress. Boundaries of each zone can be calculated from the conditions of each mode mentioned above. The results are shown in Figure 6-1. In failure modes of HY-CR or VY-CR, two cases are included: concrete crushing due to truss and arch mechanisms and concrete crushing due to truss mechanism only.

6.4.2 Shear strength of the joint

To show how the shear strength of the joint varies with reinforcement amount in x- and y-directions, the strength of a square beam-column joint with no axial column force is taken as an example In this case, $c = 0.25h$, $j_{ct} = 0.85h$ and $\theta = \pi/4$. Shear strength can be calculated by using Eq. (6-13).

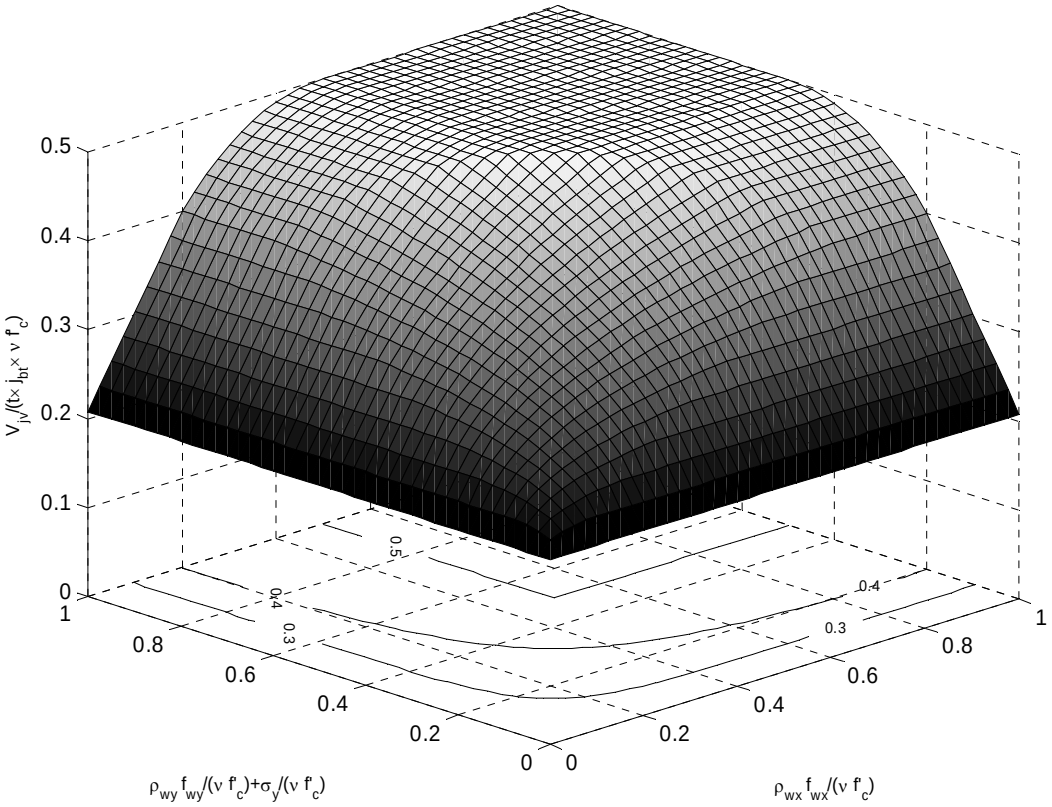

Figure 6-2 Nominal shear strength varying with $\frac{\rho_{wx} f_{wx}}{v f_c^{'}}$ and $\frac{\rho_{wy} f_{wy}}{v f_c^{'}} + \frac{\sigma_y}{v f_c^{'}}$

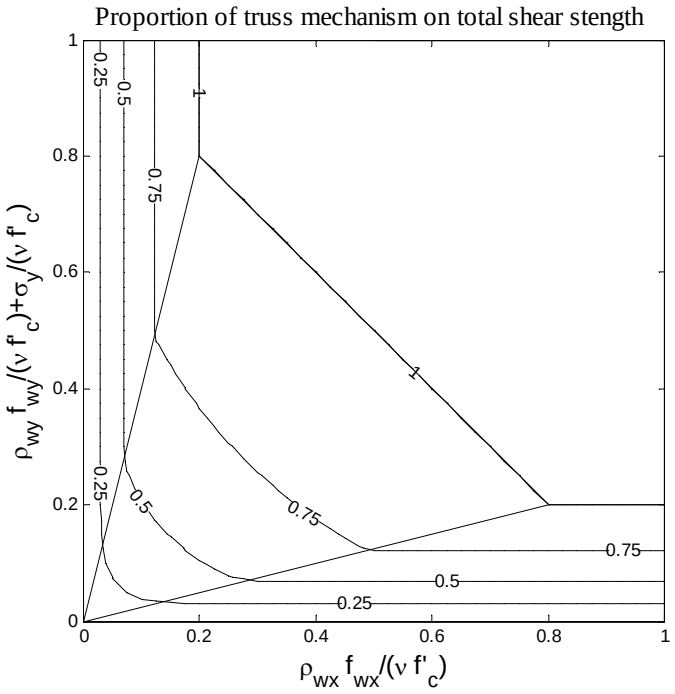

Figure 6-3 Proportion of truss mechanism on whole shear strength

Contour plotting of vertical shear strength in terms of reinforcement ratio, yield stress of reinforcement, the effective compressive strength of concrete and axial stress is shown in Figure 6-2.

From Figure 6-2, it is found that the shear strength of the joint increases with the increment of reinforcement ratio when the reinforcement ratio is relatively low, while the shear strength of the joint will not increase any more when the reinforcement ratio is large enough i.e. both $\frac{\rho_{wx} f_{wx}}{v f_c^{'}}$ and $\frac{\rho_{wy} f_{wy}}{v f_c^{'}} + \frac{\sigma_y}{v f_c^{'}}$ reach 0.5.

6.4.3 Proportion of truss mechanism on total shear strength

The proportion of truss mechanism on total strength is defined as $V_{jv}^t / V_{jv}^t + V_{jv}^a$. The proportion is the function of reinforcement ratio in x- and y-directions, yield stress of reinforcement in x- and y-directions, axial stress, arm lever of column and width-to-depth ratio of the joint. To show the proportion of truss mechanism on total shear strength varying with reinforcement ratio, yield stress of reinforcement, the effective compressive strength of concrete and axial stress, a square beam-column joint with no axial column force is taken as an example. In this case, $c = 0.25h$, $j_{ct} = 0.85h$ and $\theta = \pi/4$. Shear strength can be calculated by using Eq. (6-13). Contour of proportion of truss mechanism on total strength is shown in Figure 6-3.

From Figure 6-3, it is found that proportion of truss mechanism on total shear strength is zero when there is no reinforcement in the joint core. With the increment of reinforcement ratio, the proportion of truss mechanism on total shear strength increases. When reinforcement ratio is large enough, i.e. $\frac{\rho_{wx} f_{wx}}{v f_c^{'}}$ is greater than 0.2, $\frac{\rho_{wy} f_{wy}}{v f_c^{'}} + \frac{\sigma_y}{v f_c^{'}}$ is greater than 0.2 and $\frac{\rho_{wx} f_{wx}}{v f_c^{'}} + \frac{\rho_{wy} f_{wy}}{v f_c^{'}} + \frac{\sigma_y}{v f_c^{'}}$ is greater than 1, the proportion of truss mechanism reaches 1.0. At that time, the contribution of arch mechanism is negligible small.

6.4.4 Effect of axial load

The effect of axial load can be reflected from shear resistance of two mechanisms separately. On shear resistance contributed by arch mechanism, larger width of diagonal strut due to axial load increases the shear resistance. The axial load will increase the width of diagonal strut as shown in Eq. (6-30). On shear resistance contributed by truss mechanism, the additional stress in vertical direction due to axial load increases the shear resistance.

Normalised shear strength due to axial load, $V_{jv}(N)/V_{jv}(N=0)$, is not only the function of axial load, but also the function of reinforcement ratio in x- and y-directions. A square beam-column joint is taken as an example. In this case, $j_{ct} = 0.85h$, f'_c=30 MPa, f_{wx}=f_{wy}=300 MPa, ρ_{wx}=1%, $\theta = \pi/4$, the width of compression strut c is determined by Eq. (6-30) and the factor of effective concrete strength ν is determined by Eq. (6-31). Shear strength can be calculated by using Eq. (6-13). Three curves of relationship between normalised shear strength due to axial load and axial load ratio based on different reinforcement ratio in y-direction ρ_{wy} are shown in Figure 6-4.

From Figure 6-4, it is found that the relationship between normalised shear strength due to axial load and axial load ratio can be quite different with different reinforcement ratio in y-direction. Therefore, a shear strength estimation equation of the joint must include the effect of axial load and reinforcement ratio

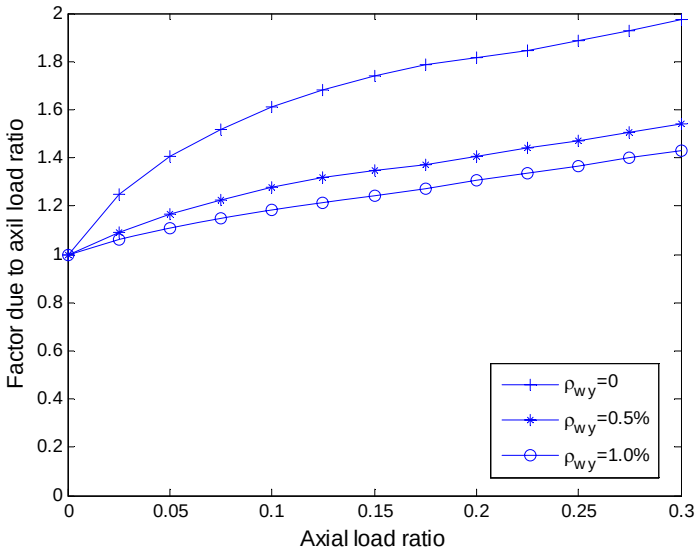

Figure 6-4 Factor of axial load v.s. axial load ratio

6.5 Parameters used in the equation

In arch mechanism, the depth of diagonal strut is a very important factor. It will affect the resistance of arch mechanism. When there is no reinforcement in x- or y-directions, truss mechanism does not contribute to shear resistance. Then the depth of diagonal strut becomes the most important factor to determine the shear resistance of joint.

The width of diagonal strut show in Figure 6-5 is empirically expressed by Paulay (1989) as

$$c = \left(0.25 + 0.85 \cdot \frac{N}{f_c^{'} A_g}\right) h_c \tag{6-30}$$

where

h_c is the depth of column

N is the axial load in column

$f_c^{'}$ is compressive concrete strength

A_g is the area of column

Compressive concrete strength is reduced due to crack in the diagonal direction. Therefore, effective compressive concrete strength should be used in the equation instead of original compressive concrete strength. The factor of effective compressive concrete strength proposed by Nielsen (1998) is used, and expressed as

$$\nu = 0.7 - \frac{f_c}{200} \tag{6-31}$$

The joint is simplified as a two-dimensional problem, and effective width of the joint is calculated according to the definition of ACI-318-05 code as the smaller of the width of column and the average of the width of beams and columns.

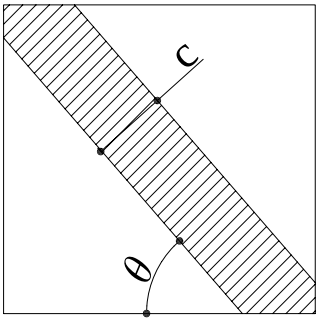

Figure 6-5 Parameters in the arch mechanism

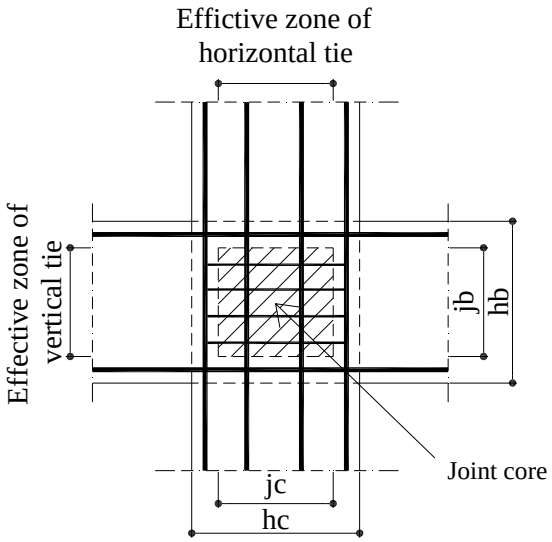

Figure 6-6 Concrete core of the joint

According to Hwang and Lee (2000), in truss mechanism, joint hoops contribute to the horizontal ties, and intermediate column bars contribute to the vertical ties. The effective horizontal and vertical ties in the calculation are indicated in Figure 6-6. All the reinforcement is smeared into the whole joint.

Because all the calculations are based on concrete core of the joint (Figure 6-6), reinforcement ratio is defined according to dimension of core of the joint. The dimension of the concrete core of joint is defined as

$$j_b = \frac{7}{8} h_b \tag{6-32}$$

$$j_c = \frac{7}{8} h_c \tag{6-33}$$

6.6 Verification of shear strength equation

A wide range of beam-column joints involving 33 specimens subjected to lateral loads is chosen. The variables of the test series are as follows:

(1) Concrete strength ranges from 26 to 82 MPa;

(2) Yield strength of reinforcement ranges from 276 to 1165 MPa

(3) Axial force ratio in the column ranges from 0 to 0.35

Details of each experiment can be found in Table 6-1. Definitions of specimen dimension are shown from Figure 6-7.

The accuracy of the equation is proved through comparison between the ratio of V_{Exp} to V_M and the ratio of V_{Cal} to V_M. V_{Exp} is the experimental column shear force. V_{Cal} is the calculated column shear force due to joint failure. V_M is the column shear force due to beam or column failure. When V_{Exp}/V_M is less than 1.0, it means the strength of joint is lower than those of adjacent members. The failure mode of the beam-column assemblage in experiments is joint failure. Due to stress hardening, moments of the adjacent members can increase after yielding of reinforcement. Therefore, when V_{Exp}/V_M is greater than 1.0 but less than 1.15, it is still considered to be joint failure.

The predicted failure mode and experimental failure mode are listed in Table 6-2. From the collected 33 specimens, the mean of V_{Exp}/ V_{Cal} is 0.98, and standard deviation of V_{Exp}/ V_{Cal} is 0.24. the comparison between experimental results and prediction is shown in Figure 6-8.

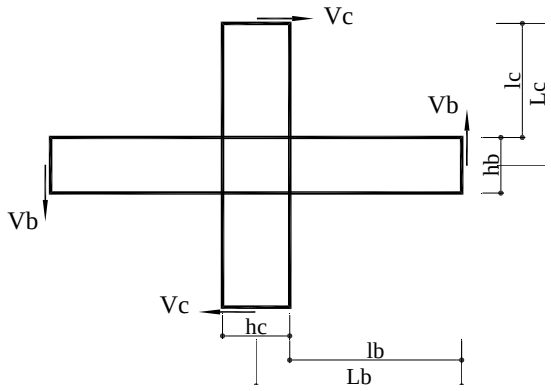

Figure 6-7 Dimension of beam-column joint and loads on it

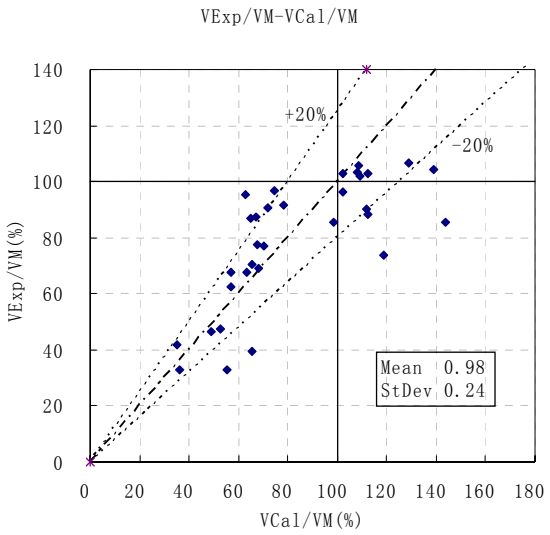

Figure 6-8 Comparison between experimental results and prediction

Table 6-1 Details of specimens for joint shear strength estimation equation

Specimens		Specimen dimensions			Material Properties			Reinforcement ratio			Axial Load Ratio	V_{col}
		h_b (mm)	h_c (mm)	t (mm)	f_c (MPa)	f_{yh} (MPa)	f_{yv} (MPa)	ρ_h (%)	ρ_v (%)	h_c/d_b	$\frac{N}{f_c A_g}$	(Exp) (kN)
Agbabian (1994)	**SA1**	203.2	177.8	127.0	27.6	413.7	413.7	0.71	0.00	18	0.00	9.1
	SA2	203.2	177.8	127.0	27.6	413.7	413.7	0.71	0.00	18	0.05	9.1
	SA3	203.2	177.8	127.0	27.6	413.7	413.7	0.71	0.00	18	0.10	10.9
Attaally (1997)	**SOC3**	203.2	177.8	127.0	47.1	551.2	413.4	0.56	0.00	15	0.25	16.9
	SHC1	203.2	177.8	127.0	56.5	551.2	413.4	0.28	0.00	15	0.22	16.5
	SHC2	203.2	177.8	127.0	59.5	551.2	413.4	0.56	0.00	15	0.22	16.9
Durrani (1985)	**X1**	419.1	362.0	320.7	34.3	275.8	413.7	0.86	1.00	16	0.05	141.9
	X2	419.1	362.0	320.7	34.3	275.8	413.7	1.29	1.00	16	0.05	141.9
	X3	419.1	362.0	320.7	34.3	275.8	413.7	0.86	0.56	16	0.05	111.9
Fujii (1991)	**A1**	250.0	220.0	190.0	41.0	297.0	656.0	0.41	2.18	22	0.08	50.0
	A2	250.0	220.0	190.0	41.0	297.0	395.0	0.41	2.18	22	0.08	46.1
	A3	250.0	220.0	190.0	41.0	297.0	656.0	0.41	2.18	22	0.25	50.0
	A4	250.0	220.0	190.0	41.0	297.0	656.0	1.09	2.18	22	0.25	51.0

Table 6-1 Details of specimens for joint shear strength estimation equation (continued)

Specimens		Specimen dimensions			Material Properties			Reinforcement ratio			Axial Load Ratio	V_{col}
		h_b (mm)	h_c (mm)	t (mm)	f_c (MPa)	f_{yh} (MPa)	f_{yv} (MPa)	ρ_h (%)	ρ_v (%)	h_c/d_b	$\frac{N}{f_c A_g}$	(Exp) (kN)
Hakuto (2000)	**O1**	500.0	300.0	380.0	41.0	339.0	325.0	0.00	0.00	13	0.00	89.0
	O4	500.0	600.0	380.0	53.0	398.0	398.0	0.00	0.00	25	0.00	177.0
	O5	500.0	600.0	380.0	33.0	398.0	398.0	0.00	0.00	19	0.00	150.0
Joh (1991)	**JX0-B8-MHUB**	350.0	300.0	250.0	26.1	377.0	325.0	0.49	1.21	23	0.17	56.9
Leon (1990)	**BCJ2**	304.8	254.0	228.6	30.2	413.7	413.7	1.04	1.50	19	0.00	58.5
	BCJ3	304.8	304.8	228.6	27.3	413.7	413.7	1.09	1.09	23	0.00	59.3
	BCJ4	304.8	355.6	228.6	27.3	413.7	413.7	1.09	0.62	26	0.00	61.4
Bertero (1980)	**BC8**	406.4	431.8	330.2	28.6	413.7	413.7	1.15	0.91	25	0.35	151.0
Liu (Park,2002)	**Unit 1**	500.0	300.0	380.0	43.8	318.0	321.0	0.00	0.00	13	0.00	72.0
	Unit 2	500.0	300.0	380.0	48.9	318.0	321.0	0.00	0.00	13	0.12	95.0

Table 6-1 Details of specimens for joint shear strength estimation equation (continued)

Specimens		Specimen dimensions			Material Properties			Reinforcement ratio			Axial Load Ratio	V_{col}
		h_b (mm)	h_c (mm)	t (mm)	f_c (MPa)	f_{yh} (MPa)	f_{yv} (MPa)	ρ_h (%)	ρ_v (%)	h_c/d_b	$\frac{N}{f_c A_g}$	(Exp) (kN)
Sugano (1991)	**J4-0**	400.0	440.0	370.0	31.0	941.0	408.0	1.73	1.07	20	0.33	594.0
	J6-0	400.0	440.0	370.0	61.7	941.0	408.0	1.73	1.07	20	0.17	706.0
	J6-1	400.0	440.0	370.0	63.5	941.0	408.0	1.73	1.07	20	0.16	683.0
	J8-0	400.0	440.0	370.0	79.1	941.0	579.0	1.73	1.07	20	0.13	691.0
	J8H-0	400.0	440.0	370.0	81.7	941.0	579.0	1.73	1.07	20	0.13	906.0
Teng(2003)	**S1**	400.0	300.0	300.0	33.0	510.0	510.0	0.90	0.80	19	0.08	120.0
Xin (1992)	**UNIT1**	500.0	450.0	275.0	30.9	348.0	477.0	1.81	0.58	38	0.32	152.0
	UNIT2	500.0	450.0	275.0	40.8	352.0	453.0	1.14	0.37	28	0.24	125.0
	UNIT3	500.0	450.0	275.0	42.5	348.0	469.0	1.68	0.58	28	0.23	170.0
	UNIT4	500.0	450.0	275.0	47.2	348.0	466.0	1.38	0.37	23	0.21	120.0
	UNIT5	500.0	450.0	275.0	60.7	341.0	469.0	1.89	0.58	23	0.16	225.0
	UNIT6	500.0	450.0	275.0	59.3	341.0	469.0	1.89	0.58	16	0.17	210.0

Table 6-2 Comparison of shear strength and failure modes of the joint between estimation by proposed equation and experimental results

Specimens		V_{ColB} (kN)	V_{ColC} (kN)	V_M (kN)	V_{Cal} (kN)	V_{Exp} (kN)	V_{Exp}/V_{cal} (%)	V_{cal}/V_M (%)	V_{Exp}/V_M (%)	Failure-Mode Cal[a]	Failure-Mode Exp[a]
Agbabian (1994)	**SA1**	27.7	28.8	27.7	10.0	9.1	91	36	33	J	J
	SA2	27.7	33.4	27.7	15.3	9.1	60	55	33	J	J
	SA3	27.7	36.8	27.7	18.2	10.9	60	66	39	J	J
Attaally (1997)	**SOC3**	24.0	49.6	24.0	15.7	16.9	108	65	70	J	J
	SHC1	24.4	51.2	24.4	15.5	16.5	107	63	68	J	J
	SHC2	24.4	45.0	24.4	16.6	16.9	102	68	69	J	J
Durrani (1985)	**X1**	138.0	227.0	138.0	141.1	142.0	101	102	103	J	J
	X2	138.0	227.0	138.0	155.0	142.0	92	112	103	J	J
	X3	105.0	139.0	105.0	135.5	112.0	83	129	107	M	J
Fujii (1991)	**A1**	176.0	120.0	120.0	42.1	50.0	119	35	42	J	J
	A2	73.6	93.8	73.6	42.1	46.1	110	57	63	J	J
	A3	176.0	108.0	108.0	53.0	50.0	94	49	46	J	J
	A4	176.0	108.0	108.0	56.7	51.0	90	52	47	J	J

Table 6-2 Comparison of shear strength and failure modes of the joint between estimation by proposed equation and experimental results (Continued)

Specimens		V_{ColB} (kN)	V_{ColC} (kN)	V_M (kN)	V_{Cal} (kN)	V_{Exp} (kN)	V_{Exp}/V_{cal} (%)	V_{cal}/V_M (%)	V_{Exp}/V_M (%)	Failure-Mode Cal[a]	Failure-Mode Exp[a]
Hakuto (2000)	**O1**	149.0	93.2	93.2	58.8	89.0	151	63	95	J	J
	O4	200.0	244.0	200.0	224.6	177.0	79	112	89	J	J
	O5	175.0	244.0	175.0	172.0	150.0	87	98	86	J	J
Joh (1991)	**JX0-B8 -MHUB**	59.0	132.0	59.0	62.2	56.9	92	105	96	J	J
Leon (1990)	**BCJ2**	102.0	60.5	60.5	46.3	58.5	126	77	97	J	J
	BCJ3	103.0	76.5	76.5	54.0	59.3	110	71	78	J	J
	BCJ4	106.0	79.6	79.6	59.0	61.4	104	74	77	J	J
Bertero (1980)	**BC8**	217.0	522.0	217.0	216.5	160.0	74	100	74	J	J
Liu (Park,2002)	**Unit 1**	147.0	82.9	82.9	54.1	72.0	133	65	87	J	J
	Unit 2	150.0	140.0	140.0	80.5	95.0	118	58	68	J	J

Table 6-2 Comparison of shear strength and failure modes of the joint between estimation by proposed equation and experimental results (Continued)

Specimens		V_{ColB} (kN)	V_{ColC} (kN)	V_M (kN)	V_{Cal} (kN)	V_{Exp} (kN)	V_{Exp}/V_{cal} (%)	V_{cal}/V_M (%)	V_{Exp}/V_M (%)	Failure-Mode Cal[a]	Failure-Mode Exp[a]
Sugano (1991)	**J4-0**	649.0	779.0	649.0	536.1	594.0	111	83	92	J	J
	J6-0	669.0	1050.0	669.0	723.5	706.0	98	108	106	J	J
	J6-1	669.0	1060.0	669.0	730.9	683.0	93	109	102	J	J
	J8-0	669.0	1250.0	669.0	724.8	691.0	95	108	103	J	J
	J8H-0	1000.0	1270.0	1000.0	716.7	906.0	126	72	91	J	J
Teng(2003)	**S1**	137.0	165.0	137.0	91.9	120.0	131	67	88	J	J
Xin (1992)	**UNIT1**	146.0	201.0	146.0	202.6	152.0	75	139	104	M	J
	UNIT 2	146.0	162.0	146.0	209.8	125.0	60	144	86	M	J
	UNIT 4	120.0	216.0	120.0	230.3	120.0	52	192	100	M	J
	UNIT 6	233.0	277.0	233.0	260.3	210.0	81	112	90	J	J

a. in failure mode, J means joint failure, while M means beam or column failure

6.7 Conclusion

A shear strength estimation equation of beam-column joints is proposed. The equation is based on the combination of truss and arch mechanisms. For joint shear resistance based on truss mechanism, the joint core is simplified into a panel, and plasticity theory is applied. For joint shear resistance based on arch mechanism, resistance is provided by diagonal strut. With the assumption of concrete compression capacity is distributed in truss and arch mechanisms and the limitation for truss angle, the total shear strength estimation equation can be developed in terms of the geometry of the joint, effective concrete compressive strength and the stress of reinforcement in x- and y-directions. The stress of reinforcement in x- and y-directions can be derived according to different failure modes.

After the shear strength estimation equation of beam-column joints is developed, the failure modes of the joint, the shear strength of the joint and the proportion of truss mechanism on total shear strength varying with reinforcement ratio in x-and y-directions have been studied. Also, the effect of axial load is illustrated based on the newly developed equation.

Finally, a wide range of beam-column joints involving 33 specimens subjected to lateral loads are selected, and the accuracy of the equation is studied through the comparison with experimental results. So, the new joint strength estimation equation is recommended to estimate the strength of beam-column joint subjected lateral loads.

CHAPTER 7 CONCLUSIONS AND RECOMMENDATIONS FOR FUTURE WORKS

7.1 Summary of conclusions

The study include the development of double-panel element for 2-D finite element analysis and 12-dof joint element and spring elements for frame analysis to model the behaviour of gravity-load-designed (GLD) beam-column joints subjected to lateral loads. A joint shear strength equation to estimate the strength of GLD beam-column joints subjected to lateral loads was also proposed. In finite element analysis, the global behaviour such as the load-deflection relationship, contribution of joint deformation to total story drift as well as local behaviour such as the stress and strain distribution in the joint reinforcement, bond slip distribution along the reinforcement in the joint has also been investigated.

A new double-panel element combining concrete panel, reinforcement panel and bond interface has been developed. The double-panel element has 16 nodes, with 8 nodes representing concrete panel and another 8 nodes representing reinforcement panel. Bond effect is simulated between the concrete and reinforcement panels.

To develop the stiffness matrix of the new double-panel element, the concrete and reinforcement panels are analysed based on fixed-angle crack theory. The local monotonic and cyclic bond slip behaviour is based on Eligehausen et al's model (1983), except the reloading part is modified according to experimental data. After the newly developed element is implemented in finite element program WCOMD, verifications have been carried out on pull-out test, axial tension test, push-pull test and cyclic push-pull test. From the comparisons, it is shown that newly developed double-panel element can simulate bond slip behaviour accurately and effectively.

With the newly developed double-panel element, shear and bond behaviour of beam-column joints subjected to lateral loads can be analysed with 2-D finite element method. Because of the characteristics of the joint, some parameters of the models were modified. These parameters include parameters in post-peak concrete

compression constitutive model, parameters in the concrete shear transfer model and parameters in the bond slip model. Then four groups of specimens, which all fail due to shear or bond, were selected. Monotonic and cyclic load-deflection curves from the experimental and analytical results were compared to show the accuracy and effectiveness of double-panel element. Besides load-deflection curves, contribution of the beam and column flexure, joint shear deformation and bond slip to the total story drift was analysed and compared with experimental results to show the significant contribution of joint shear deformation and fixed-end-rotation deformations to the total story drift. Another observed fact in the experiment, the initial tension of tensile beam reinforcement turns into compression due to bond-slip in the joint, can also be simulated in the analysis.

A model of 12-dof joint element has been developed to simulate the soft joint in frame analysis. This element has 9 Gauss points to simulate the non-constant strain field in the joint. In each Gauss point, shear modulus was calculated based on fixed-angle crack theory, which can accurately describe the shear dominated behaviour after cracking. With this element, the strength and deformation of frames with soft joints can be calculated.

A model with a combination of spring elements has also been developed to take into account the strength and stiffness reductions due to bond slip. The combination of spring element is to take into account both rotational and translational bond slip effect at the interface between the joint and the adjacent members. In GLD structures, bond slip at the upper and lower longitudinal beam reinforcement are not always symmetrical because the beams are usually asymmetrically reinforced. Then, bond slip effect at the interface includes not only rotational but also translational slip, which can not be modelled by rotational spring element only. To obtain more accurate results, the effective reinforcement ratio and bond stiffness were determined through verification with experimental data. Finally, four groups of specimens were selected, and comparison between experimental and analytical results was carried out to show the effectiveness and accuracy of the 12-dof joint element with the combination of spring elements.

A simple equation was developed to estimate the joint strength under lateral loads. The new equation is based on the combination of truss and strut mechanisms. For joint strength based on truss mechanism, the joint core is simplified into a panel, and plasticity theory is applied to calculate the strength. For joint strength based on strut mechanism, resistance is provided by diagonal strut. With the assumptions of concrete capacity distribution in each mechanism and limitation of truss angle, the total shear strength estimation formula can be developed in terms of geometry of the joint, concrete strength and the stress of reinforcement in x- and y-directions. The stress of reinforcement in x- and y-directions can be derived according to different failure modes.

After the shear strength estimation formula of beam-column joints was developed, the failure modes of the joint, the shear strength of the joint and the proportion of truss mechanism on total shear strength as the function of reinforcement ratio in x-and y-directions were studied. The effect of axial load was also illustrated based on the newly developed formula. Finally, 38 specimens were selected, and comparison between experimental results and the prediction with the formula was carried out to show the accuracy of the shear strength estimation formula.

7.2 Recommendation for future work

It is necessary to implement cyclic model of concrete, reinforcement and bond into the model of 12-dof joint element with a combination of spring elements, so that the element can be applied in frame analysis program to analyse the cyclic behaviour of frame with soft joints.

It is recommended to study the effect of splitting failure on bond behaviour in the joint. The bond behaviour with a combination of pull-out failure and splitting failure is affected by confining pressure. The confinement can be provided from out-of-plane forces coming from the transverse beams, from stirrups around the main bar, or from the above cover concrete. The out-of-plane confinement can not be included in the 2-D problem, but the confinement from cover concrete can be studied.

It is also recommended to study the effect of transverse crack on bond behaviour. The

effect of crack width on bond strength has been studied by using discrete element by Ueda and Sato (2002). In this study, the effect of crack on bond is significant in the joints subjected to lateral loads, and modelled by a factor in terms of tensile strain. To obtain accurate results, the factor considering the effect of crack should be verified from experimental data of more specimens. It is recommended to carry out an experiment program to study the effect of crack on bond behaviour.

It is recommended to study bond behaviour in concrete in post-peak compression. Concrete at the corner of joint is believed to undergo severe damage even in the early loading stage. Then, bond in these areas can deteriorate due to high compressive concrete strain. The effect of the surrounding concrete strain has been listed as the factor to affect the bond behaviour by CEB (1996). But the quantitative description is not given. It is recommended to carry out an experiment program to study the effect of concrete strain on bond behaviour.

REFERENCES

ACI-ASCE Committee 318-05 (2005) "Building Code Requirements for Structural Concrete and Commentary" *American Concrete Institute*, Detroit, Michigan, 1992

ACI-ASCE Committee 352R-02 (2002) "Recommendations for Design of Beam-Column Connections in Monolithic Reinforced Concrete Structures" *American Concrete Institute*, Detroit, Michigan, 2002.

ACI-ASCE Committee 408.2R-92 (1992) "State-of-the-art Report on Bond under Cyclic Loads" *American Concrete Institute*, Detroit, Michigan, 1992.

Agbabian, M.S., Higazy, E.M. and Abdel-Ghaffa, A.M. (1994) "Experimental Observations on the Seismic Shear Performance of RC Beam-to-Column Connections Subjected to Varying Axial Column Force", *Earthquake Engineering and Structural Dynamics*, v 23, n 8, Aug, 1994, p 859-876.

Architectural Institute of Japan AIJ (1994) "Structural Design Guidelines for Reinforced Concrete Buildings", Tokyo, 1994,

Attaalla, S.A.A. (1997) "Seismic Shear Capacity of Beam-Column Joints in Multistory Reinforced Concrete Frame Buildings" Ph.D. Dissertation, Civil Engineering Department, University of Southern Californian, Aug, 1997, p 63-92.

Aycardi, L.E., Mander, J.B. and Reinhorn, A.M. (1992) "Seismic Resistance of RC Frame Structures Designed Only for Gravity Loads: Part II – Experimental Performance of Subassemblages" *Technical Report* NCEER-92-0028, State University of New York at Buffalo, 1992

Ayoub, A. and Filippou, F.C. (1999) "Mixed Formulation of Bond-Slip Problems under Cyclic Loads" *Journal of Structural Engineering*, v 125, n 6, Jun,

1999, p 661-671

Balan, T.A., Spacone, E. and Kwon, M. (2001) "A 3D hypoelastic model for cyclic analysis of concrete structures" *Engineering structures* v. 23, 2001, p.333-342

Balázs, G. (1991) "Fatigue of Bond." *ACI Materials Journal,* v 88, n 6, Nov-Dec, 1991, p 620-629.

Bažant, Z.P. and Planas, J. (1997) "Fracture and Size Effect in Concrete and Other Quasibrittle Materials" CRC Press, New York.

Belarbi, A. and Hsu, T.T.C., (1994) "Constitutive Laws of Concrete in Tension and Reinforcing Bars Stiffened by Concrete", *ACI Structural Journal (American Concrete Institute),* v 91, n 4, Jul-Aug, 1994, p 465-474

Belarbi, A. and Hsu, T.T.C., (1995) "Constitutive Laws of Softened Concrete in Biaxial Tension-Compression", *ACI Structural Journal*, v 92, n 5, Sep-Oct, 1995, p 562-573

Bertero, V.V., Popov, E.P. and Forzani, B. (1980) "Seismic Behaviour of Lightweight Concrete Beam-Column Subassemblages" *Journal of The American Concrete Institute*, v 77, n 1, Jan-Feb, 1980, p 44-52.

Biddah, A. and Ghobarah, A. (1999) "Modeling of Shear Deformation and Bond Slip in Reinforcement Concrete Joints", *Structural Engineering and Mechanics*, v 7, n 4, Apr, 1999, p 413-432

Bracci, J.M., Reinhorn, A.M. and Mander, J.B. (1992) "Seismic Resistance of RC Frame Structures Designed Only for Gravity Loads: Part III – Experimental Performance and Analytical Study of a Structural Model" *Technical Report* NCEER-92-0029, State University of New York at Buffalo, 1992

Cervenka, V. (1970) "Inelastic finite element analysis of reinforced concrete panels under in-plane loads" *Ph.D. Thesis*, University of Colorado.

Chen, W-F and Saleeb, A.F. (1982) "Constitutive equations for engineering materials" *John Wiley & Sons*, 1982, New York

Collins, Michael P., Mitchell, Denis, Adebar, Perry and Vecchio, F.J. (1996) "A General Shear Design Method" *ACI journal* January-February 1996

Collins, M. P, Vecchio, F. J. and Mehlhorn, G. (1985) "An International Competition to Predict the Response of Reinforced Concrete Panels" *Canadian journal of civil engineering* V. 12, 1985

Comité Européen du Béton CEB (1996) "RC Frames under Earthquake Loading", *Bulletin 220: State-of-the-Art Report*, Thomas Telford Ltd, London, 1996.

Comité Européen du Béton-Fédération Internationale de la Précontrainte CEB-FIP (1993) "Model Code 90", Th. Telford, London, 1993.

Cope, R., Rao, P., Clark, L. and Norris, P. (1980) "Modelling of reinforced concrete behaviour for finite element analysis of bridge slabs" *Numerical Methods for Non-linear Problems*, Pineridge Press , pp. 457–470.

D'Ambrisi, A. and Filippou, F.C. (1999) "Modelling of Cyclic Shear Behaviour in RC Members", *Journal of Structural Engineering*, v 125, n 10, Oct, 1999, p 1143-1150

Durrani, A.J. and Wight, J.K. (1985) "Behaviour of Interior Beam-to-Column Connections Under Earthquake-Type Loading" *Journal of The American Concrete Institute*, v 82, n 3, May-Jun, 1985, p 343-349.

Eligehausen R., Popov E.P., Bertero V.V. (1983) "Local Bond Stress-Slip Relationships of Deformed Bars under Generalized Excitations", Report No. UCB/EERC 83-23, Univ. of California, Berkeley, 1983.

fédération internationale du béton fib (2000) "Bond of Reinforcement in Concrete" *Bulletin 10: State-of-the-Art Report*, Lausanne, Switzerland, 2000

Fujii, S. and Morita, S. (1991) "Comparison between Interior and Exterior RC Beam -Column Joint Behaviour" in *Design of Beam-Column Joints for Seismic Resistance* ACI, SP-123, 1991, p 145-166.

Ghobarah, A. and Biddah, A. (1999) "Dynamic Analysis of Reinforced Concrete Frames Including Joint Shear Deformation", *Engineering Structures*, v 21, n

11, Nov, 1999, p 971-987.

Gupta, A. and Akbar, H. (1984) "Cracking in reinforced concrete analysis" *Journal of Structural Engineering* 110, 1735–1746.

Hakuto, S., Park, R. and Tanaka, H. (2000) "Seismic Load Tests on Interior and Exterior Beam-Column Joints with Substandard Reinforcing Details" *ACI Structural Journal*, v 97, n 1, January/February, 2000, p 11-25.

Hegger, J., Sheriff, A. and Roeser, W. (2004) "Nonlinear Finite Element Analysis of Reinforced Concrete Beam-Column Connections" *ACI Structural Journal* v 101, n 5, September/October, 2004, p 604-614.

Hodge, P. (1957) "Discussion of the Prager Hardening Law" *ASME J. Appl. Mech.*, 24, pp. 482–484.

Hsu, T.T. C. (1998) "Unified Approach to Shear Analysis and Design" *Cement and Concrete Composition*, v 20, n 6, Dec, 1998, p 419-435.

Hwang, Shyh-Jiann and Lee, Hung-Jen (1999) "Analytical Model for Predicting Shear Strength of Exterior Reinforced Concrete Beam-Column Joints for Seismic Resistance", *ACI structural Journal*, v 96, n 5, September/October, 1999, p 846-857.

Hwang, Shyh-Jiann and Lee, Hung-Jen (2000) "Analytical Model for Predicting Shear Strength of Interior Reinforced Concrete Beam-Column Joints for Seismic Resistance", *ACI structural Journal*, v 97, n 1, January/February, 2000, p 35-44.

Ichinose, T. (1992) "Shear Design Equation for Ductile R/C Members" *Earthquake Engineering & Structural Dynamics*, v 21, n 3, Mar, 1992, p 197-214

Jiang, D.H., Shah, S.P., and Andonian, A.T. (1984) "Study of the Transfer of Tensile Forces by Bond", *ACI Structural Journal*, v 81, n 3, May-Jun, 1984, p 251-259

Joh, O., Goto, Y. and Shibata, T. (1991) "Influence of Transverse Joint and Beam Reinforcement and Relocation of Plastic Hinge Region on Beam-Column

Joint Stiffness Deterioration" in *Design of Beam-Column Joints for Seismic Resistance*, ACI, SP-123, 1991, p 317-358.

Keuser, M. and Mehlhorn, G. (1987) "Finite Element Models for Bond Problems", *Journal of Structural Engineering*, v ll3, n l0, Oct, 1987, p 2l60-2173

Kunnath, S.K., Hoffmann, G., Reinhorn, A.M., Mander, J.B. (1995) "Gravity-load-designed reinforced concrete buildings - part I: seismic evaluation of existing construction" *ACI Structural Journal*, v 92, n 3, May-Jun, 1995, p 343-354

Kupfer, H (1969) "Das verhalten des betons unter Zweiachsign Beanspruchung" *Bericht Nr 18, Lehrstuhl fur Massivbau*, Technische Hochschule, Munchen, 1969

Kwak, H.G. and Filippou, F.C. (1990) "Finite Element Analysis of Reinforced Concrete Structures under Monotonic Loads" *Report No EERC 90-14*, Earthquake Engineering Research Center, University of California, Berkeley, 1990

Leon, R.T. (1990) "Shear Strength and Hysteretic Behavior of Interior Beam-Column Joints", *ACI Structural Journal (American Concrete Institute)*, v 87, n 1, Jan-Feb, 1990, p 3-11.

Lertsrisakulrat, T., Watanabe, K., Matsuo, M. and Niwa, J. (2000) "Localized Fracture Length and Fracture Energy of Concrete in Compression" *Transactions of the Japan Concrete Institute*, v 22, 2000, p 99-104

Limkatanyu, S and Spacone E. (2003) "Effect of reinforcement slippage on the non-linear response under cyclic loadings of RC frame structures" *Earthquake Engineering Structural Dynamics*, v.23, 2003, p.2407-2424

Limkatanyu, S. and Spacone, E. (2002) "Reinforced Concrete Frame Element with Bond Interfaces: Displacement-based, Force-based, and Mixed formulations", *Journal of Structural Engineering*, v 128, n 3, March, 2002, p 346-355

Liu, T.C.Y, Nilson, A.H. and Slate, F.O. (1968) "Biaxial Stress-Strain Relations for Concrete" *journal of structural engineering*, ASCE, V98, No. ST5, May 1968

Lowes, L.N. (1999) "Finite Element Modeling of Reinforced Concrete Beam-Column Bridge Connections " Ph.D. Dissertation, Civil Engineering Department, University of Californian, Berkeley, 1999.

Lowes, L.N., Mitra, N. and Altoontash, A. (2004) "A beam-column joint model for simulating the earthquake response of reinforced concrete frames" *PEER Report 2003/10*, Pacific Earthquake Engineering Research Center College of Engineering University of California, Berkeley

Maekawa, K., Okamura, H. and Pimanmas, A. (2003) "Nonlinear Mechanics of Reinforced Concrete" SPON PRESS, 2003

Markeset, G. and Hillerborg, A. (1995) "Softening of Concrete in Compression - Localization and Size Effects" *Cement and Concrete Research*, v 25, n 4, May, 1995, p 702-708

Menétrey P. and Willam K. J. (1995) "Triaxial failure criterion for concrete and its generalization" *ACI Structural Journal*, Vol. 92, No. 3, May-June 1995, pp. 311-318

Monti, G. and Spacone, E. (2000) "Reinforced Concrete Fiber Beam Element with Bond-Slip", *Journal of Structural Engineering*, v 126, n 6, Jun, 2000, p 654-661

Monti, G., Filippou, F.C., and Spacone, E. (1997a) "Analysis of Hysteretic Behavior of Anchored Reinforced Bars" *ACI Structural Journal*, v 94, n 3, May-Jun, 1997, p 248-261.

Monti, G., Filippou, F.C., and Spacone, E. (1997b) "Finite Element for Anchored Bars under Cyclic Load Reversals", *Journal of Structural Engineering*, v 123, n 5, May, 1997, p 614-623

Ngo, D and Scordelis, A.C. (1967) "Finite element analysis of reinforced concrete

beams" *American Concrete Institute – Journal* v 64, n 3, Mar, 1967, p 152-163

Nguyen, X.H. (2005) "Behaviour of reinforced concrete short columns subjected to multi-directional loading", PhD Dissertation, School of Civil and Environmental Engineering, Nanyang Technological University, 2005

Nielsen, M.P. (1998) "Limit Analysis and Concrete Plasticity" second edition CRC

Noguchi, H. and Naganuma, K. (1984) *"Nonlinear Finite Element Analysis of Restoring Force Characteristics of Reinforced Concrete Beam-Column Joints"*, Proceeds of the 8th Conference on Earthquake Engineering volume Ⅳ July, San Francisco California U.S. , 1984.

Okamura, H. and Maekawa, K., (1991) "Nonlinear Analysis and Constitutive Models of Reinforced Concrete" Gihodo-Shuppan, 1991

Ottosen N. S. (1977) "A failure criterion for concrete" *Journal of the Engineering Mechanics Division*, Vol. EM4, August 1977, pp. 527-535

Pang, Xiao-Bo "David" and Hsu, T.T.C. (1996) "Fixed Angle Softened Truss Model for Reinforced Concrete" *ACI Structural Journal*, v 93, n 2, Mar-Apr, 1996, p 197-207.

Pang, Xiao-Bo "David" and Hsu, Thomas T.C. (1996) "Fixed Angle Softened Truss Model for Reinforced Concrete" *ACI journal* Mar-April 1996

Pantazopoulou, S. and Bonacci, J. (1992) "Consideration of Questions about Beam-Column Joints", *ACI structural journal*, v 89, n 1, Jan-Feb, 1992, p 27-36.

Park, R. (2002) "A Summary of Results of Simulated Seismic Load Tests On Reinforced Concrete Beam-Column Joints, Beams and Columns with Substandard Reinforcing Details" *Journal of Earthquake Engineering*, v 6, n 2, 2002, p 147-174.

Paulay, T. (1989) "Equilibrium Criteria for Reinforced Concrete Beam-Column Joints", *ACI Structural Journal*, v 86, n 6, Nov-Dec, 1989, p 635-643.

Pessiki, S.P., Conley, C., White, R.N. and Gergely, P. (1990) "Lightly-reinforced concrete frame structures" *Proceedings of the US National Conference on Earthquake Engineering*, 1990, p 707

Rashid, Y. (1968) "Analysis of prestressed concrete pressure vessels" *Nuclear Engineering and Design*, Balkema Ed. , pp. 265–286.

Salem, H. and Maekawa, K. (1999) "Spatially Averaged Tensile Mechanics for Cracked Concrete and Reinforcement under Highly Inelastic Range" *J. Mater. Conc. Struct. Pavements*, JSCE, v 42, n 613, 1999, p 277-293

Schafer, K. (1996) "Strut-and-Tie Models for the Design of Structural Concrete" *Notes of Workshop*, Department of civil engineering, National Cheng Kung University, Taiwan, Mar. 1996.

Shima, H., Chou, L. and Okamura, H. (1987) "Micro and Macro Models for Bond Behaviour in Reinforced Concrete" *J. Faculty Eng.*, University of Tokyo (B), v 39, n 331, p 167-180, 1987

Soltani, M., An, X. and Maekawa, K. (2005) "Localized Nonlinearity and Size-Dependent Mechanics of In-Plane RC Element in Shear" *Engineering Structures*, v 27, n 6, May, 2005, p 891-908

Soroushian, P., Chio, K., Park, G. and Aslani, F. (1991) "Bond of Deformed Bars to Concrete: Effect of Confinement and Strength of Concrete", *ACI material Journal*, v 88, n 3, May-Jun, 1991, p 227-232.

Soroushian, P., Obaseki, K., Nagi, M., and Rojas, M.C. (1988) "Pullout Behavior of Hooked Bars in Exterior Beam-Column Connections", *ACI structural journal*, v 85, n 3, May-Jun, 1988, p 269-276.

Spacone, E. and Limkatanyu, S. (2000) "Responses of Reinforced Concrete Members Including Bond-slip Effects" *ACI Structural Journal*, v 97, n 6, November/December, 2000, p 831-839.

Stevens, N.J., Uzumeri, S.M., Collins, M.P., and Will, G.T. (1991) "Constitutive Model for Reinforced Concrete Finite Element Analysis" *ACI journal*

January-February 1991

Sugano, S., Nagashima, Kimura, T.H. and Ishikawa, A. (1991) "Behaviour of Beam-Column Joints Using High-Strength Materials" in *Design of Beam-Column Joints for Seismic Resistance*, ACI, SP-123, 1991, p 359-378.

Suidan, M. and Schnobrich, W. (1973) "Finite element analysis of reinforced concrete" *Journal Structural Division* 99, 2109–2122.

Tassios, T.P. and Yannopoulos, P. J. (1981) "Analysis Studies of Reinforced Concrete Members under Cyclic Loading Based on Bond Stress-Slip Relationships" *ACI Structural Journal*, v 78, n 3, May-Jun, 1981, p 206-216

Teng, S. and Zhou, H (2003) "Eccentric Reinforced Concrete Beam-Column Joints Subjected to Cyclic Loading" *ACI Structural Journal*, v 100, n 2, March/April, 2003, p 139-148.

Thurlimann (1979) "Plastic Analysis of Reinforced Concrete Beams", *Introductory Report*, IABSE Colloquium Copenhagen, 1979

Ueda, T. and Sato, Y. (2002) "Prediction of Tension Behavior of Reinforced Concrete Member with Bond Model" *Bond in Concrete – from research to standards* 2002, Budapest

Ueda, T., Lin, I., and Hawkings, N. M. (1986) "Beam Bar Anchorage in Exterior Column-Beam Connections" *ACI Structural Journal*, v 83, n 3, May-Jun, 1986, p 412-422.

Vecchio, F.J. (1989) "Nonlinear Finite Element Analysis of Reinforced Concrete Membranes" *ACI structural journal* Jan-Feb 1989

Vecchio, F.J. and Collins, M.P. (1986) "Modified Compression-Field Theory for Reinforced Concrete Elements Subjected to Shear" *Journal of The American Concrete Institute*, v 83, n 2, Mar-Apr, 1986, p 219-231

Vecchio, F.J., Collins, Michael P. and Aspiotis, Jim (1994) "High-Strength Concrete Elements Subjected to Shear" *ACI journal* July-August 1994

Viwathanatepa, S., Popov, E.P. and Bertero, V.V. (1979) "Effects of Generalized

Loadings on Bond of Reinforcing Bars Embedded in Confined Concrete Blocks". Report No EERC 79-22, Earthquake Engineering Research Center, University of California, Berkeley.

Wang, T. and Hsu, T.T.C. (2001) “Nonlinear Finite Element Analysis of Concrete Structures Using New Constitutive Models”, *Computers & Structure* v 79, n 32, Dec. 2001, p 2781-91.

Willam K. and Warnke E. P. (1974) “Constitutive model for triaxial behavior of concrete, concrete structures subjected to triaxial stresses” *International association for bridges and structural engineering*, Bergamo, Italy, 1974.

Willam, K., Pramono, E. and Stur, S. (1987) “Fundamental issues of smeared crack models” *Proc. SEM-RILEM Int. Conf. on Fracture of Concrete and Rock*, SEM, pp. 192–207.

Xin, X.Z. (1992) “Behaviour of reinforced concrete interior beam-column joints designed using high strength concrete and steel” Master Thesis, Dept. of Civil Engineering, University of Canterbury.

Yin, H. (2001) “Behaviour of Lightly Reinforced Interior Beam-Column Joints under Reversed Cyclic Loading” Master Thesis, School of Civil and Environmental Engineering, Nanyang Technological University, 2001.

Youssef, M. and Ghobarah, A. (2001) “Modelling of RC Beam-Column Joints and Structural Walls” *Journal of Earthquake Engineering*, v 5, n 1, 2001, p 93-111.

Zhang, L. and Jirsa, J.O. (1982) “A study of Shear Behaviour of Reinforced Concrete Beam-Column Joints”, *PMFSEL* report No. 82-1 department of civil engineering, University of Texas at Austin. 1982.

Zhang, L.X. “Bob” and Hsu, T.T.C. (1998) “Behaviour and Analysis of 100 MPa Concrete Membrane Elements” *Journal of Structural Engineering*, v 124, n 1, Jan, 1998, p 24-34

Zhu, Ronnie R.H., Hsu, Thomas T.C., and Lee, Jung-Yoon (2001) “Rational Shear

Modular for Smeared-Crack Analysis of Reinforced Concrete" *ACI structural journal* July-August 2001